Biomass Combustion in Domestic Boilers with Low Emissions

Quan Gu

Faculty of Engineering

University of Nottingham

Project supervisors: Prof. Hao Liu, Dr. Chenggong Sun

Thesis submitted to the University of Nottingham for the degree of

Doctor of Philosophy

22 August 20

Abstract

Compared with conventional fossil fuels, biomass has its unique advantages in terms of wide availability, potential high energy generation and carbon neutrality. Up to now, biomass combustion has made huge contributions to meet the heating demands of both commercial and domestic fields. However, one of the main challenges of biomass combustion is its pollution emissions, including NOx, CO and hydrocarbons. Meanwhile, the release of CO_2 from biomass combustion which contributes to the greenhouse effect, should be paid more attention as well. The present PhD study aims to explore the combustion behaviours of biomass fuels by burning individual biomass pellets under different combustion atmospheres (air and oxy-fuel) and develop catalytic methods of NOx emission abatement for the potential use in small-scale and domestic biomass boilers.

In this study, five different types of biomass (wood, straw, miscanthus, peanut and torrefied wood) pellets were applied as the fuels in a visible drop tube furnace (V-DTF) to investigate the combustion behaviours under both conventional air and oxy-fuel (O_2 fraction of 21%, 25% and 30%) combustion atmospheres. Four combustion phases, namely pre-heating, volatile combustion, volatile/ char overlap combustion and char combustion were observed and identified. As expected, a shorter total burnout time of a biomass pellet was observed when increasing the combustion temperature (from 800°C to 900°C), which was mainly contributed more rapid char combustion. Increasing oxygen fraction from 21% to 30% also accelerated the pellet combustion, shortening the

total burnout time in oxy-fuel atmospheres while the total burnout time under conventional air combustion condition was between those of 21% O_2-79% CO_2 and 25%O_2-75% CO_2 atmospheres for untreated (raw) biomass fuels. Due to the impacts of C-CO_2 gasification reaction and torrefaction, torrefied wood was observed to have shorter char burning time under 21% O_2-79% CO_2, hence resulting in shorter total burning time than the air combustion. By means of high-speed camera and MATLAB software processing the flame images, the volatile flame brightness was found to increase with O_2 fraction in oxy-fuel atmospheres while the brightness of volatile flame in air was close to the one in 30% O_2-70% CO_2 atmosphere.

The tests to investigate the combustion performance and gaseous emissions (e.g. NOx, CO and CH_4) were carried out in a domestic 50kW biomass boiler with different primary and secondary air settings by using typical wood pellets. The results showed that the boiler had good performance in terms of NOx emissions under all conditions. Continuously fluctuating CH_4 and CO were detected in the combustion chamber during normal combustion processes due to insufficient mixing and limited chamber space. More importantly, both CH_4 and CO concentrations followed the same variation trend. The generation of CH_4 and CO was found to be determined by the amount of primary air while that of NOx was more dependent on the nitrogen content of the fuel. Both CH_4 and CO can potentially be utilized to reduce NOx emissions in suitable SCR processes.

Performance of CH_4-SCR and catalytic NOx-CO reactions were experimentally tested in a lab-scale fixed bed reactor with simulated flue gas atmospheres. For

CH_4-SCR tests, Co-ZSM-5 displayed great activity to reduce NOx with the help of excess oxygen. The optimum NOx conversion rate reached over 60% when using 2.89% or 4.89% Co-ZSM-5 (Si/Al ratio of 12.5) under the furnace setting temperature of 400℃. The catalytic performance of NOx reduction over Co-ZSM-5 was suppressed significantly in the absence of oxygen although there was activity between NOx and CH_4 at high temperatures due to thermal reactions. Fe-supported catalyst was inactive in CH_4-SCR system, but it could promote catalytic NOx-CO reactions in the absence of oxygen (with the maximum NOx reduction of 92.62% @ 500℃). However, the catalyst lost its activity when there was O_2 in the feed gas.

Acknowledgements

First and foremost, my deep gratitude goes to my supervisors, Prof. Hao Liu and Dr. Chenggong Sun for their patience, motivation and unwavering support during my research. I appreciate all their contributions of time and ideas to make my Ph. D experience stimulating.

I would like to thank Dr Lee Stevens, Dr Farooq Sher, Dr Hetian Chi and Dr Wenbin Zhang for the lab training. Likewise, I would like to thank our laboratory technicians, Tony Gospel, Andy Matthews, Jonathan Moss, Adrian Quinn, and Karl Booker for their kind help of manufacture and repair of parts for the experimental rigs.

I would like to thank Dr. Gary Lu for his advice on induvial pellet combustion tests, Dr. Md Moinul Hossain for Matlab code tips, Dr Xiaolei Fan for his suggestion and help on catalytic tests, and Dr Xiaoxia Ou and Rongxin Zhang for catalyst synthesis. Special thanks to my SRB and ETB colleagues and lovely Jubilee SCR team for their kindest support in the past four years.

Last but not the least, I would like to express my deepest gratitude to my parents for their unconditional love, understanding and support.

Contents

List of Figures

List of Tables

CHAPTER 1. INTRODUCTION

1.1 Background

As a large amount of fossil energy is continuously consumed in the 21st century, it becomes necessary and urgent to expand the use of other alternative energy resources to meet the future energy demand. Biomass, the most promising renewable resource, has shown its huge potential due to its wide availability, potential high energy generation and carbon neutrality. Apart from the most commonly used type of wood, other types of biomass, such as straw and miscanthus also show their great potential for future use.

Up to now, biomass has been recommended to be used in both commercial and domestic heating fields. For instance, a government scheme called ‘Renewable Heat Incentive’ (RHI) has been published by the UK government to encourage households to use biomass heating systems (boilers/ stoves) for the purposes of carbon reduction and sustainable heating. However, there are several issues with small-scale (domestic) biomass boilers that need to be addressed while reducing emissions of nitrogen oxides (NOx) is probably the most challenging issue facing the manufacturer of small-scale biomass boilers. Here, NOx is used to represent the mixture of nitrogen dioxide (NO) and nitric oxide (NO_2). Ideally, biomass combustion should only generate carbon dioxide (CO_2) and water as the final products under complete combustion conditions. However, in reality, biomass combustion always produces various pollutants such as NOx and unburnt hydrocarbons as well as carbon monoxide (CO) which not only damage the environment but also affect the health of general public, especially those with existing ailment such as asthma. Therefore, RHI requires that the NOx emission from the qualified small-scale boilers must not exceed 150g/ GJ. Similarly, emissions of other pollutants such as CO are also strictly restricted by the European Standard (EN 303-5:2012).

1.2 Aims and Objectives

The overall aims of this study are to explore the combustion behaviours of various biomass fuels and develop catalytic methods of NOx abatement for the potential use in small-scale biomass boilers. The objectives are：

1. To investigate the combustion behaviours of some typical biomass fuels (wood, straw, miscanthus, peanut shell and torrefied wood) under conventional air and different ratios of oxygen-rich atmospheres.
2. To characterise a small-scale domestic biomass boiler (the Ashwell 50kW biomass boiler), in terms of gaseous composition and temperature distribution in the combustion chamber.
3. To test the performance of NOx reduction by HC-SCR and catalytic NOx-CO reactions (after-combustion treatments) with the help of suitable catalysts under the conditions of simulated flue gas.

1.3 Thesis Layout

The schematic of thesis layout is shown in Figure 1.1, which indicates the relationship between individual chapters. The brief introduction of each of the seven chapters is presented below.

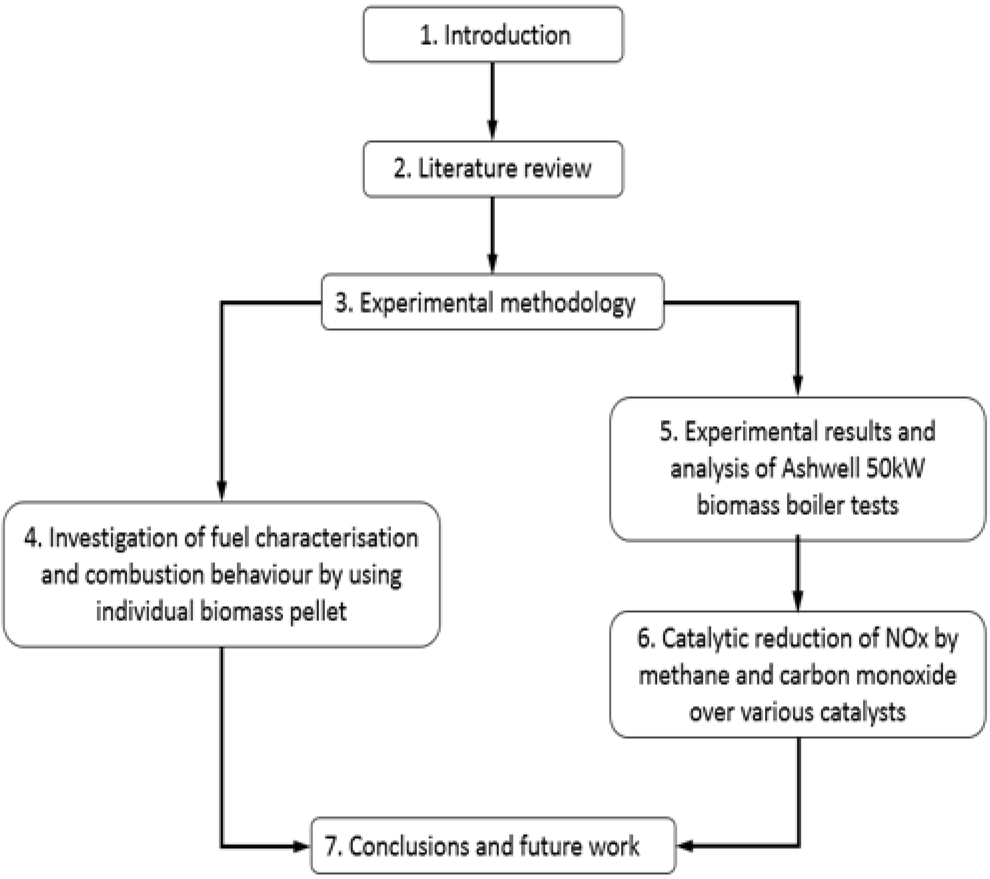

Figure 1.1: Schematic of thesis layout

Chapter 1 describes the general background of this PhD research, research aims and objectives and thesis layout.

Chapter 2 reviews literature on the biomass fuels, mechanism of biomass combustion, formation of major greenhouse gas (CO_2), pollutants (NOx, CO and hydrocarbons) and their control methods, Selective Catalytic Reduction (SCR) technology, especially hydrocarbon (HC)-SCR and corresponding catalysts and supports. Moreover, the latest cases of catalytic emission reduction in small-scale combustion systems are reviewed.

Chapter 3 includes the description of experimental set-ups used in Chapter 4-6. The experimental conditions of each set of experiments are described. The experimental uncertainties are also discussed in this chapter.

Chapter 4 focuses on the experimental results of individual biomass pellet combustion. Five biomass fuels (wood, straw, miscanthus, peanut shell and torrefied wood) are selected and characterised. The experimental findings of different atmospheres (air and oxy-fuel) and background temperatures on combustion behaviours of these fuels are presented and discussed.

Chapter 5 reports the experimental results of small-scale biomass boiler tests under different primary and secondary air setting conditions. The NOx and CO emissions of the boiler are investigated. The temperature distribution and several main gas components (CH_4, CO and O_2) in the combustion chamber are measured and discussed for the potential catalytic experiments in Chapter 6.

Chapter 6 presents the experimental results of CH_4-SCR tests over cobalt supporting catalysts (Co-ZSM-5 and Co-ZSM-5/SiC foam) and catalytic NOx-CO reactions over iron supporting catalyst (Fe-ZSM-5/SiC foam). The catalysts with various parameters are used to investigate the catalytic performance of NOx reduction under different simulated flue gas conditions.

Chapter 7 summarises the main findings and conclusions achieved from this research. Future work has been recommended at the end of this chapter.

CHAPTER 2. LITERATURE REVIEW

2.1 Biomass

2.1.1 Definition of Biomass

Biomass is a renewable, carbon-neutral energy source, extensively available and progressively used as an alternative source to fossil fuel for power and heat purposes. According to Higman and Burgt (2003), biomass can be defined as the materials which are formed naturally and collected from living plants or other organisms. This kind of raw material can be directly used as feedstock to generate energy. It should be noted that conventional fossil fuels are not in this group though they appear to fit the above definition as well. Fossil fuels are believed to be derived from animals or plants that were buried in the ground for millions of years. Also, there are overlapping portions between the classification of waste and biomass, which is less important to discuss further. From the chemical angle, the term 'biomass' means carbon-based and made up of a mixture of organic molecules, including oxygen, nitrogen, hydrogen and other atoms such as heavy metals, alkali and alkaline earth (Forestry.gov.uk, 2016).

2.1.2 Classification of Solid Biomass Materials

Solid biomass covers a wide range of materials, including trees, energy crops, agricultural and industrial waste etc. Some examples of biomass sources can be seen in Figure 2.1. Various classifications of solid biomass materials can be found based on different characteristics. In this study, two main classifications are introduced based on their original types and nitrogen contents. In terms of original types, solid biomass can be classified as three sub-categories, energy crops, natural vegetable growth and organic wastes and residues (see Figure 2.2). Owing to the importance of nitrogen content in combustion, sometimes biomass can also be divided into three board categories based on the nitrogen content (see Table 2.1). Among them, woody biomass normally has the lowest nitrogen content while biomass coming from agricultural and herbaceous has the highest value.

Figure 2.1: Various sources of biomass (Singh and Shukla, 2014)

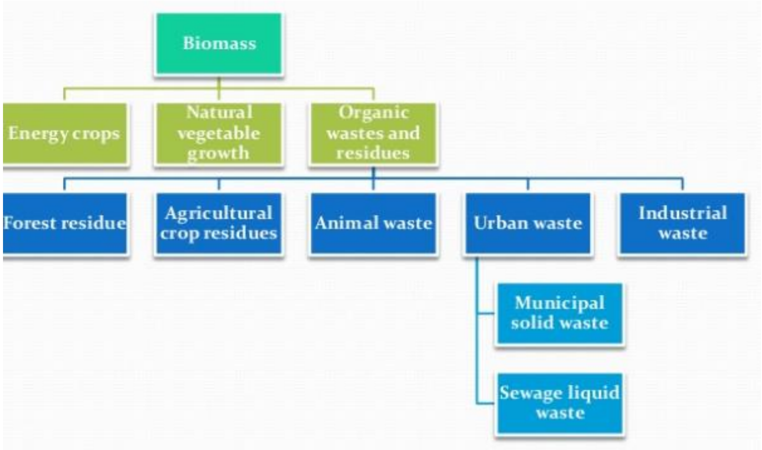

Figure 2.2: Classification of biomass materials based on original types (Singh and Shukla, 2014)

In addition to nitrogen (N) content, comparing with woody biomass, agricultural and herbaceous types normally contain higher ash content, sulfur (S) and chlorine (Cl), but less hydrogen (H) and carbon (C) (Fournel et al., 2015). These elements all have effects on the combustion process and/or performance. For instance, high ash content has an impact on particulate matter (PM) emission and combustion process such as slag formation which may further reduce boiler efficiency. Hydrogen and carbon contents affect the heating value of the fuel (Tissari et al., 2008; Werther et al., 2000).

Table 2.1: Classification of biomass fuels based on nitrogen content (Hustad, Skreiberg and Sønju, 1995)

Class	Type	Nitrogen content (w%, d.a.f)
1	Woodlike	<0.3
2	Strawlike	0.3~1.0
3	N-rich (agricultural & herbaceous)	>1

2.1.3 Forms of Solid Biomass Materials

Solid biomass materials have a variety of forms, including traditional forms such as straws and logs and processed forms such as pellets, chips and particles (see Figure 2.3). The processed forms of biomass follow the standards concerning moisture content, ash and nitrogen content. In the pelletizing process, tiny particles of the biomass are compressed under heated steam. Sometimes binder is also necessary to be added into pellets (Nati, Spinelli and Fabbri, 2010; Ståhl et al., 2004). In recent years, the trend is to use pellets instead of traditional forms because they are more suitable for small-scale boilers and easier to transport and store. More importantly, biomass materials in pellet form have higher combustion efficiency and lower pollutant emissions when comparing with other forms of biomass under the same/ similar combustion conditions (Duan et al., 2014). For example, Fournel et al. (2015) showed that the emitted PM emission was 22-52% less when changing the fuel type from uncompressed biomass to pelletised ones.

Figure 2.3: Different forms of solid biomass materials: a: logs; b: chips; c: pellets; d: particles (pulverized)

2.1.4 Health and Environmental Effects of Pollutants

With the increasing use of biomass, especially in combustion filed, more attention is now paid to the health and environmental effects of pollutants generated from the use of biomass. According to the report from World Health Organization, over 3 billion people in the world are affected by various emissions from biomass fuels, resulting in more than 4 million deaths per year

(WHO, 2016). NOx, CO, and unburnt hydrocarbon are the main pollutions and their health and environmental effects have to be considered, showing below (see Table 2.2).

Table 2.2: Health and environmental effects of NOx, CO, PM and unburned hydrocarbon (Air Pollution in the UK 2016, 2017)

Pollutant	Health Effects	Environmental Effects
Nitrogen Oxides **(NOx)**	Short-term exposure to concentrations of NOx (NO_2) higher than 200 µg m^{-3} can cause inflammation of the airways.	NOX contributes to the formation of secondary nitrate particles in the atmosphere. High levels of NOx can harm plants. NOx also contributes to eutrophication of terrestrial and aquatic ecosystems, damaging habitats and leading to biodiversity loss.
Carbon Monoxide **(CO)**	CO affects the ability of the blood to take up oxygen from the lungs and can lead to a range of symptoms.	CO contributes to the formation of ground-level ozone.
Particulate Matter (PM)	Fine particulate matter is linked with a range of health outcomes including respiratory and cardiovascular effects.	Black carbon in PM is implicated in climate change.
Unburned hydrocarbon	Hydrocarbon vapours can cause health effects. Inhaling formaldehyde can cause irritation. It is a major contributor to eye and respiratory irritation caused by photochemical smog.	Incomplete combustion of hydrocarbons also results in carbon monoxide pollution, then generating indirect effects on the environment

2.2 Policy and Regulation

In recent years, concern about air quality has received more attention. It is all agreed that the air quality is a global issue because the pollutants released in one city or country may contribute to or result in poor air quality elsewhere. Many countries have published related policies and strategies to control and improve air quality. Specifically, although each country or region has different standards for the use of boiler with solid biomass fuel, there is a uniform standard in Europe. In 2012, a new edition of the standard was released, called 'Heating boiler for solid fuels, manually and automatically stokes, nominal heat output of up to 500kW terminology, requirements, testing and marking' (EN 303-5; 2012). In this version of standard, specification of heating boiler, for example, minimum heating efficiency, exhaust gas temperature and exhausting emissions are specified. Some safety requirements are also in the new standard such as adequate air intake, pressure or electricity. All the required performance standards should be met when the boiler operation is at its nominal heat output.

Regarding the emission standard, emissions of carbon monoxide (CO), volatile hydrocarbons (OGC) and particles are standardized from Class 3 to 5 according to the way of manufacture and nominal output, which are shown in Table 2.3. For all the boilers belonging to Class 1 or 2, since they do not meet the new standard in terms of emission requirements in the European market, they are not allowed to be sold anymore and hence not included in the table below as a result.

Table 2.3: Threshold values for emissions on the operation of boilers (EN 303-5:2012)

	Nominal output	CO			OGC			Particles		
	(kW)	(mg/m^3 @ 10% O_2)								
		Class			Class			Class		
		3	4	5	3	4	5	3	4	5
Manual	≤ 50	5000	1200	700	150	50	30	150	75	60
	>50 ≤ 150	2500			100					
	>150 ≤ 500	1200			100					
Automatic	≤ 50	3000	1000	500	100	30	20	150	60	40
	>50 ≤ 150	2500			80					
	>150 ≤ 500	1200			80					

For the emission limit of nitrogen oxide (NOx), it was standardized and mentioned in the EU Ecolabel water-based heaters Commission Decision (2014/314/EU). With this standard, the nitrogen oxide concentration in the exhaust gas for solid fuel heaters should not exceed the limit value (150mg/ Nm^3 at 10% O_2). Here, NOx value is the sum of nitrogen dioxide (NO) and nitrogen monoxide (NO_2).

Also, in the UK, one scheme called Renewable Heat Incentive (RHI) was published by the UK government in March 2016. The market was encouraged to increase the proportion of heat generated from renewable sources. In the scheme, it said the emissions from the RHI-qualifying domestic biomass boiler must not exceed 150g/GJ for NOx and 30g/GJ for PM.

2.3 Mechanism of Biomass Combustion

In general, the combustion process of any fuel is an exothermic process. In the case of biomass combustion, it is a process through burning organic materials.

Now combustion is the most mature technology to convert fuels into energy and the conversion efficiency could be over 90%. The whole biomass combustion process is a sequence of chemical reactions and significantly affected by many different factors and conditions. Generally, three main stages can be identified in the evolution of fuel in the combustion process as shown in Figure 2.4: I) pre-heating process to make the moisture evaporate and devolatilisation process to produce volatiles and char, II) volatile combustion, III) char combustion (Calvo et al. 2014).

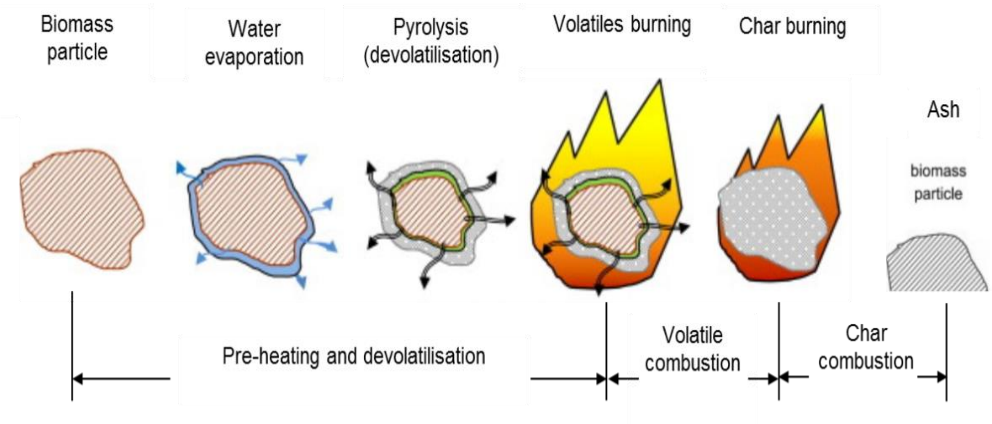

Figure 2.4: Flow chart of combustion process

The main reactions involved in biomass combustion can be represented by equations 2.1 to 2.6. The time spent on for each stage depends on the particle size and properties of fuel, combustion conditions and combustion temperature while other details of each stage will be further discussed in the following parts.

$$\text{Wet Biomass} \rightarrow \text{heating up/ drying} \rightarrow \text{dry biomass} \qquad [2.1]$$

$$\text{Biomass} \rightarrow \text{volatiles (tars and gases)} + \text{char} \qquad [2.2]$$

$$\text{Volatiles} + O_2 \rightarrow CO + CO_2 + (\text{PAH} + \text{unburned hydrocarbons}) \quad [2.3]$$

$$\text{Char} + O_2 \rightarrow CO + CO_2 \quad [2.4]$$

$$\text{Volatiles } (N, S, K, \text{etc}) \rightarrow N, S, K \text{ based pollutants} \quad [2.5]$$

$$\text{Char } (N, S, K, \text{etc}) \rightarrow N, S, K \text{ based pollutants} \quad [2.6]$$

I) Pre-heating

Pre-heating process consists of the evaporation of moisture contained in the biomass material. It should be mentioned that moisture content plays an important role in the biomass combustion process. The amount of heat required in this stage depends on the moisture content of biomass material while the necessary heat is commonly from other stages of combustion process. That means the higher moisture content, the more heat loss during combustion system. The direct result is that the conversion rate from biomass to heat goes down because the combustion chamber temperature becomes lower. Therefore, the biomass with less than 10% moisture is suggested to be high quality fuel for combustion (Mishra and Mohanty, 2018). Hamelinck et al. (2004) pointed out that the preheating and drying processes finish completely when the temperature reaches 150°C.

Devolatilization

Devolatilization, which is also called as thermal pyrolysis, takes place at the beginning of solid biomass combustion. To activate the devolatilization process, the start temperature should be around from 160°C to 250°C (Williams et al., 2012). During devolatilization process, different forms of products (solid, liquid and gaseous yields) are produced. The composition and amount of each yield are affected by biomass (fuel) type, heating rate, final temperature and other factors. The solid fraction which is called ‘char’ includes a high carbon content fraction and some inert materials. The liquid fraction is also named as ‘tars’.

II) Volatile combustion

Volatile combustion dominates the biomass combustion process. Comparing with coal, the volatile content of biomass normally accounts for a larger portion (around 70%) of the total heat of combustion. Also, this process is responsible for many harmful emissions including PAH, soot, VOC and tars. CO, CO_2, H_2, hydrocarbon(s) and other vapours are generated in this process.

III) Char combustion

Char only represents around 10% to 30% of total weight of biomass, depending on the biomass fuel itself and the combustion conditions. Char combustion is less important than volatile combustion in terms of heat generation and combustion efficiency. However, this process can generate significant amount of pollutants especially nitrogen oxides and other inorganic species (Williams et al., 2012).

2.4 Carbon Dioxide Control

In conventional air combustion, carbon dioxide (CO_2) is always one of the final products. Although CO_2 is not treated as harmful emission, it is the major component of greenhouse gas emissions (GHG) and contributes to greenhouse effect. From Figure 2.5 and 2.6, it can be found that CO_2 generated from energy accounts for a significant share of the total GHG emissions, whether in Europe or around the world. Hence, more attention should be paid to control the CO_2 emission in order to combat climate change.

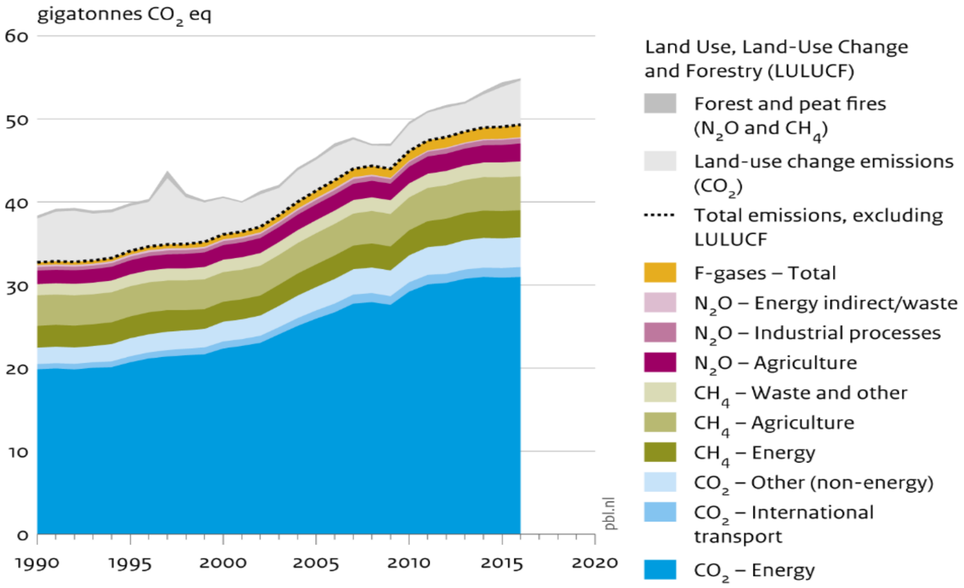

Figure 2.5: Trends in global greenhouse gas emissions from 1990 to 2015

Source: EDGAR 4.3.2 (EC-JRC/PBL 2017)

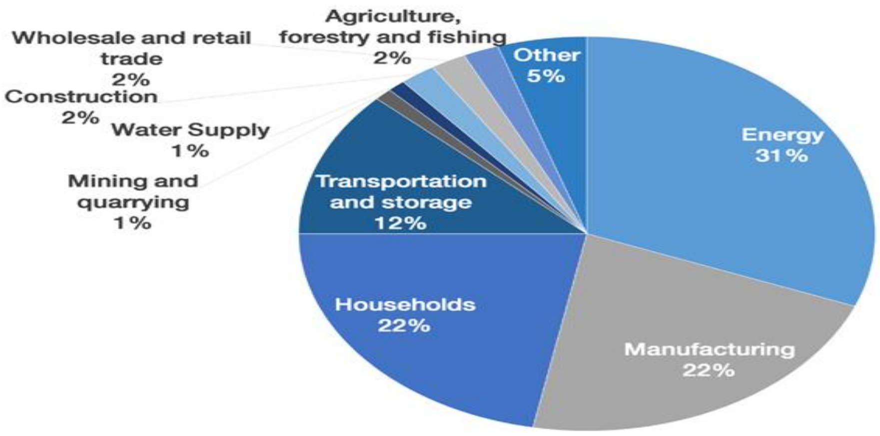

Figure 2.6: Sources of CO_2 generated in European

Source: World Economic Forum (2019)

2.4.1 Carbon Capture and Storage (CCS)

Carbon capture and storage (CCS), a promising and effective CO_2 approach, includes the separation of CO_2 from energy utilization processes such as thermal power industry, transportation of the captured CO_2 to a storage site and isolation from the atmosphere for long term purposes (Wennersten, Sun and Li, 2015). Until now, several CCS approaches have been developed to deal with CO_2 emissions. Generally, these approaches can be divided into three groups (see Figure 2.7, Rackley, 2017) with each being briefly discussed below:

a. Capture by modifying the process: generate a pure or relatively pure CO_2 stream by separating from a current process or generating a by-pass process to produce the CO_2 stream.

b. Post-process capture: separate CO_2 to obtain a pure or relatively pure CO_2 stream from the exhaust gas of industrial process.

c. Direct capture: directly capture CO_2 from atmospheric air or capture CO_2 to a chemical end product.

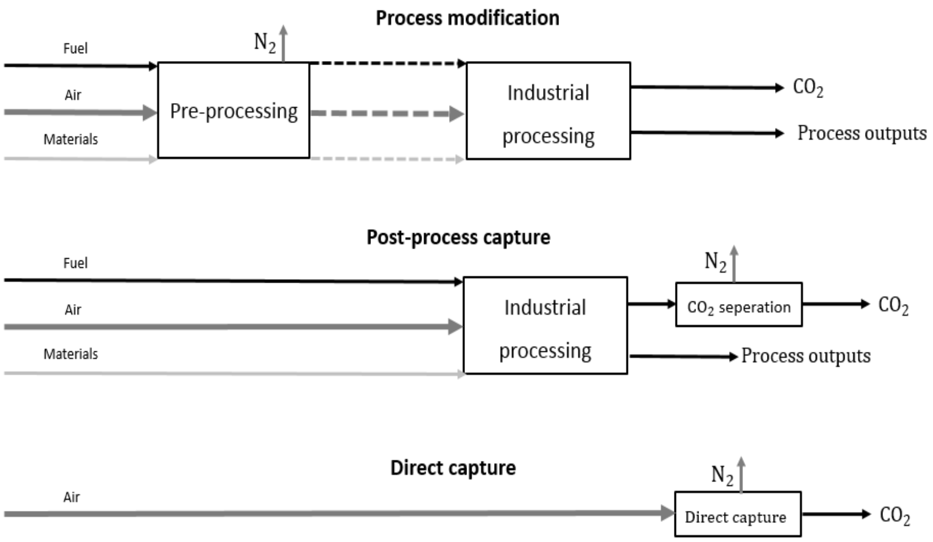

Figure 2.7: Main approaches of CO_2 capture

2.4.2 Oxy-fuel Combustion

Oxy-fuel combustion, one of the process modification approaches, has been widely studied for power plants as it has potential not only to effectively control CO_2 emission, but also to generate ‘negative’ CO_2 emission in some cases. In traditional air combustion, the N_2 coming from air still exists in exhaust gas and dilutes the concentration of generated CO_2. Although the CO_2 can be separated from exhaust gas by using some chemical methods (post-process capture) such as amine stripping, this would incur additional process steps and cost (Singh et al., 2003). In oxy-fuel combustion, O_2 is separated from air prior to combustion (ideally pure O_2, but typically of greater than 95% purity). Then it mixes with the recycled exhaust gas consisting mainly of CO_2 and water vapour used for combustion process. With the absence of N_2, enriched CO_2 (more than 95% of the total) can be found in the final product of exhaust gas, producing a more concentrated CO_2 stream for easier purification and capture.

However, compared with traditional air combustion, replacing the high content with CO_2 in oxy-fuel combustion can change the combustion behavior of solid fuel significantly. Some properties of CO_2 such as heat capacity, thermal conductivity or diffusivity can have a significant effect on ignition properties, flame features, burning time and gaseous emissions when the combustion is under oxy-fuel atmosphere (Buhre et al. 2005; Heuer et al., 2016). Hence, it is necessary to study and understand the influence of oxy-fuel combustion conditions on solid fuel combustion.

Research on oxy-fuel combustion has started since the technology was first proposed in 1981. Until now, the combustion behavior of different kinds of coal under oxy-fuel conditions has been widely investigated. For example, Kim, Li and Jeon (2014) studied the combustion performance of pulverized coal particles with different sizes, which mainly focused on the ignition step by using a flat flame burner and technology of high speed image capture. They found that the homogeneous-heterogeneous ignition of tested coals was affected by the coal ranks and particle sizes under oxy-fuel environment. Similarly, the ignition behaviour was also researched by Riaza et al. (2017) later. They observed that there was a clear sequential step under air combustion conditions while it was different under oxy-fuel conditions due to the existence of CO_2 and concentration of oxygen. The trend was to be heterogeneous under 21% O_2 and turning to be more homogeneous under 40% O_2 atmosphere. Results from the study of Rathnam et al. (2009) showed that some pulverised coal samples had obvious improvement in terms of burnout time under oxy-fuel conditions while some of them showed similar performance compared with air combustion.

Compared with coal, biomass has different characteristics due to its chemical properties. For oxy-fuel combustion, biomass also shows large difference in many parameters, for example, ignition properties, burning time of volatile or char. Riaza et al. (2014) tested four types of biomass particles (olive residue, torrefied pine sawdust, pine sawdust and sugarcane bagasse) in a lab-scale drop tube furnace. Their tests were carried out under air and different ratios of oxy-fuel conditions, including 21%, 30%, 35% and 50% of dry oxygen contents. High-magnification cinematography images were captured during the experiment. They pointed out that combustion intensity under normal air condition (21% O_2- 79% N_2) was stronger than that in oxy-fuel combustion with the same oxygen concentration in CO_2 (21% O_2- 79% CO_2). The combustion intensity was enhanced when the oxygen concentration in the O_2- CO_2 mixture was increased under oxy-fuel conditions. Both the burnout times of volatiles and chars decreased with the increasing oxygen concentration in O_2- CO_2 mixture. From the literatures above, it can be found that most of the research is related to the coal/ biomass experiments with particle size. Therefore, the research gap is found and the investigation of oxy-fuel combustion of biomass pellets should be further tested in this research.

2.5 Pollutant Formation and Control Methods

Apart from the inevitable CO_2 emissions mentioned above, biomass combustion still generates other harmful emissions such as NOx, CO, hydrocarbons and PM, especially under incomplete combustion conditions. It can be seen from Figure 2.5 that the CO generated from residential combustion and NOx from industrial combustion still account for large proportions of the global emissions. Therefore, it is necessary to study the formation mechanisms of these pollutants and analyze the reduction technologies that can be used in biomass combustion processes. It should be mentioned that although PM could cause some harmful environmental issues, the formation and control methods of PM will not be discussed in this research.

2.5.1 Carbon Monoxide Formation and Control Methods

Carbon monoxide (CO) is colourless and tasteless gas which is also a noncorrosive gaseous material (Kuo, 2005). Most of CO is emitted due to insufficient oxygen in incomplete combustion happened in combustion devices used in households, transport and industry. Evidently, in order to control the emission of CO, the simplest method without extra cost is to provide enough oxygen/air and enhance the mixing between supplied oxygen/air and fuel to reduce the extent of incomplete combustion, which means to produce CO_2 as the combustion product, instead of CO.

2.5.2 Hydrocarbon Formation and Control Methods

The term ‘unburned hydrocarbons’ is defined as the all species detected by the analyzer model 880A and they can be divided into two types, light hydrocarbons such as methane and higher hydrocarbon such as propene, propyne, propane (Soares Neto et al., 2009). Total unburned hydrocarbons, also called THC, are the emission products from incomplete combustion. Since most of combustion in small-scale domestic biomass cannot achieve 'complete' combustion, some unburned hydrocarbons are always emitted by these biomass boilers.

Rabaçal, Fernandes and Costa (2013) reported that the unburned hydrocarbon emissions were significantly affected by boiler operating conditions, especially the way of ignition. Also, they found that the higher thermal input, the more THC emissions were generated when their three different kinds of biomass fuel pellets (pine, peach stones and industrial wood wastes) were burnt in a domestic boiler. Similarly, Vicente et al. (2015) claimed that the initial stage was a critical step because the devolatilisation process generated high concentration of THC in a short period. Methane (CH_4) as the typical type of hydrocarbon in THC has been also studied. Nasir Uddin, Daud and Abbas (2013) reported that there was up to 20% of hydrocarbons in dry exhaust compositions, mainly including CH_4, C_2H_4 and C_2H_6 by testing different kinds of biomass materials (pine sawdust, legume straw and tobacco stalk). Among these hydrocarbons, CH_4 kept the largest percentages when comparing with other higher hydrocarbons. Furthermore, Calvo et al. (2011) found that the trend of CH_4 emission profile was generally similar to that of the CO when they used log-size hardwood and softwood in two different boilers (fireplaces and wood stoves), which agreed with the viewpoint of Rabaçal, Fernandes and Costa (2013). Amorim et al. (2013) proposed that the amounts of CH_4 and CO were mainly determined by the biomass type among all the variables in biomass combustion. Both CH_4 and CO emissions were found to be lower when solid biomass with smaller particle size was burnt.

The cost-effective way to control CH_4 and CO emissions is to improve the combustion process and use biomass fuel with optimized particle size. Combined with the introduction of solid biomass forms in section 2.1.3, the combustion applications with biomass pellets look an encouraging method to achieve the low CH_4 and CO emissions.

2.5.3 NOx Formation and Control Methods

Nitrogen oxides can be generated by any fuel combustion process, whether fossil or biomass fuels. NOx is one of the main precursors for the formation of photochemical smog and acid rain. Since the RHI policy has been introduced in the UK, NOx emissions of domestic biomass boilers have received a lot of attention. Compared with coal, biomass fuels have much lower nitrogen content. However, it is interesting that the combustion of biomass fuels releases much more NOx than other fossil fuels such as natural gas, and hence NOx emissions from biomass combustion especially in domestic biomass boilers need to be considered and addressed (Verma et al., 2011).

2.5.1.1 NOx Formation

The NOx generated from boilers or engines is usually made up of a mixture of around 95% NO and 5% NO_2 (Roy, Hegde and Madras, 2009). Although the amount of NO_2 is far less than NO, the toxicity level of NO_2 is much higher than that of NO, around five times (Last, Sun and Witschi, 1994). This is to say, attention should be paid to both NO and NO_2 due to their harmful effects.

In general, NOx is mainly formed through three routes, which are thermal-NOx, fuel-NOx and prompt-NOx. Thermal-NOx is formed typically when the combustion temperature is over 1200℃. Fuel-NOx is produced due to the nitrogen content from biomass fuel. Prompt-NOx is generated in the flame region through the reactions of hydrocarbons and molecular air nitrogen (Baukal, 2005). Further details of each NOx formation mechanism are given below:

i) Prompt-NOx

Prompt-NOx was termed by Fenimore in 1970. Also, he found that some NOx was generated in the flame zone preferentially before they had enough time to produce NOx via thermal-NOx route. It is well accepted that prompt-NOx is formed mainly due to the primary reaction between CH and N_2, which is shown below:

$$\mathrm{CH} + \mathrm{N_2} \leftrightarrow \mathrm{HCN} + \mathrm{N} \qquad [2.7]$$

In general, the NO mechanism which based on the theory of Fenimore published in 1971 is that the hydrocarbon radicals such as CH or CN_2 reacts with molecular nitrogen to form hydrocyanic acid or amines. After that, the products would be reacted further to generate NOx. The main relevant reactions include the following:

$$\mathrm{CH_2} + \mathrm{N_2} \leftrightarrow \mathrm{HCN} + \mathrm{NH} \qquad [2.8]$$

$$CH_2 + N_2 \leftrightarrow H_2CN + N \qquad [2.9]$$

$$C + N_2 \leftrightarrow CN + N \qquad [2.10]$$

Until now, the mechanism of prompt-NOx formation has not been fully understood. Since the proportion of prompt-NOx only accounts for a small percentage in total NOx emissions of domestic biomass combustion boilers, the mechanism will not be further discussed in this study.

ii) Fuel-NOx

Fuel-NOx plays a vital role in the NOx formation of a solid fuel combustion process because the conversion rate from fuel-N to fuel-NOx can be over 80%. Also, the contribution of fuel-NOx in biomass combustion is much higher than that in coal combustion since the reaction temperature of biomass combustion is not as high as that of coal combustion, which reduces the amount of thermal-NOx (Houshfar et al. 2012). More importantly, it seems that the fuel-NOx is not primarily affected by specific boiler operating conditions (Rabaçal, Fernandes and Costa, 2013). Although it is well known that the NOx emission increases with the nitrogen content of the biomass, the correlation between NOx emissions and fuel-N content is not linear. In fact, the conversion rate from fuel nitrogen content to NOx emissions shows a downward trend when nitrogen content increases (Carroll et al., 2015).

iii) Thermal-NOx

In fuel combustion with an oxidizer containing N_2 such as air, NO is formed mainly based on the Zeldovich mechanism which can be described by the following three reactions.

$$\mathrm{O + N_2 \leftrightarrow NO + N} \qquad [2.10]$$

$$\mathrm{N + O_2 \leftrightarrow NO + O} \qquad [2.11]$$

$$\mathrm{N + OH \leftrightarrow NO + N} \qquad [2.12]$$

The formation of thermal-NOx is strongly affected by combustion temperature. As mentioned before, the active temperature of thermal-NOx is over 1200℃ while the normal combustion temperature in small-scale biomass boilers is under this value. Therefore, the formation of thermal-NOx in small-scale biomass boilers is pretty insignificant in most of the cases. (Nussbaumer, 2003; Johansson et al., 2004).

2.5.1.2 Control technologies

Reducing NOx emissions can be achieved by either primary or secondary strategies (see Figure 2.8). The primary strategies are to modify and improve the biomass combustion process to generate less harmful emissions while the secondary strategies are to achieve low emissions by controlling and reducing the NOx emissions after the combustion process (Carroll et al., 2015). The commonly used primary strategies include flue gas recirculation, staged combustion (air or fuel staging), low NOx burner. Secondary strategies for NOx emissions control mainly include absorption, Non-Catalytic Reduction (SNCR) and Selective Catalytic Reduction (SCR). A brief of NOx control strategies is presented below.

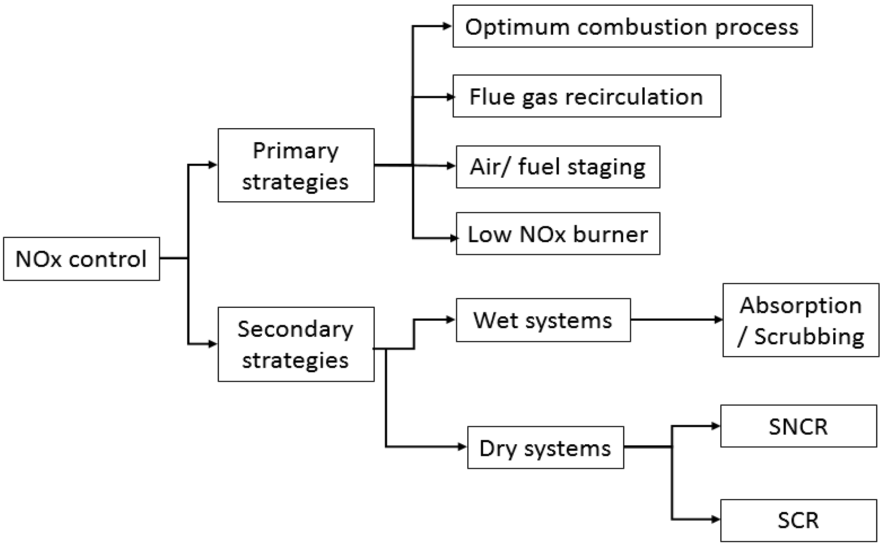

Figure 2.8: Main NOx control methods

(i) Flue gas recirculation

Flue gas recirculation is one of the most mature methods to reduce NOx emission. It is achieved by recycling a part of exhausting gas from chimney to the combustion chamber. The temperature of flame region can be reduced by mixing the recirculated flue gas with combustion air. Also, the residence time of recirculated flue gas is increased by passing combustion chamber for the second time. As a result, thermal NOx can be decreased due to the lower combustion temperature (Chen et al., 2015). Although the method of flue gas recirculation could be used in the existing biomass boilers with low cost, the efficiency of flue gas recirculation using in biomass combustion system is not as high as that in oil or natural gas combustion system (Houshfar et al. 2012). Also, it is not widely applied in small-scale biomass combustion systems when taking the relatively low combustion temperature into account.

(ii) Air staging

The idea of air staging is to control NOx generation by reducing the air supplying into the primary combustion zone but keeping the total amount of air inlet constant. Under air staging conditions, the intermediates such as HCN and NH_i (i=0,1,2,3) generating from fuel-N would react and form harmless N_2 (for example reaction 2.13) in the primary combustion zone where air/oxygen is below the stoichiometric value. Otherwise, fuel-N intermediates would likely be oxidized into NOx in a traditional combustion process.

$$NO + NH_2 \leftrightarrow N_2 + H_2O \qquad [2.13]$$

When discussing the technology of air staging, the term 'excess air ratio' should be fully explained. Excess air ratio is a ratio between the amount of air actually adding to the combustion chamber and the amount of air needed for complete combustion theoretically. If the excess air ratio below 1, incomplete combustion would take place and there would be part of fuel being wasted and high emissions of CO and unburnt hydrocarbons etc. On the other hand, if the excess air ratio is well over 1, it would cool the combustion chamber down and cause additional thermal loss. The most significant advantage of air staging combustion is that it can create a fuel-rich zone when using a lower primary air ratio (< 1) in primary combustion zone. After that, the secondary air is then introduced into the combustion chamber to achieve an overall air-rich atmosphere in order to make sure that the fuel is completely burnt (Munir, Nimmo and Gibbs, 2011). Houshfar et al. (2011) found that the optimal total excess air ratio should be around 1.5. A higher or lower value would cause an increase in NOx emission. Moreover, it proved by Brunner et al. (2009) that if the total injected air volume is kept in constant, reducing the amount of primary air is useful to control the temperature of combustion chamber to operate in optimal condition. Meanwhile, secondary combustion air injection may also reduce NOx emissions because it can create a favourable condition for better mixing and higher turbulence.

Air staging is a popular technology applied in medium and small-scale biomass boilers so far. It has been proved that the combustion with air staging is more effective to achieve low NOx reduction compared with conventional combustion (Buchmayr et al., 2015; Liu et al., 2013; Khodaei et al., 2016; Qiu, 2013). In general, air staging is to introduce the air into the combustion boiler at two different positions and separate the combustion into two zones, as shown in Figure 2.9. When applying the method of air staging, a total excess air ratio between 1.1 and 1.8 is used in large-scale applications and 1.5 to 2.0 in small-scale applications would create optimal combustion. So far, small-scale biomass combustion with air staging has been tested by many researchers and NOx reduction efficiency can be achieved up to 90% (Caposciutti and Antonelli, 2018; Houshfar et al., 2012; Li et al., 2019; Nussbaumer, 2003).

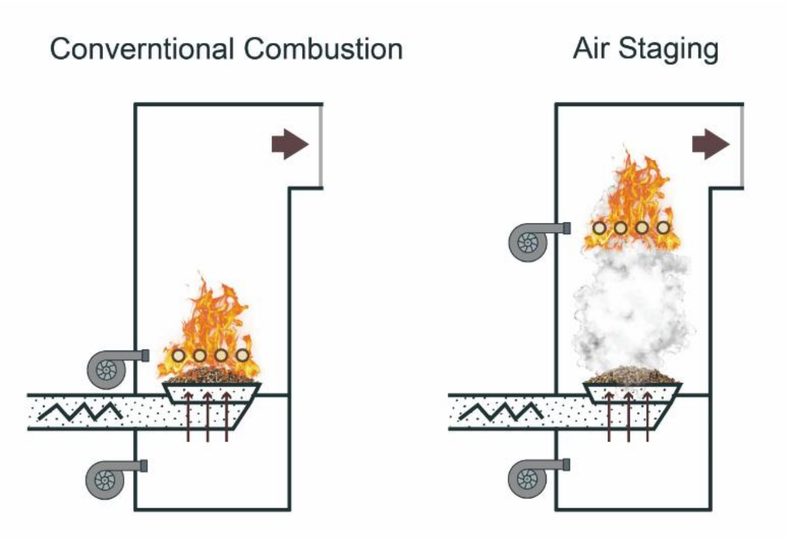

Figure 2.9: Diagram of the difference between conventional combustion and combustion with air staging

(iii) Fuel staging

Fuel staging, also called reburning technology, is another method of primary NOx strategies. Similar to air staging, a small proportion of fuel (typically 10 to 20% of the total) is introduced to the position above primary combustion zone, generating a secondary combustion zone with fuel-rich environment. That step can effectively reduce NOx formation which mainly happens in primary combustion zone through decomposition (Hodžić, Kazagić and Smajević, 2016). Some advanced methods are used to combine some new additives (e.g. Fe) with fuel staging to achieve better performance for NOx removal.

(iv) Additive

When the biomass market is getting larger, woody biomass has been far from meeting market demand, more and more non-woody biomass has been studied and tested. The results show that non-woody biomass such as agricultural kinds (straws, crops, miscanthus) normally have higher content of potassium (K), sulfur (S), chlorine (Cl) and ash contents when comparing with woody biomass. The problem is that the high concentration of these alkali metals could form harmful compounds which have relatively low melting temperature and cause some operational problems such as fouling and slagging. Furthermore, high amount of inorganic elements would also increase the emission of fly ash, NOx and particulate matter. It should be mentioned that potassium and chlorine are the main elements to cause these problems (Nussbaumer, 2003). The fly ash is mainly from potassium compounds such as potassium chlorides (KCl), potassium sulfates (K_2SO_4). Meanwhile, a high concentration of chlorine would promote the process of volatile alkali metal chlorides and release of alkali metals (Olsson, Jaglig and Pettersson, 1997).

Using additives is a potential method to eliminate these harmful effects and reduce the emissions of NOx and particulate matter as well. In simple terms, the mechanism of using additives is to bind potassium to potassium-aluminum silicates which have relatively stable and large particles with high melting temperatures while keeping chlorine in gas phase then emitting with flue gas.

Based on the reactive compounds, additives can be roughly divided into following four categories: (1) Calcium based additives, (2) Phosphorus based additives, (3) Sulphur based additives, (4) Aluminium-silicate based additives (Damoe et al., 2014). Various kinds of additives can be used in different situations to handle specific problems based on the chemical properties of fuel. Among four groups of additives, Aluminium-silicate based additives have been widely studied and have shown great potential to abate NOx and particulate matter emissions during biomass combustion (Carroll and Finnan, 2015; Tissari et al. 2008). The Aluminium-silicate based additives normally include kaolin and clay which are mainly consisted of mineral kaolinite ($Al_2Si_2O_5(OH)_4$ which has the ability to capture alkali metals. The overall reactions are below:

$$Al_2Si_2O_5(OH)_4 + 2KCl \rightarrow 2KAlSiO_4 + H_2O + 2HCl \qquad [2.14]$$

$$Al_2Si_2O_5(OH)_4 + 2KCl + 2SiO_2 \rightarrow 2KAlSi_2O_6 + H_2O + 2HCl \qquad [2.15]$$

Many reports have been published regarding the experiments of adding additive to small-scale biomass combustion processes with different kinds of biomass materials. Boström et al. (2009) reported that a large number of potassium was captured in the bottom ash and NOx emission was significantly reduced when kaolin was added into oat grain before combustion happening. In the same year, Bäfver et al. (2009) used the same fuel to do the similar experiments. The results showed that adding a certain amount of kaolin (2% to 4%) had the optimal conversion performance. More percentage of potassium was found in the bottom ash and chloride was almost eliminated in the fly ash particles while the concentration of HCl rose. Later, Bäfver, Boman and Rönnbäck (2011) found that 3% and 6% wet basis of kaolin had the best performance of particulate matter reduction in the combustion of straw pellets. However, adding excessive kaolin seemed like have no extra effect on the performance.

Now, kaolin and clay as the mature additives have different functions in various conditions. The trend is to use them to reduce sintering and deposit formation in large plants and to reduce NOx and particulate matter emission in small scale applications (Sommersacher et al., 2013).

2.6 Selective Non-catalytic Reduction (SNCR) and Selective Catalytic Reduction (SCR)

In last section, many separated primary technologies have been introduced to control the emission of NOx. From Figure 2.8, there are also some after-treatment (secondary) technologies. So far, Selective Non-catalytic Reduction (SNCR) and Selective Catalytic Reduction (SCR) have been globally studied. The main difference between SNCR and SCR technologies is whether the system uses catalyst or not. Both SNCR and SCR technologies allow the NOx removal reactions happening in oxidizing environment. The purpose of these methods is to convert NOx existing in flue gas to harmless N_2, then directly discharging into atmosphere (Fu et al., 2014). The reason why these techniques are developed is that, in the actual reaction process, the concentration of O_2 in flue gas is much higher than NOx, normally several orders of magnitude higher. Also, O_2 as oxidizing agent is much easier to be oxidized than NOx, which means the oxidation order of O_2 is higher than that of NOx. Owing to SNCR or SCR technology, NOx could be oxidized first due to a suitable reductant, especially in the presence of catalyst(s) (Cheng and Bi, 2014). That is the reason why it called ‘selective’.

⊙ ***Selective Non-catalytic Reduction (SNCR)***

In the SNCR technology, a chemical additive such as ammonia or urea is introduced into system which works as a reductant to mix with flue gas to reduce NOx to N_2 through desired reactions and a catalyst would not be required (Fan et al., 2014). Admittedly, the detailed reactions are pretty complicated since the process includes many free radical reactions (TayyebJaved, Irfan and Gibbs, 2007). The overall reactions of NOx removal are shown below when adding ammonia or urea into the system.

With ammonia:

$$4NO + 4NH_3 + O_2 \rightarrow 4N_2 + 6H_2O \qquad [2.16]$$

$$6NO_2 + 8NH_3 + O_2 \rightarrow 7N_2 + 12H_2O \qquad [2.17]$$

With urea:

$$H_2NCONH_2 + 2NO + \frac{1}{2}O_2 \rightarrow 2N_2 + CO_2 + 2H_2O \qquad [2.18]$$

The most significant advantage of SNCR is that the capital and maintaining cost is relatively low since the process can be conducted without the use of any catalyst. However, the disadvantages are clear as well. The performance of SNCR system is greatly influenced by the operating temperature window. The efficiency of NOx reduction could achieve up to 80% though it can only work in a narrow temperature range, from about 820℃ to 940℃. However, the performance drops dramatically if the operating temperature is outside the optimal range (Bae, Roh and Kim, 2006; Nussbaumer, 2003). Furthermore, many factors such as residence time or mixing could cause worse performance in actual applications.

⊙ ***Selective Catalytic Reduction (SCR)***

The SCR technology is used to convert NOx to N_2 over an ideal catalyst by using suitable reductant(s). Although it has relatively higher capital cost and maintaining cost compared with SNCR, the SCR technology can achieve greater removal performance than SNCR. At the present time, a modern SCR system with good design could achieve over 90% NOx reduction efficiency (Hums, 1998; Nussbaumer, 2003). This technology was firstly applied in the thermal power plant of Japan in the 1960s. With the development of SCR technology, there are a large number of automotive applications existing in the market, for both heavy-duty diesel engines and light-duty diesel vehicles and applications for large-scale coal combustion systems (Sawatmongkhon, 2011). The SCR system can be installed at different locations within the application plant depending on the characteristics of catalysts (Strege et al., 2006).

In the process of SCR, there are two different and competitive paths for reductant to react, which are the selective reaction by NOx and oxygen oxidation reaction. The former path is the positive reaction which expected to take place in SCR system while the latter path is negative. As mentioned before, the suitable reductant and catalyst must be able to promote the former path in order to achieve the purpose of NOx reduction.

So far, many researchers have sought and developed suitable reductants for different SCR technologies. Two interesting reductants (ammonia and hydrogen) are introduced in section 2.6.1 and 2.6.2. The detailed information on SCR with hydrocarbon is presented in section 2.6.3 due to its potential use in this research. The corresponding mechanisms and catalysts of HC-SCR are presented in section 2.6.3.1 and 2.6.3.2.

2.6.1 Selective Catalytic Reduction by Ammonia or Urea (NH_3-SCR)

Ammonia is one of the most effective and common reductants for SCR. The SCR with ammonia is a pretty mature technology and typically used in large-scale stationary applications and thermal power plants (Gawade et al., 2012). However, this technology cannot be popularized because it requires a large number of harmful reductants (ammonia), which could form ammonium salts further and have a noxious effect on human body (Heck, 1999). As a result, SCR with ammonia is unsuitable in automatic vehicles and small scale boilers. To overcome these disadvantages, non-toxic urea instead of ammonia was developed to work within the SCR systems. The combination of SCR and urea is proved to be a promising method since it has high NOx removal efficiency. Urea is an odourless and colourless solid with the chemical formula of its main component of $(NH_2)_2CO$ (Koebel, Elsener and Kleemann, 2000). The related reactions of SCR-urea for NO_x removal as follow:

$$(NH_2)_2CO\ (l) \rightarrow NH_3 + HNCO \qquad [2.19]$$

$$HNCO + H_2O \rightarrow NH_3 + CO_2 \qquad [2.20]$$

$$4NH_3 + 4NO + O_2 \rightarrow 4N_2 + 6H_2O \qquad [2.21]$$

$$4NH_3 + 2NO + 6NO_2 \rightarrow 4N_2 + 6H_2O \qquad [2.22]$$

The first step [2.19] is the thermolysis process, which causes endothermic decomposition while the second step [2.20] is an exothermic hydrolysis reaction, mainly generating ammonia for further reactions. The reactions 2.21 and 2.22 are named as the standard SCR and fast SCR reactions respectively. It should be mentioned that the former reaction $[2.21]$ is the main path for ammonia-SCR while the latter one $[2.22]$ is the secondary path but could accelerate the whole process because of its faster reaction rate. Thus, higher proportion of NO_2 is expected in system to achieve the purpose of efficient SCR reaction. However, there exists another trade-off, which is another reaction (see reaction 2.23) would take place if the amount of NO_2 exceeds the acceptable limit. The reason is that the reaction rate of reaction 2.23 is pretty slow, even slower than the rate of standard SCR reaction.

$$4\mathrm{NH_3} + 3\mathrm{NO_2} \rightarrow 3\frac{1}{2}\mathrm{N_2} + 6\mathrm{H_2O} \qquad [2.23]$$

Due to the reasons stated above, it is necessary to control the amount of injected urea to ensure that the process has the optimal reaction ratio. Either too high or too low ratio of NO_2/ NOx would cut the overall NOx removal efficiency. Also, if the value of urea exceeds the acceptable limit, ammonia slip could happen, which would lead to ammonia emissions to the air. Furthermore, there are also some side reactions which may have negative effects on the performance of ammonia-SCR such as N_2O formation and ammonium nitrate formation (Song, Johnson and Naber, 2014). These have become barriers for the development and practical applications of NH_3-SCR technology.

2.6.2 Selective Catalytic Reduction by Hydrogen (H_2-SCR)

Apart from NH_3-SCR, NOx reduction by SCR with hydrogen (H_2-SCR) is another hot research field. This is mainly due to the fact that hydrogen has proven its existence during combustion process and its concentration is even higher than any hydrocarbon found by many reseachers (Balat and Kırtay, 2010; Tanksale, Beltramini and Lu, 2010). Relevant H_2-SCR technologies have been studied and developed over the past decades. The efficiency of NOx reduction with H_2-SCR technology could reach 95% under low operating temperature conditions with ideal catalyst(s) such as Pt/HZSM-5, Pt/ZSM-35 or Pt/H-FER (Machida and Watanabe, 2004; Yang et al., 2011; Yu et al., 2010; Zhao et al., 2015). H_2-SCR technology has not been experimentally studied in this research due to safety restrictions within university laboratories and hence will not be further discussed in this thesis.

2.6.3 Selective Catalytic Reduction by Hydrocarbon (HC-SCR)

Taking the weakness or concerns of SCR technology with ammonia or H_2 into account, the use of hydrocarbon instead of ammonia or hydrogen as reductant has been considered as a potentially promising alternative NOx removal strategy. The reaction 2.24 describes the generic HC-SCR reaction in the presence of oxygen. The idea of using hydrocarbon in SCR technology was proposed by Iwamoto et al. (1989). Now it becomes a globally popular technology being widely used in mobile applications and stationary sources (Roy, Hegde and Madras, 2009). Since there are unburned hydrocarbons such as methane and/or other higher hydrocarbons existing in exhaust gas of any combustion devices or internal combustion engines, they could be directly used as the reducing agent to improve economic efficiency because the additional reducing agent will not be needed for the SCR system anymore. Meanwhile, hydrocarbons, as one of the pollutants, are also controlled.

$$\mathrm{HC} + \mathrm{NO} + \mathrm{O_2} \rightarrow \mathrm{N_2} + \mathrm{CO_2} + \mathrm{H_2O} \qquad [2.24]$$

2.6.3.1 Catalysts for HC-SCR

The term 'catalyst' is defined by The International Union of Pure and Applied Chemistry (IUPAC) as a substance that improves the reaction rate without altering the overall Gibbs energy change in the reactions. This shows the importance of choosing an appropriate and powerful catalyst.

It is known that the NO molecule is thermodynamically unstable, even at the standard state (1atm and 298K). However, the fact is that even at high-temperature conditions, there is no nitric oxide decomposition that could be observed due to the electronic structure of bond in nitric oxide. Also, since the formation of NO is spin-forbidden and it has a high activation energy (364 kJ/mol), the NO decomposition rate is pretty low (Mrad et al., 2015). Therefore, the use of a catalyst is necessary to reduce the activation energy to promote the decomposition process (Roy, Hegde and Madras, 2009).

A large number of catalysts have been discovered and tested for SCR technology with various hydrocarbon(s) in terms of durability, activity and stability. These catalysts can be stratified into three categories, metal ion-exchanged zeolites, metal oxide-based catalysts and supported precious metals (see Table 2.4).

Among these three categories, zeolite supporting metal ion-exchanged catalysts are the most studied and developed group. In a HC-SCR system, zeolite could work as carrier due to its characteristics such as narrow pores, ion exchangeability and internal channel structure. Ion-exchanged zeolite catalysts represent high performance on NOx removal with hydrocarbons when there is excess oxygen in flue gas while the performance does not rely on the properties of reductant. Also, some zeolites have shown advanced activity in terms of storage capacity of hydrocarbons, comparing with silica or other traditional supports (Pérez-Ramírez et al., 2000). More importantly, ion-exchanged zeolite catalysts have a much wider working temperature range when comparing with other groups of catalysts.

Table 2.4: Summary of current catalysts for HC-SCR (Kim and Nam, 2001; Mrad et al., 2015; Xu et al., 2020)

(1) Bare zeolites: MFI, MOR, FER, FAU, CLI

(2) Metal ion-exchanged zeolites:

MFI with Cu, Fe, Co, Ce, Ga, Ag, Na, Zn, Ni, Mn, Mg, Mo, V, Cr, Ca, La, Pr, Nd, Ln, In, Ir, Pb, Pt, Rh, Ru and Pd

MOR with Cu, Fe, Co, Pt, Rh, Ru, Pd, Ti, W, Mo, Ce, Mg, Zr; Sn, Na, V, Cr, Ni, Zn, Ca, Ga, Sr, Ba and La

FER with Cu, Fe, Co, Cr, V, Zn, Pt, Pd, Mn and Ni

LTL with Cu, Co and Fe

BEA with Cu and Co

(3) Metailosilicates: Cu-, Fe-, Ga-, AI-, Co-, Ni-, Mn-, Mo-, Ti-silicate

Metal oxides and related materials

(1) Single metal oxides: Al_2O_3, SnO_2, TiO_2, ZrO_2, La_2O_3, Fe_3O_4 and Ag_2O

(2) Mixed metal oxides: Al_2O_3-BaO, Al_2O_3-La_2O_3, ZnO-SiO_2, TiO_2-AL_2O_3, SiO_2-Al_2O_3

(3) Sulfate-promoted single and mixed metal oxides: Al_2O_3, TiO_2, ZrO_2, Fe_2O_3, ZrO_2-Al_2O_3 and ZrO_2-TiO_2

(4) Metal oxides supported on (1) to (3): Cu, Co, Ag, V, Ni, La, Mn, Ga, Cr, Ba, Ca, Sr, Mg, Zr, Cs, Sm, Mo, Ce and Fe

Noble metals

(1) On zeolites: MFI, MOR, FER and FAU

(2) On metal oxides: Al_2O_3, SiO_2, TiO_2, ZrO_2, La_2O_3, CeO_2, Cr_2O_3, ZnO, TiO_2-Al_2O_3, ZrO_2-TiO_2

The first kind of ion-exchanged zeolite catalyst which showed high capability in HC-SCR in the presence of air was Cu-ZSM-5, also known as Cu-MFI, (Iwamoto and Hamada, 1991). Cu/ZSM-5 could work in a range of temperature from 300℃ to 550℃ by using different reductants, such as ethylene (C_2H_4) (Sullivan and Cunningham, 1998), propene (C_3H_6) (Shelef, Montreuil and Jen, 1994), propane (C_3H_8) (Mongkolsiri et al., 2000) and decane ($C_{10}H_{22}$) (Čapek et al., 2005). However, Erkfeldt, Palmqvist and Petersson (2011) reported that oxygenated hydrocarbons do not play well in the HC-SCR system with Cu/ ZSM-5. Other metals such as Co, Ni, Mn and Zr have also been tested for the further development of ion-exchanged zeolite catalysts (De Lucas et al., 2005; Seo et al., 2012). Generally, various kinds of zeolite catalysts are used under different conditions. For example, Fe-zeolite catalysts show great potential in relatively high-temperature conditions while Cu-zeolite catalysts have good performance under relatively low-temperature conditions (Luo et al., 2012). Some typical examples of NO removal systems by HC-SCR, including applied catalyst, experimental condition and catalytic performance are shown in Table 2.5. However, the common issue of these catalysts is that they could be deactivated in the presence of water vapor (Pavulescu, Granger and Delmon, 1998).

Table 2.5: Some examples of NOx reduction by HC-SCR over various ion-exchanged zeolites

Catalyst	Reaction conditions				T_{max}	Performance		Ref.
	NO (ppm)	O_2 (vol %)	Reductant	H_2O (vol %)	(°C)	NO conversion (%)	N_2 selectivity (%)	
Cu/ZSM-5	1000	2	1000 ppm C_3H_6	NA	573	NA	70	(Iwamoto et al., 1992)
Ir/ZSM-5	750	8	1800 ppm C_3H_6	NA	450	NA	80	(Wögerbauer et al., 2001)
Co (0.91) ZSM-5	900	2	1000 ppm C_3H_8	NA	450	50	NA	(Stakheev et al., 1996)
Co (1.13)+ Ca/ ZSM-5	900	2	1000 ppm C_3H_8	NA	500	54	NA	
Co (1.28)+ Ba/ZSM-5	900	2	1000 ppm C_3H_8	NA	500	76	NA	
Co-Pd/ ZSM-5	500	5	2500 ppm CH_4	5	450	90	NA	(Pieterse et al., 2003)
Cu/ZSM-5	1730	3	1280 ppm i-C_4H_{10}	NA	375	94	NA	(Deeng, Mohamed and Bhatia, 2004)
Ag/ZSM-5	1000	5	1500 ppm C_3H_6	NA	700	60	NA	(Schuricht and Reschetilowski, 2012)
Fe/ZSM-5	1000	2	1000 ppm C_4H_{10}	NA	800	75	NA	(Heinrich et al., 2002)

In addition, ion-exchanged zeolites, metal oxide-based and related catalysts have also been found to have huge potential to accelerate and improve the HC-SCR process. Ag/Al_2O_3 is a typical representative of metal oxide-based catalysts. Previous research showed that owing to Ag/Al_2O_3 average NO conversion rate could achieve over 60% under the high-temperature condition (600℃) and up to 90% under the medium temperature condition (450℃) (Eränen et al., 2003). Many kinds of hydrocarbons have been tested and proved that Ag/ Al_2O_3 could adapt to a variety of hydrocarbons and have great NO conversion performance. Other metals supported on aluminum oxides (precious metal) have also been studied. For example, Meunier et al. (2000) tested the performance of NO conversion with C_3H_6 over Pt/ Al_2O_3 in lab-scale test. They found that the NO reduction activity was only available in the presence of oxygen while the NO reduction activity was low in the absence of oxygen. Because of the limitation of catalyst synthesis, the research with supported precious metals and metal oxide-based catalysts has been excluded from this thesis.

2.6.3.2 Mechanisms of HC-SCR

Many reaction mechanisms have been proposed and discussed for catalytic NOx reduction with hydrocarbons. The specific mechanisms may be different when using different kinds of catalysts. They may also depend on the type of hydrocarbon and reaction conditions. The mechanisms of CH_4-SCR over Co-ZSM-5 have been studied. Different schemes including N_2 formation, possible intermediates and active sites have been proposed by numerous studies (Chupin et al., 2006).

At the early stage of Co-ZSM-5 development, Li and Armor (1994) found that methane was activated through a Co-bound NO_2 species such as NO_2^- and formed CH_3 radicals. Then, intermediate like CH_3NO_2 would react with gaseous NO to generate N_2 Two years later, Aylor et al. (1996) used situ infrared method to investigate CH_4-SCR over Co-ZSM-5 and they found that NO_2 was generated via NO oxidation at the beginning of catalytic process. Then CN species were produced as reactive intermediates and further reacted with NO_2 to form CO_2 and N_2. Similarly, Sun, Fokema and Ying (1997) reported that oxygen or nitric oxide + oxygen interacted with Co^{2+} first to generate Co-oxygen complex, then it interacted with gaseous nitric oxide and oxygen to form adsorbed nitrogen dioxide intermediates. As the existence of CH_4 , the adsorbed NO_2 intermediates reacted with CH_4 to form nitromethane intermediates. Finally, the nitromethane reacted with nitrogen dioxide and/or nitric oxide-oxygen mixture to produce N_2, H_2O, and CO_2

(see Figure 2.10). After entering the 21st century, Wang, Chen and Sachtler (2001) proposed that NO, the initial element, was oxidized and adsorbed as NOy species which reacted with CH_4 while isocyanate species were measured as possible intermediates in their case. Lónyi et al. (2014) found that the CH_4-SCR reaction practically occurred in the channels of zeolite, and Co^{2+} ions exchanged in matrix have been considered to be the active sites.

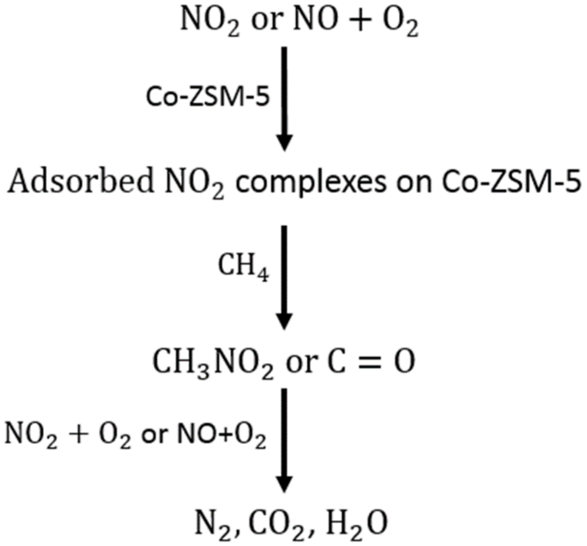

Figure 2.10: Proposed mechanism of CH_4-SCR over Co-ZSM-5 in the presence of oxygen (Sun, Fokema and Ying, 1997)

2.7 Advanced Support for Catalyst(s)

As shown in Table 2.4, zeolite is normally used in fixed bed of SCR tests as the support (carrier) of catalysts. It is known that zeolite has microporous structure with well-defined pore architecture and size. Also, zeolite can be loaded via various methods by cations to meet the specific requirement of catalytic reaction. ZSM-5, a high-silica type zeolite discovered by Mobil Oil Corporation in 1972, has been a popular one for various catalytic processes, such as methanol to gasoline and propylene (Jiao et al., 2012).

However, there are also some disadvantages of the use of zeolite, listed below (Ivanova et al., 2007; Shelef, Montreuil and Jen, 1994):

(a) Only around 10% of zeolite volume is occupied by catalytically active coating while the rest of volume is empty channel, which results in low contacting areas and affects the efficiency of NOx removal.

(b) Low radical mixing and heat and mass transfer rates, which can also cause some operating problems.

(c) Flow maldistribution, which may bring selectivity loss of reaction.

(d) The small size of zeolite (normally in micrometre level) is vulnerable to dust and not easy to integrate with practical applications.

To overcome the drawbacks of zeolite, many advanced porous supports have been proposed to combine with the use of zeolite catalysts in practical applications. Monolithic support which has uni-body structure is one of the candidates. It is regularly made by metal or ceramic materials though it can be composed of plastic material as well (Heck, Gulati and Farrauto, 2001). So far, the common honeycomb types are metal and ceramic ones (see Figure 2.11).

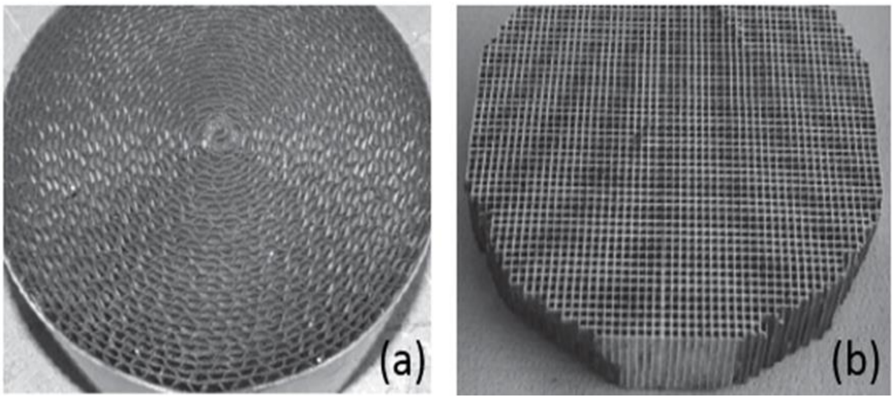

Figure 2.11: Photos of (a) metal honeycomb and (b) ceramic honeycomb (Matthes and Hartmann, 2017)

2.7.1 Introduction of Open-cell Foam

Apart from the honeycomb, open-cell foam, another potential support, has become a hot issue because it offers some crucial intrinsic properties such as higher heat and mass transfer and lower pressure drop (Patcas, Garrido and Kraushaar-Czarnetzki, 2007). Because of these valuable properties, the use of open-cell foam shows a promising future in the potential field where mass transfer and heat transfer are of great importance. It is necessary to investigate the application of open-cell foam with coating catalysts for SCR technology.

Generally, open-cell foam is an extremely porous reticulated cellular material and its structure looks like a sponge. The open-cell foam is comprised of a network of interconnected solid strut building cells which communicates via windows. The open-cell foam can be made of metals (e.g., aluminum, iron-chromium) or ceramics (e.g., silicon carbide, aluminum oxide). Various kinds of foams have different porosities. The porosity of ceramic foams is from 75% to 85% while that of metal foams can achieve around 95% porosity (Cheng and Bi, 2014).

Among all the types, silicon carbide (SiC) including alpha (α) or beta (β) SiC polymorphs, is a promising material to manufacture open-cell foam working as catalyst support (see Figure 2.12). Wong (2009) reported that silicon carbide has great mechanical strength, high thermal conductivity ($> 300\mathrm{Wm}^{-1}\ \mathrm{K}^{-1}$), low thermal expansion coefficient and high thermal and chemical resistance.

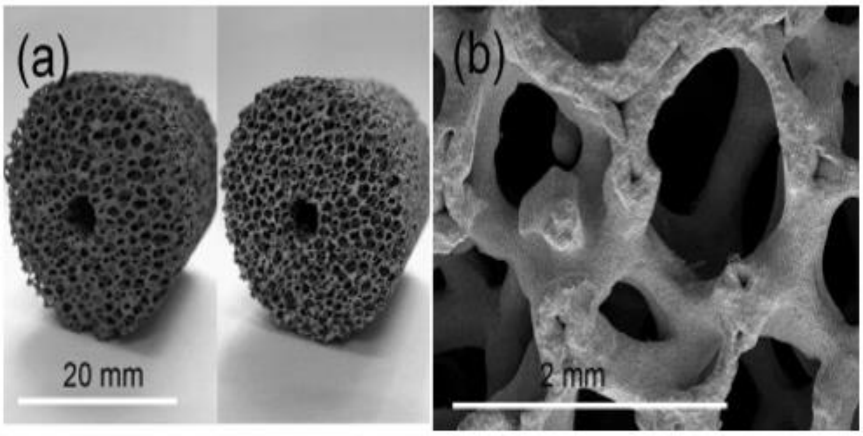

Figure 2.12: (a). Photo of ZSM-5/SiC foam (b). Micrograph of ZSM-5/SiC foam (Jiao et al., 2012)

So far, it has been proved that some factors such as pressure drop and specific surface area have a significant impact on the performance of SiC open-cell foam.

(i) Pressure drop

When SiC open-cell foam is used as SCR catalyst carrier, the pressure drop, i.e. the pressure difference between the inlet and outlet of flue gas (see Figure 2.13) is an important factor that needs to be considered as flue gas is near atmosphere pressure. The low pressure drop of SiC open-cell foam is created by the open structure and high catalytic surface area. The pressure drop of SiC open-cell foam is several times lower than that of traditional spherical packing (Lacroix et al., 2007). Skibinski et al. (2015) studied the relationship between pore volume variation and pressure drop and they found that the low pressure drop could be gained for SiC open-cell foams through the structure with inhomogeneous pore volume distribution. Although the exact relationship cannot be concluded due to different designed structures, the general trend could be used to optimize the porosity of SiC open-cell foam. So far, many correlations have been published for prediction of pressure drop in open-cell foams. For instance, a predicted pressure drop correlation was established by Dietrich (2012) for SiC and other types of open-cell foams based on over 2500 literature data. Four years later, a universal correlation for prediction of pressure drop in open-cell foam was proposed by Inayat et al. (2016). In this prediction, the pressure drop was only determined by two factors, open porosity and window diameter. However, there is another sound that the deviation between theoretical and experimental results of pressure drop could have three orders of magnitude difference because most of the correlations were gained based on experimental tests (Kumar and Topin, 2014). Additionally, geometrical parameters play an important role in the pressure drop of open-cell foams, which could not be ignored.

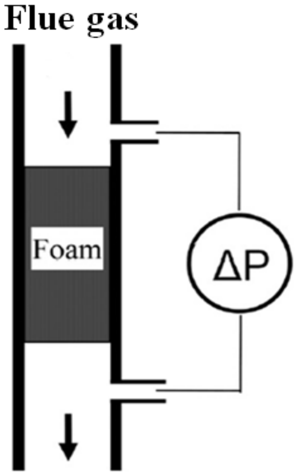

Figure 2.13: Diagram of pressure drop of open-cell foams

(ii) Specific surface area

According to Incera Garrido et al. (2008), the specific surface area of an open-cell foam is the total external surface area of foam struts per unit volume assuming that struts have a perfectly smooth surface. Higher specific surface area could increase heat and mass transfer and provide a larger contact surface for reactants and catalyst, as demonstrated by Saber et al. (2012). So far, medium to high specific area is normally from 25 to 110 m^2/g (Truong-Phuoc et al., 2014). Higher pores per inch (PPI) could achieve the increase of specific surface area (Inayat et al., 2011). Figure 2.14 shows the SiC open-cell foams with different PPIs.

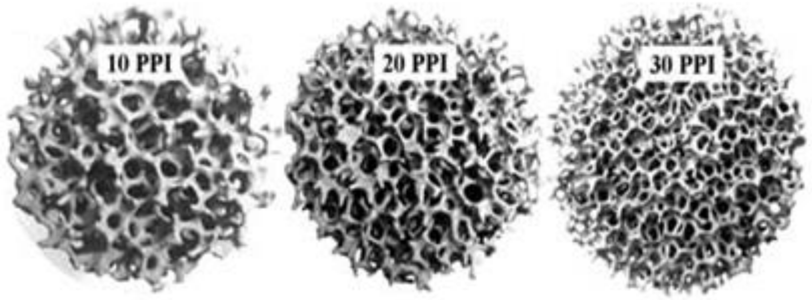

Figure 2.14: Diagram of ZSM-5/SiC foams with different PPI (Jiao et al., 2012)

Other advantages of SiC open-cell foam include: chemical inertness, ease of shaping, lightweight, high surface to volume ratio and high catalytic surface, making open-cell foam a potential solution to replace honeycomb and monolithic catalysts (Schwieger et al., 2000). Meanwhile, the open-cell foam is known as a great inherent filtering material because it could capture the majority of particulates in tortuous structure, effectively reducing PM emissions (Kim and Lee, 2014).

2.7.2 Applications of Open-Cell Foam

Owing to these attractive properties, open-cell foams have been widely used in various applications such as methane and propane combustion (Cerri, 2000), waste and flue gas purification (Fino et al., 2005; Vansetten et al., 2003), design of compact heat exchangers (Mahjoob and Vafai, 2008) and catalytic substrates for internal combustion engines (Bianchi et al., 2012).

Furthermore, open-cell foam has already been tested as the substrate for automatic catalyst applications (Bach and Eggenschwiler, 2011; Dimopoulos Eggenschwiler et al., 2009).

2.8 Applications of Catalytic Emission Abatement in Small-scale Combustion Systems

Since the 1990s, the use of catalytic emission abatement in small-scale combustion systems has received a lot of research and development attentions. Carno (1996) used two commercial pelletized catalysts (one platinum supporting catalyst and one manganese and copper oxides on alumina carrier) in chimney to achieve the reduction of unburned hydrocarbon and CO in exhaust gas. Doggali et al. (2011) tested Al_2O_3, TiO_2 and ZrO_2 support in domestic stoves using solid fuel. They found that these catalysts were helpful for the oxidation of CO and PM. Similarly, a series of La-Cr perovskite catalysts were applied in a household wood-fired stove to reduce CO and hydrocarbon (Bensaid et al., 2012).

The use of porous materials (e.g., ceramic foams or honeycomb supports) with or without the help of catalyst to control emissions of biomass combustion stoves/ boilers is also on the increase. It is believed that these kinds of porous materials with suitable catalyst(s) have attractive capability to decrease most of gaseous emissions such as CO and PM. For example, in the study of Matthes and Hartmann (2017), ceramic foam (cordierite as catalyst) and other three catalyst samples (knitted steel wire catalyst, ceramic honeycomb and metal honeycomb) were placed in the inlet of heat exchange of a standard 7kW wood log stove. Their results showed that there was noticeable CO reduction in all cases comparing with reference values. Nevertheless, there was a small rise of NOx values in flue gas. In the same year, Wöhler et al. (2017) tested the emission reduction and combustion performance by using foamed ceramic catalyst coating which contains palladium (Pd), platinum (Pt) and rhodium (Rh) in a 8kW firewood stove. Their idea was to use the foams to cover upper half of combustion chamber. That generated a 20% CO and 40% PM reduction. Recently, Reichert et al. (2018) investigated the performance of honeycomb carriers with a coating of aluminum oxide (Al_2O_3) which also contained noble metals palladium and platinum while the catalysts were placed at the inlet of the flue gas chimney. Over 80% of CO reduction and approximately 20% of PM reduction were observed in their tests.

2.9 Summary

From the review of the existing literature, it can be concluded that many technologies have been developed to improve the performance of small-scale biomass combustion devices/boilers in terms of emissions such as NOx, CO and unburned hydrocarbon. Among them, SCR-related technologies are worth further study due to their unique advantages. According to the applications shown in section 2.9, the focal point in most of current research is on the emissions of CO and unburnt hydrocarbons when applying catalytic or non-catalytic technologies in small-scale heating applications. This leads to some knowledge gaps in the feasibility of NOx reduction of HC-SCR by potential reductants and catalysts. Also, the biomass combustion behaviour under oxy-fuel conditions should be further investigated in order to control CO_2 emissions by the use of CCS.

CHAPTER 3. EXPERIMENTAL METHODOLOGY

3.1 Experimental Set-up for Chapter 4

In this section, the basic experimental set-up for the Chapter 4 (investigation of fuel characterisation and combustion bevaviours by using individual biomass pellet) is reviewed, including the introduction of Visual Drop Tube Furnace (V-DTF) and its configurations, selection and preparation of five types of biomass pellets (wood, straw, peanut shell, miscanthus and torrefied wood pellets). The high-speed camera which was used to record the combustion process of individual biomass pellet is introduced in section 3.1.3. Also, the testing procedure is mainly presented in section 3.1.4. The thermal analysis of biomass samples is mentioned in section 3.1.5.

3.1.1 Visual Drop Tube Furnace (V-DTF)

The Visual Drop Tube Furnace (V-DTF) manufactured by Elite Thermal Systems Ltd was a laminar flow furnace (see Figure 3.1 a). There was a quartz tube vertically located at the centre of furnace as work tube, which had 1400mm length, 50mm internal diameter and 5mm wall thickness. The V-

DTF was electrically heated by the surrounding heating elements (resistive wire on ceramic tubes, see Figure 3.1 c) and it has a maximum rated temperature of 1200°C and continuous running temperature of 1150°C. The setting temperature was monitored and controlled on the control panel (see Figure 3.1 b), sitting close to the furnace. The heating rate of V-DTF was set at 20°C per minute in this research.

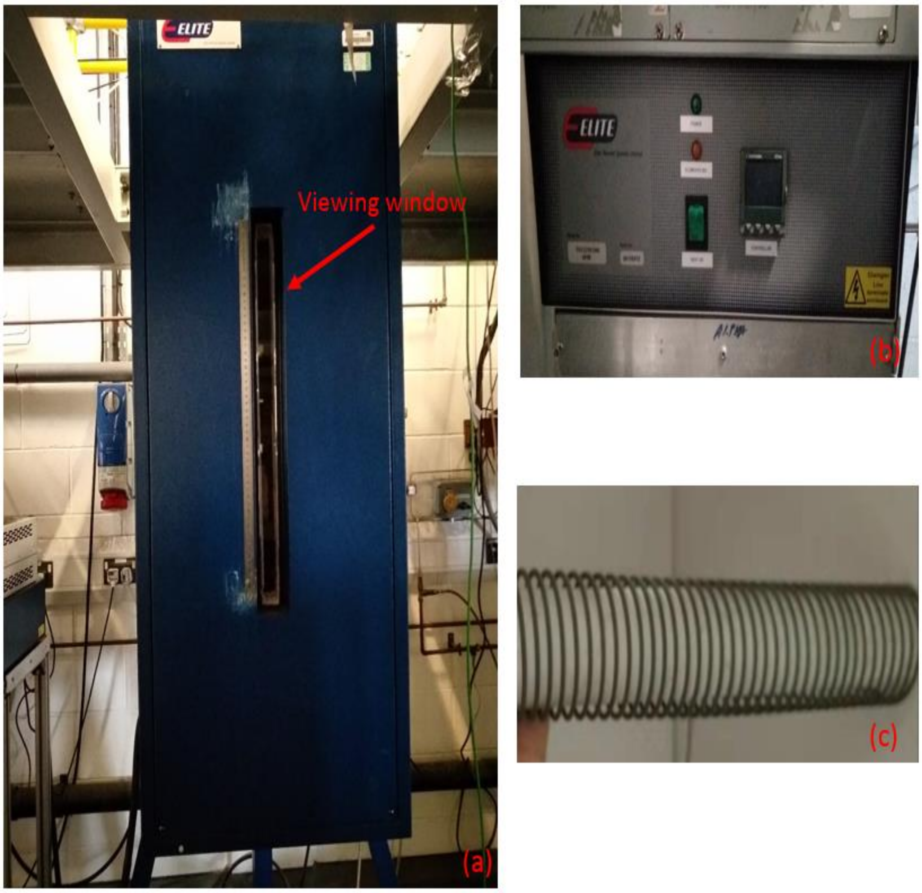

Figure 3.1: Photos of (a) Visual Drop Tube Furnace (V-DTF) with viewing window, (b) control panel, (c) One of the heating elements in V-DTF

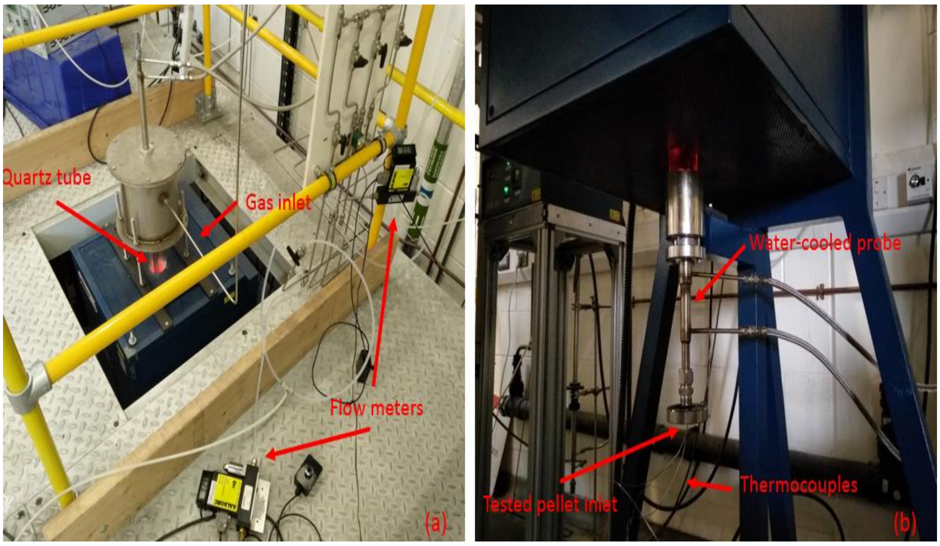

Figure 3.2: Photos of (a) top part of V-DTF, (b) bottom part of V-DTF

Distinguishing from other drop tube furnaces, there was a custom-designed viewing window with a size of 30mm width and 450mm length placed on the front of V-DTF and parallel to the quartz tube. Also, two water-cooled probes are placed axially at the top and bottom of quartz tube. Both of them had the same internal diameter (5mm), but different length (760mm for the top probe and 610mm for the bottom one). A support situated at the bottom of V-DTF was used to assist the insertion of biomass pellets for future experiments (see Figure 3.2).

3.1.2 Selection of Biomass Pellets

In order to study the combustion and ignition performance of a variety of biomass fuels, five kinds of biomass pellets were chosen and used in a group of experiments (see Figure 3.3), two woody pellets (wood – W, torrefied wood – T) and three non-woody ones (miscanthus - M, straw - S, peanut shell - P).

Figure 3.3: Photos of the five kinds of selected biomass pellets (top row: miscanthus pellets, peanut shell pellets and straw pellets; bottom row: torrefied wood pellets and wood pellets)

All the pellets are easy to find from the current market due to their widespread use and availability. Some of them are commonly used in power industry such as wood and straw pellets. The peanut shell pellet is an interesting one since it is produced from wasted peanut husks which is the main by-product of peanut processing factories. The potential use of peanut shell pellets can solve the storage and reuse issues of peanut husks. Compared with four raw biomass pellets (W, M, S, P), torrefied wood pellet (T) is slightly different in terms of production method. It is made from torrefaction which is a mild pyrolysis process under an inert atmosphere with in the temperature range of 200°C~300°C (Kymäläinen, Havimo and Louhelainen, 2014). Because of this step, although the torrefied wood pellet may lose some moisture content and volatile matter depending on the torrefaction temperature, it can achieve higher heating value compared with its raw (untreated) type. It has been reported that the use of torrefied pellets can generate better performance for industrial applications, for example co-firing with coal in pulverized coal boilers (Eddings, McAvoy and Coates, 2017).

For each type of biomass fuel, pellets with similar sizes were chosen for the experiments. Averagely, the wood pellets had the longest length while the peanut shell pellets had the largest width. The size (length and width) and weight of all induvial pellets were carefully measured before the experimental tests, which can be found in Figures A.1 and A.2. The chemical and physical properties of these biomass pellets were characterised by using TA instrument SDT Q600 and elemental analyzer, which will be further introduced in detail in section 3.1.5. The results of proximate and ultimate analysis are presented in Table 3.1. It should be mentioned that the values of oxygen in ultimate analysis were determined by the difference. In addition, since the wood pellets and torrefied wood pellets came from different types of raw wood, no direct comparison between them can be made.

Table 3.1: Proximate and ultimate analysis of the selected biomass pellets (wood, straw, peanut shell, miscanthus, torrefied wood), based on dried basis

	Wood	*Straw*	*Peanut shell*	*Miscanthus*	*Torrefied wood*
	Proximate analysis (wt%, as received)				
Moisture	7.32	4.00	7.73	4.42	6.40
Ash	0.35	7.57	2.78	3.67	1.97
Volatile matter	76.96	73.96	68.50	75.91	72.90
Fixed carbon	15.37	14.47	20.99	16.00	18.73
	Ultimate analysis (wt%, d.a.f)				
Carbon	46.68	44.03	46.69	45.55	49.32
Hydrogen	6.44	5.93	6.42	6.13	6.04
Nitrogen	0.24	0.67	1.38	0.66	0.51
Oxygen	46.64	49.37	45.51	47.66	44.13
high heating values (HHV), kJ/kg	18.57	17.50	18.72	18.11	19.62

3.1.3 High Speed Camera

Since typically small size of biomass were chosen in the related research of ‘fuel performance’, residue time and tiny change of fuel samples in tube furnace are challenging to find. Hence, the high speed camera was found to offer high-speed imaging technology to monitor and record the combustion behaviour of fuel samples in drop tube furnaces. For example, in the research of Riaza, Gibbins and Chalmers (2017), a high-speed camera with a rate of 500 frames per second (FPS) was used. Because of the high frame rate, slight changes in the flame could be observed. In the same paper, they also observed a ‘blue colour’ in the flame before it turning into a ‘yellow colour’ at the beginning of the ignition stage, which only happened under a few milliseconds.

3.1.4 Test Conditions and Measurement

Three N-type thermocouples with Nicrotherm DTM Sheaths were used to assist the experiment. The N-type thermocouple was ideally suited for accurate measurement in air up to 1200℃ and kept good thermoelectric stability, which was superior to other type thermocouples. Two of them (N1 and N2) had the length of 1000mm and external diameter of 1mm while the other one (N3) had a longer length (1500mm×1mm). Each biomass pellet sample was drilled a suitable hole by using a lab-made driller before conducting the experiments (see Figure 3.4 a). All the holes were located in the centre axis and drilled to the half depth of pellet.

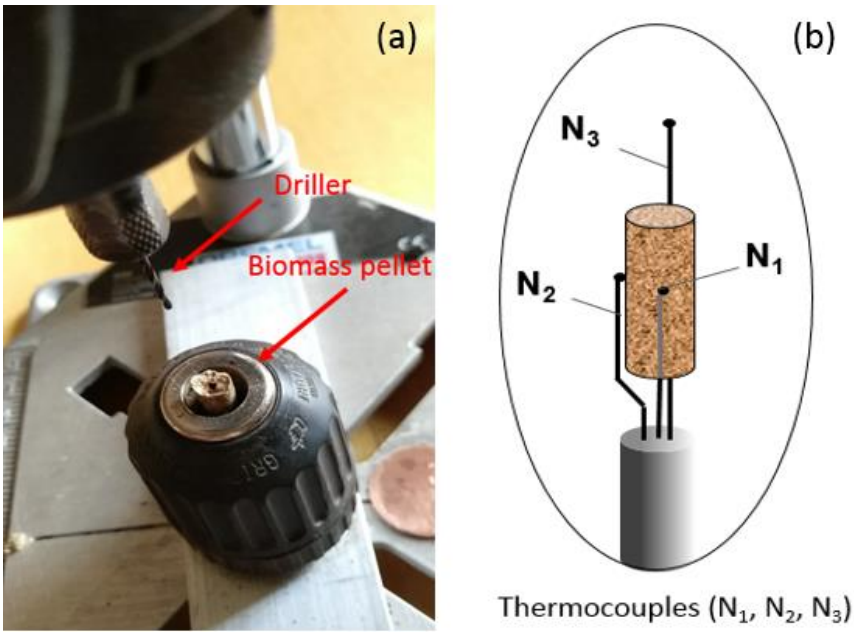

Figure 3.4: (a) Photo of the lab-made driller and pellet sample, (b) Schematic of experimental setting of three thermocouples

The experimental tests to investigate the combustion behaviour were carried out by preheating the furnace to these setting temperature and introducing the feed gas mixture from the top of furnace (see Figure 3.4 b) to work tube. The tested individual biomass pellet and three thermocouples were inserted manually from the bottom side of furnace to a fixed position after the furnace Reached the target temperature and stabilised for at least half an hour (see Figure 3.2 b). One of the thermocouples (N1) was not only used to hold the biomass pellet, but also to measure the centre temperature of pellet during combustion process. The other two thermocouples (N2 and N3) were used to measure the side surface and top surface temperature of the pellet sample. The whole combustion process of each pellet sample was recorded by the high-speed camera.

The tested pellet samples were burnt under different flow conditions (see Table 3.2) and temperatures of 800˚C and 900˚C which represented typical fixed bed and fluidised bed biomass combustion temperatures. The total flow rate of the feed gas mixture was set at 10L/ min in all tests in order to reduce the effect of flow rate on combustion behaviour, which has studied in Shan et al., (2017). Two oxygen-enriched conditions (25% O_2-75% CO_2 and 30% O_2-70% CO_2) and a normal oxygen fraction oxy-fuel condition (21% O_2-79% CO_2) were chosen while the condition of conventional air (21% O_2-79% N_2) was used as baseline. Pure O_2 and CO_2 were coming from two separate gas cylinders, controlled by two mass flow meters which had 0 to 30 L/ min measuring range. It should be mentioned that the flow rates were slightly modified based on correction factors as both flow meters were manufactured for air flows.

Table 3.2: Flow conditions of feed gas for individual pellet tests

Condition (L/min)	O_2 (L/min)	CO_2 (L/min)
Air (21% O_2-79% N_2)	10 (L/min)	
21% O_2-79% CO_2	2.1	7.9
25% O_2-75% CO_2	2.5	7.5
30% O_2-70% CO_2	3.0	7.0

3.1.5 Biomass Sample Analysis

3.1.5.1 Milling

Since pulverised biomass samples were required for the tests of thermogravimetric analysis (TGA), it was necessary to brittle all the biomass samples from pellet to particle sizes. In that case, a laboratory bench-top planetary Retsch PM100 ball mill was used (see Figure 3.5 a). It had eight stainless steel grinding balls inside sample bowl which would be put in the mill when it was running. About 5g of each sample was placed in the sample bowl (see Figure 3.5 b) and milled at the rotational speed of 350 RPM (Revolutions Per Minute) for four to five minutes, depending on different types of samples. Milled biomass powders were stored in clean sample bags for both proximate and ultimate analysis.

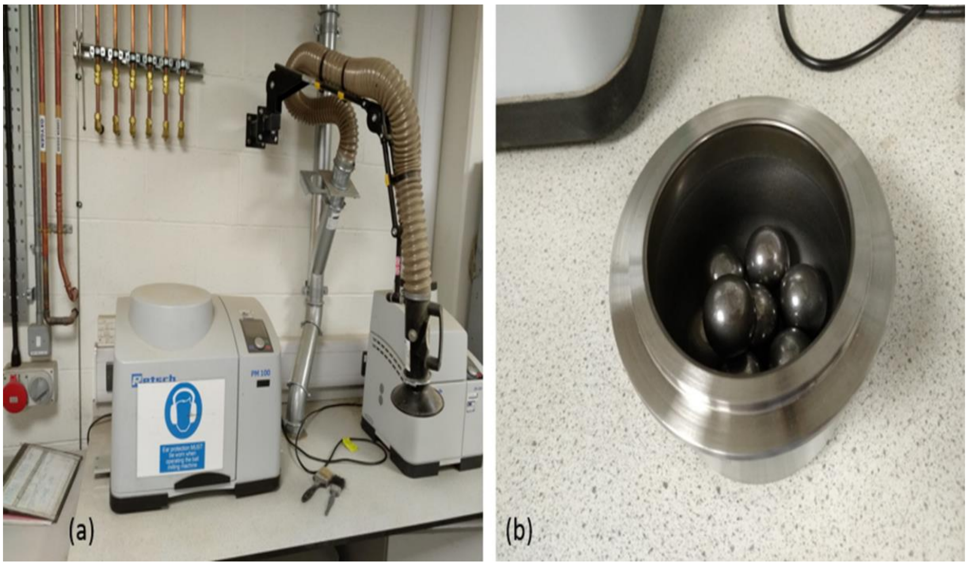

Figure 3.5: Photos of (a) the PM 100 mill, (b) the sample bowl and stainless steel grinding balls

3.1.5.2 Thermogravimetry

Thermogravimetric analysis (TGA) was used to estimate the performances of proximate analysis (moisture, volatile matter, fixed carbon and ash). In this work, a lab bench called 'TA instrument SDT Q600' (upper temperature limit of 1100℃) was employed for all TGA tests (see Figure 3.6).

The TGA proximate analysis process was performed based on a customer-build program. Around 30 mg of sample was heated to over 100℃ (110℃ was chosen in our program) under a nitrogen atmosphere with flow rate of 100 ml/ min and kept under isothermal condition for 10 minutes. Then, keeping the same supply gas, the testing temperature of unit was heated to 920 ℃ with heating rate of 50 ℃/ min and also kept under isothermal condition for 10 minutes to make sure that all the volatile matter were removed entirely. After that, the supply gas was switched from nitrogen to air and had another twenty-min test to consume the char completely. Finally, the unit was cooled down to ambient temperature under air atmosphere. After run finished, the result of curve with residual weight over time can be found in corresponding TA universal analysis software. An example of TGA results is shown in Figure 3.7.

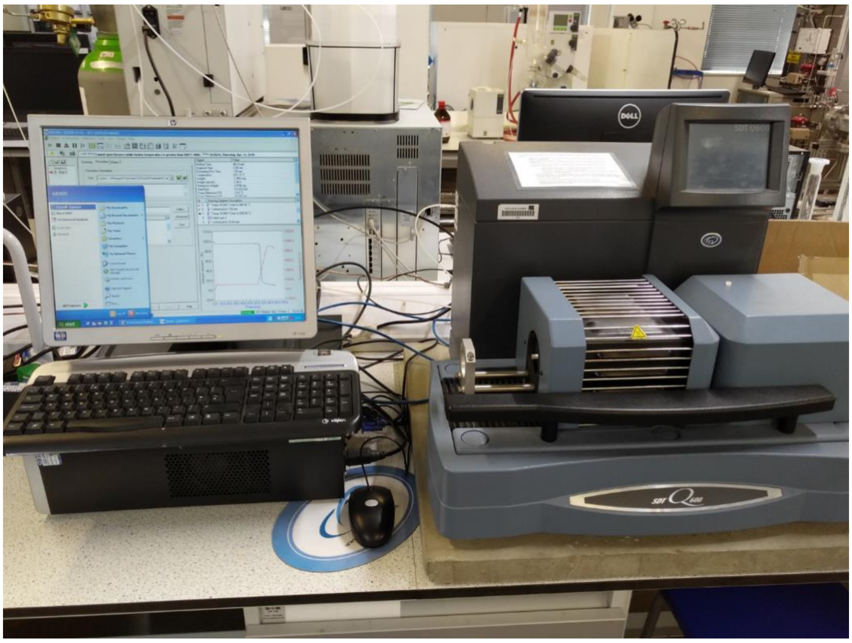

Figure 3.6: Photo of the TA instrument SDT Q600

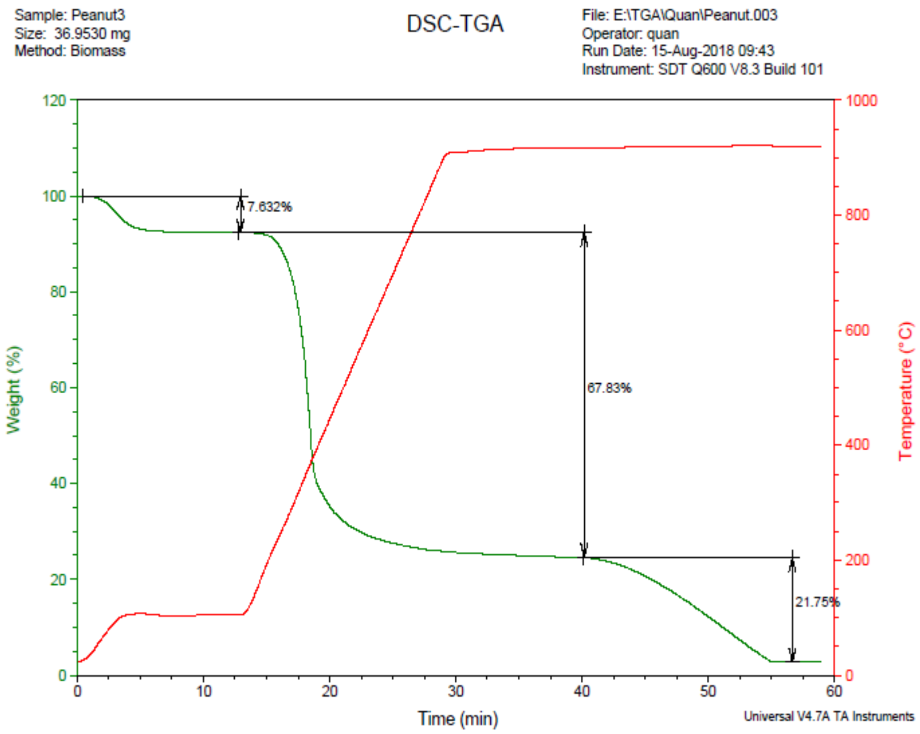

Figure 3.7: One example of the TGA results

3.1.5.3 Ultimate analysis

An apparatus called CNH-628 series elemental analyzer (see Figure 3.8) was used to conduct the ultimate analysis, determining the elemental composition of carbon (C), nitrogen (N) and hydrogen (H).

Before running each elemental test, a blank test called ‘BBOT test’ was done first to standardise and calibration the elemental analyzer. Then the sample to be tested was wrapped by a foil before being put into the elemental analyzer. The sample was combusted in the analyzer at 900°C and under excess oxygen conditions. The combustion products including CO_2, N_2 and H_2O were used as the basis to calculate the contents of C, N and H of the sample.

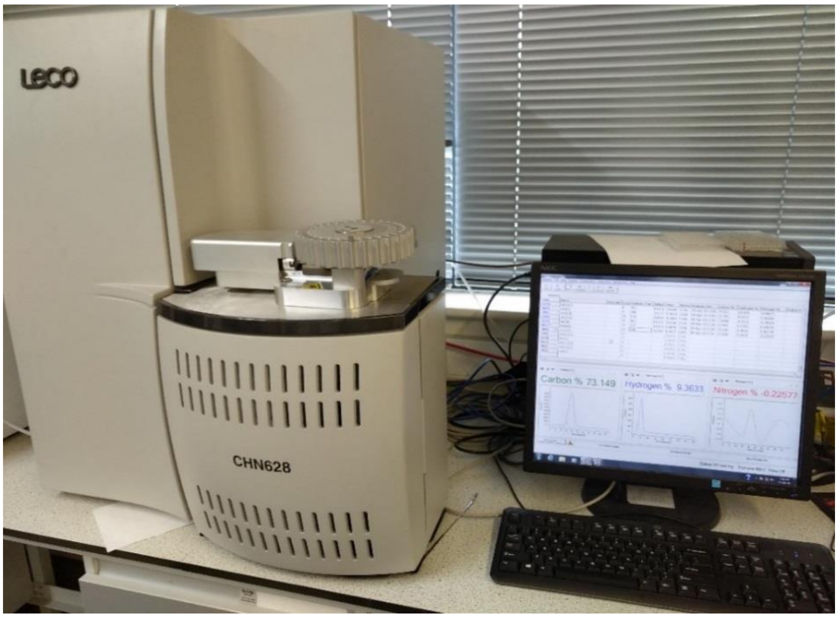

Figure 3.8: Photo of the CNH-628 Series elemental analyzer

3.1.5.4 Determining Heating Values

The high heating value (also known as gross calorific value) of biomass is a significant parameter to predict the amount of heat produced by complete combustion of the fuel. In this study, the high heating values (HHV, dry basis) of tested biomass samples were calculated by using the correlation developed by Friedl et al. (2005). The results from ultimate analysis were used to calculate the HHV values.

$$\mathrm{HHV} = 3.55\mathrm{C}^2 - 232\mathrm{C} - 2230\mathrm{H} + 51.2\mathrm{C} \times \mathrm{H} + 131\mathrm{N} + 20600 \qquad [3.1]$$

Where the higher heating value, HHV, is in kJ/kg; C, H, N are wt% of carbon, hydrogen and nitrogen, respectively.

3.2 Experimental Set-up for Chapter 5

In this section, the basic experimental set-up for Chapter 5 (small-scale biomass boiler tests) is presented including: the boiler configurations and its recommended biomass fuel (section 3.2.1 and 3.2.2). The gas sampling and analysis system is introduced in section 3.2.3. The general testing steps and conditions are also described in section 3.2.4.

3.2.1 Ashwell 50kW Biomass Boiler

The biomass pellet boiler used in this research was Ashwell Green-tech 50 kW biomass pellet boiler, which was designed as a domestic biomass pellet boiler for hot water and space heating purposes. It was a pellet fired boiler with automatic electric ignition and bottom screw feed system. Meanwhile, it was a low maintenance wood pellet boiler of modular design which allowed an extremely versatile configuration of fuel feeds. The main dimension of the boiler was 1450mm× 1650mm× 850mm and other details can be found in Figure 3.9. The net weight of the boiler was 550 kg and it had a pellet hopper with 250 kg capacity. The compact design resulted in a smaller footprint compared to similar output biomass boilers. More importantly, as one of the most significant advantages, the temperature of hot water heated by biomass boiler can be monitored and controlled through the supporting control panel. Also, many parameters such as the boiler load, fuel feeding rate and 'kindle time' rate can be adjusted based on different conditions by adjusting the parameters on control panel (see Figure 3.10). Here, the 'kindle time' rate was applied and used to control the periodic pulsing of feed screw when the boiler control was turned off. It allowed the boiler to maintain hot embers in the combustion retort and reduced the chance of 'burn back' condition occurring.

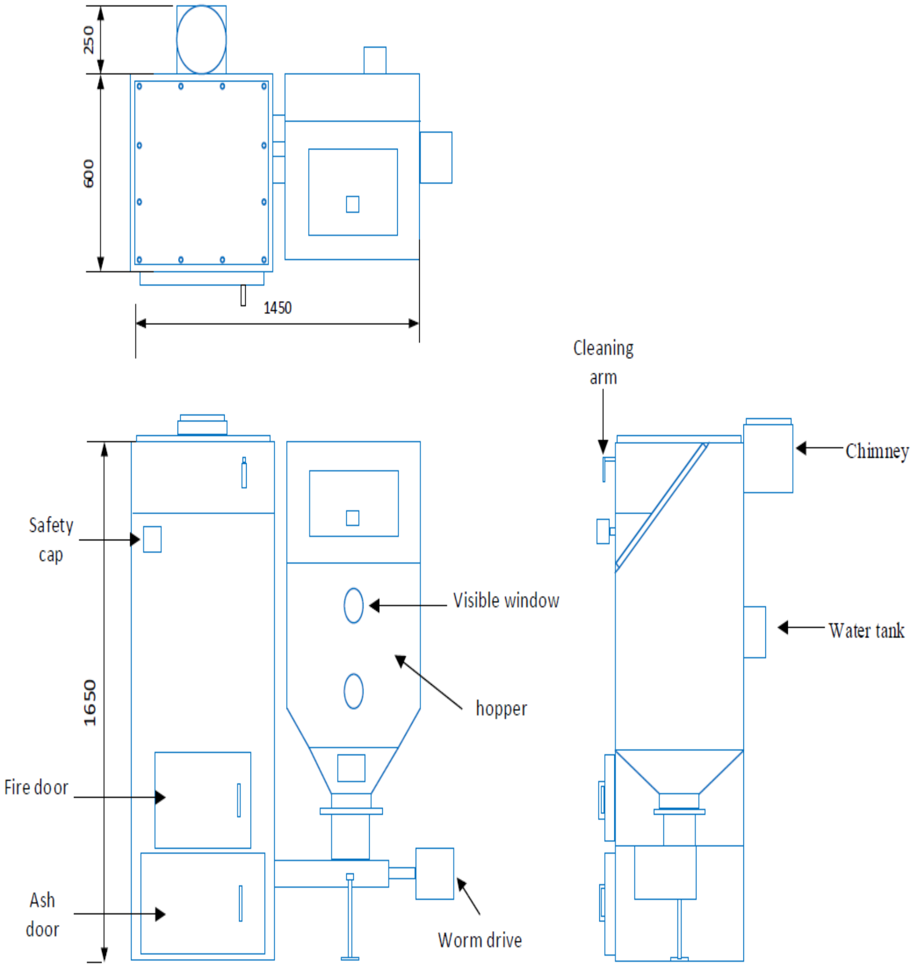

Figure 3.9: Schematic diagram of the 50 kW biomass pellet boiler

Figure 3.10: Photo of the 50kW biomass pellet boiler and its control panel

3.2.1.1 Boiler configurations

The internal layout of biomass boiler is shown in Figure 3.11 by using a 3D dimension model. Ignition was triggered by the heat gun located in the fire pot. The boiler has the staged air supply, primary air with being supplied below the fuel bed while secondary air above the fuel bed being supplied by four one-centimeter inner diameter nozzles placed at two different heights (see Figure 3.12). A flame deflection plate was placed above the fuel bed and below the heat exchanger to boost mixing process between the primary combustion products and the secondary air and promote complete combustion.

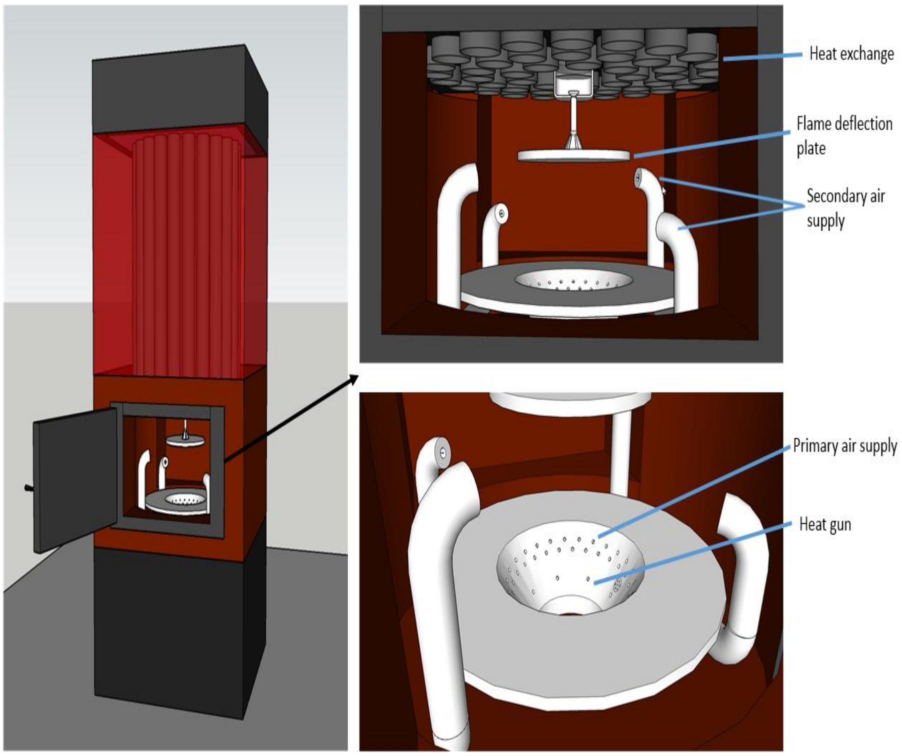

Figure 3.11: 3D dimension of internal layout of the biomass boiler

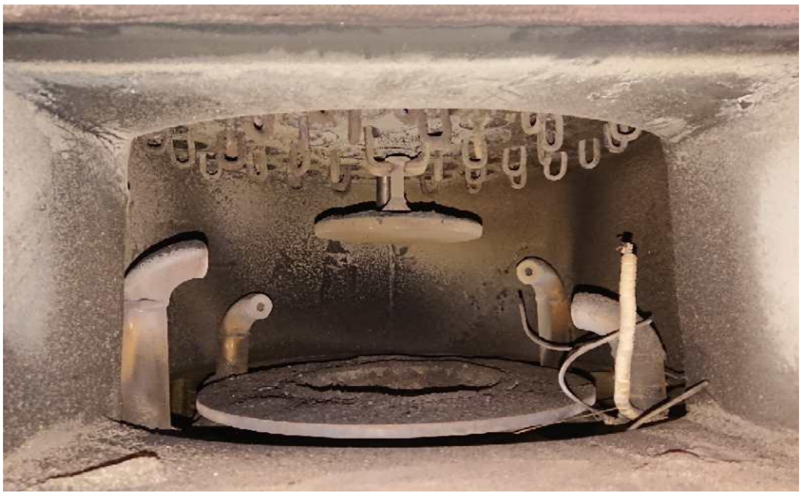

Figure 3.12: Photo of the combustion chamber

3.2.1.2 Boiler operation procedure

When the boiler was turned on (switch on the controller on control panel), biomass pellets were delivered from fuel hopper to the bottom of the fuel bed via the feeding convey screw while the air was provided by primary and secondary air fans located at the back side of boiler. Then biomass combustion started automatically in the combustion chamber because of the automatic electric ignition (the heat gun in fire pot). Hot combustion products generated from the combustion chamber was used to heat the water inside the heat exchanger. The warmed hot water leaving the boiler to the heat DUMP fan via supply route and flowing back to the boiler via the return route, forming a water loop. As the boiler was used for research purpose, not heating purpose, the heat of the hot water was dumped by a heat dissipation fan installed outside the laboratory (see Figure 3.13, which also shows the other parts of the water loop (schematic hydraulic system).

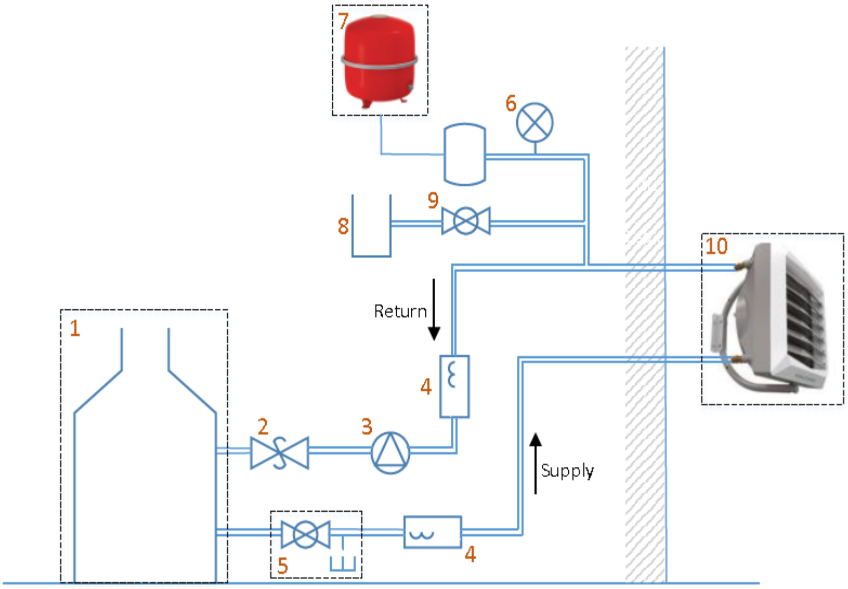

1. Biomass boiler 2. Vent valve 3. Circulation pump 4. Thermometer(s) 5. Ball valve and drain 6. Monometer 7. Expansion vessel 8. Water tank (supply) 9. Ball valve 10. Heat dump fan

Figure 3.13: Schematic of the hydraulic system

3.2.2 Boiler Design Fuel

The Ashwell Green-tech biomass boiler was designed to burn 6mm or 8mm quality wood pellets. The reason was that it had shown that the diameter of pellets played an important role in the transport process of the biomass pellets from the hopper to combustion chamber where the pellets were ignited and burned. For the 50 kW biomass boiler used in this study, the diameter of 6 mm or 8 mm was optimal for the transport system. Generally, domestic biomass pellet boilers only use qualified pellets with good mechanical and chemical properties in order to maintain end-user confidence on the biomass boilers. These properties of the pellets affected the quality of combustion, performance and emissions. To maintain optimal burning performance, pellets should be adhered to: D06 or D08 (pellet diameter 6 or 8mm), M10 (＜10% moisture content), A1.5 (≤1.5% ash content), S0.05 (＜0.05% sulphur), DU 97.5 (durability> 97.5) and F1.0 (≤1% fines). The effect of different biomass pellets such as woody and non-woody pellets in small-scale boiler has been widely researched (Carvalho et al., 2013; Dias, Costa and Azevedo, 2004; Kluska, Turzyński and Kardaś, 2018). Therefore, only standard but commonly-used wood pellets were used as fuel in this series of biomass boiler tests since the main objectives were to study the boiler performance and internal temperature distribution more than the adaptability of biomass fuels.

The selected wood pellets for the biomass pellet combustion tests described in Chapter 5 have been shown in Figure 3.3, with diameter of 6mm ± 1mm and max length of 40mm, and meet the requirement of ENplus A1 quality scheme (Woodlets, 2019). The proximate and ultimate analysis results of the wood pellets can be found in Table 3.1.

3.2.3 Gas Sampling and Analysis System

The photo and schematic of the experimental set-up and gas sampling system are shown in Figures 3.14 & 3.15 respectively. Two sets of gas sampling systems were used for the biomass boiler, one for sampling chamber gas and the other for sampling flue gas. The main gases analyzed from the combustion chamber included CO, CO_2, O_2, CH_4 while for the flue gas they were CO, CO_2, O_2, NOx. As pointed out in Chapter 2, CH_4 was the main hydrocarbon expected to be found within the combustion chamber. Hence, CH_4 was chosen as the focus of the measurement for the combustion chamber gas. Although numerous researchers have conducted gas sampling and analysis with domestic biomass boilers, however, the concentration of CH_4 has rarely been measured in small-scale boilers so far. The concentration of NO_x in the flue gas is one of the most critical indicators for the environmental performance of the boiler.

As too many particles were generated during the ignition and initial combustion stage, the gas sampling systems were only connected to the boiler after combustion process approached the stable condition. The temperature of flue gas shown on control panel was used to monitor the boiler initial operation before gas sampling and analysis system were used. A small flow of chamber gas and flue gas was sampled and analyzed while most of the flue gas was discharged to the atmosphere through the chimney.

As Figure 3.15 shown, both the sampled chamber gas and flue gas had to pass through a cleaning system first to cool down and get rid of moisture and dust (details are in section 3.2.3.2), before flowing into their respective gas analyzers. The real-time gaseous composition and emissions were measured by different types of Horiba and ABB gas analyzers. Data were sent and stored to the computer at the terminal by using data logger.

Figure 3.14: Photo of the biomass boiler with gas sampling system

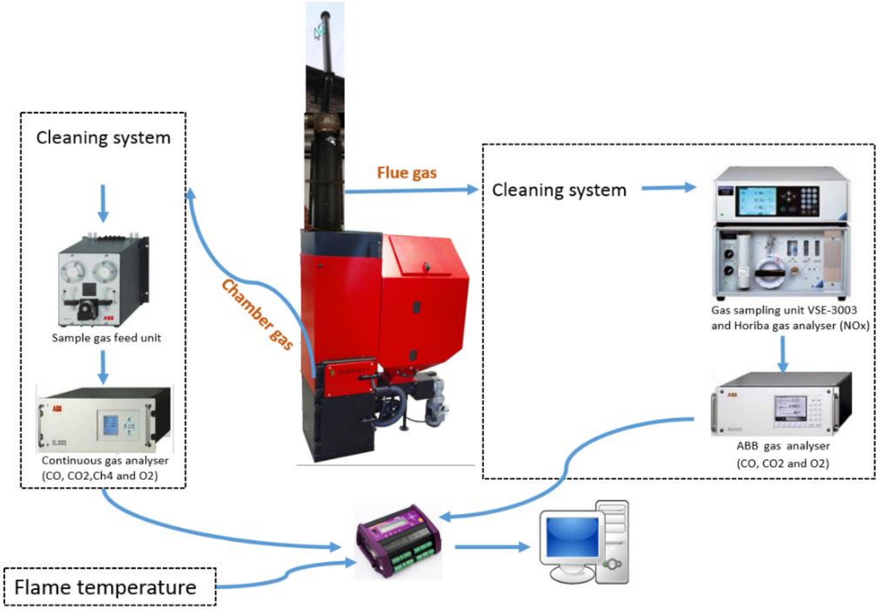

Figure 3.15: Schematic of the sampling system for chamber gas and flue gas

3.2.3.1 Gas analyzers

Two sets of analyzers (a Horiba VA-3003 multi-gas analysis unit and ABB AO2020 gas analyzers) were used to monitor the sampled combustion chamber gas and flue gas compositions. Both gas analyzers were designed for continuous measurement of the concentration of individual components. The combustion chamber gas was sampled and analyzed by a set of ABB apparatus including a sample gas unit and gas analyzers (see Figure 3.16 a). Similarly, the flue gas was sampled by Horiba gas sampling unit VS-3003 with a built-in sampling pump, and then passing Horiba VA-3003 and ABB AO2020 analyzer for analysis (see Figure 3.16 b).

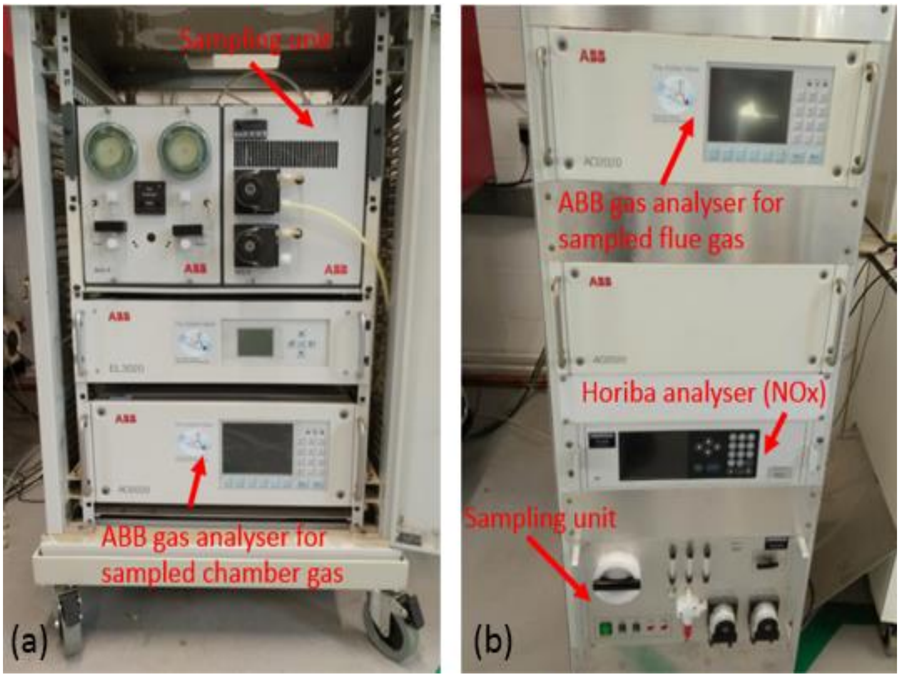

Figure 3.16: Photos of the gas analyzers for the sampled combustion chamber gas (left) and flue gas (right)

Horiba VA-3003 was a single gas analyzer that can measure a wide selection of gas components by using different sensor technologies. To measure NOx, a sensor module utilizing the proprietary interference free chemiluminescence (CLA) method was used and allowed to measure low-concentration NOx, even low as 0 to 10 ppm. The measuring principle of NOx was that when the O_3 reacting with NO in the sample gas, part of NO was oxidized to NO_2 Then the generated NO_2 emitted light when it returned to the ground state while the emitted light according to the reaction was detected by the photodiode. The light emitted volume was proportional to its concentration. (Multi-Component Gas Analyzer VA-3000 Series, n.d.)

With ABB gas analyzer, non-dispersive infrared (NDIR) modules were applied to measure the concentrations of CO and CO_2. As a mature technology, the main measuring principle of NDIR was that each gas in the sample would absorb some infrared at a particular energy. The NDIR detector can measure the volume of absorbed infrared in the sample cell. Thus, the detector can measure the volumetric concentration of particular gas in the sample gas.

Furthermore, the measuring ranges of different channels in gas analyzers were critical as well since it was related to the accuracy of measurement. Most of measuring ranges were fixed by the manufacturer while the NOx channel was changeable which can be set up to 2000 ppm. Its span range was set at 200 ppm for the biomass boiler tests when taking the result of blank tests into account. The details of range and stability of measured channels for gas analyzers are shown in Table 3.3.

To maintain the accuracy of the gas analyzers, it was necessary to be calibrated before running the experiments. All O_2, CO, CO_2, CH_4 and NOx gas channels were calibrated their zero and span points. Following the manuals of analyzers: zero points should be calibrated first, then span points.

The zero points of CO and NOx were calibrated by using atmospheric air while zero points of O_2, CH_4 and CO_2 were calibrated by using the special gas supplied by BOC (150 ppm NO_2/ N_2 balance). Atmospheric air was used to calibrate span point of O_2 into 20.9 vol%. The span points of NOx, CO, CO_2 and CH_4 were calibrated by the special gases supplied by BOC (150 ppm NO_2/ N_2 balance, 1500 ppm CO & 15% CO_2/ N_2 balance and 2% CH_4/ N_2 balance respectively).

Table 3.3: List of range and stability of measured channels in gas analyzers

	Device and measured channel		**Range**	**Stability**
Chamber gas	ABB EL3020	O_2	0-100 vol%	≤0.5% of span
		CO	0-20 vol%	≤1% of span
		CO_2	0-20 vol%	≤1% of span
		CH_4	0-10 vol%	≤1% of span
Flue gas	ABB AO2020	O_2	0-21 vol%	≤0.5% of span
		CO	0-5 vol%	≤1% of span
		CO_2	0-100 vol%	≤1% of span
	Horiba VA-3000	NOx	0-200 ppm	≤0.5% of span

3.2.3.2 Sample Gas Cleaning System

As required in the manuals of Horiba and ABB analyzers, the temperature of sample gas entering into sampling units should be in the range from 5°C to 50°C. Also, water vapor and dust were not allowed to enter the sampling units and gas analyzers to avoid any operating problem. Hence, it was essential to clean the sample gas before gas analysis. To achieve this, two sample gas cleaning systems (see Figure 3.15) were built for the two routes of the sample gases. Each gas sample/ cleaning system consisted of three parts, each for cooling, drying and dust elimination respectively (see Figure 3.17).

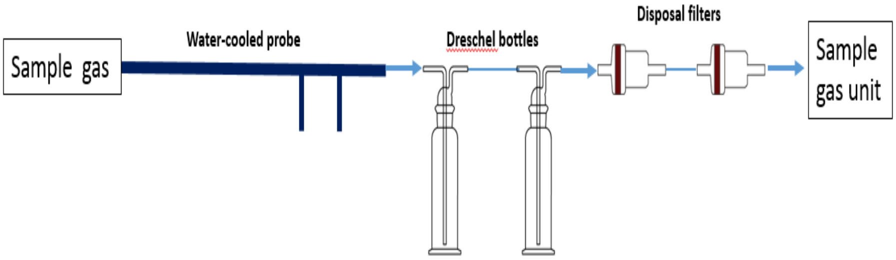

Figure 3.17: Schematic of the cleaning system for sample gas

A) Water-cooled flue gas sampling probe

After the sample gas leaving chamber or chimney, the top priority was to reduce the temperature of sample gas from high temperature (several hundred degrees) to the required temperature. Two same water-cooled gas sampling probes were designed and used to cool down the combustion chamber gas & flue gas (see Figure 3.18 and 3.19). Generally, each sampling probe consisted of three concentric tubes with different diameters and lengths which were welded together. Since the temperature of flue gas was much lower than that of the combustion chamber gas, two water-cooled sampling probes were formed a water loop to save cooling water, which meant the outlet of the flue gas sampling probe was connected to the inlet of the combustion chamber gas sampling probe. The flow rate of the cooling water was fixed at around 1L/ min.

Figure 3.18: The water-cooled probe for sampling flue gas

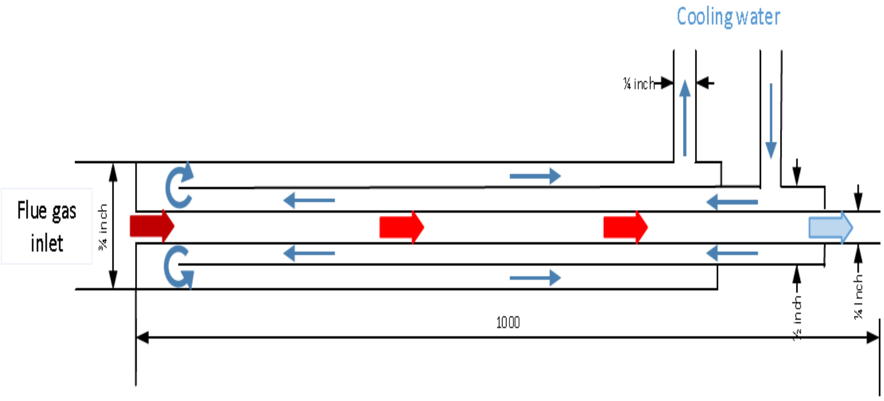

Figure 3.19: Cross sectional diagram of the water-cooled sampling probe

B) Dreschel bottles

After leaving sampling probes, the sample gas passed two dreschel bottles, which acted as water knockouts and initial particle removers (see Figure 3.20). Some glass wool were placed inside the bottles to aid particle and moisture removal and plenty of ice were placed around the bottles were used to cool down the gas inside the bottles helping condensing the moisture.

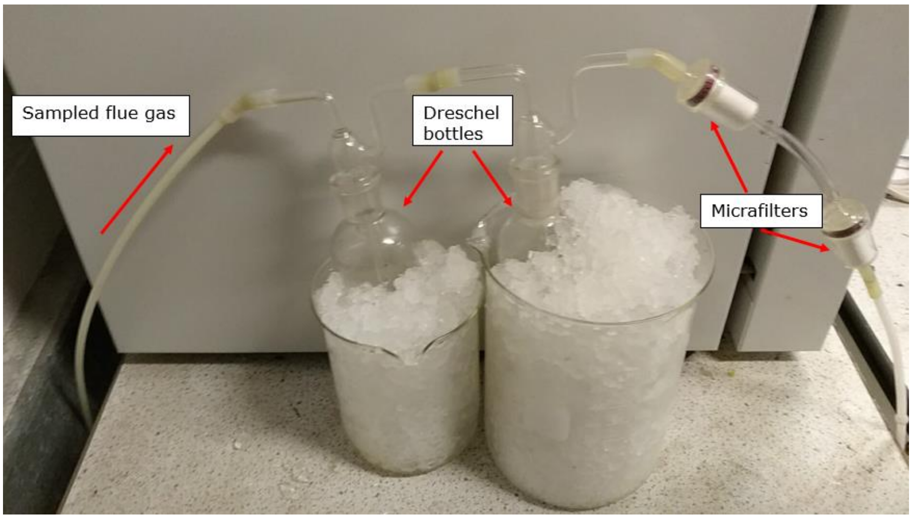

Figure 3.20: Dreschel bottles and disposable filters

C) Disposable Filters

To further protect the Horiba and ABB analyzers, small particles need to be completely eliminated in the sample gas before it entering the analyzers. Therefore, two disposal filters Micrafilter MDE-123 and MDC-123 with efficiency of 95% and 99.99% at 0.3 micron were connected series in the sample gas cleaning system (see Figure 3.20).

3.2.3.3 Data collection

Data collection is one of the essential parts of any experimental test. Data logger is a helpful instrument to provide accurate sensor readings. In this study, dataTaker DT80 was used to measure and record the data based on the created program. As DT80 can only offer five analog input channels, numbered 1 to 5, another CEM 20 (Channel Expansion Module) was used to work with DT80 to expand the number of input channels, up to 20 digital channels. Then, the digital channels were enough to record all the monitors. Details have been listed in Table 3.3.

3.2.4 Test Conditions

As mentioned before, the Ashwell biomass boiler was designed to burn biomass pellets with staged air supplies, therefore, the experiments under three different air staging conditions, named as normal air setting, weak primary air setting and weak secondary air setting were carried out in this study. In the experimental stage, as the primary and secondary air fans were controlled by the single fan inverters, air staging can be only changed by increasing or decreasing the air inlet area of each fan (see Figure 3.21). The details of different air staging conditions are following.

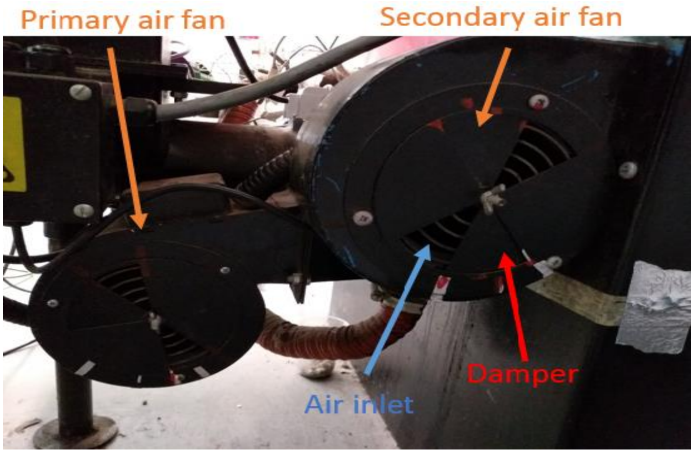

Figure 3.21: Photo of the primary and secondary air fans

Normal air setting: Under this condition, the air fans were operating with the original settings set by the manufacturer at the commissioning stage. The settings of air fans are displayed in Figure 3.22. The red part is the fixed damper which cannot be rotated while the black part is moveable and can be used to change the area of air inlet (white part). A bigger area of the white part means the larger air inlet area.

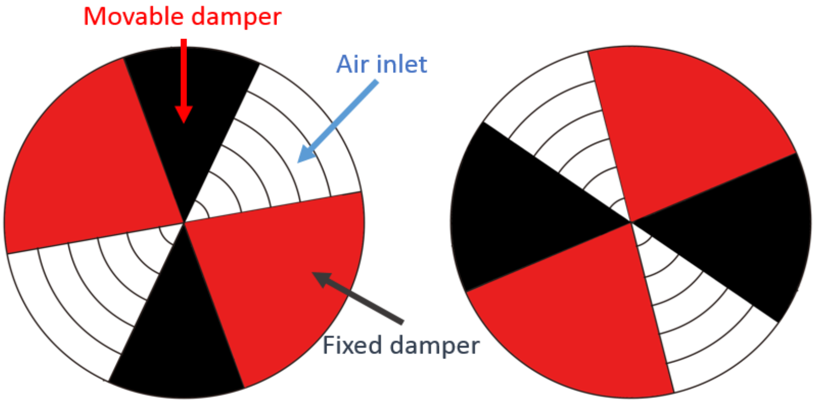

a) Primary air fan setting b) Secondary air fan setting

Figure 3.22: Fans setting for normal air staging condition

Weak primary air setting: Under this condition, the area of primary air fan inlet was reduced by one-third of original position in comparison to the normal air staging by increasing the area of the movable damper part. Hence, the inlet volume for the primary air was reduced to about two-thirds of the value under normal air staging condition while the inlet volume of the secondary air was kept at the same value as the original. The settings of weak primary air fans are displayed in Figure 3.23.

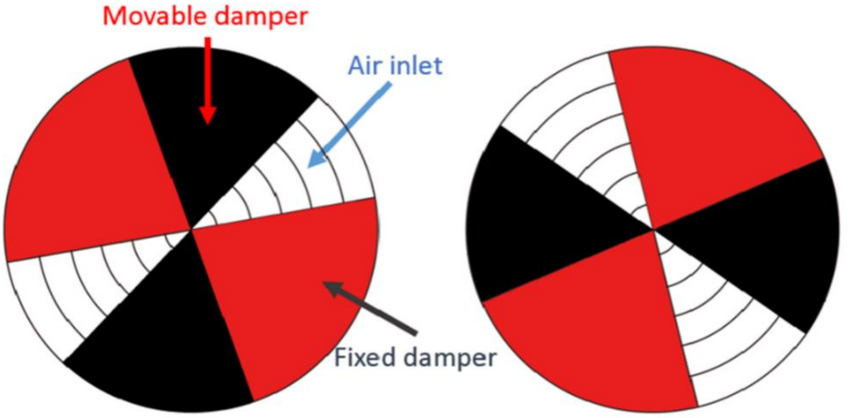

a) Primary air fan setting b) Secondary air fan setting

Figure 3.23: Fans setting for weak primary air condition

Weak secondary air setting: Similar to the weak primary air setting, this time the area of the secondary air fan inlet was reduced by one-third of the original position, which meant the inlet volume of secondary air was reduced to about two thirds while the inlet volume of primary air inlet was kept the same as the original. The settings of weak secondary air fans are shown in Figure 3.24.

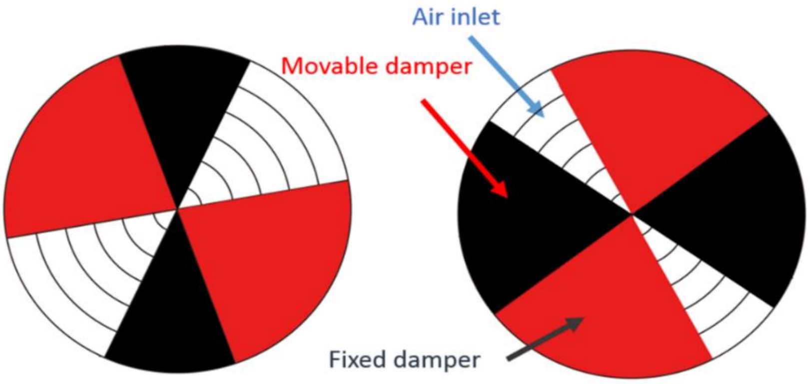

a) Primary air fan setting b) Secondary air fan setting

Figure 3.24: Fans setting for weak secondary air staging condition

The operational procedure of biomass boiler has been presented in section 3.2.1.2. All the tests on the Ashwell biomass boiler were conducted under three air staging conditions to compare the difference. Fuel feeding rate and fan speed were set on the control panel and kept constant for all tests.

3.3 Experimental Set-up for Chapter 6

In this section, the general experimental set-up for Chapter 6 (catalytic tests) is presented, including the synthesis of various catalysts (Co-ZSM-5 pellets, Co and Fe supporting ZSM-5/SiC foams), V-DTF modification and the new synthetic gas analysis system. Moreover, since the nature of V-DTF, the experimental uncertainty of catalytic tests is also discussed at the end of this section.

3.3.1 Catalysts Synthesis

Cobalt (Co) supporting ZSM-5 and ZSM/Silicon Carbide (SiC) catalysts were chosen and synthesized for the potential CH_4-SCR experiments. Also, the other Iron (Fe) supporting ZSM/SiC catalyst was selected to test the catalytic performance in the condition of absence of oxygen. The synthesis methods of catalysts are described below.

3.3.1.1 Synthesis of Co-ZSM-5 pellets

Up to now, there are three main methods to synthesize Co-ZSM-5, including wet ion exchange, impregnation and sublimation. Many studies have been conducted to investigate the effect of synthesis methods on the CH_4-SCR performance. For instance, Wang, Chen and Sachtler (2001) reported that, under the condition of excess oxygen, the catalyst prepared via sublimation had the best performance under 425°C while the catalyst prepared via wet ion exchange had the highest NOx reduction over 425°C. However, Smeets et al. (2008) reported that the difference of performances between different synthesis methods was not evident when keeping other parameters the same or close.

Therefore, the method of wet ion exchange was applied to synthesize Co supporting ZSM-5 catalysts with expected 2.44% and 4.89% Co loading. The pellet type Co-ZSM-5 was prepared by using an aqueous solution of Cobalt (II) nitrate hexahydrate: $Co\ (NO_3)_2 \cdot 6H_2O$ salt (Sigma Aldrich, see Figure 3.25 a). The bare materials for making catalyst were H-ZSM-5 with Si/Al ratios of 12.5 and 60.

Table 3.4: Catalyst synthesis

Catalyst	c (Co salt)
2.44% Co-ZSM-5	0.005 Co nitrate
4.89% Co-ZSM-5	0.05 Co nitrate (threefold ion exchange)

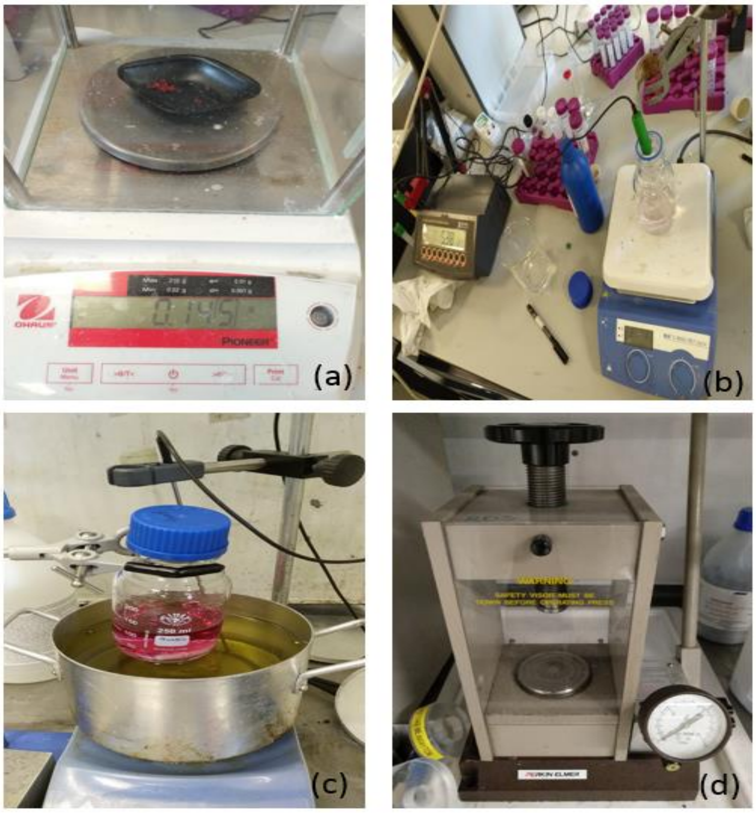

Figure 3.25: Synthesis of Co-ZSM-5 pellets (a).Weighing of Cobalt salt (b). PH adjustment of aqueous solution (c). Suspension stirring (d). Tablet press

The synthesis was carried out in the lab at University of Manchester according to the method of Bellmann et al. (2018). Specifically, 1g of H-ZSM-5 was introduced to 100ml aqueous solution when the solution was heated to 60°C and PH was set to 6.9 by using ammonium hydroxide ($NH_3 \cdot H_2O$) (see Figure 3.25 b). Then the suspension was stirred (24 hours at 60°C condition, see Figure 3.25 c), centrifuged (400 mL water per 1g zeolite) and dried (overnight at 90°C condition). After that, the sample catalyst was calcined in a Nabertherm muffle furnace LE6/11 with P300 controller (5 hours under 550°C condition), pelletized (see Figure 3.25 d), crushed into pellet type and sieved to specific size (250 to 600μm). Some bare H-ZSM-5 pellets with the same size as Co-ZMS-5 pellets were also prepared for the use of blank experiments (see Figure 3.26).

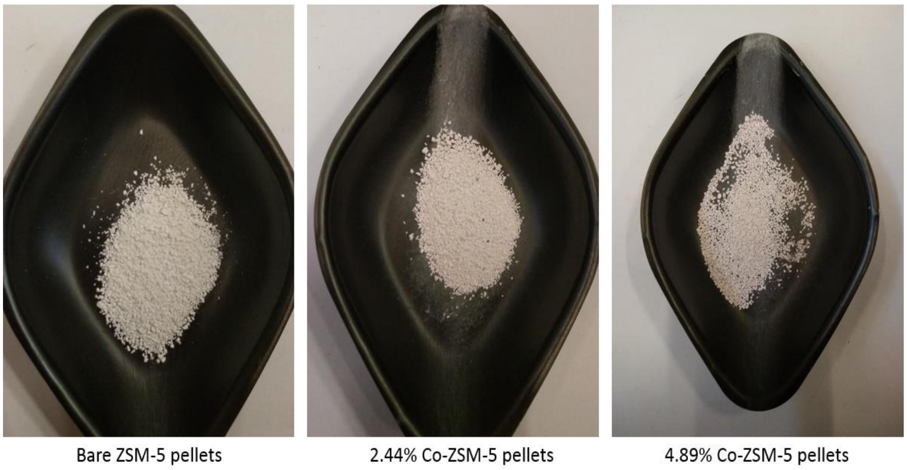
Bare ZSM-5 pellets
2.44% Co-ZSM-5 pellets
4.89% Co-ZSM-5 pellets

Figure 3.26: Photos of the bare ZSM-5, 2.44% & 4.89% Co-ZSM-5 pellets

3.3.1.2 Synthesis of Co-ZSM-5/SiC foams

The synthesis of silicalite-1 seeds was carried out by hydrothermal synthesis. The synthesis solution was prepared with the molar composition of TEOS:

TPAOH: H_2O: C_2H_5OH = 1:0.4:19.5:4 and aged at room temperature under stirring for 24h. The solution was placed in an autoclave reactor and heated by an oven (Memmert UM 400) at 100 °C for one day. The solid product was separated from the liquid phase by centrifugation at 9500 RPM and then washed five times with distilled water and centrifugated in order to reach a neutral pH value. The recovered solid product was dried overnight and used as the silicalite-1 seeds.

ZSM-5/SiC foams were synthesized using the secondary growth method. The SiC foams (ca. 0.3g weight each, 50mm length and 9.5mm diameter) were dip-coated with the silicalite-1 in ethanol solution (C_2H_5OH, 0.65 wt.%) and then dried in an oven at 160°C. Seeded SiC foams were transferred to a reactor for the secondary growth of silicalite-1 seeds into ZSM-5 crystals in the aged synthesis solution with sodium aluminate as the aluminum source. The synthesis solution was prepared with the molar composition of TEOS: NaCl: TPAOH: $NaAlO_2$: H_2O = 1: 0.22: 0.19: 0.08: 178 and aged at room temperature under stirring for 24h. The synthesis process was carried out at 160 °C for 4 days to allow the growth of ZSM-5 crystals on SiC foams. After the synthesis, ZSM-5/SiC foams were washed with distilled water in an ultrasonic bath for 15 min, dried in an oven at 100 °C and calcined in the mentioned muffle furnace at 550 °C for 4h with a ramp rate at 1 °C to remove the template.

H-ZSM-5/SiC foams were obtained by the ion exchange method in aqueous ammonium nitrate solution (1.0 M) at 80℃ for 24h, followed by drying at 100℃ (12h) and calcination at 550℃ (6h). Co-ZSM-5/SiC foams (see Figure 3.27 a) were obtained by the ion exchange in aqueous at 80℃ for 24h, followed by drying at 100℃ (12h) and calcination at 550℃ (6h). The gain weight of Co-ZSM-5 on SiC foam is determined by the weight difference between the dry SiC foam and Co-ZSM-5/SiC foam (ca. 0.1g Co-ZSM-5 in each foam).

Figure 3.27: Photos of (a). Co-ZSM-5/SiC foams and (b). Fe-ZSM-5/SiC foams

3.3.1.3 Synthesis of Fe-ZSM-5/SiC foams

The Ferrisilicate/SiC foams (see Figure 3.27 b) were also synthesized by using the secondary growth method. The detailed introduction of synthesis procedure can be found in Ou et al. (2018). The gained weight of Fe-ZSM-5 in SiC foams was measured by the difference values between the weight of dry SiC foams and that of dry ferrisilicate/SiC foams (ca. 0.4g Fe-ZSM-5 in each foam). 0.5% Fe loading was expected in the synthetic Fe-ZSM-5/SiC foams.

3.3.2 Visual Drop Tube Furnace (V-DTF) Modification

The Visual Drop Tube Furnace (V-DTF) was re-designed to test the viability of emission (mainly NOx) reduction by catalytic technologies with potential catalyst(s). The main functions of V-DTF have been introduced in section 3.1.1. One important point should be pointed out is that although any temperature (high temperature, e.g., above 200°C) can be achieved theoretically by setting specific temperature on the control panel, the actual temperature at some parts of furnace may be far away from the setting temperature. Its impact and related experimental uncertainty will be discussed in section 3.3.5.

Compared with the original setting of V-DTF, the quartz tube and corresponding supports were removed and a new stainless steel flow tube was placed in the V-DTF. The tube had 2030 mm length and was placed vertically along the central axis of furnace, surrounded by the electric heating elements. As the flow and reaction medium of synthesis gas, the stainless steel tube consisted of two 6mm outside diameter (OD) tubes at two ends and a 10mm OD tube with 290mm length in the middle as the main reactor where the catalyst was placed. The schematic of new V-DTF system is shown in Figure 3.28.

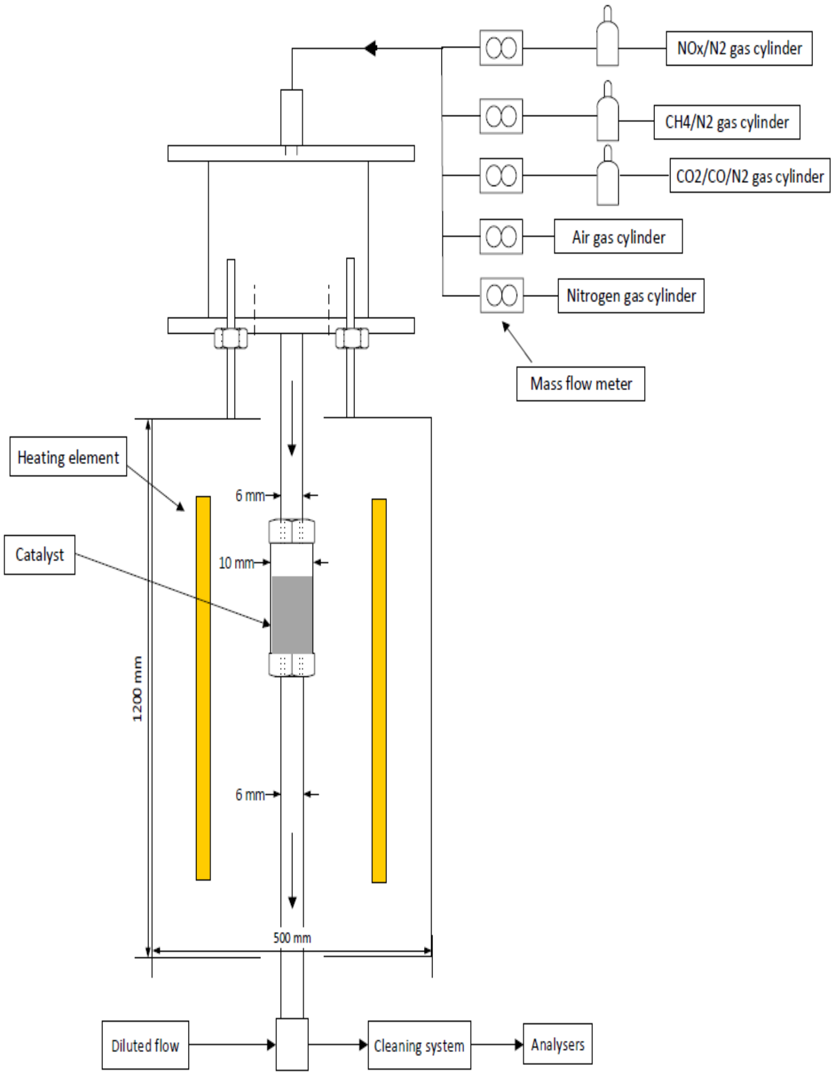

Figure 3.28: Schematic of the modified V-DTF

3.3.3 Synthesis Gas

Although the synthesis gas for catalytic tests was largely different in terms of composition and proportion, the potential synthesis gas was made up of the following five gases:

1) 2% methane (CH_4), balance in Nitrogen

2) 1000ppm NOx, balance in Nitrogen

3) 1500ppm carbon monoxide (CO), 15% carbon dioxide (CO_2), balance in Nitrogen

4) Compressed air

5) Pure Nitrogen (99.5% purity)

Five Aalborg mass flow meters were used to control the flow rates of different synthesis gases (see Figure 3.29). In order to get accurate measured data, the mass flow meters were needed to change their routes in some cases as they had different flow ranges, e.g., 250mL/min, 1000mL/min and 5L/min. Five supply gas routes were connected by flexible plastic tubes, generating a final channel to ensure a sufficient mixing before entering the reaction tube (See Figure 3.28).

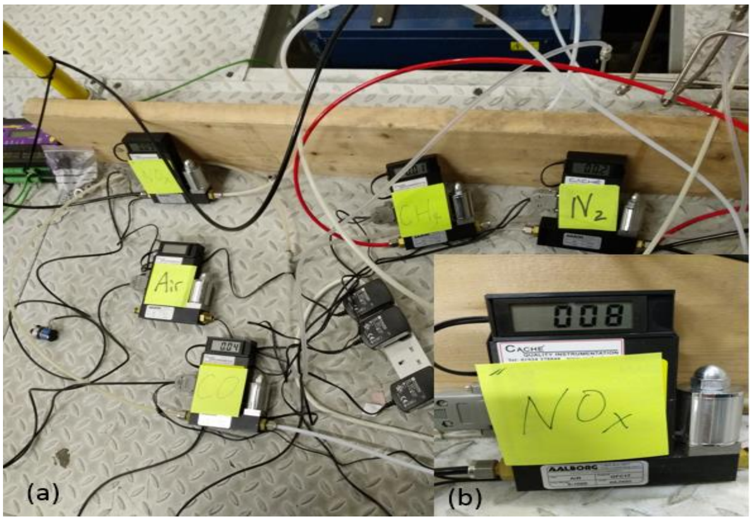

Figure 3.29: Photos of the Aalborg mass flow meters

3.3.4 Synthesis Gas Analysis System

The performance of the proposed catalytic technologies was evaluated by comparing the concentration variation of synthesis gas compositions before and after flowing through the fixed bed (catalytic reactor). A new synthesis gas analysis system was built up in order to analyze and record the variation of some main components (NOx, CH_4, CO, CO_2 and O_2) (see Figure 3.30).

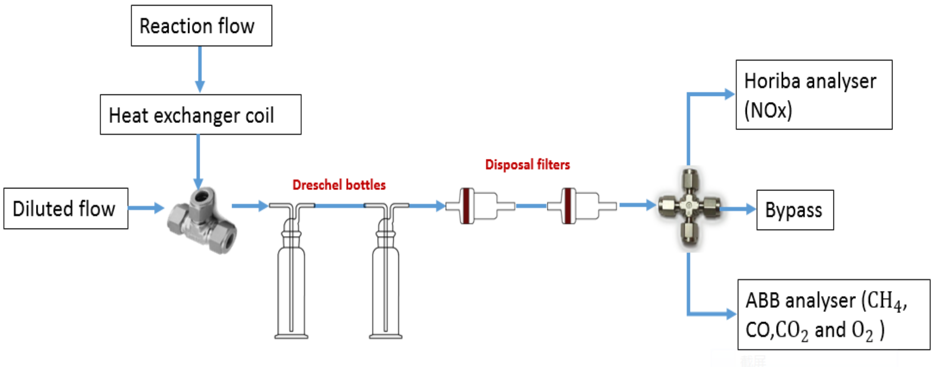

Figure 3.30: Schematic of the synthesis gas analysis system

The new synthesis gas analysis system for catalytic tests was generally similar to the one designed for biomass boiler tests. Two sets of Horiba and ABB gas analyzers were used to measure and record the concentration of the synthesis gas. The introduction of these analyzers has been presented in section 3.2.3.1. Compared with the system used for the biomass boiler tests, a homemade copper heat exchanger coil was made (see Figure 3.31) to replace the water-cooled probe (see Figure 3.18) in the system. The copper coil was placed in a large plastic bucket surrounded by a mixture of ice and water to cool down the synthesis gas to the required temperature (5°C to 50°C) for further gas analysis. A bypass route was also built in the gas analysis system to release the extra gas flow and protect the gas analyzers in case ‘overflow’ issue happened.

Figure 3.31: Photos of the homemade copper heat exchanger coil

Furthermore, due to the small flow rate of synthesis gas used for the catalyst tests, another diluting flow route (using either air or nitrogen, depending on the specific case) was included to add the diluting gas to the synthesis gas flow (reaction gas) in some cases in order to meet the required lower flow rate limit of the gas analyzers. However, the dilution method also brought in a problem that the concentration of synthesis gas was diluted by the large flow before entering gas analyzers. Therefore, the results of emission reduction at high temperature were shown in percentage term (%), the ratio of emission variation to the reference value obtained at room temperature. The equations of emission conversion rates are shown below:

$$\text{NOx conversion rate (\%)} = \frac{\text{NOx}_{\text{RT}} - \text{NOx}_{\text{HT}}}{\text{NOx}_{\text{RT}}} \qquad [3.2]$$

$$\text{CH}_4 \text{ conversion rate (\%)} = \frac{\text{CH}_{4\ \text{RT}} - \text{CH}_{4\ \text{HT}}}{\text{CH}_{4\ \text{RT}}} \qquad [3.3]$$

$$\text{CO conversion rate (\%)} = \frac{\text{CO}_{\text{RT}} - \text{CO}_{\text{HT}}}{\text{CO}_{\text{RT}}} \qquad [3.4]$$

Where RT means the emission value obtained at room temperature, HT means the emission value obtained at a high temperature.

3.3.5 Experimental Uncertainty

As mentioned before, there may be a temperature difference between the actual testing temperature inside the furnace and the operating temperature showing on the control panel of V-DTF. According to Sarroza et al. (2017), at a fixed setting temperature, the furnace temperature profile inside the furnace was uneven. Also, based on the original design of the V-DTF, the furnace set temperature was controlled according to the temperature measurement of a single thermocouple placed at the center of the furnace. Hence, it was necessary to measure the temperature profile of V-DTF and determine the position of main reactor before conducting catalytic eq when taking the size of furnace (1200mm × 500mm × 500mm) and internal heat transfer into account.

CHAPTER 4. INVESTIGATION OF FUEL CHARACTERISATION AND COMBUSTION BEHAVIOUR BY USING INDIVIDUAL BIOMASS PELLETS

4.1 Introduction

As mentioned in literature review (Chapter 2), oxy-fuel combustion as one of the CCS technologies has shown its promising future to control CO_2 emission and achieve clean combustion. In this chapter, combustion behavior of various biomass fuels under both air combustion and oxy-fuel combustion conditions is investigated by conducting individual pellet combustion tests in the Visual Drop Tube Furnace (V-DTF) integrated with a high-speed camera. The details of experimental set-up, including apparatus, selected biomass fuels and test conditions have been introduced in section 3.1. The obtained experimental results are shown and analyzed in the following sections.

4.2 Phases in Individual Pellet Combustion

As introduced in section 3.1.4, three thermocouples were used to measure center temperature (N1), side surface temperature (N2) and top surface temperature (N3) of the pellet sample during individual pellet combustion process (see Figure 3.4). The combustion phases can be spotted and separated by using the temperature variations observed during the individual pellet combustion process.

These combustion phases are illustrated by using the temperature distribution of one of the wood pellet combustion tests (30% O_2-70% CO_2 and pre-set furnace temperature of 800°C) in Figure 4.1. The flame images captured during the wood pellet combustion test under the same conditions are displayed in Figure 4.2, which supports the identification of the combustion phases defined in Figure 4.1. The details of video-image conversion procedure will be presented in section 4.5.1.

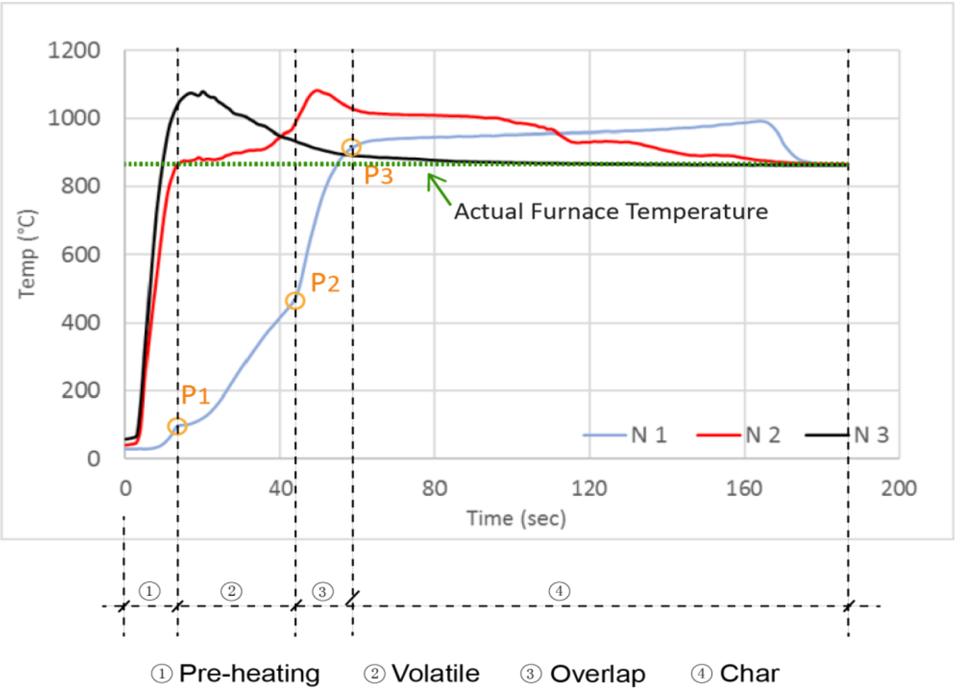

Figure 4.1: One example of temperature distribution of the individual pellet combustion (Wood pellet under 30% O_2-70% CO_2 and 800 °C)

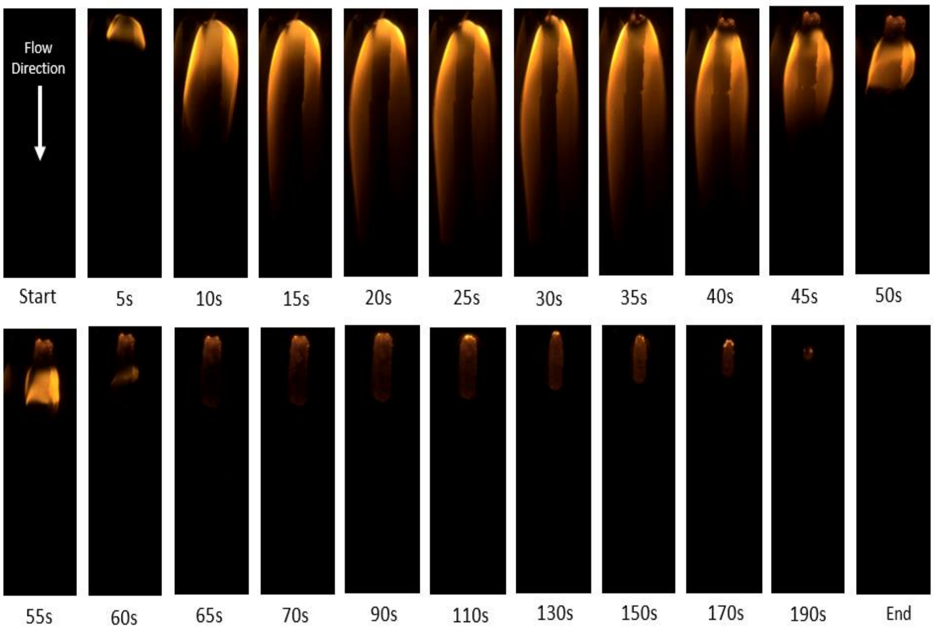

Figure 4.2: One example of sequential steps of the individual pellet combustion (Wood pellet under 30% O_2-70% CO_2 and 800 °C)

Stage 1, Pre-heating phase: The biomass pellet underwent a pre-heating phase at the beginning of combustion after being rapidly inserted into the quartz tube (reactor). The measured side surface temperature (N2) and top surface temperature (N3) had sharp increases as they were exposed to the high pre-set temperature for the quartz tube reactor, which itself was heated by the high-temperature heating elements in the furnace through thermal radiation. By contrast, the heating rate of the center of the pellet (N1 temperature) was much slower. The pellet center was heated mainly by heat conduction before the pellet was ignited. During the heating process, the moisture inside the pellet was gradually evaporated. The P1 which was assumed to be the end point of pre-heating phase and the starting point of volatile released combustion phase was defined as the first infection point of N1 temperature curve (blue line). The N1 temperature of P1 was around 110°C to 150°C, slightly different with various cases due to different heat transfer rates under different test conditions, thermocouple reaction time and data logger trigger time.

Stage 2, Volatile combustion phase: After finishing the pre-heating, the tested pellet was further heated, resulting in volatile release and volatile combustion. In this phase, a clear volatile flame could be observed, for example the images from 10s to 35s in Figure 4.2. From the temperature perspective, N3 (black line) was seen to reach its peak temperature of the whole combustion process in a short time, and then decrease gradually. It should be pointed out that the feed gas flow was introduced from the top of V-DTF to bottom. Hence, the top part of pellet sample was always ignited first with the help of oxygen flow and the high ambient temperature. The captured images shown in Figure 4.2 from the corresponding video support this explanation. The tendency and direction of flame generation are also shown in Figure 4.2. The volatile flame appeared and heated the thermocouple which measured the top surface temperature of pellet sample, resulting in the mentioned peak N3 temperature. Then, the flame grew downward along with the flow direction, having less effect on the measured temperature of N3 temperature, which gradually approaching the ambient (furnace) temperature. During this stage, the N2 temperature was still increasing though its increment was getting slower than that in stage 1. It was attributed by the additional heat generated from volatile combustion of the tested pellet when it was over pre-set furnace temperature. Similarly, when analyzing the N1 temperature curve, it can be seen that the center temperature of pellet sample had a more rapid increase due to the occurrence of volatile combustion after pre-heating phase. The characteristics of volatile flame can be affected by many factors such as ambient temperature and combustion gas composition and this will be further discussed in section 4.5.2. The volatile combustion phase was assumed to end when the N1 temperature reached the second temperature inflection point (P2).

Stage 3, Overlap phase: Depending various factors such as fuel particle sizes, properties, combustion conditions, the volatile combustion phase and char combustion phase may occur consecutively. In this study, from temperature perspective (based on Figure 4.1), it was interesting to observe that the heating rate of N1 in this new defined phase was steeper than that in volatile combustion (stage 2). From the flame images (such as the 55s and 60s images shown in Figure 4.2 which was already entering the char combustion stage), there was still a weak flame surrounding the pellet sample. Although volatile flame was not visible from the original images near the end of this stage (for instance the 65s one), the weak flame could be still observed by using post-image technology (MATLAB software). That proved volatile combustion continued when char combustion started to take place as the colour of pellet top turned into 'orange and alight'. Hence, an overlap stage of volatile combustion and char combustion using the N1 temperature was defined. Similar to the definition for the end of stage 2, this overlap phase was considered to terminate when N1 curve reached the third temperature inflection point (P3), which was also the moment when volatile flame entirely disappeared from the processed images.

Stage 4, Char combustion phase: In the final stage, the pellet sample turned into full char combustion phase and the char residue was heated continuously. In this stage, bright char could be observed until the end of char combustion (burnout). From Figure 4.1, it can be found that the char combustion phase took a much longer time than that in the volatile combustion phase or the overlap phase. The N1 temperature kept rising due to the heat from char combustion and achieved its peak temperature when heat was transferred to the center of pellet where the thermocouple was placed. By observing the captured images of char combustion in Figure 4.2, it can be found that the shape of biomass pellet remained intact though its size was getting smaller during char combustion. Also, no breakage or bending of pellet was observed during the tests.

Apart from the discussed wood pellet sample (30% O_2-70% CO_2 and pre-set furnace temperature of 800°C), results of other tested samples can also be divided into four phases mentioned above. Correspondingly, three temperature inflection points can also be found in each pellet sample test. The only exception happened in the group of peanut shell pellet tests. Specifically, the second temperature inflection points (P2) in some peanut shell tests (e.g. all the pellet tests under 800°C condition) were vague to find when comparing with other types of pellets. This is likely due to by the bigger size of peanut shell pellets, especially larger diameter (c.a. 8.5mm, others are c.a. 6mm). Due to distinct temperature gradient inside the pellet sample, char combustion would be already started when the pellet was still undergoing intensive volatile combustion. As the heating rate of char combustion was much lower than that of volatile combustion, the effect of char combustion on temperature was less evident in peanut shell pellet samples, which made the inflection point between volatile combustion and overlap phases hard to observe.

4.3 Temperature Measurement of Individual Pellet Combustion

4.3.1 Temperature Distribution

The temperature distributions of various biomass pellets under different pre-set temperature (800°C and 900°C) and ambient gas (conventional air and different ratios of O_2-CO_2 mixture) conditions are shown in Figure 4.3 & 4.4 (wood pellets) and Figures A.1 to A.8

(straw, miscanthus, torrefied wood and peanut shell pellets). It should be mentioned that each condition (a specific type of biomass pellet in one condition of ambient gas and pre-set furnace temperature) was repeated at least three times to reduce experimental error, but only a typical set of results is presented in this chapter due to a large number of samples. The actual furnace temperatures at the locations where pellets were placed for combustion tests were measured to be around 770°C and 865°C by applying all the thermocouples (N1, N2, N3) at the end of each pellet combustion test corresponding to the set furnace temperature of 800°C and 900°C, respectively.

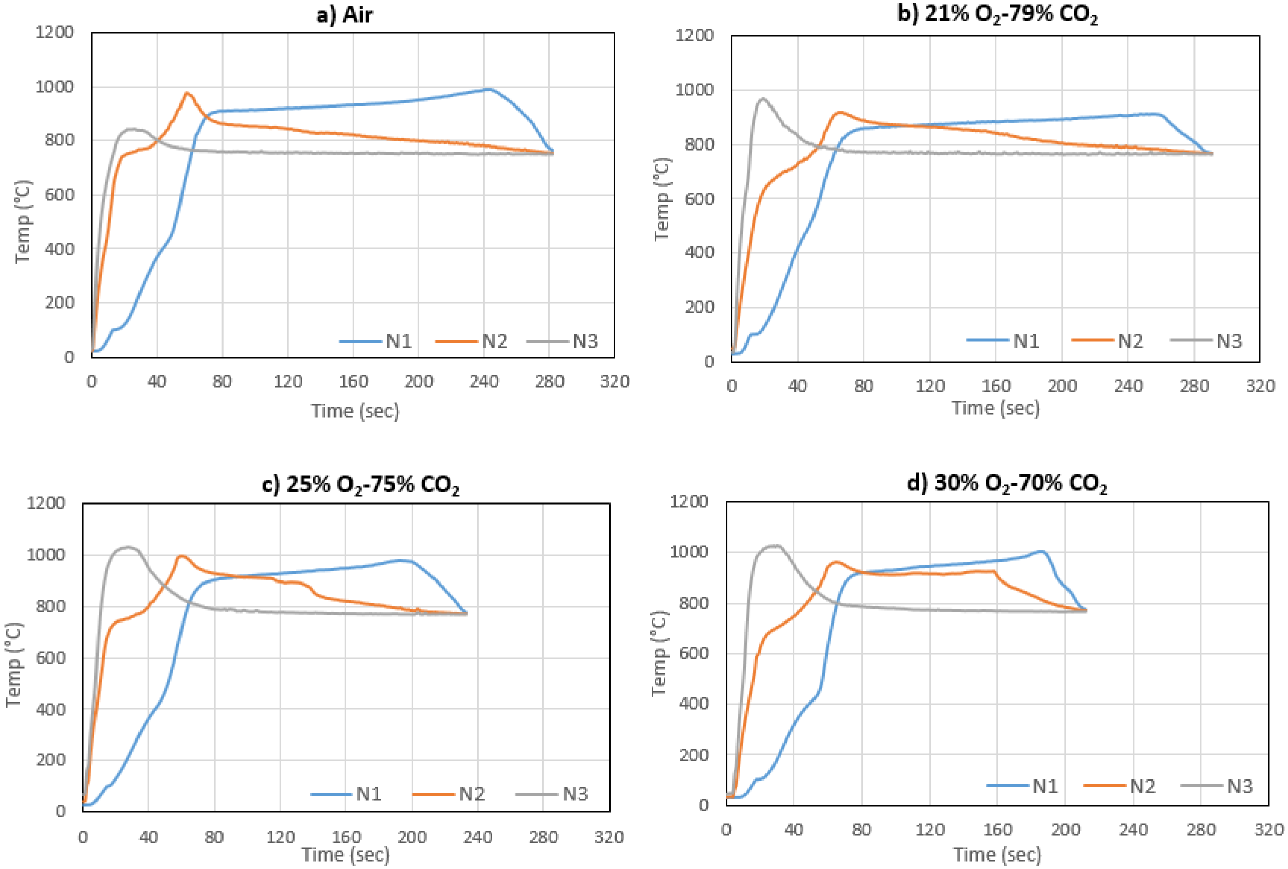

Figure 4.3: Temperature distributions of wood pellet combustion test with the furnace set temperature of 800°C: a) air; b) 21%O_2-79% CO_2; c) 25%O_2-75% CO_2; d) 30%O_2-70% CO_2

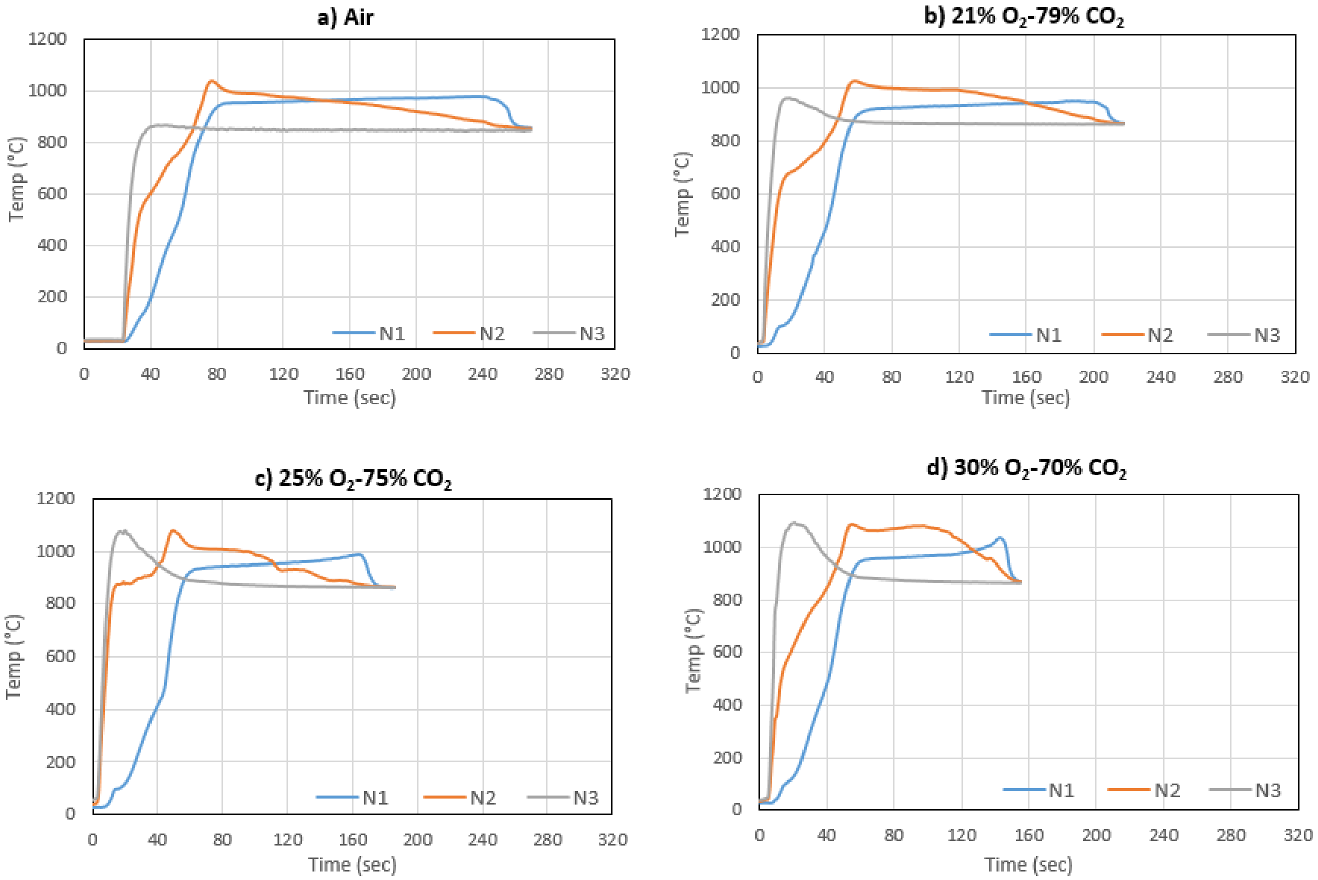
a) Air

b) 21% O_2-79% CO_2

c) 25% O_2-75% CO_2

d) 30% O_2-70% CO_2

Figure 4.4: Temperature distributions of wood pellet combustion test with the furnace set temperature of 900°C: a) air; b) 21%O_2-79%CO_2; c) 25%O_2-75%CO_2; d) 30%O_2-70%CO_2

4.3.2 Thermocouple Measurement Error

It is well-known that the measured temperature of a hot gas or flame may differ from the actual temperature when using thermocouple(s). That is due to various potential errors which affect temperature measurement process, including heat conduction loss along the thermocouple wires, catalytic loss because of the reactions happened at the junction part and heat radiation loss from the thermocouple to the cooler or hotter source (Heitor and Moreira, 1993; Pitts et al., 1998). The schematic of potential heat losses of a thermocouple is shown in Figure 4.5.

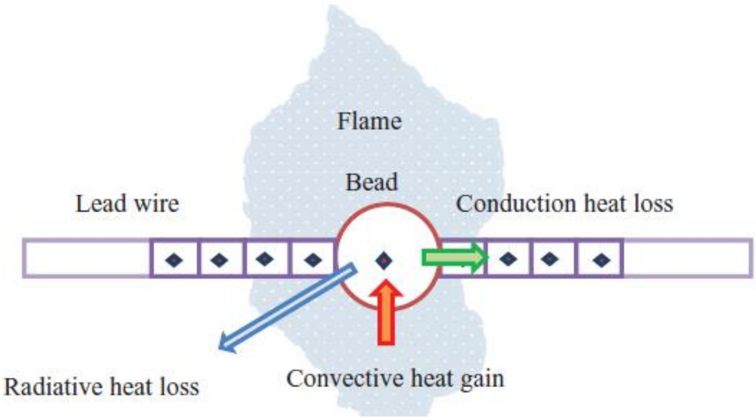

Figure 4.5: Schematic of heat losses of a thermocouple with the existence of flame (Hindasageri, Vedula and Prabhu, 2013)

Among all the losses, the catalytic and conduction ones can be largely avoided or minimized by selecting a suitable type of thermocouples while the radiation loss remains the most significant error when measuring high-temperature gas.

The loss leads to a lower measured temperature than the actual gas temperature in some applications. For instance, there was up to 250°C temperature error out of 1400°C level in the measurement of Attya and Whitelaw (1981) when they applied a 3mm diameter thermocouple in a spray flame.

4.3.2.1 Correction Methods

It has been proposed that the level of radiation error is affected by some properties of the hot gas and thermocouple. Specifically, more radiation error is generated by broader temperature gap between the measured gas and surrounding environmental temperature, larger diameter of thermocouple and slower feed gas velocity (or smaller Reynolds number) (Brohez, Delvosalle and Marlair, 2004; Hindasageri, Vedula and Prabhu, 2013). There are two common experimental methods to correct the readings of thermocouples used for flame temperature measurement in combustion environment, the reduced radiation error method and the extrapolation method, which were detailed by in Lemaire and Menanteau, (2017). Although the two methods are slightly different in terms of mechanism, both of them are used to estimate the radiation error by using two thermocouples with the same material but different diameters.

In addition to the two experimental methods mentioned above, there are some theoretical methods to calibrate the measured temperature. For example, Pitts et al. (2003) used reaction 4.1 to correct the temperature measured in a fire environment.

$$\mathrm{T} = \mathrm{T_c} + \frac{\mathrm{d}^{0.55}}{\mathrm{U}^{0.45}} * \left(\mathrm{T_c}^4 - \mathrm{T_s}^4\right) \qquad [4.1]$$

Where T was the actual gas temperature (K), Tc was the temperature measured by thermocouple (K), $\mathrm{T_s}$ was the environmental temperature (K) which was the actual furnace temperature, d was the thermocouple diameter (m) and U was the flow velocity (m/s) over the thermocouple. Reaction 4.1 shows that the temperature difference between the actual and measured temperatures (T-$\mathrm{T_c}$) becomes smaller with a smaller diameter thermocouple and a larger gas flow velocity. However, the computed temperature showed an unreasonable result (temperature error rate＞100%) when applying reaction 4.1 in this study.

Then, an upgraded method (reactions 4.2 to 4.4) was applied based on Hossain et al. (2013).

$$\mathrm{T} = \mathrm{T_c} + \epsilon \cdot \sigma \cdot \frac{(\mathrm{T_c}^4 - \mathrm{T_s}^4)}{\mathrm{h_c}} \qquad [4.2]$$

$$\mathrm{Nu} = \frac{\mathrm{h_c} \cdot \mathrm{d}}{\mathrm{k}} \qquad [4.3]$$

$$\mathrm{Re} = \frac{\mathrm{v} \cdot \mathrm{d_h}}{\gamma} \qquad [4.4]$$

Where T, T_c and T_s were the same terms introduced in reaction 4.1. ε was the emissivity of the thermocouple (ε = 0.28) and σ was the Stefan–Boltzmann constant ($\sigma = 5.67 \times 10^{-8}\mathrm{W} \cdot \mathrm{m}^{-2} \cdot \mathrm{K}^{-4}$), $\mathrm{h_c}$ was the convective heat transfer coefficient ($\mathrm{W} \cdot \mathrm{m}^{-2} \cdot \mathrm{K}^{-1}$) which was determined by the Nusselt (Nu) number. In the equation of Nu number (see reaction 4.3), d was the diameter of thermocouple wire and k was the gas conductivity (the value varied with temperature). Meanwhile, the value of Nu number was related to Re number (laminar or turbulent flow, according to reaction 4.4). γ ($\mathrm{m^2/s}$) and u (m/s) were the kinematic viscosity and velocity of the fluid respectively.

4.3.2.2 Correction of Measured Temperature

According to the introduction of thermocouple measurement error, N2 and N3 thermocouples in this study needed to be corrected as they were used to measure the external temperature of pellet sample (side surface and top surface temperature) and mainly suffered the effect of heat radiation from the furnace. On the other hand, N1 thermocouple which used to measure the internal center temperature had less effect by heat radiation. Hence, the measured N1 temperature was assumed as actual center temperature and did not need to be corrected.

Figure 4.6 shows the uncorrected (solid line) and corrected (dashed line) temperature by using the results of miscanthus pellets under 800°C and various ambient gas conditions. It displays that the trends of temperature errors under air and oxy-fuel combustion conditions were similar, which were mainly affected by the temperature difference between measured and environment (pre-set furnace) temperatures. Generally, a broader temperature difference would result in a more significant temperature error. The most significant temperature error happened at the highest measured temperature (990.0°C), having the maximum temperature difference of 88.1°C under 30% O_2-70% CO_2 @ 800°C. The effect of changing ambient atmosphere from air to O_2- CO_2 mixture on temperature error was less noticeable since the numerical difference of gas conductivity had a minor impact on the temperature correction.

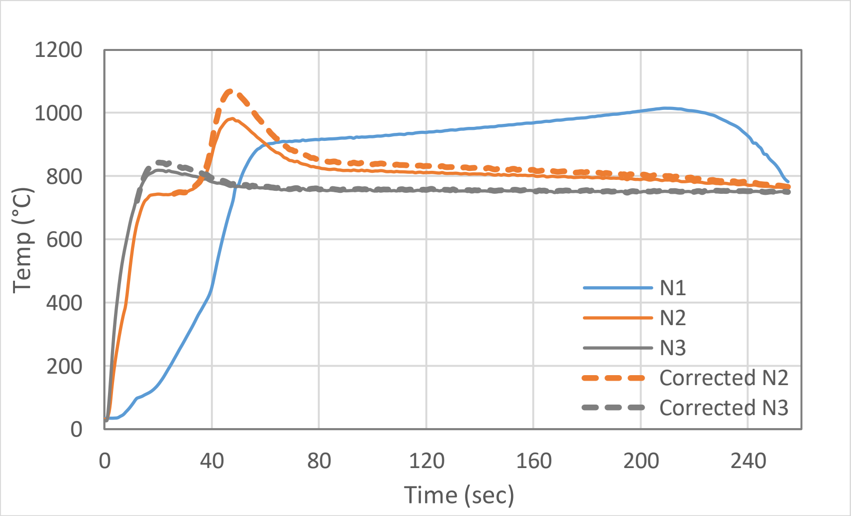

a. Air @ 800°C

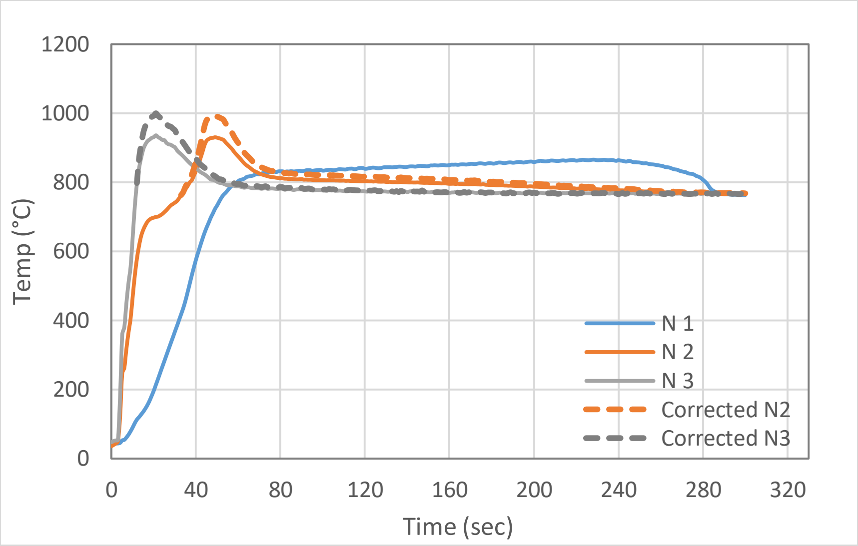

b. 21% O_2-79% CO_2 @ 800°C

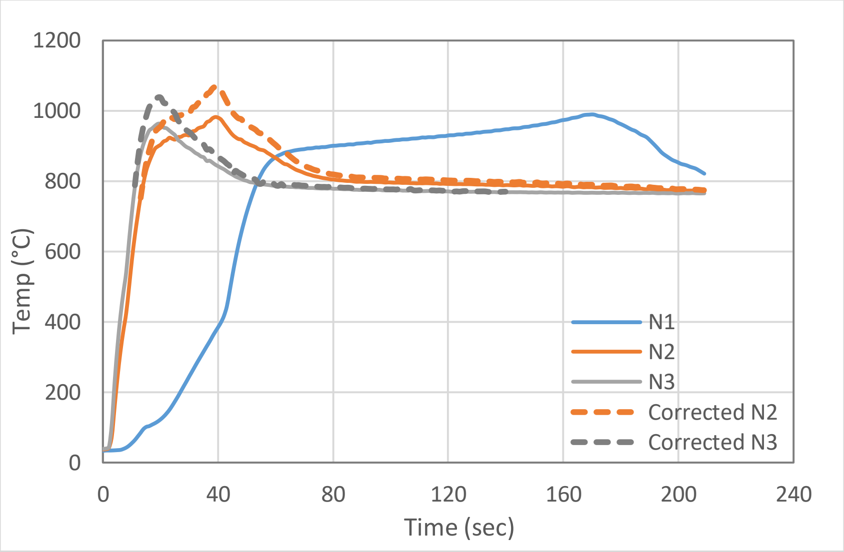

c. 25% O_2-75% CO_2 @ 800°C

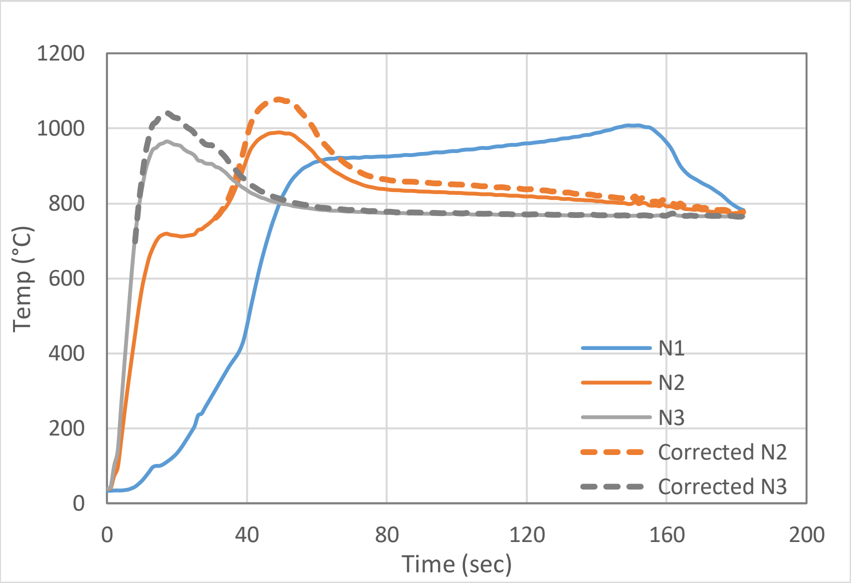

d. 30% O_2-70% CO_2 @ 800 ℃

Figure 4.6: Uncorrected and corrected temperature measured by thermocouple: a) air; b) 21%O_2-79%CO_2; c) 25%O_2-75%CO_2; d) 30%O_2-70%CO_2 (miscanthus tests at 800°C)

4.3.3 Effect of Gas Composition on Temperature Distribution

From the last section, it can be seen that the corrected temperature followed the same trends of the uncorrected temperatures. Because of this observation, the uncorrected temperature was directly used to inspect the effect of ambient gas composition on temperature distributions. As mentioned before, the highest top surface temperature of each pellet sample (peak N3 temperature) was caused by ignition and volatile combustion. However, this peak value appeared to be affected by the composition of ambient gas. In O_2- CO_2 atmospheres, the peak temperature increased significantly when the oxygen fraction was increased from 21% to 25%. Then, the peak temperature had a smaller increment when further increasing the oxygen fraction to 30%. As expected, the higher peak temperature was determined by the more mass flux of oxygen in O_2- CO_2 atmospheres. However, the relationship of peak temperature between air and 21% O_2-79% CO_2 atmospheres was vague due to the limited experimental samples and the uncertainty caused by recording device, which will be further discussed in section 4.3.4.

4.3.4 Experimental Uncertainties on Temperature Measurement

Some experimental set-up uncertainties cannot be neglected when analyzing the measured temperatures. The first uncertainty is the positions of thermocouples placed around the tested pellet. The N1 thermocouple was supposed to be located at the middle of central axis of each pellet sample. However, the hole to hold the N1 thermocouple which was manually drilled may deviate from the central axis practically, hence resulting in a lower peak temperature. Meanwhile, a position higher or lower than the middle of central axis may also cause a variation in the peak temperature. Similarly, the temperature measurements of N2 and N3 may have the similar concerns. Compared with the intended experimental set-up, the position of a thermocouple (N2 or N3) away from top or side surface of the pellet sample may result in a lower peak temperature as well. Secondly, the deviation of the measured peak temperatures may relate to the recording device and its measurement method. The data logger which was used to record the temperature data was recording the data at the frequency of once per second and the thermocouple had a specific reaction time of 0.3s. Hence, within a short combustion process with rapid temperature variations, the recorded temperatures have varying uncertainties which may include a large uncertainty to the peak temperature measurement. Thirdly, some selected pellet samples may not be in ideal cylindrical shapes as they were made by pellet manufacturing in large, especially the top or bottom part. This may have an impact on the measured top surface temperature (N3) of pellet sample.

4.4 Burning Time of Biomass Pellet

The burning time of biomass pellet is one of the hottest topics in combustion research field. Both effects of air/ oxy-fuel atmosphere and pellet type were inspected in this series of experiments. The approach to separate the phases (total, volatile, overlap and char) of combustion process of individual biomass pellet has been presented in section 4.2. The associated periods of burning time based on different phases are shown in Figure 4.7 to 4.11. It should be noted that burning time was used as the comparative criterion in this study, not burning rate based on either volume or mass which normally used in other pulverized particle experiments. Compared with the critical effect of physical parameters on small particle combustion, that effect on pellet combustion was less significant as most of the selected pellets (W, M, S and T) had similar diameter, length and density (see Table 4.1). Therefore, the burning times of different pellets were directly used to compare and analyze their combustion performance. The only exception was the peanut shell pellet, which had similar density but bigger volume (diameter) than the other four types of pellets. The same y-scale (0 to 250s) had been used for Figures 4.7 to 4.10 to enable easy visual comparison of burning tomes for wood, straw, miscanthus and torrefied wood pellet combustion under different gas environments and both furnace set temperatures. However, a bigger y-scale (0 to 450s) had to be used for Figure 4.11 as the larger peanut shell pellets had much longer burning times than the other four biomass pellets.

Table 4.1: Volume and density ranges of the tested biomass pellets

Pellet type	**Volume range (cm^3)**	**Density range (g/cm^3)**
Wood	1.40~1.60	0.51~0.55
Straw	1.38~1.92	0.47~0.57
Miscanthus	1.18~1.61	0.48~0.54
Torrefied wood	1.11~1.54	0.49~0.57
Peanut Shell	2.43~3.21	0.48~0.54

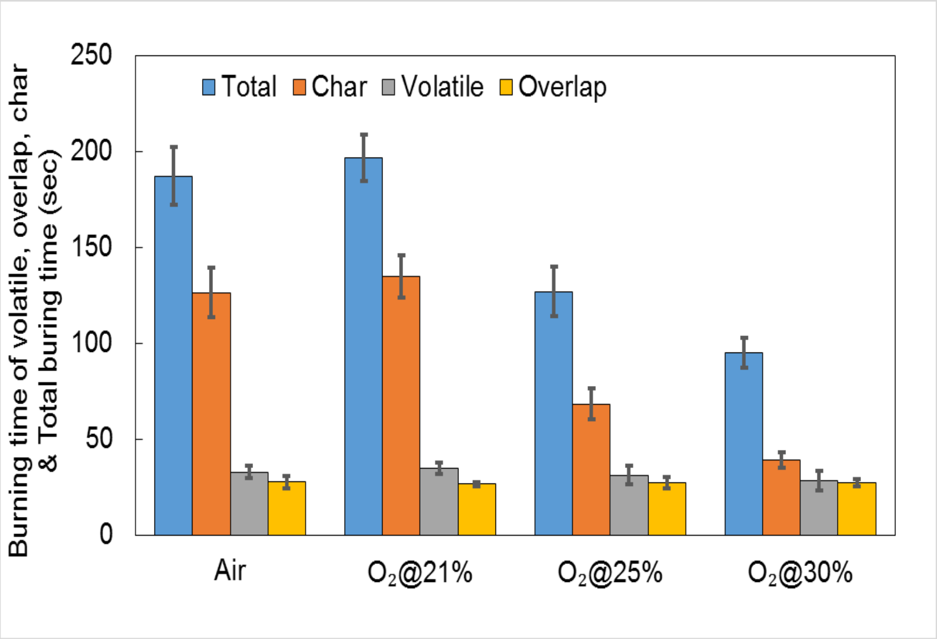

(a) Tests under 800°C

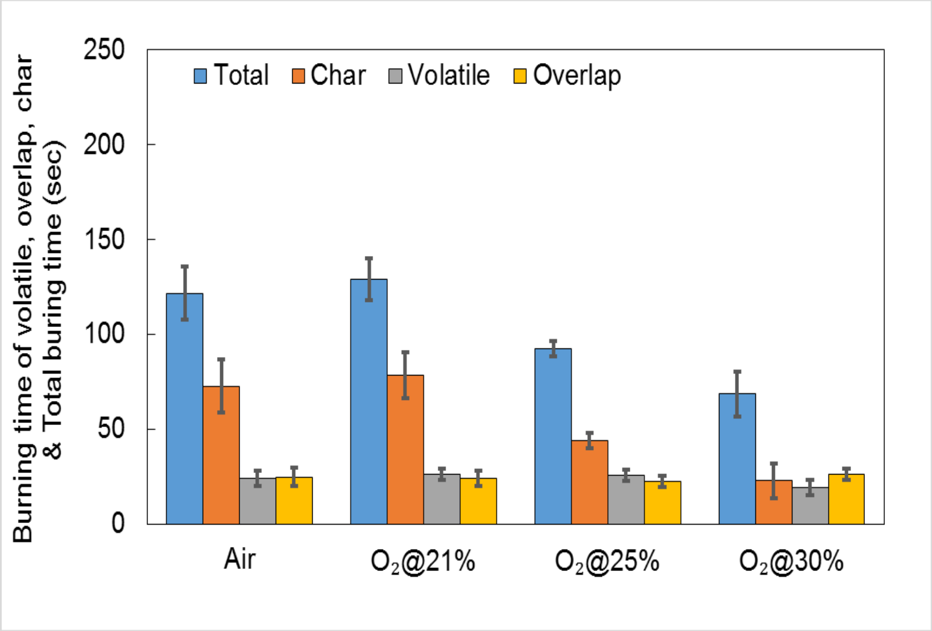

(b) Tests under 900°C

Figure 4.7: Burning times (total, volatile, overlap and char) of wood pellets under air and oxy-fuel combustion atmospheres with different ambient gases

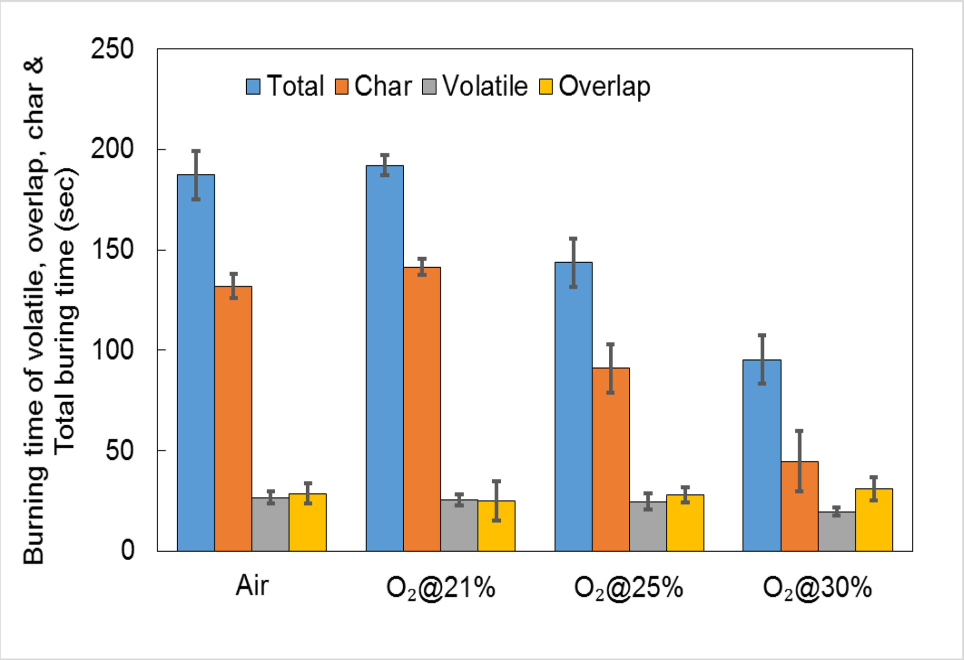

(a) Tests under 800°C

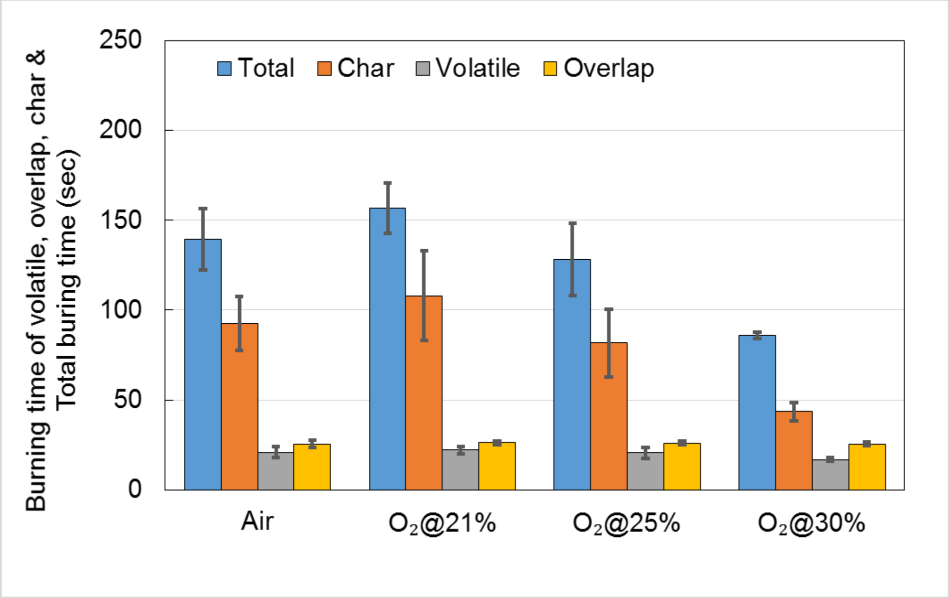

(b) Tests under 900°C

Figure 4.8: Burning times (total, volatile, overlap and char) of straw pellets under air and oxy-fuel combustion atmospheres with different ambient gases

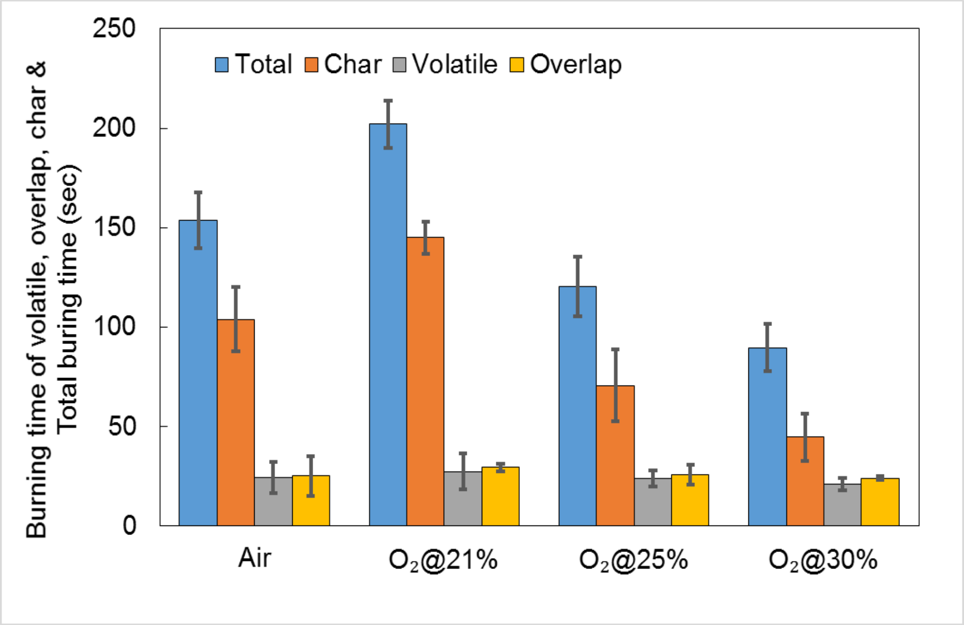

(a) Tests under 800°C

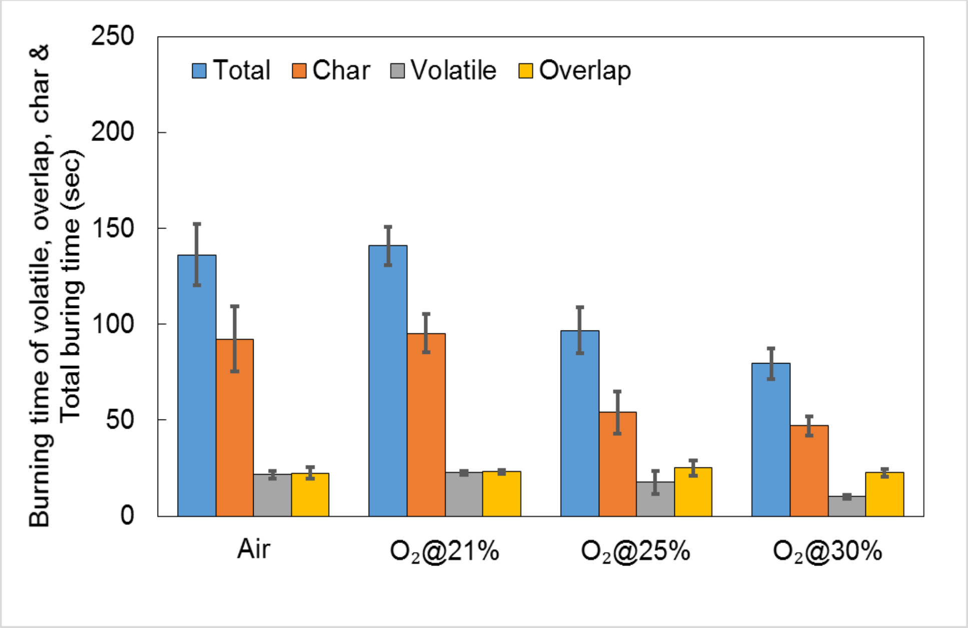

(b) Tests under 900°C

Figure 4.9: Burning times (total, volatile, overlap and char) of miscanthus pellets under air and oxy-fuel combustion atmospheres with different ambient gases

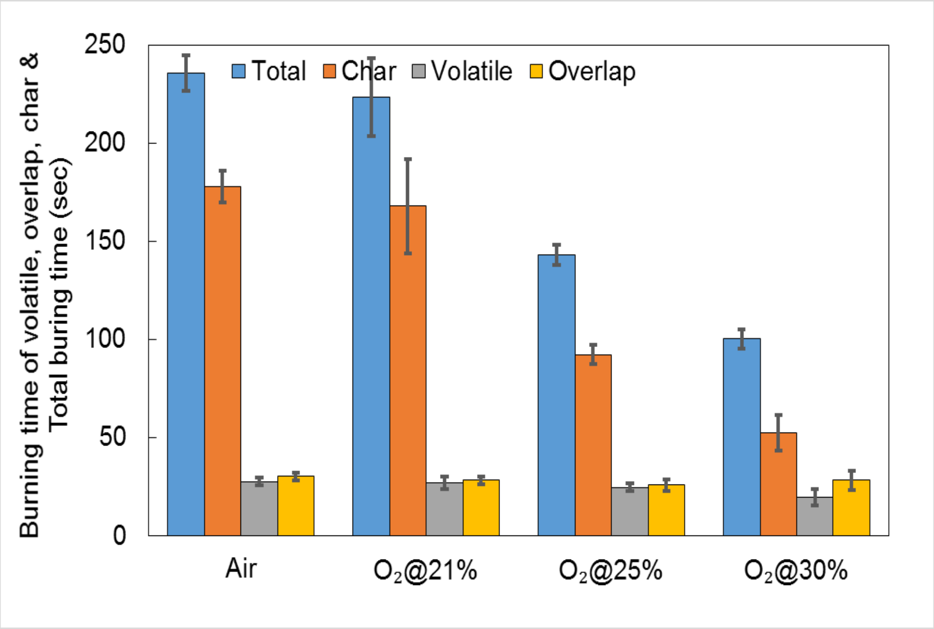

(a) Tests under 800°C

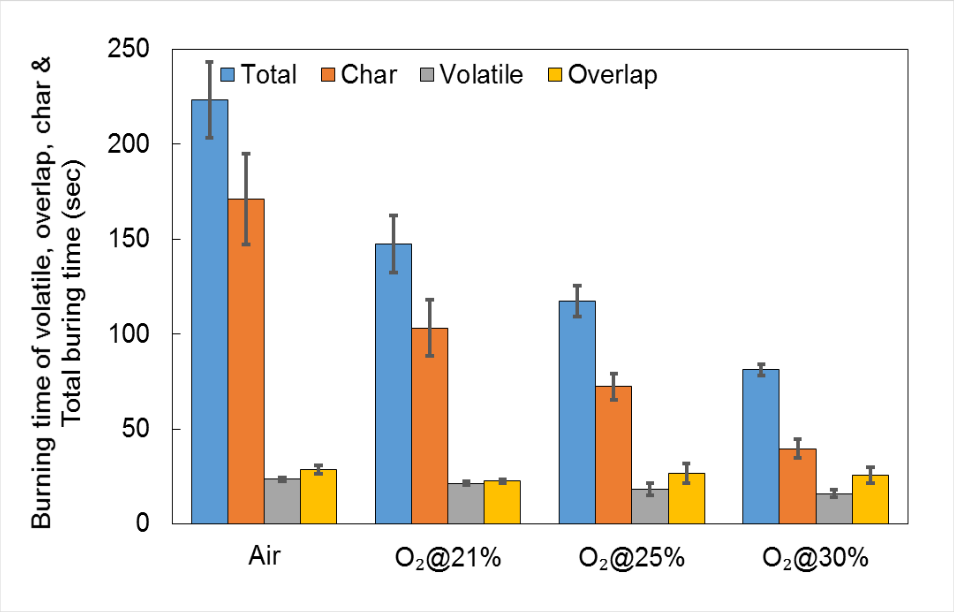

(b) Tests under 900°C

Figure 4.10: Burning times (total, volatile, overlap and char) of torrefied wood pellets under air and oxy-fuel combustion atmospheres with different ambient gases

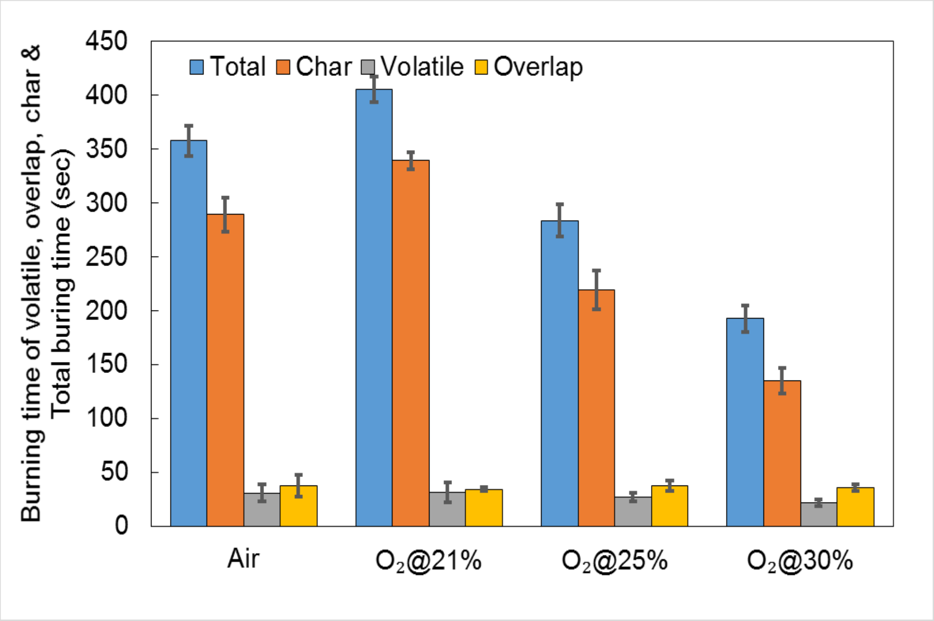

(a) Tests under 800°C

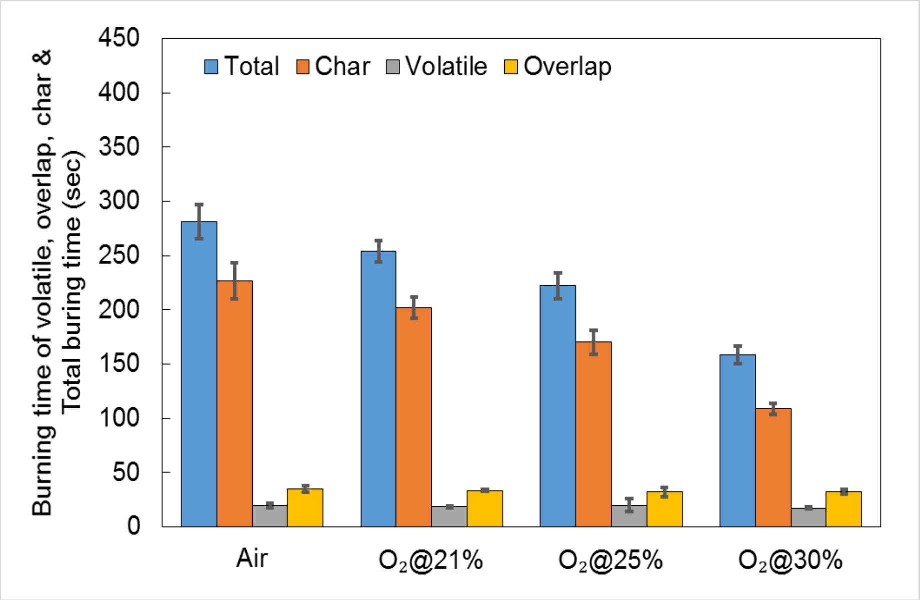

(b) Tests under 900°C

Figure 4.11: Burning times (total, volatile, overlap and char) of peanut shell pellets under air and oxy-fuel combustion atmospheres with different ambient gases

4.4.1 Effect of Ambient Temperature on Burning Time

Figures 4.7 to 4.11 compare the burning times of total, volatile, overlap and char between the air and oxy-fuel combustion atmospheres under pre-set furnace temperature of 800°C or 900°C by using five different biomass pellets. For all types of tested pellets, the ambient furnace temperature had a minor impact on burning times of volatile and overlap phases, keeping close burning times when increasing furnace temperature from 800°C to 900°C. The reason is that the fast-growing flame temperature was more dominant than ambient furnace temperature in these two phases. On the other hand, the ambient furnace temperature had a clear effect on burning time of char combustion as the heat transfer between the burning char and it surrounding environment was affecting the char combustion. With a higher furnace set temperature, a smaller amount of heat was transferred from the burning char to the environment and hence a higher char burning rate was maintained, which meant a shorter char burning time. Also, Figures 4.7 to 4.11 show that char burning time comprised more than 70% of the total burning time; thus the burning rate of char combustion played a significant role in the total combustion time. As a result, the significant decrease of char burning time led to a shorter total burning time.

4.4.2 Effect of Ambient Gas Composition on Burning Time

At the same fraction of O_2 (21% O_2-79% N_2 and 21% O_2-79% N_2), distinct trends of burning time can be observed when testing different types of pellets. For wood, straw and miscanthus pellets, the char and total burning times under 21% O_2-79% CO_2 atmospheres were slightly longer than those of air combustion at both 800°C and 900°C conditions. CO_2 has larger molar specific heat capacity than N_2, which means more heat are absorbed in O_2-CO_2 than O_2-N_2 atmosphere. As a result, a lower flame temperature was expected in the furnace when replacing N_2 by CO_2 in the oxidant and keeping O_2 concentration at 21%. In addition, the molar specific heat of ambient gas also affects the surface temperature of biomass pellet under any condition with a given O_2 fraction. Therefore, the combustion of a pellet sample under 21% O_2-79% CO_2 atmosphere was expected to have a lower temperature, thus resulting in a longer burning time. This has been proven by the studies of Liu, Zailani and Gibbs, (2005), Riaza et al. (2014) and Shan et al. (2017). Furthermore, there may be enhanced reactions between char residue (carbon element) and (gasification reaction, Equation 4.5) under O_2-CO_2 where a large amount of CO_2 was used to replace the N_2 in the background gas. As an endothermic reaction, gasification reaction can further reduce the pellet surface temperature.

However, an opposite trend was observed in the torrefied wood pellet combustion tests. Shorter char and total burning times were found when replacing N_2 by the same fraction of CO_2 at both temperature conditions (see Figure 4.10). Although the C- CO_2 gasification reaction was expected to take place during the combustion of all biomass pellets, it was more severe in the combustion of torrefied pellets as a result of the torrefaction step of pre-treatment. In the case of torrefied wood combustion, more char residue was likely to be consumed via gasification reaction during char combustion. Compared with the same fraction of O_2 in air, gasification reaction under O_2-CO_2 atmosphere can accelerate the consumption rate of char residue and then generate a shorter char and total burning times, though 21% O_2-79% CO_2 can still lead to lower pellet combustion temperature. Specific tests to verify the expected C-CO_2 gasification reactions with torrefied wood have been designed and carried out. Section 4.6.3 will discuss these tests and the results. In the case of peanut shell combustion, more interestingly, the trends under 800°C and 900°C were different in terms of char and total burning times. It may be caused by some abnormal values, which should be investigated further.

$$\mathrm{C} + \mathrm{CO_2} \rightarrow 2\mathrm{CO} \qquad \Delta\mathrm{H} = +173\ \ \mathrm{kJ/mol} \qquad [4.5]$$

In O_2-CO_2 atmospheres, the burning times of volatile and overlap were not affected by the O_2 fraction. However, the char and total burning times of all types of pellets decreased with the O_2 fraction (from 21% to 30%). Although the temperature of combustion gas was slightly increased when more O_2 was available in ambient atmosphere, the promotion of char and total burning times was more related to the higher mass flux rate of O_2, which provided additional heat for combustion process of biomass pellets. Also, it looks like the char and total burning times of individual biomass pellet in air (21%O_2-79%N_2) were between those in 21%O_2-79%CO_2 and 25%O_2-75%CO_2 atmospheres in most of the raw pellet cases (W, S and M).

4.4.3 Effect of Biomass Type on Burning Time

Figure 4.12 presents the effect of pellet type on burning times (total, volatile, overlap and char) by using a group of tests under a typical oxy-fuel atmosphere (25%O_2-75%CO_2), which has already been presented in Figure 4.7 to 4.11. Peanut shell pellet took the longest total and char burning times among all the biomass types due to its largest weight and highest fixed carbon content. Interestingly, the volatile and overlap burning times of peanut shell pellet did not have a clear difference compared with other types of pellets and the potential reasons have been discussed in section 4.4.1. Also, as mentioned before, the longer total burning time was contributed by the increase of char burning time. Among the remaining four biomass types with little difference in sizes, straw pellet had the longest total and char burning times under both temperature conditions (pre-set furnace temperatures of 800°C and 900°C), followed by torrefied wood and miscanthus pellets. Although straw pellet had the lowest fixed carbon content (14.47%) based on proximate analysis, it had the highest ash content (7.57%, about double the second highest ash content in miscanthus - 3.67%). To burnout the carbon in the char, O_2 must penetrate the ash layer and hence the fuel with the highest ash content (straw) had the longest char burning time. After them, as expected, the wood pellet with the lowest fixed carbon and ash content had the shortest char and total burning times.

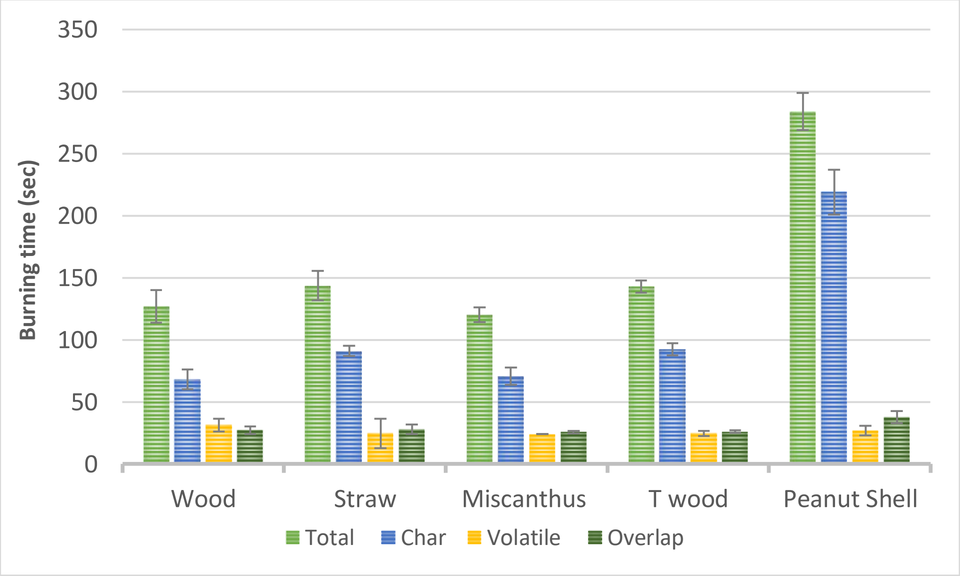

a. Pre-set furnace temperature of 800°C

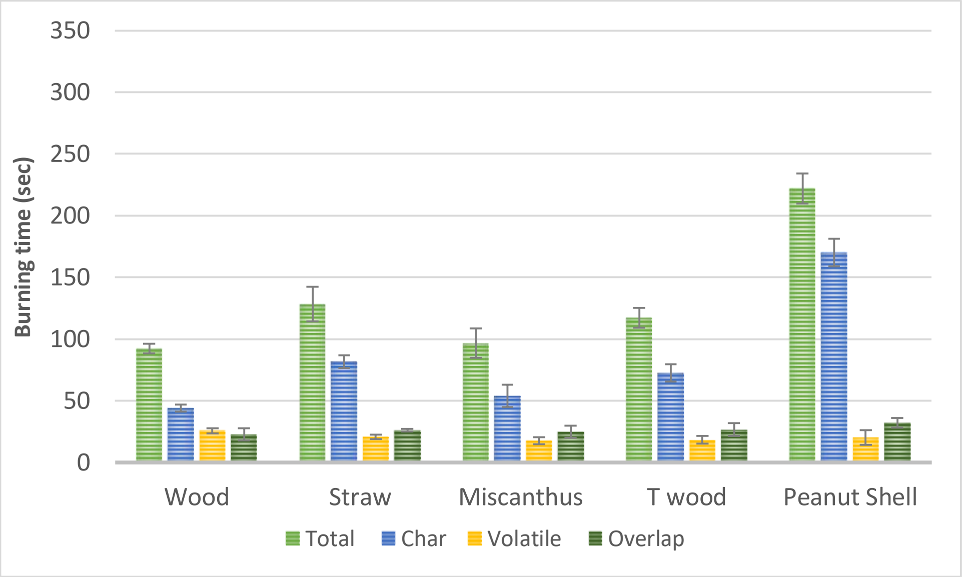

b. Pre-set furnace temperature of 900°C

Figure 4.12: Burning times (total, volatile, overlap and char) of various pellet samples under 25%O_2 -75%CO_2 and 800°C & 900°C

4.5 Visualisation of The Combustion Behaviour of Biomass Pellets by Video Imaging

4.5.1 Conversion from Video File to Images

A high-speed camera was used during the experiments to record the whole combustion process. All the recorded original video files were stored in common '.avi' format with high-quality resolutions. As introduced in section 3.1.3, the high-speed camera had sample rate of 100 fps, which means a second video file can be divided into up to 100 images. Thus, an image post-processing program was necessary to apply to analyze the combustion behaviours of different biomass fuels. As a multi-functional tool, MATLAB software (version R2014 b) was used in this study and its main purpose was to convert video file to useful image files for further investigation. The detailed code which was produced with the University of Kent is illustrated in Figure 4.13. To avoid the effect of radiation shadow, and to save storage space, a suitable intercepted screen size of each pellet test was determined based on its maximum size of the volatile flame before the conversion from '.avi' format video files to '.jpg' format images.

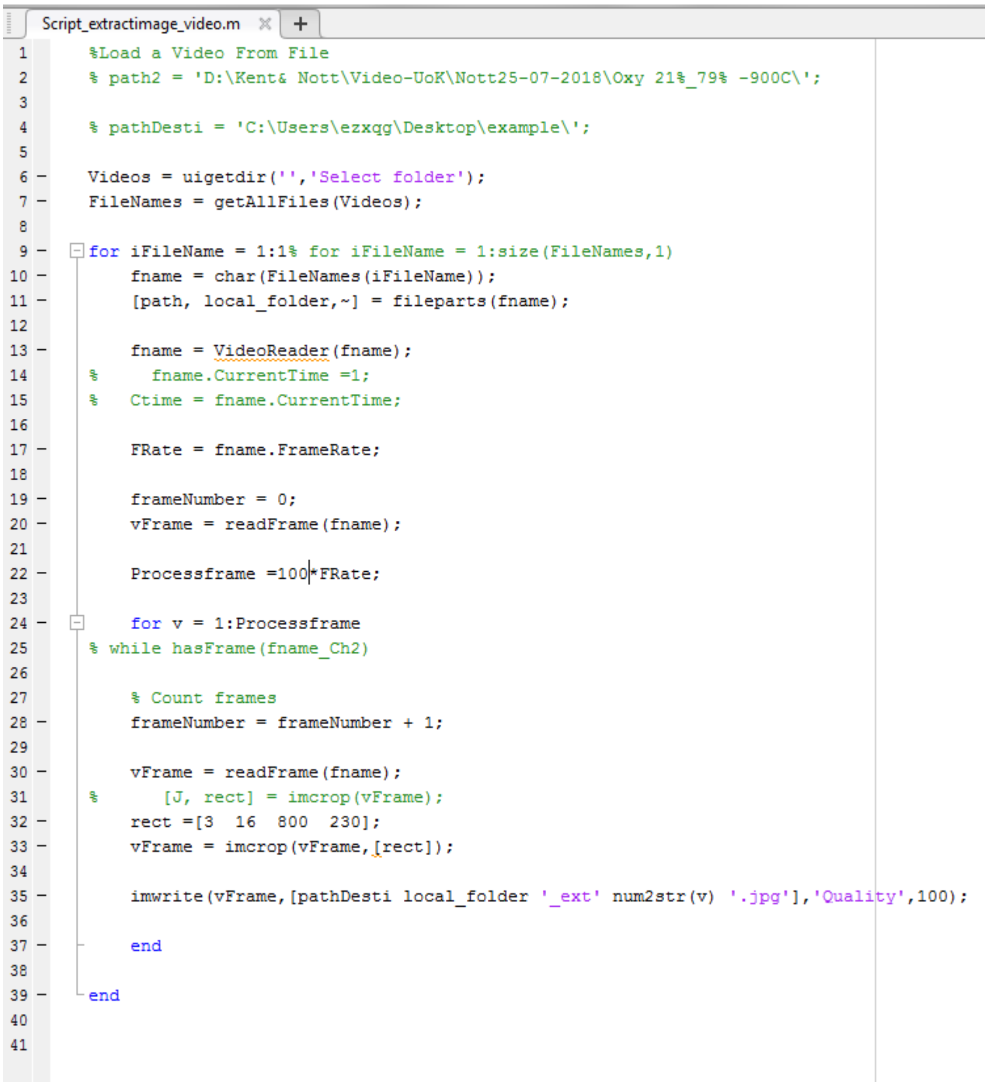

```
%Load a Video From File
% path2 = 'D:\Kent& Nott\Video-UoK\Nott25-07-2018\Oxy 21%_79% -900C\';

% pathDesti = 'C:\Users\ezxqg\Desktop\example\';

Videos = uigetdir('','Select folder');
FileNames = getAllFiles(Videos);

for iFileName = 1:1% for iFileName = 1:size(FileNames,1)
    fname = char(FileNames(iFileName));
    [path, local_folder,~] = fileparts(fname);

    fname = VideoReader(fname);
%     fname.CurrentTime =1;
%   Ctime = fname.CurrentTime;

    FRate = fname.FrameRate;

    frameNumber = 0;
    vFrame = readFrame(fname);

    Processframe =100*FRate;

    for v = 1:Processframe
% while hasFrame(fname_Ch2)

    % Count frames
    frameNumber = frameNumber + 1;

    vFrame = readFrame(fname);
%      [J, rect] = imcrop(vFrame);
    rect =[3  16  800  230];
    vFrame = imcrop(vFrame,[rect]);

    imwrite(vFrame,[pathDesti local_folder '_ext' num2str(v) '.jpg'],'Quality',100);

    end

end
```

Figure 4.13: MATLAB code for video-image conversion

4.5.2 Comparison of Volatile Flames

As the brightness of volatile flames is related to the temperature of individual biomass pellet combustion, the comparison of volatile flames of pellets under different atmospheres is investigated in this section. Figure 4.14 displays the typical volatile flame images of various types of pellets under different ambient atmospheres and temperatures. All the images were captured at the half time of volatile combustion stage for a fair comparison. For all the biomass types, under the same pre-set furnace temperature, the volatile flame of biomass pellet become more and more luminous with higher oxygen fraction in O_2-CO_2 atmospheres. Moreover, when comparing the luminance of the volatile flames between air and O_2-CO_2 atmospheres, it can be noticed that the brightness of volatile flame in air was closer to the one in 30% O_2-70% CO_2 atmosphere. As the specific heat capacity of CO_2 was higher than that of N_2 at the same oxygen fraction, the volatile flame under O_2-CO_2 atmosphere had a lower flame temperature and darker flame luminance. In addition, the lower molecular diffusivity of O_2 in O_2-CO_2 than O_2-N_2 atmosphere also decreased the flame temperature and further contributed to the observed brightness difference between the volatile flames in air and 21% O_2-79% CO_2. Furthermore, increasing the O_2 concentration under O_2-CO_2 atmosphere led to higher temperature and more luminous flame due to the enhanced combustion rate.

Moreover, it looks like that the higher ambient temperature did not improve the brightness of the volatile flame when the pellet sample was under air atmosphere. However, the brightness of volatile flame under oxy-fuel atmospheres had a significant enhancement under furnace temperature of 900°C than that of 800°C, especially under 21% and 25% oxygen fraction. Apart from the contribution of temperature increase by the ambient gas, furnace brightness was the other factor that cannot be neglected. The brightness of blank furnace under 900°C was more luminous due to the redder and brighter heating elements. Furthermore, there was no apparent brightness difference of volatile flames observed among the five types of biomass pellets under the same conditions of ambient gas and temperature.

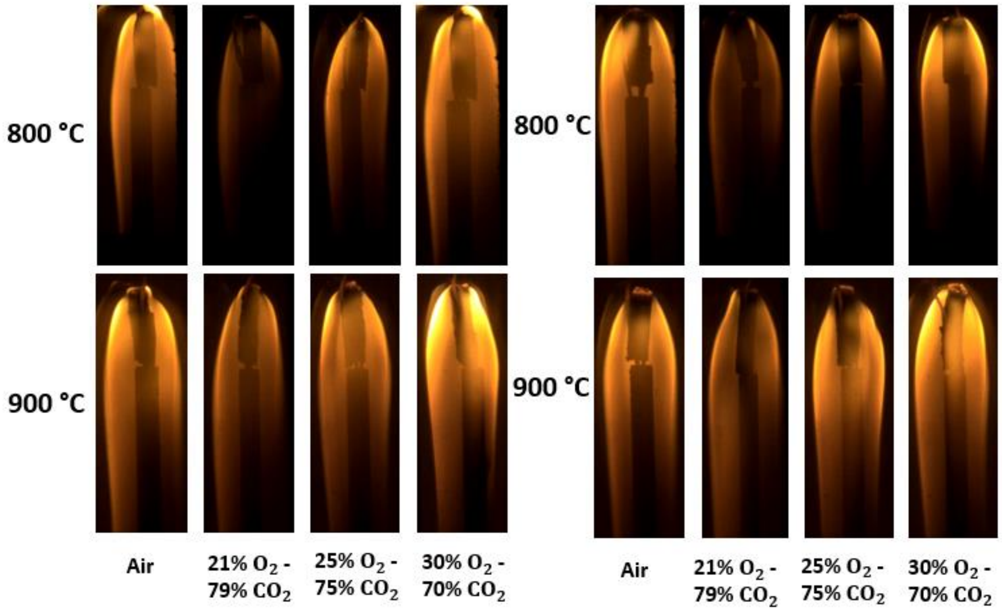

(a)Wood

(b) Straw

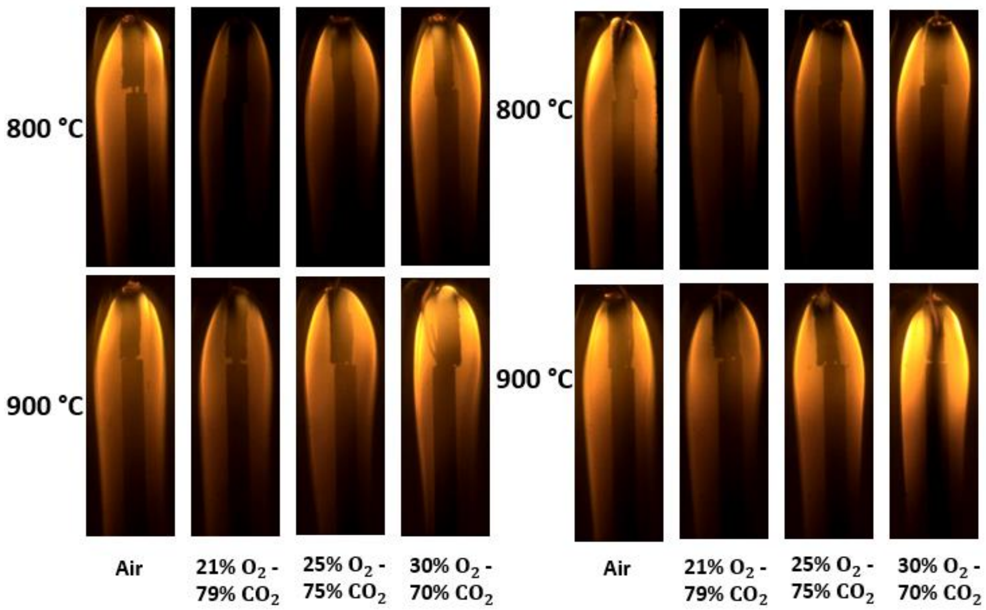

(c) Miscanthus (d) Torrefied wood

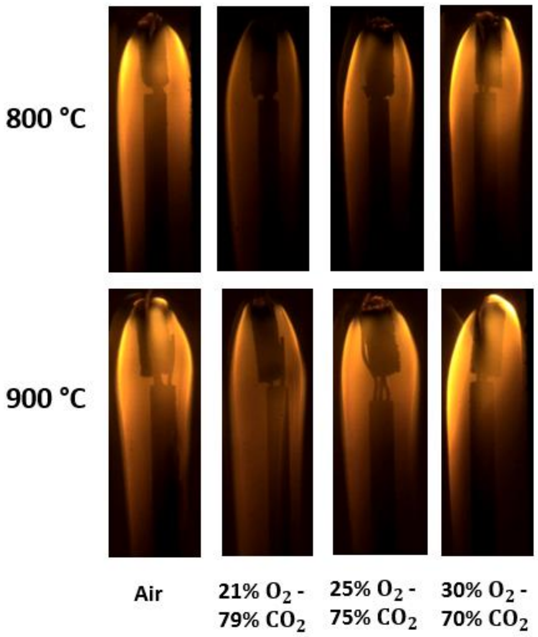

(e) Peanut shell

Figure 4.14: Comparison of volatile flame: (a) Wood; (b) Straw; (c) Miscanthus; (d) Torrefied wood; (e) Peanut shell

(Images were captured at the half time of volatile combustion phase)

4.6 Biomass Thermal Analysis in TGA

Following the study of individual biomass pellet combustion, an additional group of experiments was carried out to further explore the thermal behaviors of biomass fuels under different atmospheres.

The pulverised biomass fuels (W, S, M, T and P) were tested in different environments (N_2 and CO_2) by using TGA that has been described in section 3.1.5. About 20-30 mg of each biomass sample was used for each TGA test according to the test program shown in Table 4.2. A constant gas flow of 100 ml/ min was set for all atmosphere/ gas conditions. 800°C and 900°C were chosen as final temperatures to match the conditions of the V-DTF tests. The curves of TGA and corresponding DTG (differential thermogravimetric, rate of sample weight variation against temperature) were captured.

Table 4.2: Pre-built program for biomass thermal analysis in TGA

1: Select gas (N_2/ CO_2)
2: Ramp 10.00 ℃/min to 110.00 ℃
3: Isothermal for 10.00 min
4: Ramp 10.00 ℃/min to 800.00 ℃ or 900.00 ℃
5: Isothermal for 40.00 min
6. Cool down to ambient temperature

4.6.1 N_2 Atmosphere

Figure 4.15 (a) and 4.16 (a) show the mass variation of selected biomass fuels during TGA tests under N_2 atmosphere. With the temperature increasing gradually from ambient to 110°C, the sample mass had a small loss (<10%, different due to biomass types), as a result of moisture evaporation. The loss of moisture generated the first peak on the DTG curves shown in Figures 4.15 (b) and 4.16 (b). As the temperature increased to around 200°C, devolatilization started to take place. It was found that various biomass fuels had different peak temperatures for devolatilization (P>M>S>T>W) due to different elemental and chemical compositions (Vassilev et al., 2010). Furthermore, among the five biomass fuels, wood and miscanthus had the highest devolatilization rates while peanut shell had the lowest rate at the peak devolatilization temperature. The same trend can be observed at both 800°C and 900°C cases. Rapid mass loss rate during devolatilization was mainly contributed by the high volatile matter of selected biomass fuels as shown by their proximate analysis (see Table 3.1). After the end of devolatilization process (under 600°C), the loss mass became much smaller but continuous with the increasing temperature, and also in the final isothermal stage. Due to the inert atmosphere (N_2), the tested sample kept most of the unburnt char and ash in residue until the end of test.

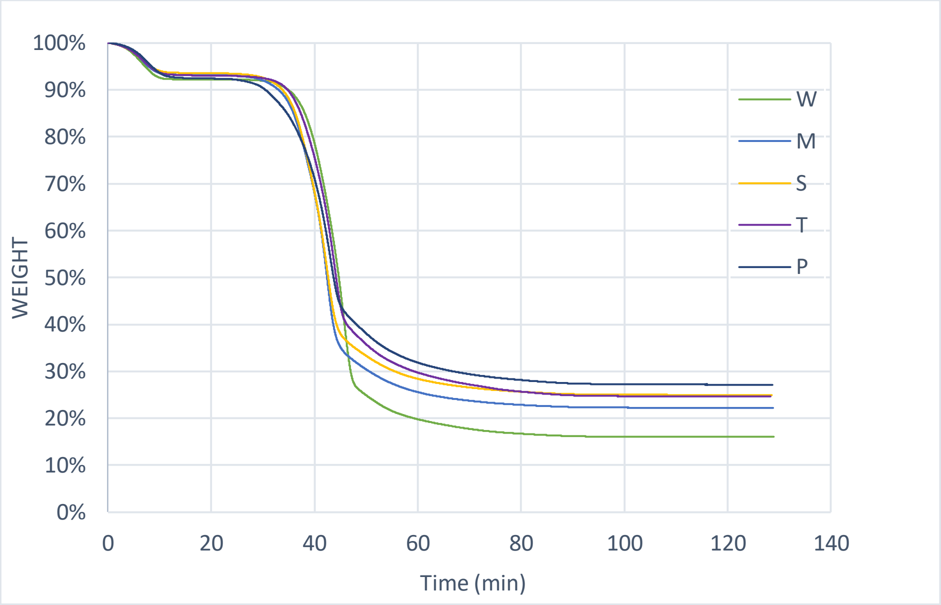

(a). TGA

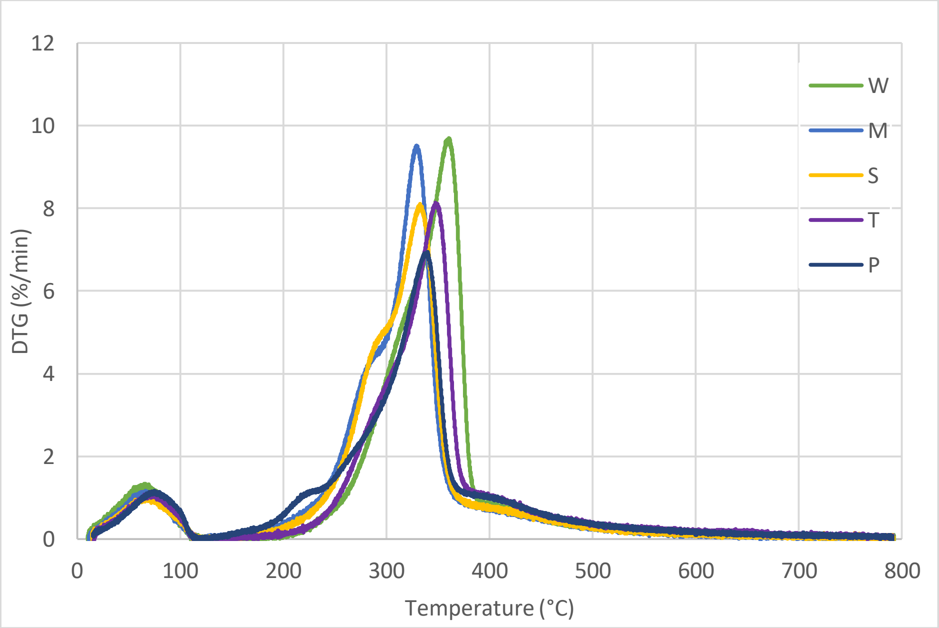

(b). DTG

Figure 4.15: Thermal behaviors of biomass fuels under N_2 atmosphere, 800°C: a) TGA; b) DTG (W-wood, M-miscanthus, S-straw, T-torrefied wood, P-peanut shell)

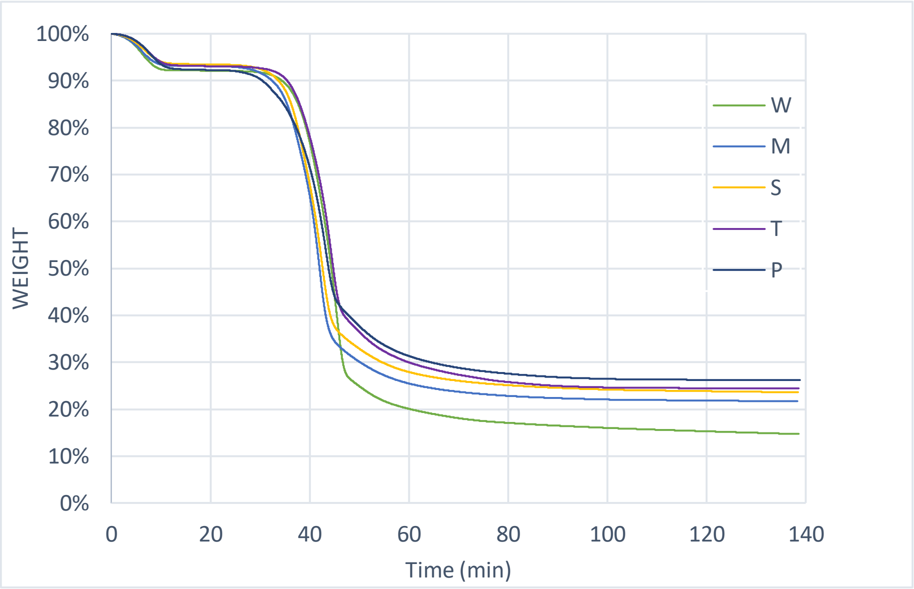

(a). TGA

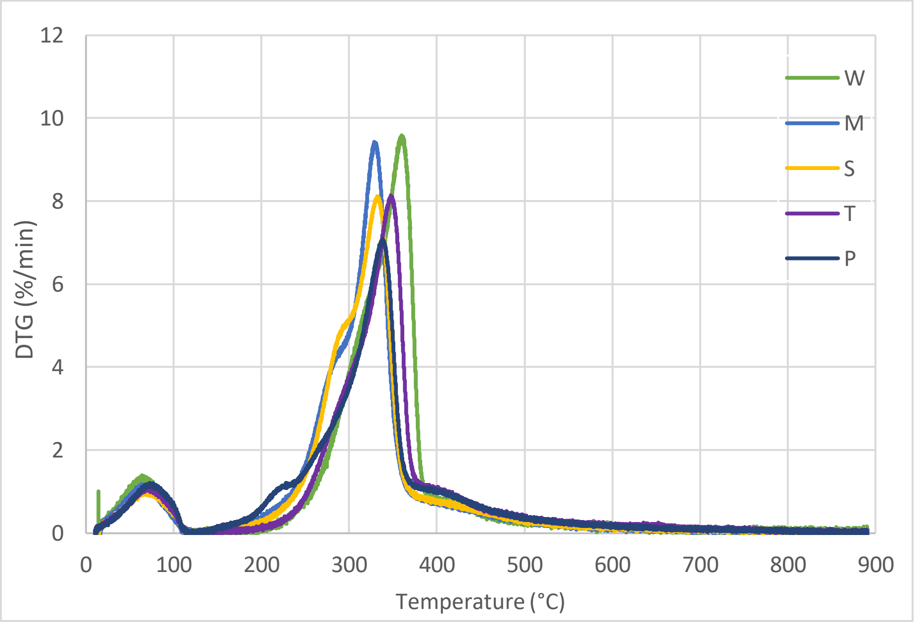

(b). DTG

Figure 4.16: Thermal behaviors of biomass fuels under N_2 atmosphere, 900°C: a) TGA; b) DTG (W-wood, M-miscanthus, S-straw, T-torrefied wood, P-peanut shell)

4.6.2 CO_2 Atmosphere

Figure 4.17 (a) and 4.18 (a) show the mass variation of selected biomass fuels during TGA tests under CO_2 atmosphere. Comparing with the tests under N_2 atmosphere, three stages of moisture evaporation, volatile matter release and fixed carbon can be clearly distinguished when using CO_2 as reaction gas. Correspondingly, three main mass loss stages can be identified in Figures 4.17 (b) and 4.18 (b). The use of CO_2 slightly delayed the active temperatures of devolatilization process compared with the ones with N_2 which shown in Figure 4.15 (b) and 4.16 (b). The difference of active temperature between two atmospheres was mainly related to their physical properties such as thermal conductivity and specific heat capacity.

Apart from the stages of moisture evaporation and devolatilization, the third stage took place over 700°C under CO_2 atmosphere. As mentioned in section 4.4.2, the gasification reaction (reaction 4.5) may be dominant at this stage. Char residue was consumed by CO_2 via the gasification reaction and the reaction rate was more apparent under the higher temperature condition (e.g. 900°C). Compared with other raw biomass fuels, the variation trend of torrefied wood in the gasification stage was more notable. The consumption rate of char residue of torrefied wood (purple line in Figures 4.17 b and 4.18 b) kept accelerated rising with the temperature from 700°C and had the highest peak mass loss rate in the third wave. Its attractive characteristic was related to the 'torrefaction' of pre-treatment and can be used to explain the phenomenon observed in section 4.4.2, i.e. torrefied wood had shorter char and total burning times under 21% O_2-79% CO_2 atmosphere than those under air under both V-DTF set temperatures of 800°C and 900°C (see Figure 4.10).

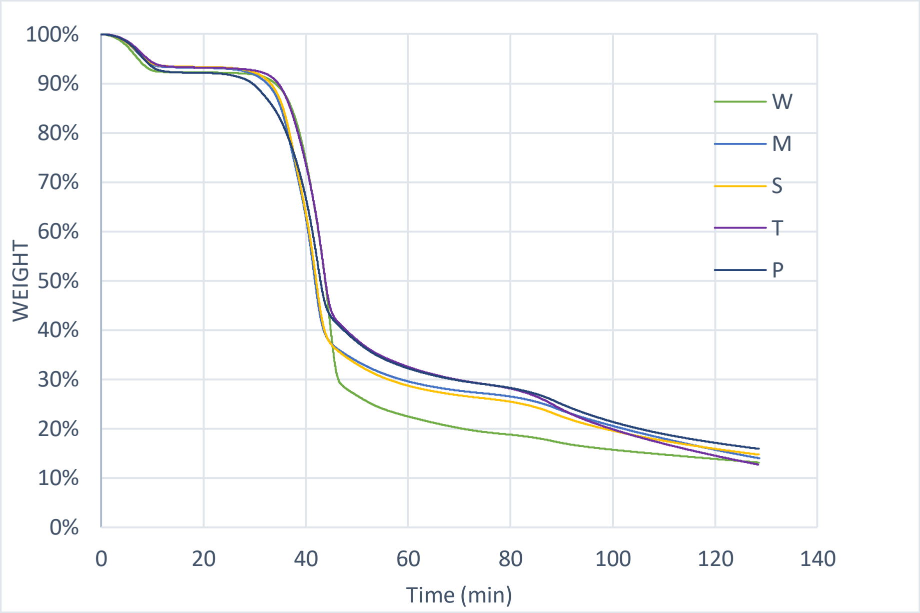

(a). TGA

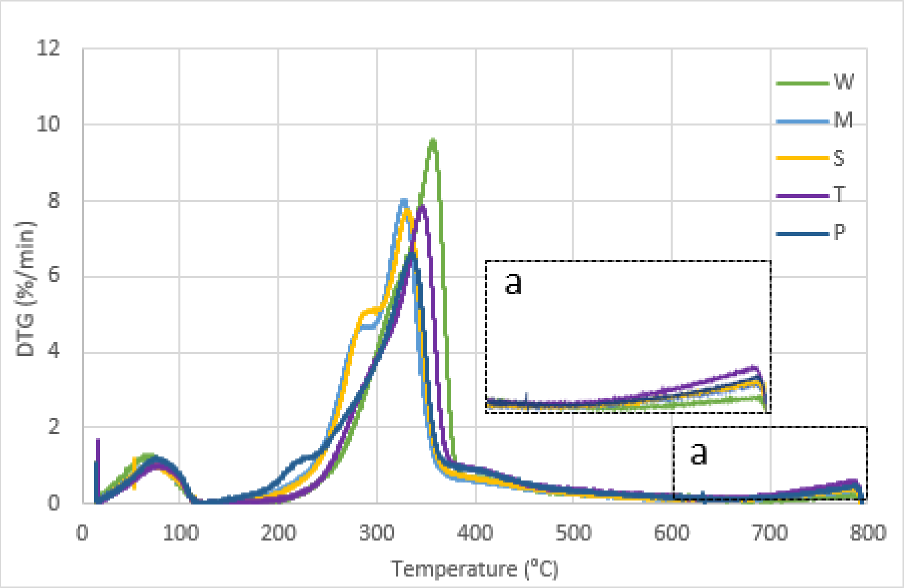

(b). DTG

Figure 4.17: Thermal behaviors of biomass fuels under CO_2 atmosphere, 800°C: a) TGA; b) DTG (W-wood, M-miscanthus, S-straw, T-torrefied wood, P-peanut shell)

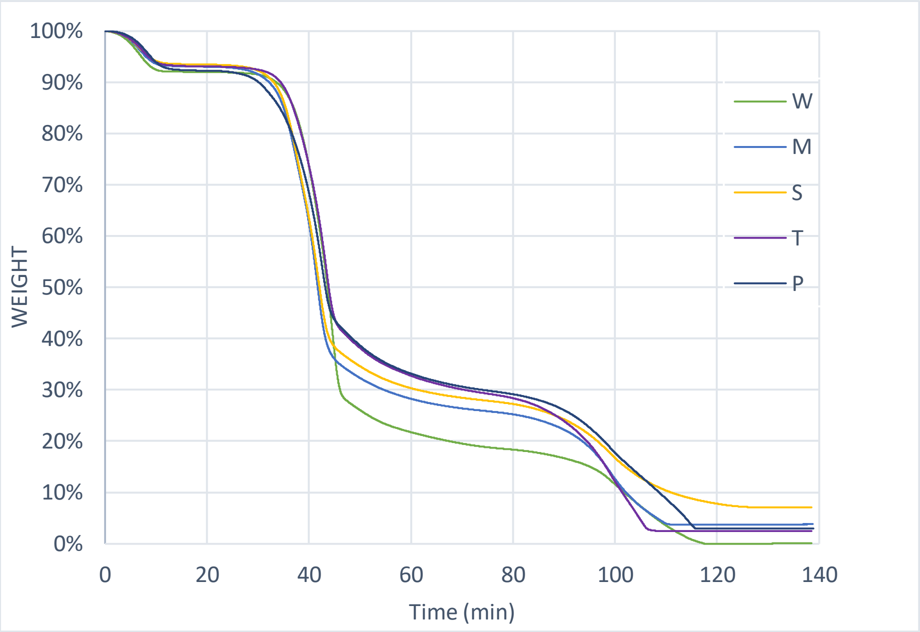

(a). TGA

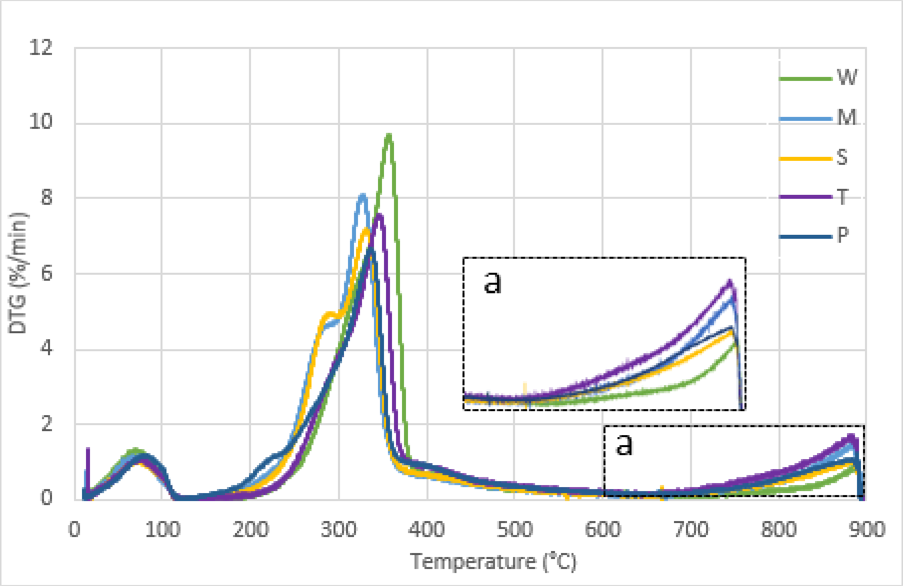

(b). DTG

Figure 4.18: Thermal behaviors of biomass fuels under CO_2 atmosphere, 900°C: a) TGA; b) DTG (W-wood, M-miscanthus, S-straw, T-torrefied wood, P-peanut shell)

4.7 Summary

The investigation of combustion behaviours has been carried out in this chapter by burning five types of individual biomass pellets (wood, straw, miscanthus, peanut shell and torrefied wood) under traditional air and oxy-fuel atmospheres in a visual drop tube furnace (V-DTF) integrated with a high-speed camera. Different combustion stages of the biomass pellets have been identified from the measured temperature distributions and the captured flame images. Further characterization of the investigated biomass fuels has been conducted by TGA under the environments of N_2 and CO_2. The following conclusions can be obtained from these V-DTF combustion tests and TGA tests:

- Four phases of biomass combustion can be identified from on the temperature distributions of individual pellet tests and the flame/ char combustion images captured by the high-speed camera for all five types of biomass pellets and under all combustion conditions (both air and oxy-fuel combustion environments and both V-DTF set temperatures of 800 ℃ or 900 ℃). These four phases are pre-heating phase, volatile combustion phase, volatile/ char overlap phase and char combustion phase.

- The pre-set V-DTF temperature (800 ℃ or 900 ℃) had a limited impact on the burning times of volatile and the volatile/ char overlap phases while it had clear effect on the burning time of char combustion phase. Higher ambient temperature led to shorter char burning time and shortened the total burning time of biomass pellet.
- In O_2-CO_2 atmospheres (O_2 fraction from 21% to 30%), an increased O_2 fraction did not clearly affect the burning times of volatile combustion and overlap stages, but evidently accelerated the char burning time, resulting in a shorter total combustion time of biomass pellet.
- The total burning time in air (21%O_2-79% N_2) was shorter than that in 21% O_2-79%CO_2 for most of the biomass pellets (wood, straw and miscanthus). Furthermore, the total burning time in air was between those in 21% O_2-79% CO_2 and 25% O_2 -75% CO_2 atmospheres.
- However, the char and total burning times of torrefied wood in air were longer than those in 21% O_2-79% CO_2. This is contributed by the fact that the C-CO_2 gasification for torrefied wood was much more significant than other raw biomass fuels.
- From the perspective of processed combustion images, the volatile flame brightness increased with the O_2 fraction under oxy-fuel combustion

conditions. The brightness of volatile flame in air was close to the one in $30\% \ O_2$-$70\% \ CO_2$ atmosphere.

- There was no breakage or bending of biomass pellets during the whole combustion stage, even near the end of the char combustion

CHAPTER 5. EXPERIMENTAL RESULTS AND ANALYSIS OF ASHWELL 50kW BIOMASS BOILER TESTS

5.1 Introduction

The experimental set-ups of the Ashwell 50kW biomass boiler tests, including the laboratory apparatus, selected fuel and test conditions (different air fan settings) have been introduced in section 3.2. This chapter presents the experimental results and corresponding analysis, including the gaseous emissions of the sampled flue gas, the composition of the combustion chamber gas, temperature distribution of the heat exchanger & combustion chamber under different air settings, shown in sections 5.2 to 5.5.

It should be noted that, based on the findings of literature review presented in Chapter 2, hydrocarbons are expected to be presented in biomass combustion. In addition, methane (CH_4) is believed to be the largest source of the hydrocarbons. However, few have quantified the concentration of CH_4 in the combustion chamber or the heat exchanger area of domestic biomass boilers. Therefore, apart from NOx and CO, CH_4 is also chosen as the focus in this chapter. Knowledge on the concentrations of hydrocarbons and CO will be used to guide the design of the catalytic tests to be described in Chapter 6. It should be also mentioned that all the tests are repeatable, but only one example result of each test is presented in this chapter.

5.2 Emission Results of Flue Gas

A 15mm × 15mm hole was drilled at the inlet of chimney (see Figure 3.18) after hot gas leaving the heat exchanger. The sampling system for flue gas was applied and its detail has been introduced in section 3.2.3.2. The details of the two sets of gas analyzers have also been presented in section 3.2.3.1. In this section, the experimental results on the measurement of main parameters of flue gas, including NOx, CO, CO_2 and O_2 are presented and analyzed.

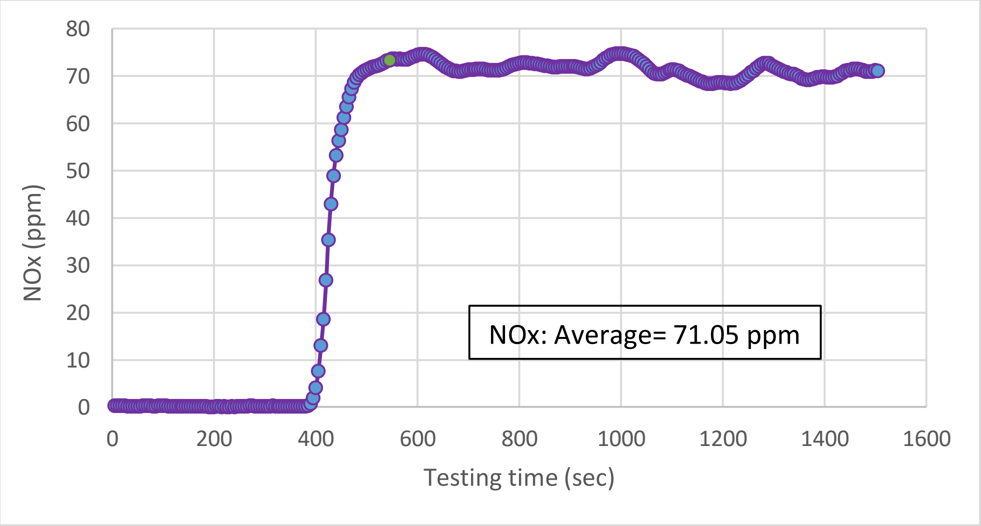

(a) NOx emissions

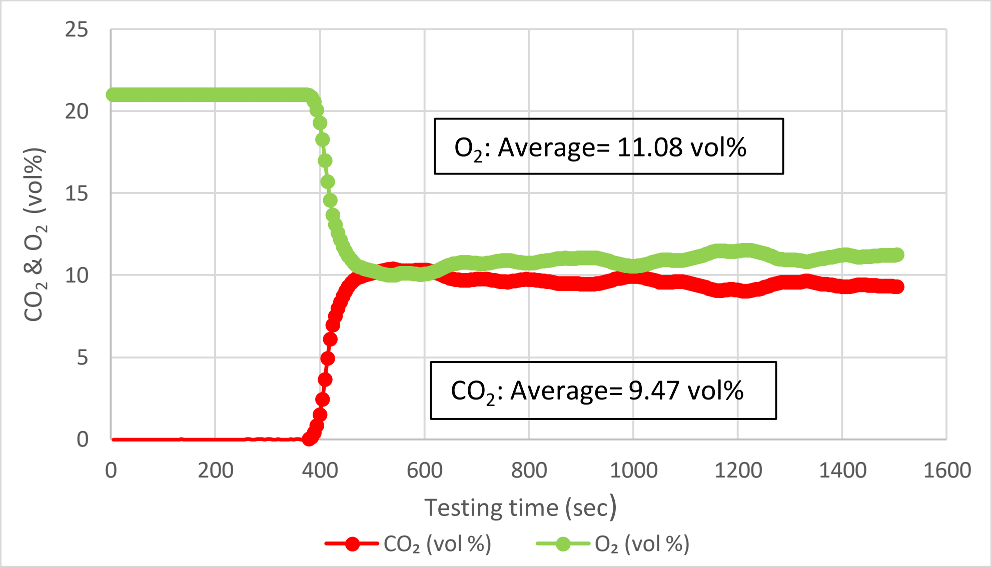

(b) CO_2 and O_2 concentrations

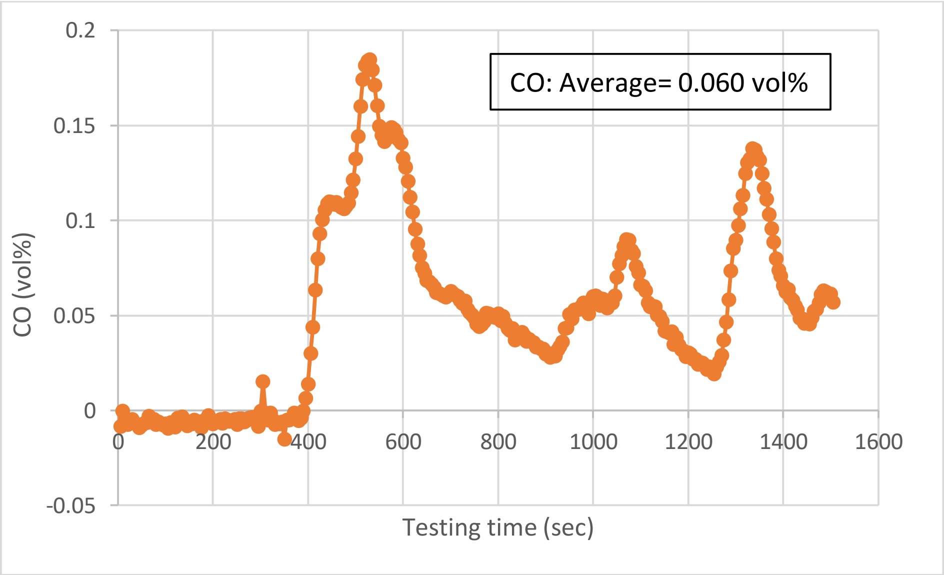

(c) CO emissions

Figure 5.1: Main flue gas compositions (CO_2 and O_2) and gaseous emissions (NOx and CO) under normal air setting

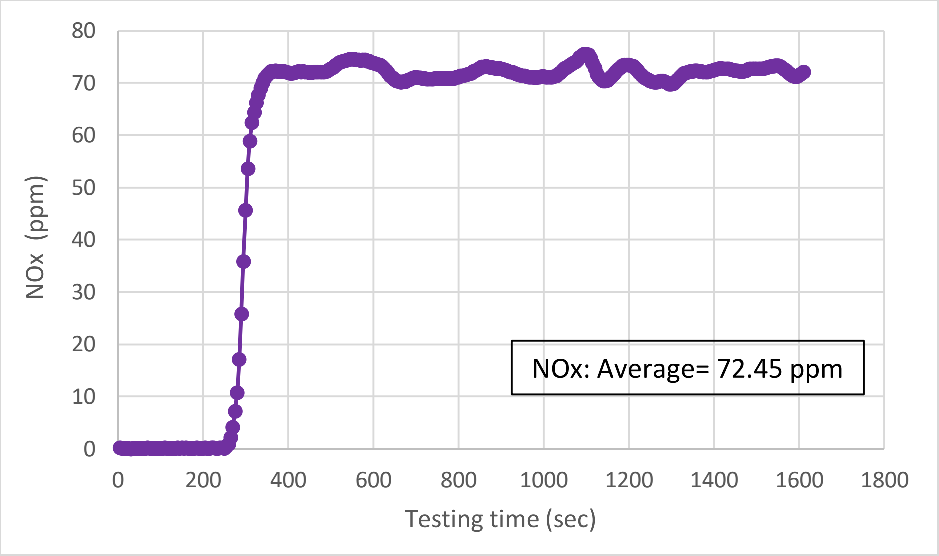

(a) NOx emissions

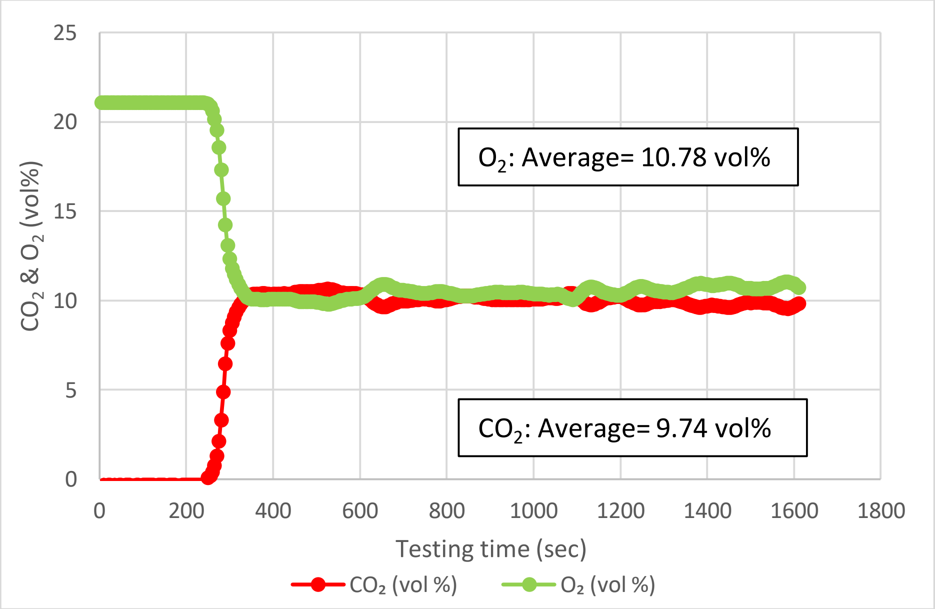

(b) CO_2 and O_2 concentrations

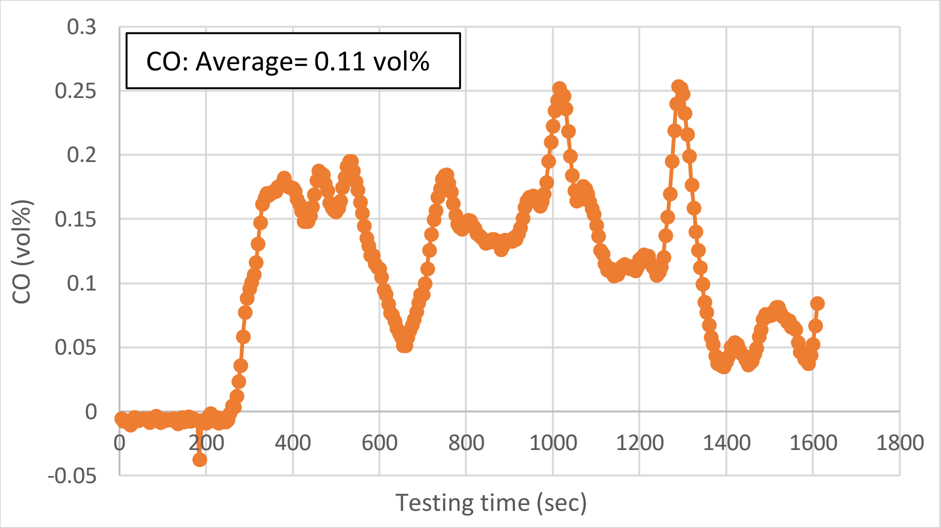

(c) CO emissions

Figure 5.2: Main flue gas compositions (CO_2 and O_2) and gaseous emissions (NOx and CO) under weak primary air setting

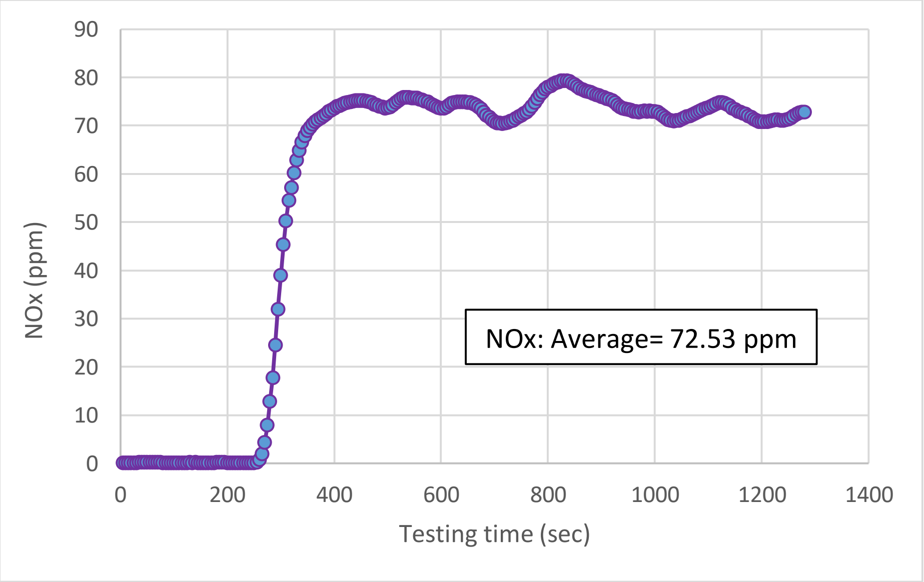

(a) NOx emissions

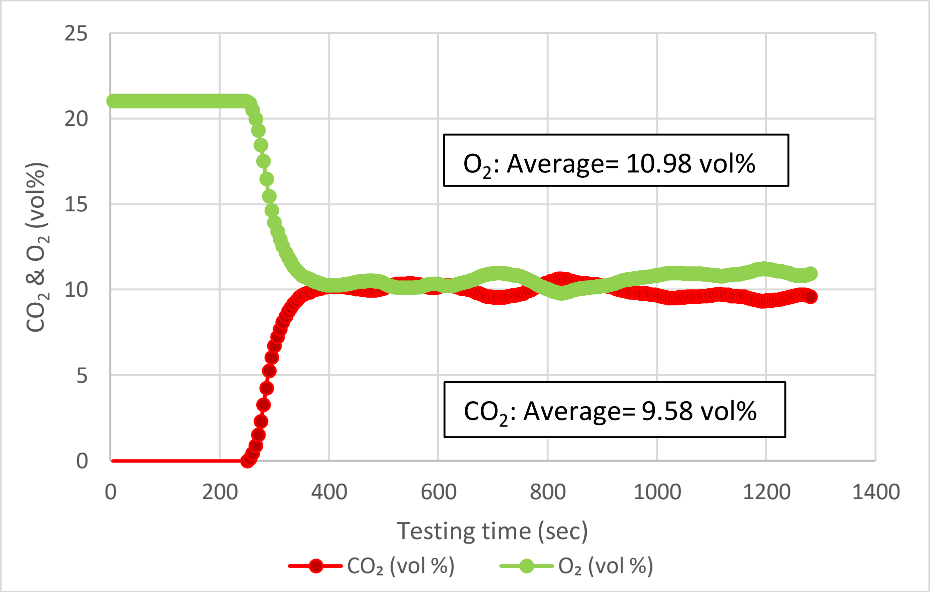

(b) CO_2 and O_2 concentrations

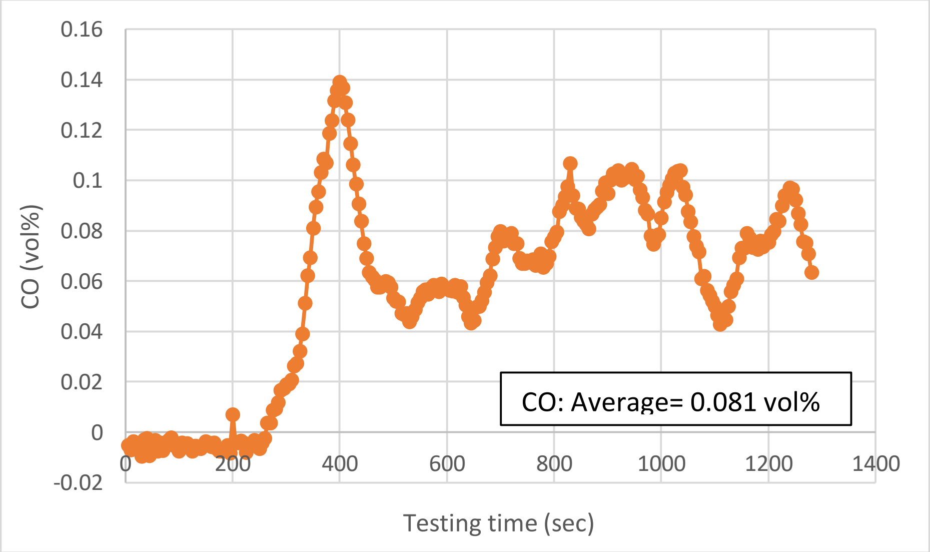

(c) CO emission

Figure 5.3: Main flue gas compositions (CO_2 and O_2) and gaseous emissions (NOx and CO) under weak secondary air setting

Figures 5.1 to 5.3 display the concentrations of the two main gas components (CO_2 and O_2) and the emissions of two gaseous pollutants (NOx and CO) under three air setting conditions. From these figures, it can be found that the values of NOx, CO_2 and O_2 emissions tended to be stable once the boiler reached the stable operating stage. However, CO emissions always fluctuated during the experimental period because of its relatively low measured concentration and wide measuring range of CO channel in ABB gas analyzer (0% to 5%). All the measured gaseous concentrations under different air settings were summarized and compared in Table 5.1. The unit of NOx emission was also converted from ppm (fixed in gas analyzer) to grams per gigajoules (g/GJ) which was the one used in the published RHI criteria. Reactions 5.1 and 5.2 were used based on the method of Stewart (2012).

Table 5.1: Main flue composition (CO_2 and O_2) and gaseous emissions (NOx and CO) under different air staging conditions

	CO (vol %)	**CO_2 (vol %)**	**O_2 (vol %)**	**NOx (ppm)**	**NOx (g/GJ)**
Normal air setting	0.060	9.47	11.08	71.05	75.66
Weak primary air setting	0.110	9.74	10.78	72.45	75.88
Weak secondary air setting	0.081	9.58	10.98	72.53	76.46

NOx emission, ppm to $\mathrm{mg/m^3}$

$$\mathrm{mg/m^3} = \mathrm{ppm} \times (\mathrm{MM}/22.4) \times (273/\mathrm{T}) \times \left(\frac{\mathrm{P}}{101.3}\right) \qquad [5.1]$$

NOx emission, $\mathrm{mg/m^3}$ to $\mathrm{g/GJ}$

$$\mathrm{g/GJ} = \mathrm{mg/m^3} \times (21 - \mathrm{O_2req})/\ (21 - \mathrm{O_2act}) \times \frac{\mathrm{SDFGV}}{1000} \qquad [5.2]$$

Where MM- the molar mass of the substance (grams), T- Temperature (Kelvin), P- Pressure (kPa)

$\mathrm{O_2req}$ - the standard percentage of oxygen for the reaction which was 10%

O_2act – the value for oxygen measured in the experiment

SDFGV- the Specific Dry Flue Gas Volume for oxygen at 10%, different values based on the biomass type. Here, the wood value from literature was chosen.

Table 5.1 indicates that the NO_x emissions had similar concentration under different air staging conditions, having 71.05ppm, 72.45ppm, 72.53ppm respectively. After converting the unit from ppm to g/GJ by using reactions 5.1 and 5.2, it can be found that the biomass boiler had excellent performance in term of NO_x emissions since all the values under different conditions (75.66 g/ GJ, 75.88 g/ GJ and 76.46 g/ GJ) conformed to the restriction of RHI policy (150g/ GJ), only reaching about half of the upper limit. Also, the similar values of NOx emissions demonstrate that the NO_x emission generated from this particular biomass boiler was quite low largely due to the low fuel-N content (0.24%) of the biomass fuel (wood pellet) and the use of air staging. The total amount of air (controlled by adjusting primary or secondary air inlet in this study) only had a slight effect on NO_x emissions. However, CO emission was clearly affected by the amount of air supply. Reducing air inlet caused the CO increasing from an average 0.060 vol% under normal air setting to 0.110 vol% (weak primary air setting) and 0.081 vol% (weak secondary air setting). Less total air supply resulted in incomplete combustion, evidenced by the increase of CO emission though the total air supply was excess in all cases. Moreover, reducing primary air led to the highest CO emission because most of CO was generated in the primary combustion zone.

The ratio of CO to CO_2 is an indicator of combustion efficiency in terms of solid fuel conversion and a low ratio shows higher combustion efficiency. According to Fernandes et al., (2011), a typical CO/CO_2 ratio for flame combustion should be lower than 0.1. The average ratios achieved from all the air staging conditions were less than the value mentioned above, which indicated the flame combustion phase was dominant during burning process. The highest combustion efficiency (i.e. the lowest ratio between CO and CO_2) was achieved with the test under normal air staging condition, which was not a surprise as the manufacturer had commissioned the boiler to the 'optimised conditions' by using the same wood pellets.

5.3 Temperature Measurement in Heat Exchanger

After investigating the performance of biomass boiler in terms of flue gas emissions, more attention was paid to the study of the feasibility of CH_4-SCR application in small-scale biomass boilers. As mentioned in Chapter 2, the reaction temperature may have a significant impact on the CH_4-SCR performance of any potential catalysts. The heat exchanger within the boiler has a wide range of temperature distribution from the combustion gas inlet to outlet. With the heat of hot gas transferred to warm up the boiler water, the gas stream temperature decreased along the tube of heat exchanger tubes from the highest temperature at gas inlet to lower temperature at higher positions.

Hence, it was necessary to measure the gas temperature profiles of the heat exchanger tubes at different heights and positions. As there was little information from literature and each boiler had its unique heat exchanger, the temperature distribution in the heat exchanger of the small-scale biomass boiler had to be experimentally measured. The results are presented and analyzed in this section below.

5.3.1 Boiler Modification

The heat exchanger (HX) of Ashwell 50kW biomass boiler used for this study had forty-eight HX tubes, vertically arranged as shown in Figure 5.4. Since it was impossible to measure the temperature distributions in all HX tubes, only some typical HX tubes were chosen and tested. Originally, two HX tubes located in the inner circle of heat exchanger (named as HX 1 and HX 2, see Figure 5.4) were chosen for the temperature measurement when taking the position of mixing plate in the chamber (see Figure 3.12) into account.

To carry out the temperature measurement in heat exchanger, two small holes were drilled from the top lid of the boiler to insert thermocouples (see Figure 5.5). Two K-type thermocouples with 3mm probe diameter and 1.5 meter cable length were used. The K-type thermocouple had the measuring range up to 1100°C and temperature error of ± 2.5°C, which could offer accurate measurement and cover the whole potential temperature range. Since the top lid of the HX was perfectly square shape, two more HX tubes in the same ring were found when rotating the top lid to seal the boiler. The final positions of four measured HX tubes are shown in Figure 5.4, HX 1 to HX 4.

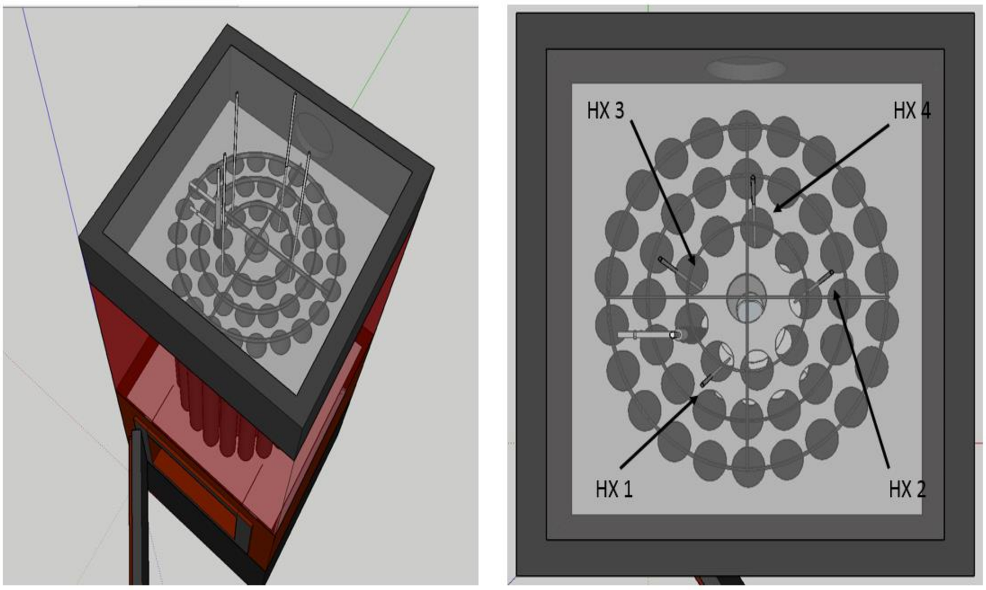

Figure 5.4: Positions of the four measured tubes in the heat exchanger

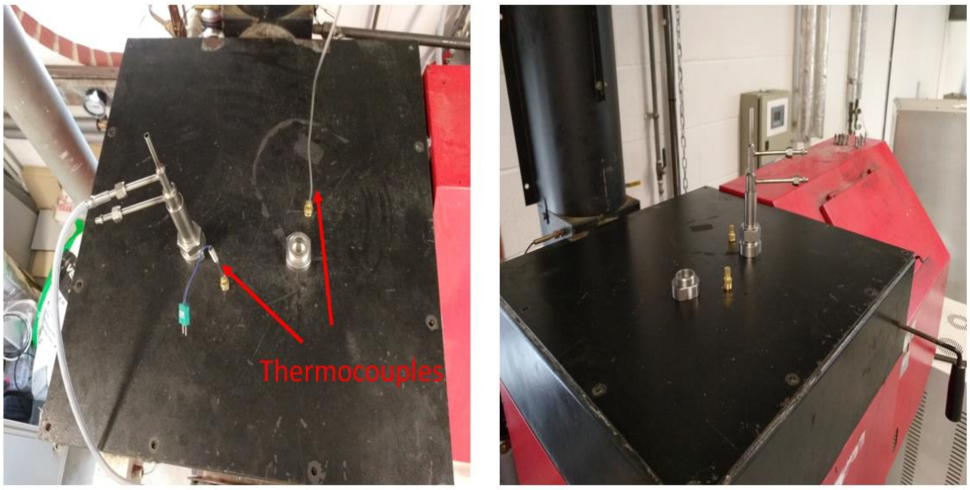

Figure 5.5: Photos of the drilled holes and corresponding thermocouples

5.3.2 Temperature Distribution of Heat Exchanger

Positions of HX 1 and HX 2 were the original places for thermocouples while HX 3 and HX 4 were the locations after rotating the top lid. From Figure 5.4, it can be seen that all the measured tubes were on the inner circle of heat exchanger and almost evenly distributed on the circle line. For each tube, temperature measurement was started from 300mm height above the tube inlet, then every 100mm drop until touching the inlet. Therefore, four temperature points within each tube were recorded in total (300mm height, 200mm height, 100mm height and tube inlet). Based on the temperatures of these measuring points, a rough temperature distribution of each tube and whole heat exchanger can be predicted. The summary of the measured temperatures in four tubes with various positions under different air staging conditions is shown in the following tables (Table 5.2 to 5.4). The detailed temperature variation of each tube can be found in Figures A.11 & A.12. It should be mentioned that the temperatures within tube HX 1 and HX 2 were obtained in one test while those of tube HX 3 and HX 4 were obtained with another test under the same conditions on a different day. All the tests were repeatable and their temperature error was acceptable (± 5 %). When conducting the pre-tests, the temperature measured at 300mm height in most of the cases was pretty low, around or under 300℃, consequently that height was chosen as start point of temperature measurement and no further temperature measurement was taken at higher positions.

Table 5.2: Temperature distribution of four heat exchanger tubes under normal air setting

Normal air setting unit: ℃				
	HX 1	HX 2	HX 3	HX 4
300mm	226.38	211.63	255.86	277.80
200mm	364.18	242.03	301.03	281.21
100mm	509.82	294.32	364.92	355.28
Inlet	868.83	574.99	820.82	675.31

Table 5.3: Temperature distribution of four heat exchanger tubes under weak primary air setting

Weak primary air setting unit: ℃				
	HX 1	HX 2	HX 3	HX 4
300mm	332.49	155.67	277.67	264.74
200mm	435.25	159.67	289.95	282.67
100mm	491.64	189.95	369.21	350.57
Inlet	839.33	517.55	794.46	647.37

Table 5.4: Temperature distribution of four heat exchanger tubes under weak secondary air setting

Weak secondary air setting unit: ℃				
	HX 1	HX 2	HX 3	HX 4
300mm	368.84	148.11	260.08	254.85
200mm	439.07	151.27	296.93	262.85
100mm	496.11	188.82	374.56	325.83
Inlet	830.36	506.51	813.25	652.40

Combining with all the measured temperatures above three tables (Table 5.2 to 5.4), it can be observed that the temperature distribution was not uniform through the heat exchanger, especially in the bottom part. When comparing the inlet temperature among four tubes, the positions of HX 1 and HX 3 which were on the left front side and left back side of chamber (positions shown in Figure 5.4) had relatively higher temperature than the temperature of HX 2 and HX 4 which were on the right front side and right backside of chamber. This phenomenon happened in all air staging conditions and the largest temperature difference between left and right sides of heat exchanger inlet was over 200°C. It could be caused by heterogeneous combustion or flame generated in the chamber. With the heat transfer proceeding (from inlet to higher positions of the tubes), the temperature drop became smaller. Using HX 3 tube under normal air setting condition as an example, there was the largest temperature drop (over 300°C) between the points of heat exchanger inlet and 100 mm height and the drop was much lower when going from 100 mm to 200 mm height, only difference of 60°C. More interestingly, when combining Figure A.10 and Figure 5.5, most of the temperature differences between HX 3 and HX 4 (back side tubes) with the same height was small (apart from the inlet point) while that difference between HX 1 and HX 2 (front side tubes) was much larger. In short, larger temperature differences mainly occurred in the front of combustion chamber.

Furthermore, when combing all the inlet temperatures under different air staging conditions, it can be found that reducing primary or secondary air created a decrease temperature of heat exchanger inlet. For instance, the inlet temperature of HX 1 tube dropped from 868.83°C to under 840°C when changing from normal air setting to weak primary or secondary air setting. It can be attributed by the weaken oxidation of volatile and char combustion when there was a depressing amount of oxygen available in combustion chamber.

Based on the temperature measurement results discussed above, it can be concluded that the temperature drop was not gradual in heat exchanger tubes. Specifically, the bottom part of tube had large temperature difference while the upper part had less effect. The temperature distribution of tubes in different parts of heat exchanger also had a huge difference. The tubes on the left side of boiler had a higher temperature, especially for inlet temperature. Also, the total amount of air had clear impact on the inlet temperature of heat exchanger and temperature distribution of the tubes. A moderate reduction of air inlet led to lower temperature distribution in the heat exchanger.

5.4 Temperature Measurement in Combustion Chamber

After the investigation of temperature measurements within the heat exchanger tubes, further characterization of temperature distribution within the combustion chamber of the biomass boiler was carried out, including primary & secondary temperatures and temperature distribution of combustion chamber under different air setting conditions.

5.4.1 Boiler Modification

Five K-type thermocouples were inserted from outside to various positions to assist the temperature measurement in combustion chamber (see Figure 5.6).

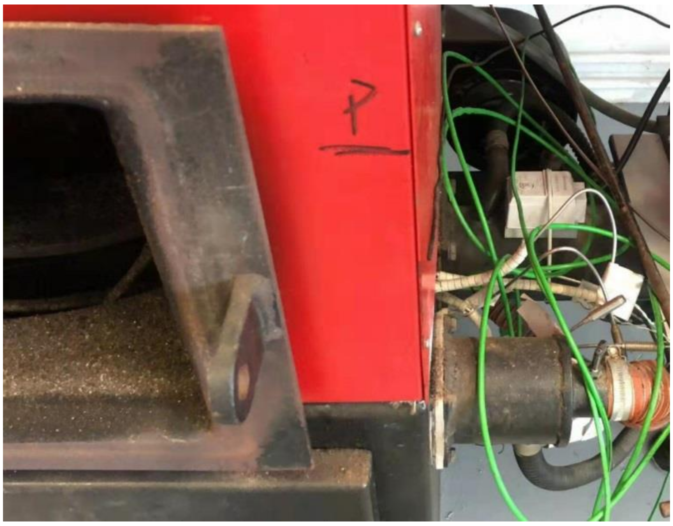

Figure 5.6: K-type thermocouples for the temperature measurement within combustion chamber, inserted from the boiler outshell

5.4.2 Primary and Secondary Air Temperatures

As shown in Figure 3.12 and Figure 5.7, the primary air was supplied below the fuel bed while the secondary air supply was blown to the combustion chamber via the four secondary air supply tubes surrounding the fire pot, two at higher heights and two at lower heights. The thermocouples were adjusted to the required positions (see Figure 5.7, a) to investigate the temperatures of primary and secondary air. Because of the limit numbers and length of thermocouples, two of four secondary vent tubes were measured, the upper-left one and the lower-right one. The temperature was measured under different air staging conditions. The temperature of measured secondary air can be seen in Table 5.5. It shows that the secondary air temperature of lower right side was much lower than the value of upper left side, which the reasons will be discussed in the next section.

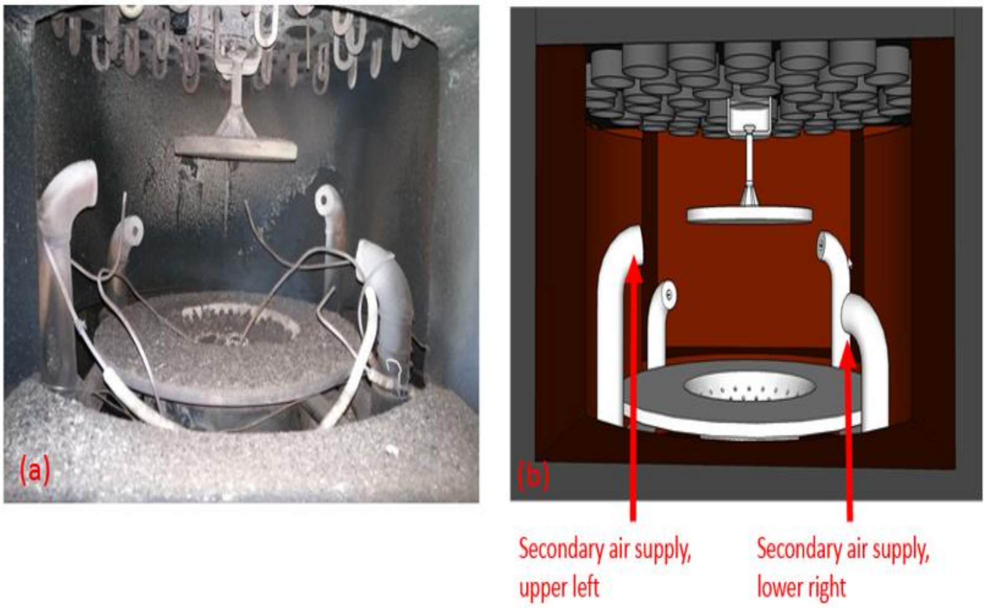

Figure 5.7: Thermocouple positions for measuring the temperatures of primary and secondary air

However, when measuring primary air temperatures, it was found that the measured temperature was over 1000°C, but the value was unreliable since the primary air holes were under fire pot and they might be blocked by biomass pellets when boiler was running. Also, the accumulated pellets pushing from conveyor may hamper the temperature measurement.

Table 5.5: Temperature of secondary air under different air staging conditions

	Upper left	Lower right
Normal air setting	851.08°C	484.53℃
Weak primary air setting	866.72°C	481.03℃
Weak secondary air setting	895.91°C	476.45℃

5.4.3 Temperature Distribution of Combustion Chamber

The boiler chamber is the place where the combustion process happens. In this section, the thermocouples placed in chamber were further adjusted to new locations to investigate the temperature distribution in combustion chamber of the boiler and verify the measured inlet temperature of heat exchanger (see Figure 5.8). Five thermocouples were placed from left to right on the central line of the combustion chamber, having similar height. The leftmost (TC 4) and rightmost (TC 5) thermocouples were below the middle ring of heat exchanger while the TC 3 and TC 2 were below the inner ring, similar to the ones set in Figure 5.5 (inlets of HX 1 and HX 2 tubes). The middle thermocouple (TC 1) was located at the central location of the boiler but above mixing plate. The temperature measurement in combustion chamber was also carried out under three different air staging conditions, normal air setting, weak primary air setting and weak secondary air setting. The results are shown in Figure 5.9.

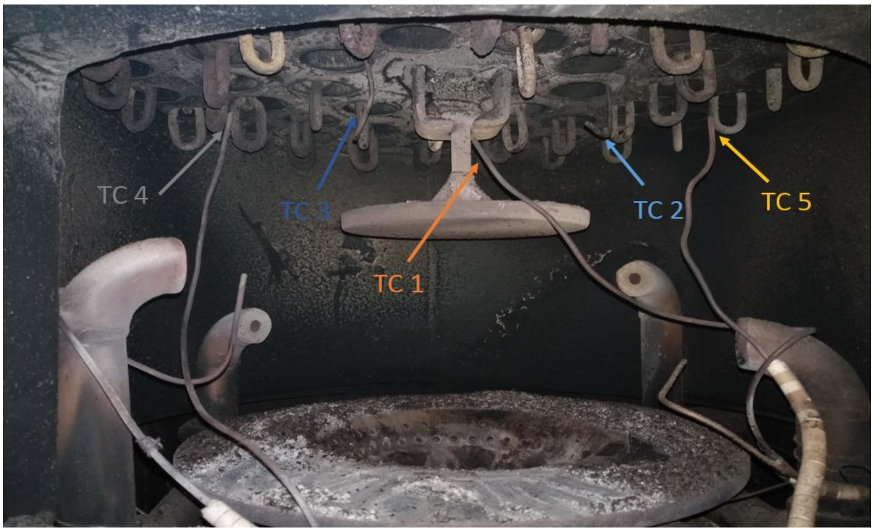

Figure 5.8: Positions of the five thermocouples placed in combustion chamber

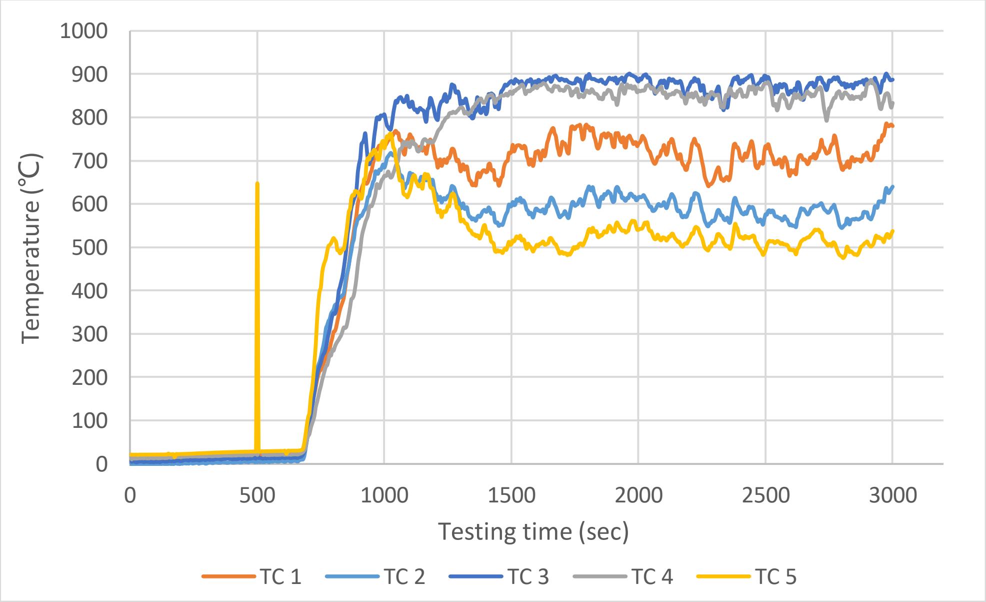

(a). Normal air setting

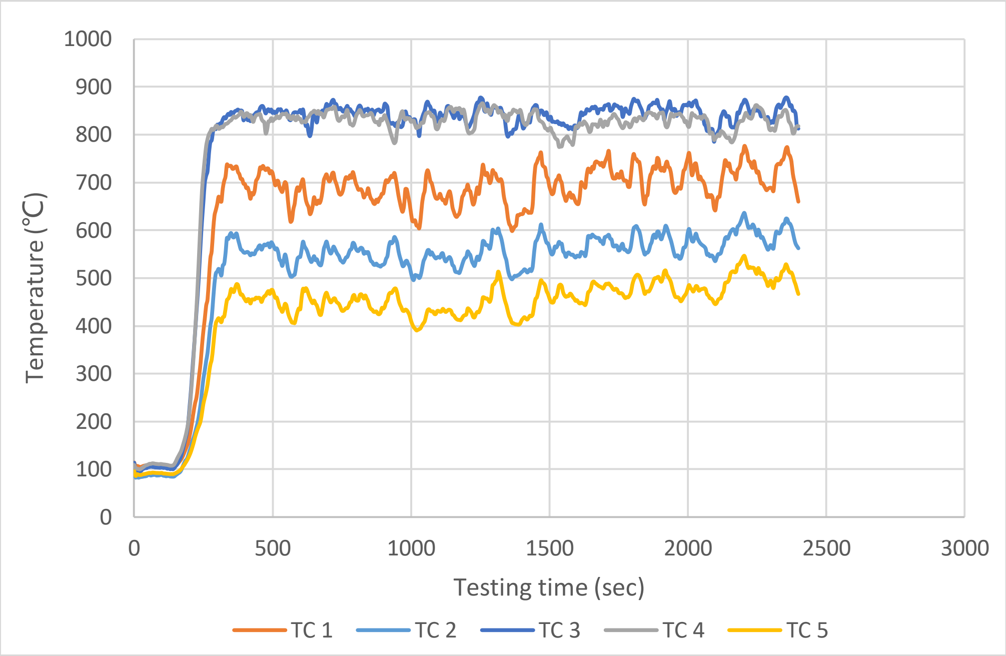

(b). Weak primary air setting

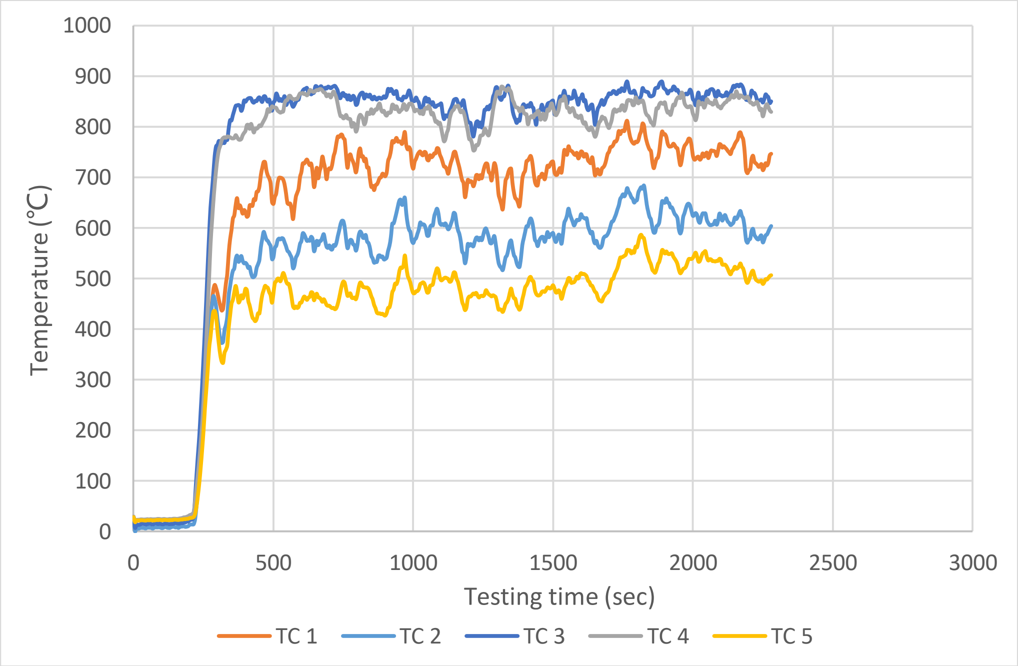

(c). Weak secondary air setting

Figure 5.9: Temperature distribution in combustion chamber under different air setting conditions

The result obtained from Figures 5.9 a, b and c can confirm the observation from section 5.3.2. The temperature of TC 3 which represented as the point of HX 1 or HX 3 due to close positions (see Figure 5.5) had a higher temperature than TC 2 which can be treated as the point of HX 2 because of similar position. That phenomenon can be observed in all air staging conditions. Furthermore, it was noted that the trends of five temperatures were the same under three air staging conditions, though the values were slightly different due to the change of air setting conditions.

When decreasing primary or secondary air inlet, the measured peak temperature in chamber reduced from 901℃ to around 850℃ and the temperature of other locations also had different levels of decline. For each air staging condition, temperatures of five thermocouples had a gradual downward trend from left to right of the combustion chamber. Using the case with normal air setting as an example, temperatures of TC 4 and TC 3 on the left side had similar and highest values. With the thermocouple moving to further right positions, the temperature decreased progressively, from 800~900℃ (TC 3& 4) to under 500℃ (TC 5).

It should be pointed out that the three tests above were carried out in one day to ensure the same or close environmental conditions, but there was at least two hours interval between two tests. The test would not be conducted until the chamber was cooled to room temperature. That was the main reason why the heating rates in weak primary and weak secondary air settings were much faster than the one with normal air setting as the biomass boiler had finished 'warm-up' in the first test. All the tests had been repeated afterward. The results showed slightly different values, but the same trends.

It is known that each experiment would generate different shape of flame in combustion chamber due to various reasons such as the boiler structure or environmental conditions, which will be stated in detail later. Combining with the observation from Figure 5.9 and Tables 5.2 to 5.4, the direction and peak of flame can be predicted when combustion process reached stable state. Specifically, for this small-scale biomass boiler, the flame would be generated and directed to the left side, mainly towards the left front. This conclusion can be verified by the phenomenon author observed when opening the boiler door during operating process (see Figure 5.10). The behaviour of ‘opening the door’ took place at the end of test when boiler was running but temperature record had been ended. Also, since the boiler was running in a closed laboratory and the door was only slightly opened to minimum the effect of atmospheric wind on combustion process in chamber, the phenomenon observed by author was reliable.

Figure 5.10: Photos of the flame from combustion chamber during operating process

The slanting flame may relate to the ignition way. When observing the design of combustion chamber, it can be found that the heat gun was located on the right side of fire pan and surrounded by primary air inlet holes (see Figure 3.11). The way of electric ignition coupling with primary air supply may generate this kind of special flame shape. If some primary air holes/ slots were blocked during operation, uneven primary air would be supplied, then affecting the combustion behaviour. That would also make the fire becoming lazy and smokey though it was not observed in our tests. Similarly, the slanting flame may be generated when the secondary air which provided by four vent tubes was uneven due to some reasons such as partial blockage in left side vent tubes. This possibility had been largely avoided since the fire pot was regularly checked and cleaned. In addition, some environmental conditions should be also taken into account. When the motor was on, both primary and secondary air were introduced by air fans, sucking atmospheric air to the chamber via connection tubes. Hence, the weather conditions on the day of experiment may have an impact on combustion behaviours. For example, the windy day may result in a larger air inlet than usual, further changing the flame characteristics. Furthermore, the transport way of biomass pellets may affect the combustion flame to some extent. The pellets were delivered from the hopper (right side of the boiler) to combustion chamber via conveyor screw, then emerging from screw to fire pot. The way pellets stacked, especially in excess condition may be one of the factors affecting the flame. Although the optimum ‘kindle time’ had been set for all the tests, insufficient air supply may aggravate the uneven accumulation of pellets. Overall, observing the flame was helpful to understand the energy conversion inside the chamber and improve the combustion process further.

5.5 Measurement of Gas Composition within Combustion Chamber

5.5.1 Boiler Modification

In this section, some modifications were made on the biomass boiler to investigate the concentrations of some main sample gas components in combustion chamber. Two holes were drilled on the top lid for inserting the water-cooled probe with one-meter length to the combustion chamber. As introduced in 3.2.3.2, the water-cooled probe was used to cool down the sampled chamber gas and deliver it to gas analyzers. Furthermore, it would protect the sampled chamber gas not be affected by any potential reactions when passing the heat exchanger. A set of ABB gas analyzers was used to detect the concentrations of some main parameters, including CO, CO_2, O_2 and CH_4, which the detailed introduction has been shown in section 3.2.3.

The positions for water-cooled probe are shown in Figure 5.11. Unfortunately, the experiments in two locations cannot be performed concurrently because of the limited number of probes. Therefore, one hole was sealed completely when the other one was used to assist measurement during the experiment. The inlet of water-cooled probe was adjusted to a suitable position (see Figure 5.12) to suck sample gas in order to match the temperature measured at heat exchanger inlet in section 5.4.3. Three air staging conditions were applied for the tests of using water-cooled probes on both left and right sides. Although ignition and the beginning phase of combustion process were important to monitor due to the generation of a large number of harmful emissions, many particles were also emitted during these phases. Thus, for the purpose of protecting gas analyzers, chamber gas sampling system was only connected to the boiler when combustion process approaching steady status by monitoring flue gas temperature.

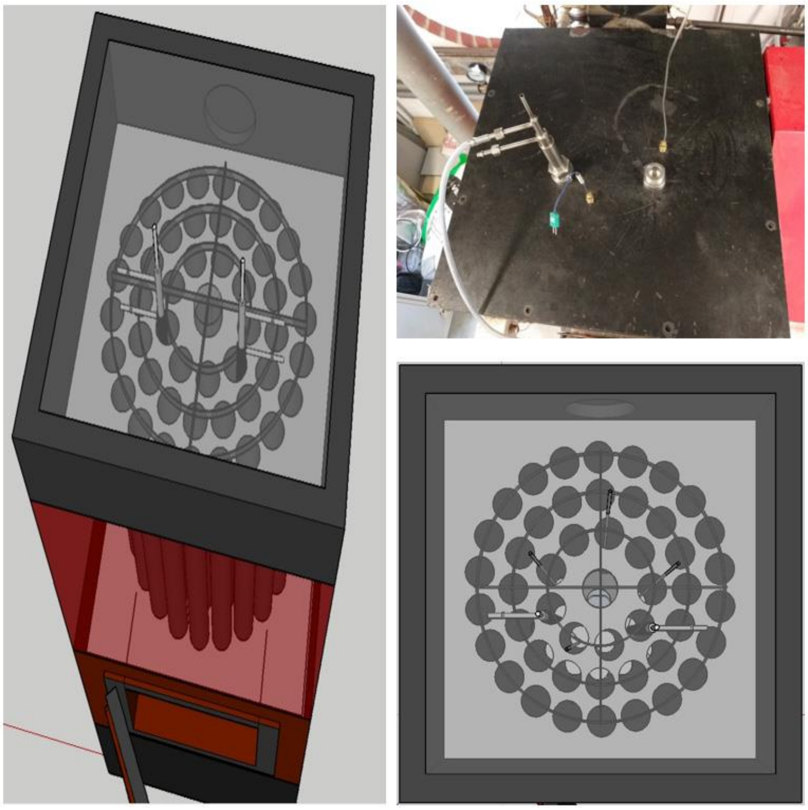

Figure 5.11: Positions of the water-cooled probe for chamber gas sampling

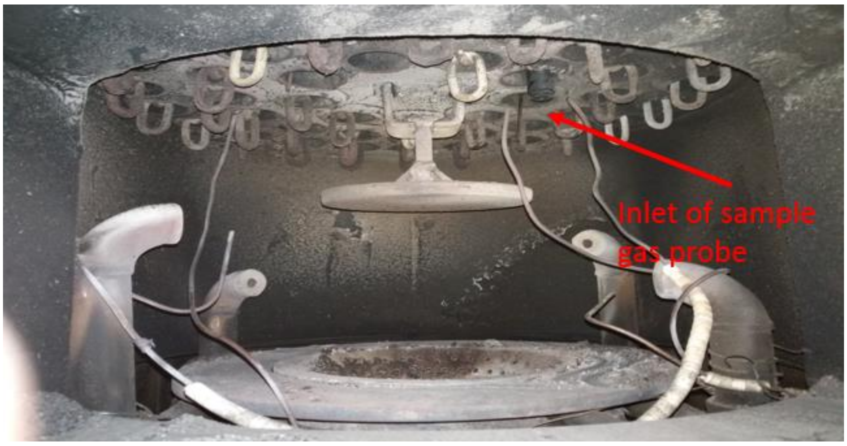

Figure 5.12: Position of the water-cooled probe inlet in combustion chamber

5.5.2 Composition Results of Left Combustion Chamber

In the first stage, water-cooled probe was put in the left side of combustion chamber to test the concentrations of some main gaseous components in sampled chamber gas. The results under different air staging conditions are shown in Figure 5.13 to 5.15.

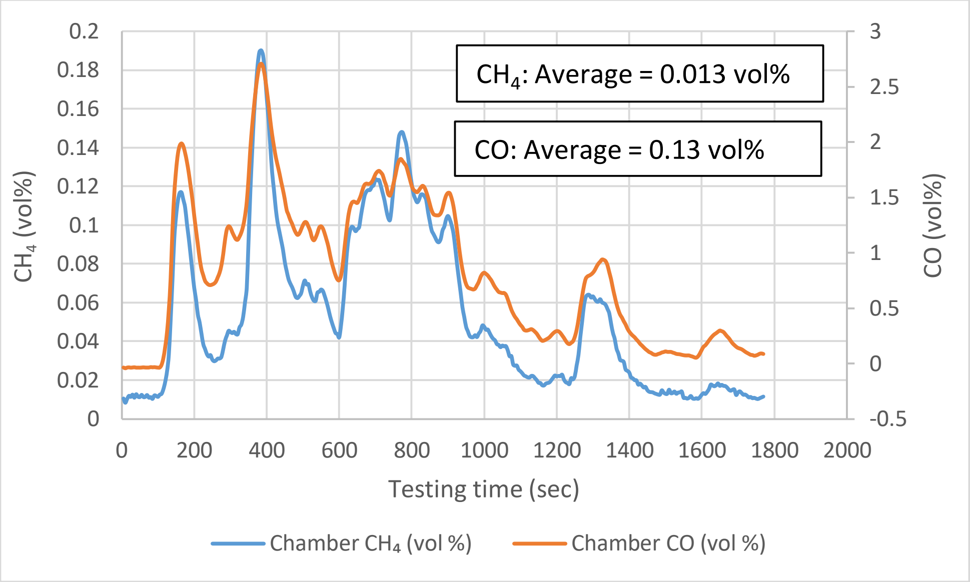

(a) CO and CH_4

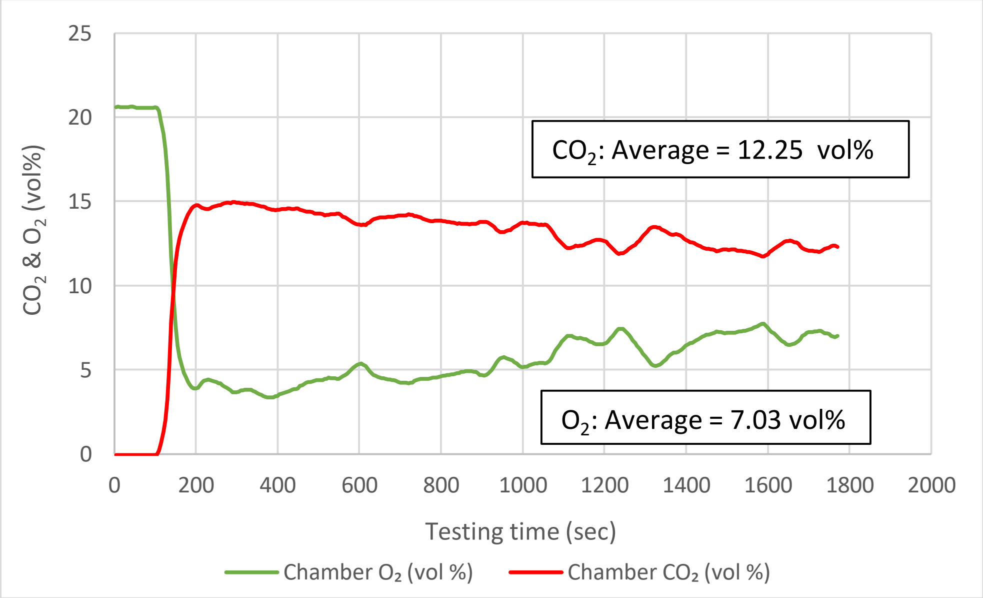

(b) CO_2 and O_2

Figure 5.13: Concentrations of some main gaseous components in the left side of combustion chamber under normal air setting

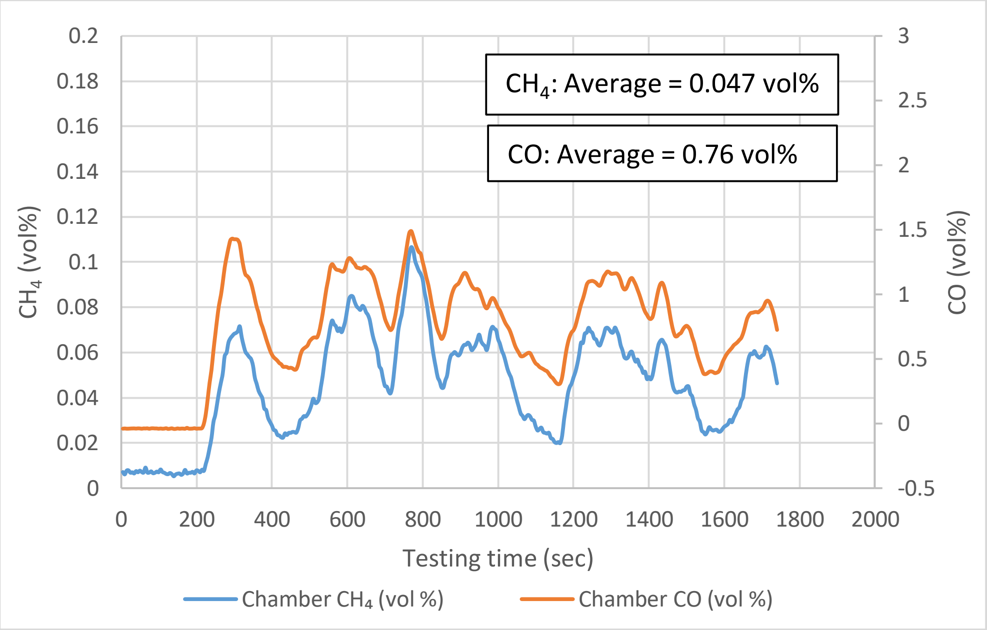

(a) CO and CH_4

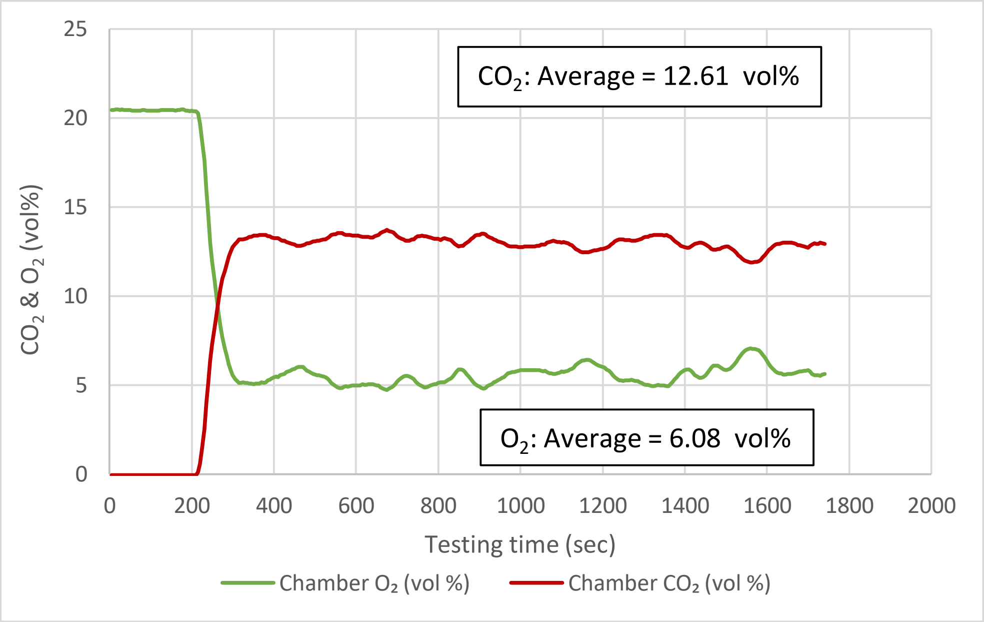

(b) CO_2 and O_2

Figure 5.14: Concentrations of some main gaseous components in the left side of combustion chamber under weak primary air setting

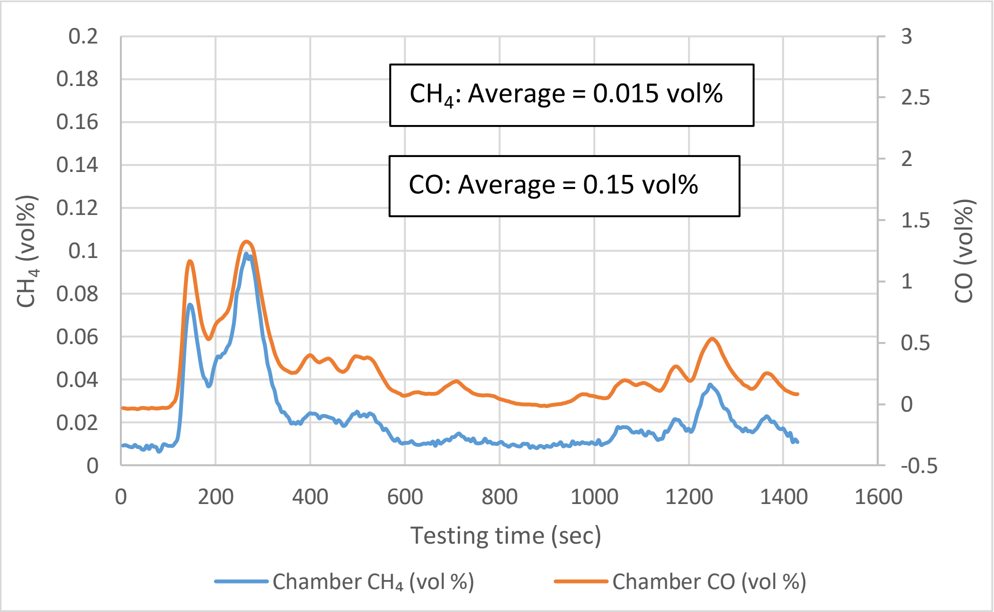

(a) CO and CH_4

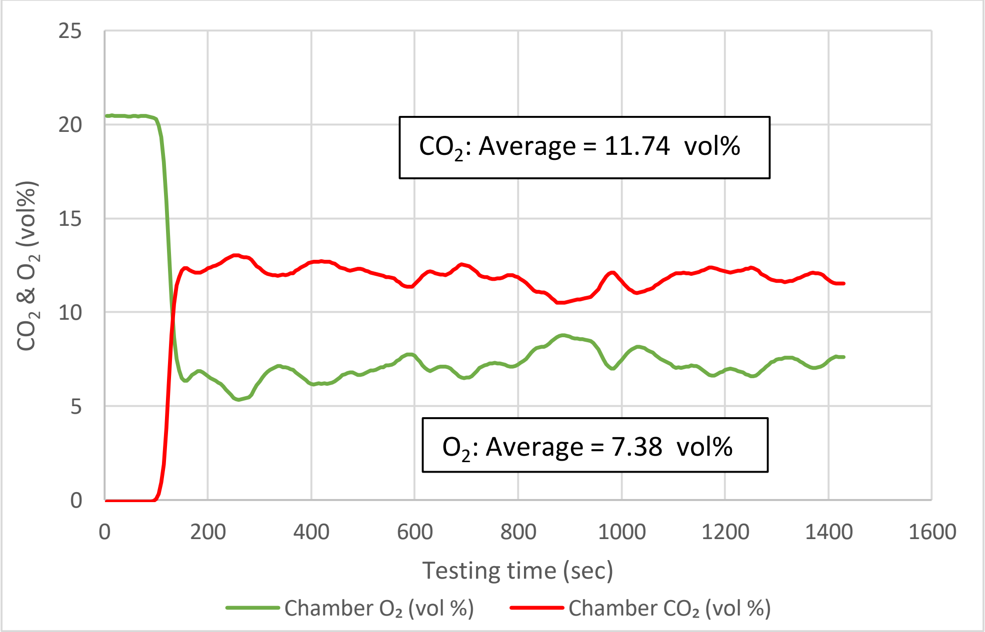

(b) CO_2 and O_2

Figure 5.15: Concentrations of some main gaseous components in the left side of combustion chamber under weak secondary air setting

Figure 5.13 displays the fluctuating trends of some main compositions (CH_4 and CO, O_2 and CO_2) under normal air setting condition. From Figure 5.13, it can be found that CH_4 and CO had relatively changeable trends while O_2 and CO_2 were comparatively stable after a period of run. The fluctuating trends of CH_4 and CO were the same while those of O_2 and CO_2 were opposite. This phenomenon also happened in the cases of weak primary and weak secondary air settings (see Figures 5.14 and 5.15).

CO was the typical residual product of incomplete combustion, which can be used to represent the state of combustion process. At the initial stage of sampling, CO had a rapid changing trend and touched its peak value of the whole process, 2.7 vol% under normal air setting. Therefore, it can be seen the combustion was incomplete in this stage, even the concentration of O_2 in the combustion chamber was high (> 7%), generating a large amount of CO in a short time. It was largely due to the uneven fuel feeding and limited combustion space in the combustion chamber, resulting in inadequate residence time of combustion gases in the room, which typically happened in the small-scale boilers. This tendency was also observed in Zeng et al., (2016) when they used blended biomass pellets in a similar small-scale boiler.

The variation of CH_4 concentration generally followed the trend of CO during combustion process. At the beginning stage, the highest CH_4 concentration was observed, having 0.18 vol% under normal air setting condition. With the experiment proceeding, the variation of CH_4 turned to gentler and more stable until the end of the test. Overall, the low values of CH_4 and CO with stable trends can confirm the ideal complete combustion happened in the combustion chamber. The only exception happened under the condition of weak primary air setting, which the trends of CH_4 and CO were still struggling until the end of the experiment.

As mentioned in section 2.5.2, biomass type and fuel size were found to be the pre-combustion factors of CH_4 emissions. In this study, it can be found that CH_4 emission was also determined by the amount of primary air during the combustion process. For instance, the CH_4 emission (average 0.015%) under weak secondary air setting was close to the value under normal air staging (average 0.013%). However, there was a significantly harmful effect on CH_4 emission when reducing the primary air. The CH_4 emission under weak primary air setting was much higher (average 0.047%) than other two conditions. That can be explained by the reason that CH_4 emission was mainly generated in the devolatilisation stage of combustion process, which strongly related to the amount of primary air. Therefore, it can be concluded that comparing with original air staging, the variation of amount of primary air affected CH_4 emissions primarily. On the other hand, the fluctuation of secondary air in combustion process had little impact on CH_4 emissions, which was consistent with the conclusion of Vicente et al. (2015). They proposed that adding secondary air to conventional combustion system only had a slight effect on CH_4 emissions.

5.5.3 Composition Results of Right Combustion Chamber

In the second stage, the water-cooled probe was then moved to the right side of combustion chamber after conducting the tests on the left side. Same components (CH_4, CO, O_2 and CO_2) of sampled chamber gas were monitored and the tests were still conducted under three different air staging conditions. The results are shown in Figure 5.16 to 5.18.

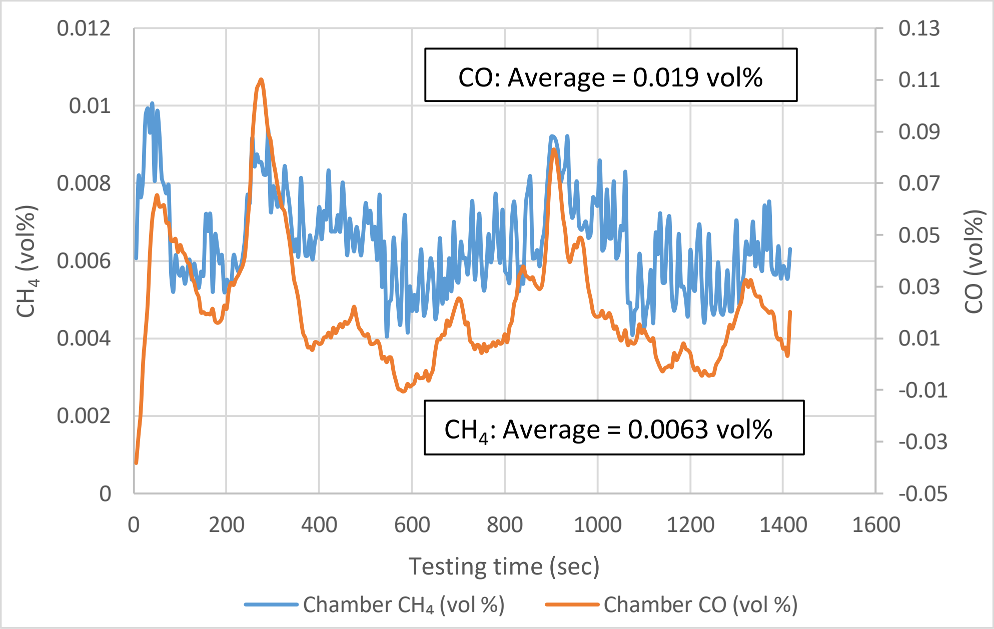

(a) CO and CH_4

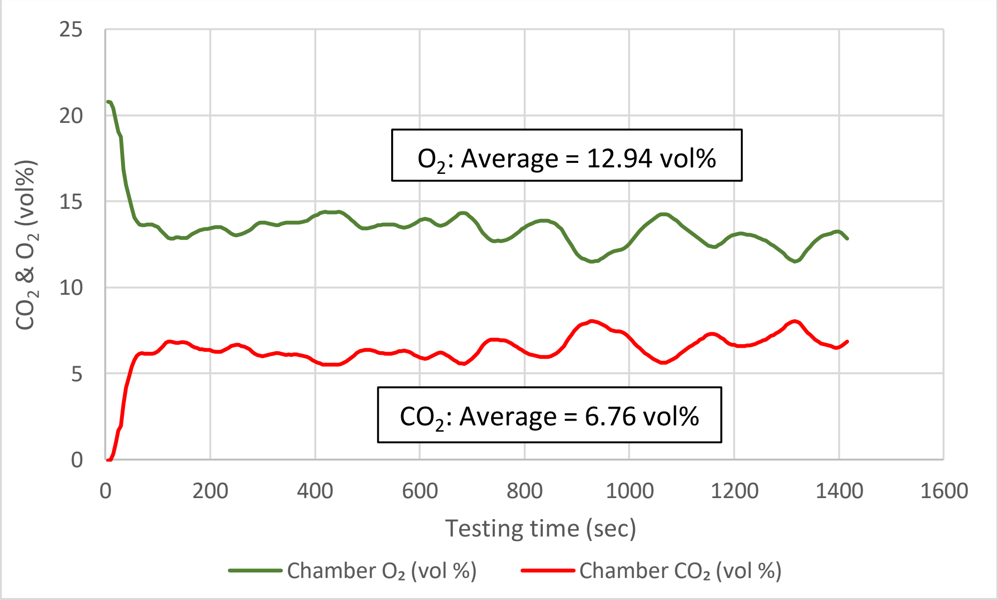

(b) CO_2 and O_2

Figure 5.16: Concentrations of some main gaseous components in the right side of combustion chamber under normal air setting

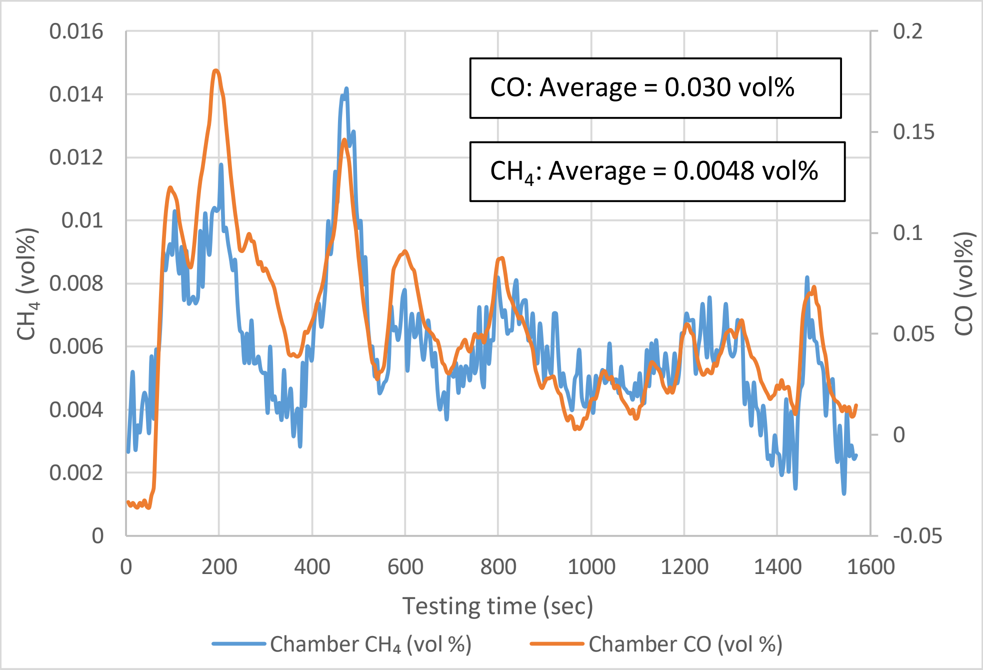

(a) CO and CH_4

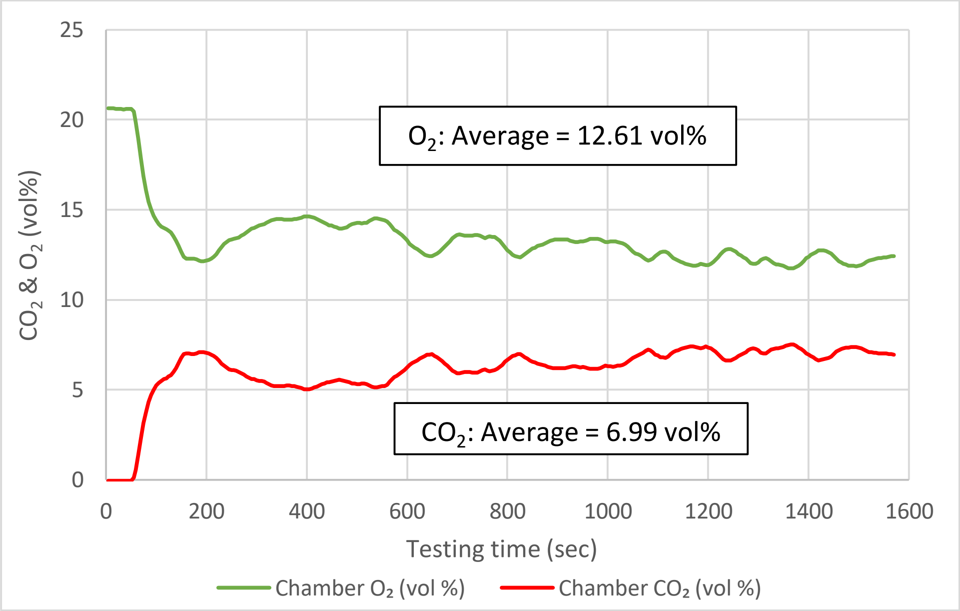

(b) CO_2 and O_2

Figure 5.17: Concentrations of some main gaseous components in the right side of combustion chamber under weak primary air setting

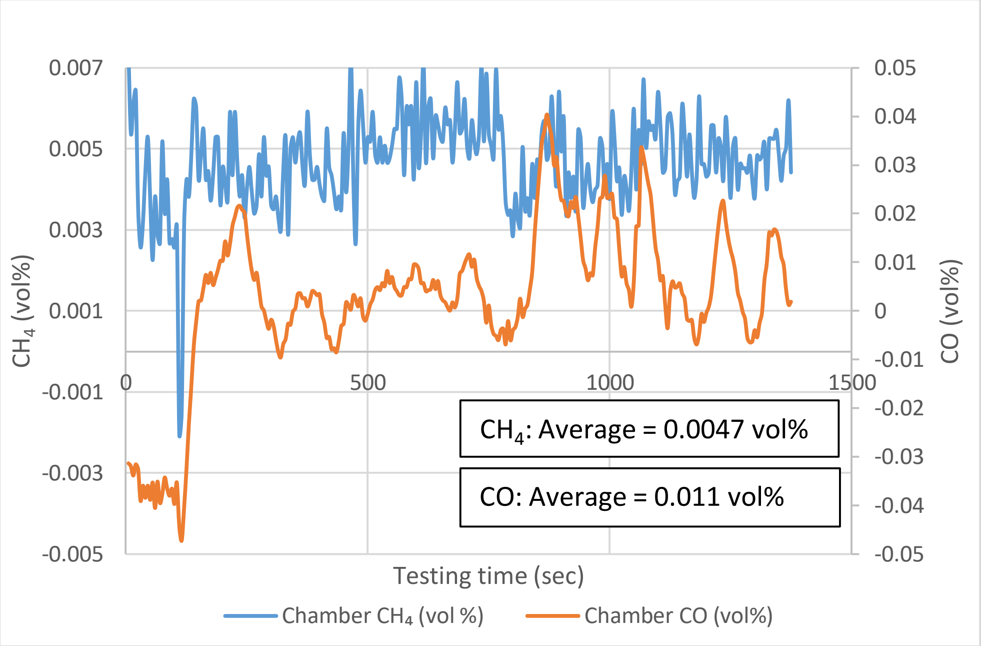

(a) CO and CH_4

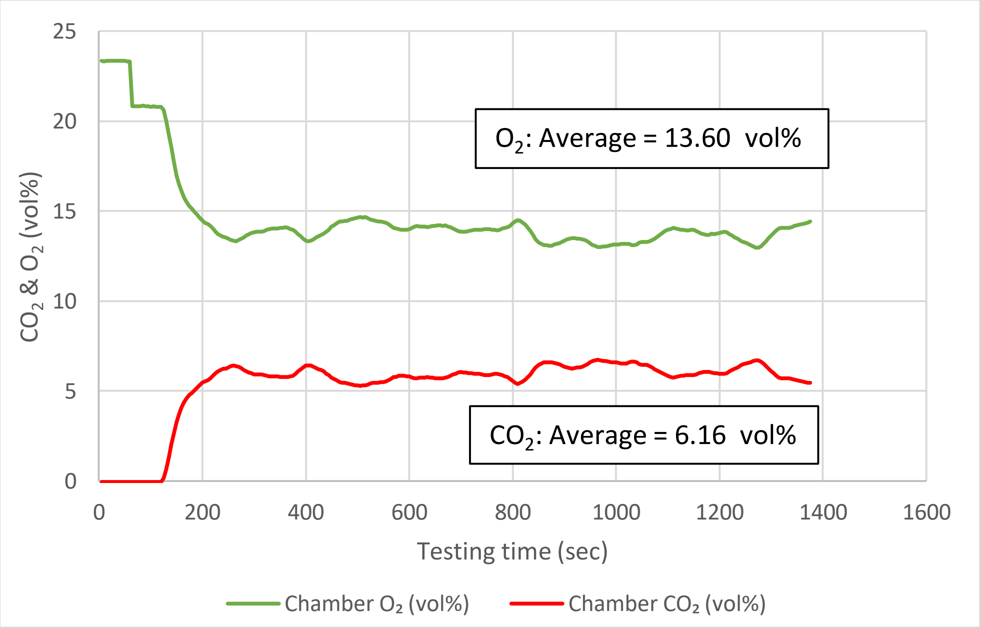

(b) CO_2 and O_2

Figure 5.18: Concentrations of some main gaseous components in the right side of combustion chamber under weak secondary air setting

From Figures 5.16 to 5.18, it can be seen that the emission concentrations obtained from right side of combustion chamber showed large difference with those from the left side. O_2 and CO_2 concentrations were around 13% and 6.5% under different air staging conditions when the probe was on the right side of chamber while they were around 5.5% and 12% on the left side. That further confirmed the uneven combustion in chamber though both sides of the chamber were in excessive air-rich environment.

Also, the trends of CH_4 concentration shown under all air staging conditions had continuous but minor fluctuation. The expected peak of CH_4 happened under normal air and weak primary air conditions. Again, the fluctuation may be caused by insufficient air during combustion process, especially during preheating and devolatilisation stages. It may also relate to the data drift caused by gas analyzer as the measured value was close to the lower limit. Overall, the CH_4 concentrations obtained under all air staging conditions were similar, 0.0063%, 0.0048% and 0.0047%, an order of magnitude lower than the values in the left chamber side. The low concentration of CH_4 illustrated that the combustion in the right side of chamber was more sufficient than the left side, then producing limited CH_4.

5.5.4 Results Comparison and Analysis

To determine the parameters for CH_4-SCR tests in next chapter, the measured result of sampled chamber gas near heat exchange inlet was needed to combine with its corresponding temperature. However, when choosing the paired position(s) for thermocouple and water-cooled probe, one tube in heat exchanger cannot be used for both temperature and emission measurements simultaneously since the cooling water in the probe may affect the temperature measurement by thermocouple. Similarly, the results of temperature and emission measurement from the same position but two separate tests were not comparative due to the potential change of ambient environment. Hence, the measured results of probes and thermocouples with close positions in the same experiment were applied. As shown in Figure 5.11, the temperatures of HX 1 and HX 2 were assumed as the corresponding temperature of two positions of sampled chamber gas. The concentrations of main sample gas components from both sides of combustion chamber and HX 1 & HX 2 temperatures which has displayed in the last two sections are combined in Table 5.5 below.

Table 5.6: Concentrations of main sample gas components in both sides of combustion chamber and corresponding temperatures

Left side of combustion chamber					
	Chamber-O_2 (vol %)	Chamber-CH_4 (vol %)	Chamber-CO (vol %)	Chamber-CO_2 (vol %)	Temperature of HX 1 (℃)
Normal air setting	7.03	0.013	0.13	12.25	868.83
Weak primary air setting	6.08	0.047	0.76	12.61	839.33
Weak secondary air setting	7.38	0.015	0.15	11.74	830.36
Right side of combustion chamber					
	Chamber-O_2 (vol %)	Chamber-CH_4 (vol %)	Chamber-CO (vol %)	Chamber-CO_2 (vol %)	Temperature of HX 2 (℃)
Normal air setting	12.94	0.0063	0.019	6.76	574.99
Weak primary air setting	12.61	0.0048	0.030	6.99	517.55
Weak secondary air setting	13.60	0.0047	0.011	6.16	506.51

As discussed earlier, CH_4 (representing unburnt hydrocarbon) always followed the trend of CO during combustion process. If the air inlet increased, especially via primary air, complete combustion may be achieved and CO & CH_4 (unburnt hydrocarbon) can be controlled or eliminated correspondingly. However, it would affect boiler efficiency and generate a higher fuel bed temperature in combustion chamber, then resulting in higher NOx emission. Therefore, it can be concluded that the emissions of NO_x, CO and unburnt hydrocarbon emissions were interrelated and interacting. There was always a trade-off between NOx and CO & unburnt hydrocarbon if using primary strategies to control gaseous emissions in small-scale boiler(s).

As a solution, the trade-off issue may be effectively solved by using suitable CH_4-SCR technology since all the reactants for catalytic reaction, including NO_x, CH_4 and O_2 are all available in the process of biomass combustion. Thereinto, there was sufficient oxygen in the most areas of combustion chamber and heat exchanger. Similarly, NO_x as the key gaseous emission had around 70 ppm existing in flue gas though the value may be affected by biomass type and other factors such as reaction temperature. According to the experimental results above, CH_4, the typical one among the group of hydrocarbons, had been proved to exist in biomass combustion and its concentration was determined by some operating conditions such as the amount of primary air. However, its existence was only in a partial area of combustion chamber in this boiler. Specifically, CH_4 concentration was limited in the right side of chamber as it was 'excessive air rich' and had relatively complete combustion. On the other hand, there was a certain amount of CH_4 generated in the left side of combustion chamber, average value of 0.047 vol% (470ppm) and the highest value of 0.118 vol% (1180ppm) when using weak primary setting. Hence, CH_4 can be used as the potential reducing agent for HC (CH_4)-SCR reaction(s). It cannot be ignored that the presence of CH_4 was also accompanied by the production of high-level CO due to incomplete combustion, especially in the beginning stage. Therefore, the effect of CO on CH_4-SCR should be studied in the next chapter since CO may be further oxidized to CO_2 in redox reaction, resulting in other potential sub-reactions.

More importantly, it was significant to find a suitable temperature range for potential CH_4-SCR application. When combining Figure 5.4 with Table 5.6, the area of left side of combustion chamber was more suitable as it had a 'methane-rich' atmosphere. In that zone, a wide optional temperature range was available depending on the location, from up to 950°C in combustion chamber and as low as 100°C~200°C in the upper of heat exchanger. In conclusion, all the elements (reactants and reaction temperature) required for the potential CH_4-SCR system can be found in the combustion process of small-scale boiler.

5.6 Summary

This chapter tested the overall performance of a 50kW biomass boiler in terms of main flue gas emissions (e.g., NOx and CO) by burning recommended wood pellets. Also, this chapter presented the temperature distributions and concentrations of some main components (e.g., CH_4, CO and O_2) within biomass chamber for the potential catalytic tests. The following conclusions can be summarized:

- The small-scale (50kW) Ashwell biomass boiler showed great performance, discharging around 72ppm (75g/GJ) NOx under different air setting conditions. The variation of primary or secondary air had a minor effect on NOx emissions and NOx emissions were mainly generated via the Fuel-N route from nitrogen content of selected fuel.
- Methane (CH_4) was proven to be present in biomass (wood) combustion process. Compared with normal air setting, reducing secondary air had limited impact on CH_4 concentration. However, the reduction of primary

air increased CH_4 concentration significantly as CH_4 was mainly generated in the devolatilisation stage of combustion process, which strongly related to the amount of primary air.

- The production of CH_4 was always accompanied by the appearance of high-level carbon monoxide (CO). As the products of incomplete combustion, both of them had the same tendency during combustion process.
- Due to the structure of this small-scale biomass boiler, concentrations of CH_4 and CO were uneven in combustion chamber though the chamber was always in an excessive oxygen environment. It was mainly caused by the small space of combustion chamber and insufficient mixing between fuel and air.
- For potential SCR applications, the presence of some main reactants (NOx, CH_4, CO and O_2) had been identified in combustion process and the corresponding reaction temperature range had been explored.

CHAPTER 6. CATALYTIC REDUCTION OF NOx BY METHANE AND CARBON MONOXIDE OVER VARIOUS CATALYSTS

6.1 Introduction

As introduced in Chapter 2, HC-SCR has shown its bright future to control NOx emissions as one of post-combustion treatments. Methane (CH_4), the classic representative of hydrocarbon, is treated as an environmental-friendly reducing agent in HC-SCR system since no more additional reducing agent is necessary in the catalytic system. It is widely accepted that NOx reduction by CH_4-SCR in the presence of oxygen proceeds under reaction 6.1 (Gao et al., 2003). Based on the tests of biomass boiler which has been presented in Chapter 5, there is a certain level of NOx, CH_4, O_2 and CO in the heat exchanger tubes where HC-SCR catalysts may be placed. However, the concentrations of these species are affected by many factors such as the position or air staging. The feasibility of NOx reduction over Co- and Fe- supporting catalysts by utilizing CH_4 and/or CO which are expected to be present in the NOx containing gases is investigated in this chapter. The synthesis of different catalysts, apparatus and synthesis gas analysis system used for experiments have been presented in section 3.3. As mentioned in section 3.3.1, compared with the effect of synthesis methods, NOx reduction is affected by catalyst loading content and temperature conditions, which will be investigated in this chapter.

$$\mathrm{CH_4 + 2NO + O_2 \rightarrow N_2 + CO_2 + 2H_2O} \qquad [6.1]$$

6.2 Furnace Temperature Measurement

It is generally accepted that the reaction temperature is one of the most critical factors which affects the performance of catalytic reaction(s). As mentioned in section 3.3.5, there is a phenomenon of uneven temperature distribution inside V-DTF which is to be used to house the catalytic reactor of this study. Hence, the temperature distribution of V-DTF was measured firstly in order to determine the ideal location of the fixed-bed reactor for the catalytic experiments.

The temperature measurement was carried out by using a two-meter long K-type thermocouple inserting from the top or bottom of reactor (stainless steel tube). The main reactor (290mm length) was equally divided into five measuring points (T1 to T5). It can be seen from Figure 6.1 that T5 and T1 were the inlet and outlet of main reactor respectively. Five measuring points were measured separately by changing the position of thermocouple under one setting temperature. Also, main reactor was adjusted its position in V-DTF to measure the temperature distribution of furnace. The rough position of main reactor was chosen at the upper part of V-DTF, not the lower part, to avoid any undesired reactions happened before synthesis gas touching catalyst. Furnace setting temperatures of 300°C, 400°C and 500°C were chosen for the experiments at this stage.

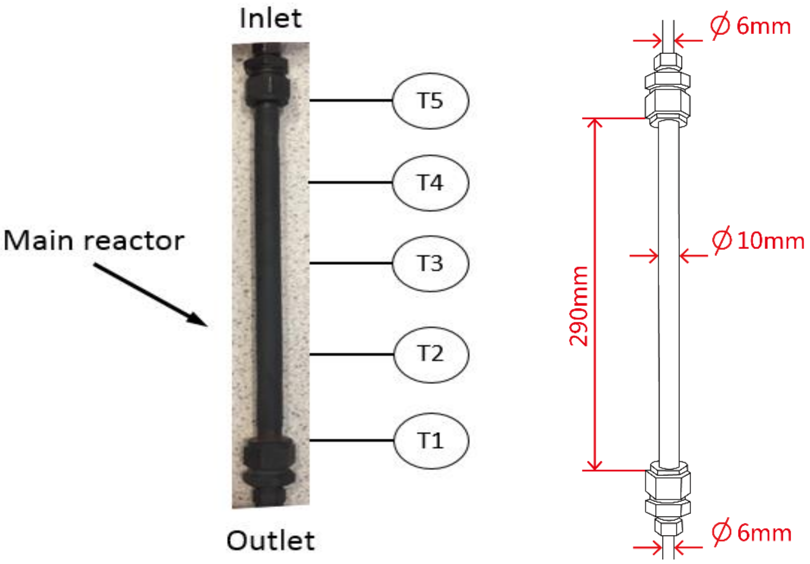

Figure 6.1: Five measuring points in the main reactor

6.2.1 Temperature Measurement without Feed Gas

First of all, temperature profiles of the main reactor within different setting temperatures were measured by merely heating the furnace without any feed gas. Five positions of the main reactor in V-DTF were chosen, including 10mm, 50mm, 150mm, 250mm and 350mm from the top (inlet) of main reactor to V-DTF inlet. The results are shown in Figure 6.2. It should be mentioned that the values in the horizontal axis of Figure 6.2 mean the distance from the measured point to the V-DTF inlet. For instance, T5 and T1 points in Figure 6.2 (a) had 10 mm and 300 mm distance to furnace inlet while they were also the inlet and outlet of main reactor.

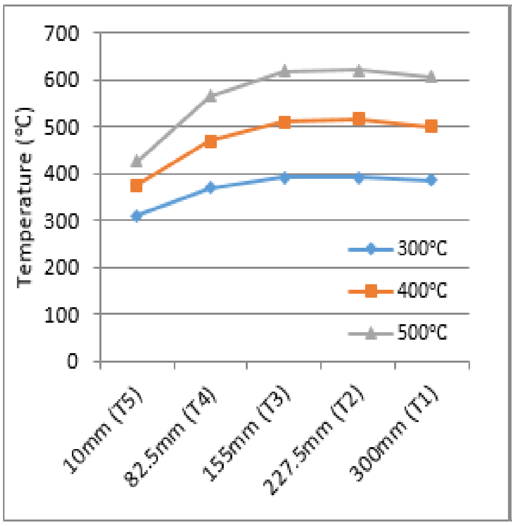

(a) 10mm from main reactor inlet to furnace inlet

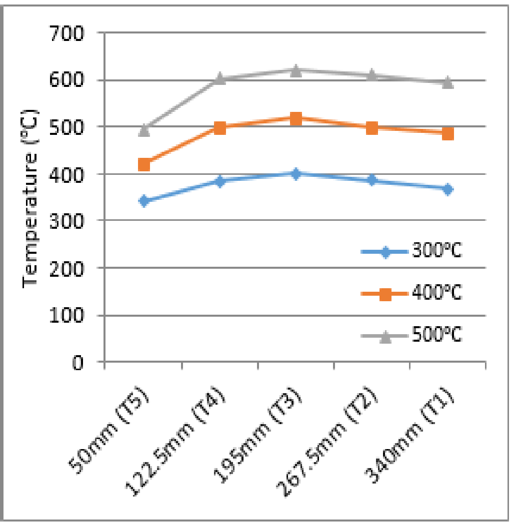

(b) 50mm from main reactor inlet to furnace inlet

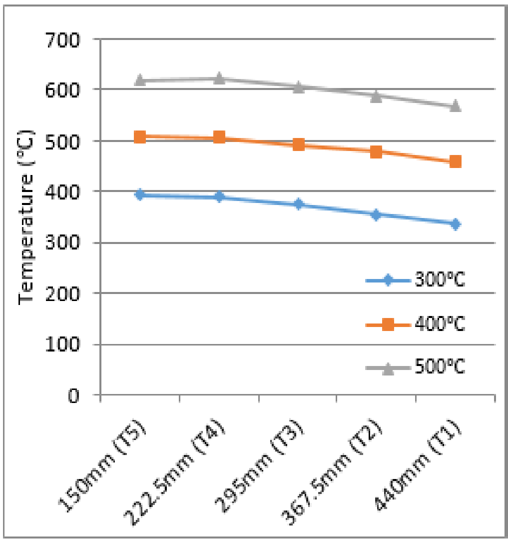

(c) 150mm from main reactor inlet to furnace inlet

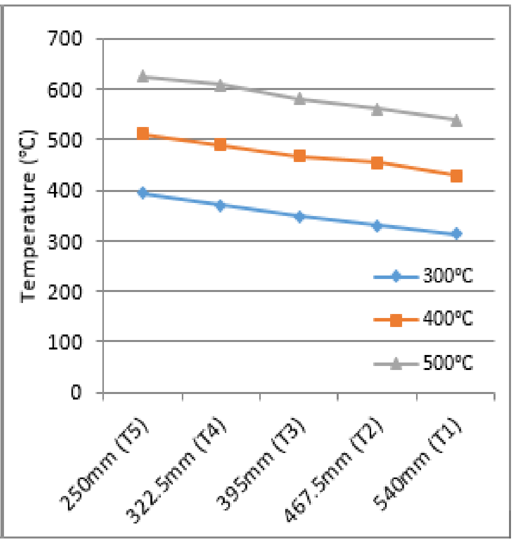

(d) 250mm from main reactor inlet to furnace inlet

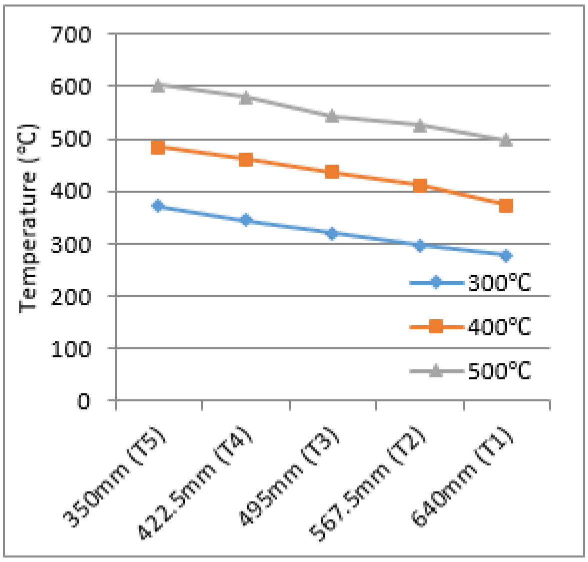

(e) 350mm from main reactor inlet to furnace inlet

Figure 6.2: Temperature profiles of the main reactor without feed gas in the conditions of different locations and setting temperatures

Based on the trends shown in Figure 6.2, it can be seen that the temperature distribution inside main reactor was hugely uneven under all setting temperature conditions. For instance, when the furnace operating temperature was set as 300°C, the measured temperature gap in the main reactor reached around 100°C (Figure 6.2 d & e), which could bring significant uncertainty of experiments in terms of catalytic performance. However, the temperature increase of a fixed point in most of the positions was smooth and close when increasing the setting temperature.

The temperature distribution of furnace (V-DTF) can be concluded when combing all the values in Figure 6.2. At a constant setting temperature, the temperature profile of upper half furnace showed the tendency to rise rapidly and then decrease gradually. For example, at setting temperature of 500℃, the highest temperature in the upper half furnace was over 600℃ at 195mm position. After that, the measured temperatures had a decreasing trend with a slow pace, touching its corresponding setting temperature at 640mm position. That can be verified by the temperature measured by the integrated thermocouple inside V-DTF since the deepest measured point (640mm) was close to the center of furnace.

Based on the measurement above, the position of '10 mm case' (see Figure 6.2 a) was roughly selected for main reactor so that the inlet temperature of reactor was reasonable and close to its corresponding setting temperature. Consequently, it can minimize the experimental uncertainty which caused by the nature (temperature error) of V-DTF.

6.2.2 Temperature Measurement with Feed Gas (Air)

After selecting the location of the main reactor in V-DTF (10mm distance from main reactor inlet to V-DTF inlet), feed gas was introduced into the reaction reactor to test the effect of flow rates on temperature profiles. Compressed air with different flow rates of (2L/min, 4L/min and 6L/min) controlled by mass flow controller was conducted in the experiments. Also, another group of tests with the furnace setting temperature of 600°C was conducted to provide the information needed for potential experiments under high-temperature conditions. The results were compared with the results without feed gas obtained from last section. The comparison results are shown in Figure 6.3 below.

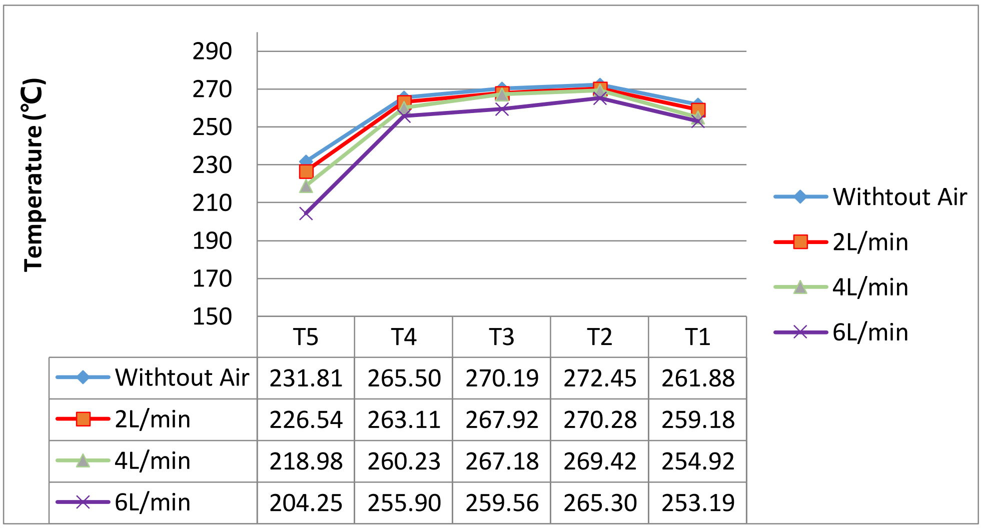

	T5	T4	T3	T2	T1
Withtout Air	231.81	265.50	270.19	272.45	261.88
2L/min	226.54	263.11	267.92	270.28	259.18
4L/min	218.98	260.23	267.18	269.42	254.92
6L/min	204.25	255.90	259.56	265.30	253.19

(a) Test at 200°C setting temperature

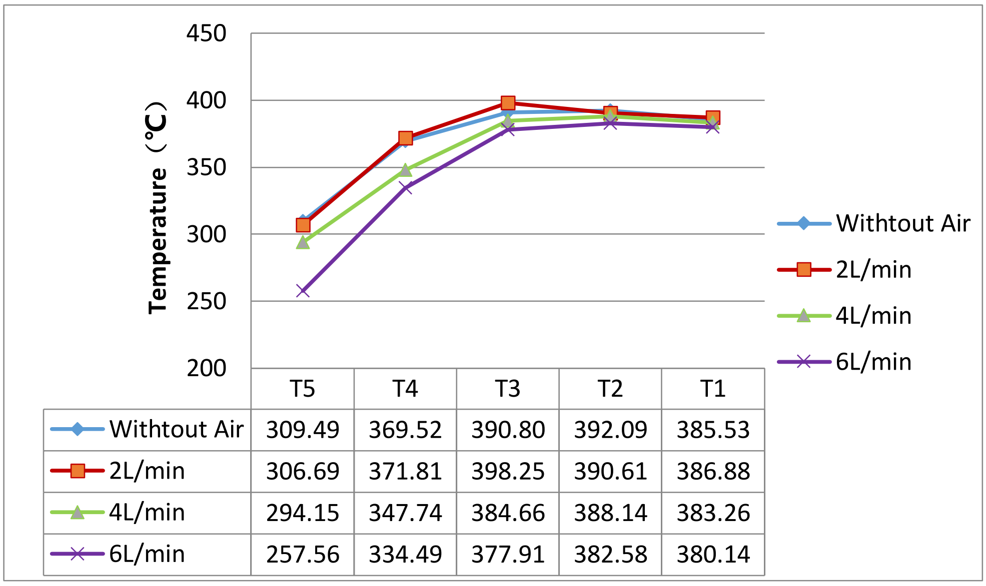

	T5	T4	T3	T2	T1
Withtout Air	309.49	369.52	390.80	392.09	385.53
2L/min	306.69	371.81	398.25	390.61	386.88
4L/min	294.15	347.74	384.66	388.14	383.26
6L/min	257.56	334.49	377.91	382.58	380.14

(b) Test at 300℃ setting temperature

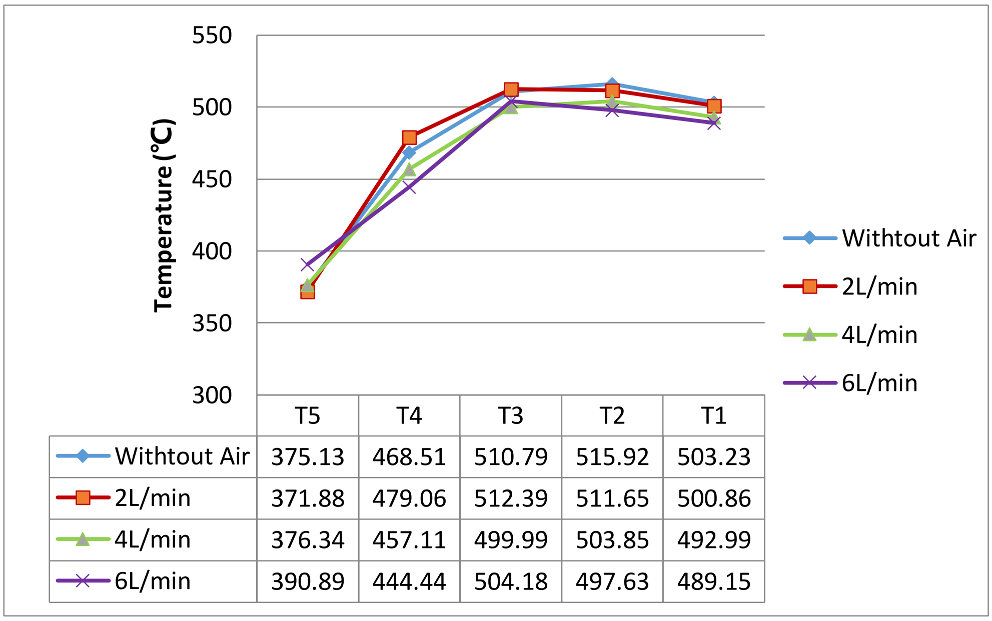

	T5	T4	T3	T2	T1
Withtout Air	375.13	468.51	510.79	515.92	503.23
2L/min	371.88	479.06	512.39	511.65	500.86
4L/min	376.34	457.11	499.99	503.85	492.99
6L/min	390.89	444.44	504.18	497.63	489.15

(c) Test at 400℃ setting temperature

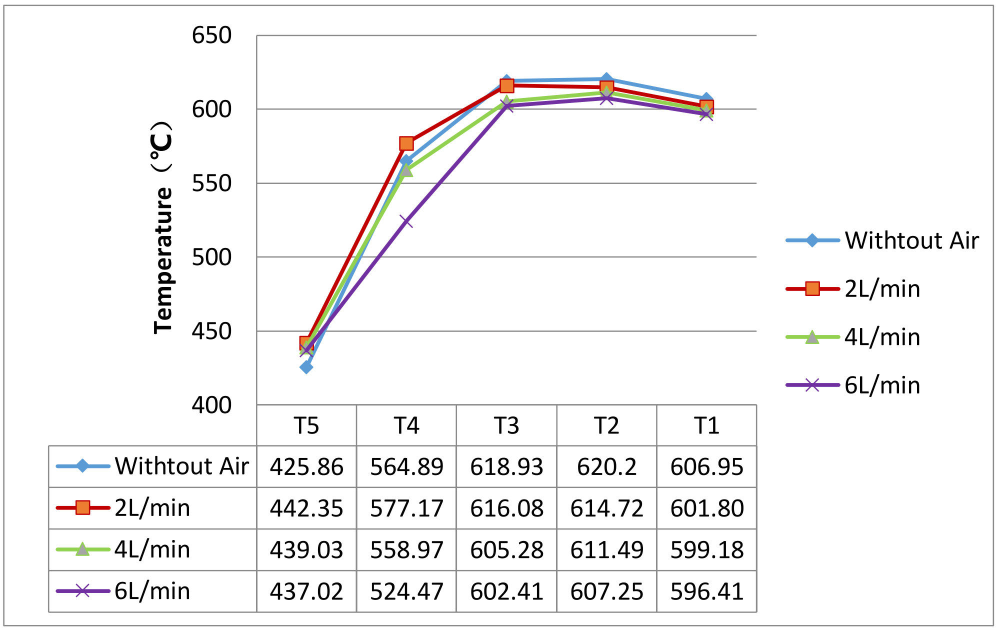

	T5	T4	T3	T2	T1
Withtout Air	425.86	564.89	618.93	620.2	606.95
2L/min	442.35	577.17	616.08	614.72	601.80
4L/min	439.03	558.97	605.28	611.49	599.18
6L/min	437.02	524.47	602.41	607.25	596.41

(d) Test at 500°C setting temperature

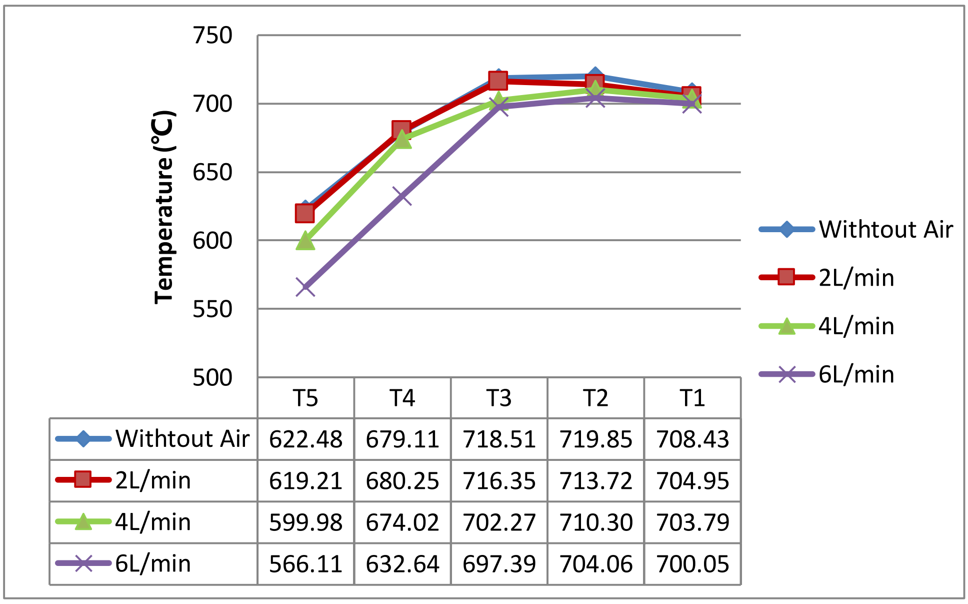

	T5	T4	T3	T2	T1
Withtout Air	622.48	679.11	718.51	719.85	708.43
2L/min	619.21	680.25	716.35	713.72	704.95
4L/min	599.98	674.02	702.27	710.30	703.79
6L/min	566.11	632.64	697.39	704.06	700.05

(e) Test at 600°C setting temperature

Figure 6.3: Temperature profiles of the main reactor under the conditions of different air flow rates and setting temperatures

Figure 6.3 displays that, with the air flowing through reaction reactor from the top to bottom, the temperatures in main reactor had varying degrees of decline. The inlet point (T5) had the most apparent temperature variation in most of the setting temperature conditions since its position was close to the top of furnace which was not fully sealed and the flowing feed gas effectively enhanced the heat convection to reduce the temperature inside tube. For the measured points close to main reactor inlet, larger flow rates resulted in lower temperatures while that phenomenon was less evident in the positions close to main reactor outlet. It should be mentioned that there may be a small measurement error due to small position difference since the temperature was measured by changing the positions of thermocouple manually.

6.3 Tests with Co-ZSM-5 Pellets

6.3.1 Reaction Temperature for Co-ZSM-5 Tests

Although the temperature measurement has been carried out in section 6.2, the V-DTF had a repair before conducting catalytic experiments due to the damage of some heating elements. As the way of electric heating for V-DTF, the replacement of heating elements may result in different temperature profiles from the ones obtained before. Also, since the new testing flow rates of synthesis gas were proposed, the measurement of reaction temperatures was applied further for both pellet and foam type tests. The results of reaction temperature for pellet type catalysts can be found in Table 6.1. Again, compressed air was used to represent ‘synthesis gas’ in the new tests of temperature measurement.

Table 6.1: Reaction temperatures for the tests with pellet-type catalysts under various flow rates

Setting temperature	**Reaction flow rate**		
	0.3L/min	0.6L/min	0.9L/min
Room temperature	17.4℃	17.4℃	17.4℃
200℃	268.8℃	268.5℃	268.0℃
300℃	401.2℃	400.6℃	400.1℃
400℃	511.8℃	511.4℃	510.8℃
500℃	615.6℃	615.4℃	615.2℃

Table 6.1 displays the measured temperatures under small but different flow rates (0.3 L/min to 0.9 L/min) were close in all setting temperature conditions. Also, when combining Table 6.1 with Figure 6.3, it can be found that the temperature difference between before (e.g., T1 temperature, group without gas supply) and after (e.g., tests with 0.3 L/min) the repair was acceptable for further experiments.

6.3.2 Effect of Co-ZSM-5 on Methane Oxidation

According to the experimental results of literature, it is acknowledged that methane oxidation with oxygen (air) occurs over the temperature of 640℃ and its reactions are below in equations 6.2 and 6.3. It should be noted that reaction 6.3 shows the complete methane oxidation process while reaction 6.2 presents the incomplete oxidation process (Kong, Eckhoff and Alfert, 1995; Robinson and Smith, 1984). The difference between two reactions is that CO_2 is the gas production in the presence of sufficient oxygen while CO is generated when oxygen is at a low level.

$$2CH_4 + 3O_2 \rightarrow 2CO + 4H_2O \qquad [6.2]$$

$$CH_4 + 2O_2 \rightarrow +CO_2 + 2H_2O \qquad [6.3]$$

The effect of Co supporting catalysts on methane oxidation was carried out in this section. The feeding gas mixture contained 2% methane (0.1 L/min), compressed air (0.1 L/min) and nitrogen (0.1 L/min). The nitrogen existing in feed gas was used to control the total testing flow rate at fixed 0.3 L/min and compare with the result of tests with additional NOx (CH_4-SCR tests), which will be shown in section 6.3.3. Another diluted air with flow rate of 2L/min was introduced and mixed with the reaction gas flow after passing through catalysts (leaving the V-DTF) in the tests to meet the requirement of lower flow rate limit for gas analyzers.

The blank test with an empty reactor (no pellet) was conducted first to test the methane oxidation in the potential temperature range for CH_4-SCR tests, from 200℃ to 500℃ setting temperature. Then, experiments over different types of ZSM-5 pellets (bare ZSM-5 pellets, 2.44% and 4.89% Co-ZSM-5 with Si/Al=12.5) were carried out to investigate the effect of cobalt supporting ZSM-5 pellets on methane oxidation. The catalyst tested in each test was fixed at 0.3g ± 0.01g weight with 250-600 μm particle size before calcination (preheating process) for fair comparisons. The catalyst was placed at a fixed position (the bottom of main reactor) and the corresponding reaction temperature has been tested in Table 6.1. The gas hourly space velocity (GHSV) in this case was 30000h^{-1}, which the definition and related formula are explained in section 6.3.4.

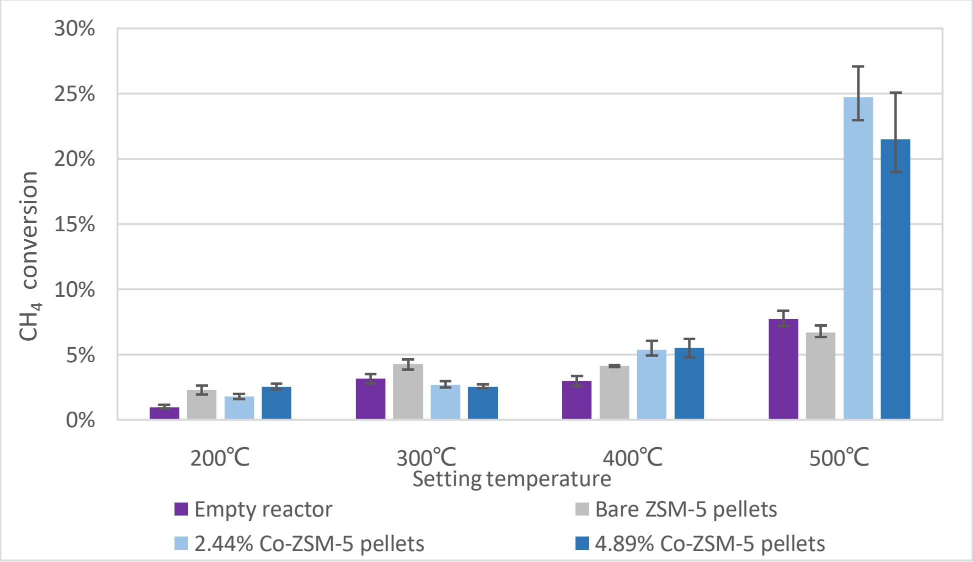

Figure 6.4: CH_4 oxidation rates over empty reactor, 0.3g bare ZSM-5 and 2.44% & 4.89% Co-ZSM-5 pellets (Si/Al=12.5) under different setting temperatures, feed gas conditions: $[CH_4]$= 0.67%, $[O_2]$= 6.98%, balance in N_2, 0.3 L/min.

Figure 6.4 compares the methane oxidation rates under different pellet-use and setting temperature conditions. It can be found that the methane oxidation rates when using empty reactor and bare ZSM-5 pellets were low for the entire testing temperature range. Top two methane conversion rates happened at 500°C setting temperature, only 7.69% with empty reactor and 6.69% with bare ZSM-5 pellets respectively. On the other hand, the methane conversion rates over Co supporting ZSM-5 pellets had evident increases, especially at 500°C setting temperature. Both 2.44% and 4.89% Co-ZSM-5 cases had conversion rates of over 20%, almost four times as the other two blank cases. This can be contributed by the catalytic effect of Co-ZSM-5 since it has been proved that CH_4 can easily generate $-CH_3$ and –H radical species over catalyzed zeolites, then generating intermediates to 'achieve' methane conversion (Lin, Wang and Lunsford, 1988; Zhang, Walters and Vannice, 1994).

Using the result of 2.44% Co-ZSM-5 test (see Table A.1) as an example, the values of CO and CO_2 had upward trends at 500°C setting temperature when there was obvious methane conversion. Although the oxygen/ methane ratios in these tests were far larger than 2, which meant methane oxidation should progress under reaction 6.3 theoretically, the experimental result displayed that the ‘carbon element’ from CH_4 was converted into both CO and CO_2 by monitoring their variations. The products of catalytic methane oxidation should be investigated in further research.

Also, it is interesting to notice that Co–ZSM-5 has the capacity to partially oxidize methane to oxygenates such as formaldehyde (CH_2O) or methanol (CH_3OH) by using oxygen as an oxidant agent under at low temperature, around 150℃-200℃ (Beznis et al., 2011). Also, it is proposed by Beznis, Weckhuysen and Bitter (2009) that the catalytic products largely depend on preparation method and cobalt speciation of catalysts. The Co-ZSM-5 prepared by ion-exchange method which is the approach used in this study mainly produces formaldehyde while the catalyst made by impregnation method mostly generates methanol. However, as complex chain reactions, partial methane oxidation is hard to achieve, even with the help of catalyst. Hence, when combining its low catalytic temperature range (150℃-200℃) and limited methane conversion rate (maximum 2.51%) over Co-ZSM-5 pellets at setting temperature of 200℃, including experimental error (see Figure 6.4), the effect of partial methane oxidation can be negligible in this study.

6.3.3 Effect of Presence of Oxygen on CH_4-SCR over Co-ZSM-5

A series of tests using two types of cobalt loading ZSM-5 pellets (expected 2.44% and 4.89% Co, both of them with Si/Al ratio of 12.5) under different setting temperature conditions were conducted in the absence or presence of oxygen (air). 0.3g ± 0.01g Co-ZSM-5 pellet with 250-600 μm particle size was chosen as the last section. To match the components of feed gas used in section 6.3.2, NOx (1000 ppm, balance in nitrogen) was used to replace the content of N_2 in the gas mixture. That was to say the total testing flow rate remained at 0.3L/min and the flow rates of NOx, CH_4 and air (or nitrogen) were all set at 0.1L/min.

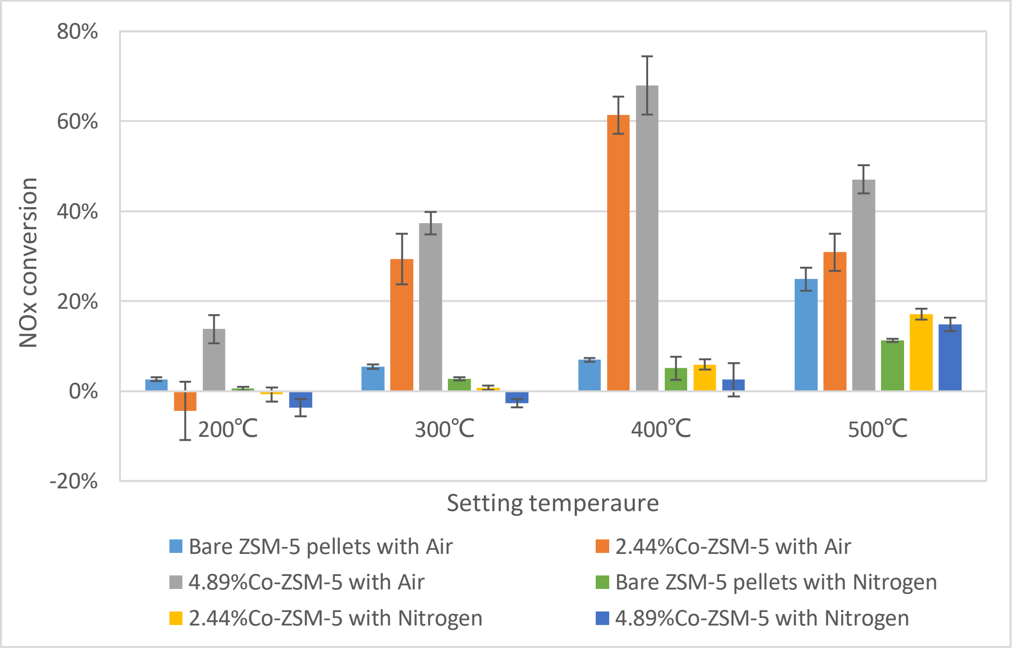

(a). NOx conversion

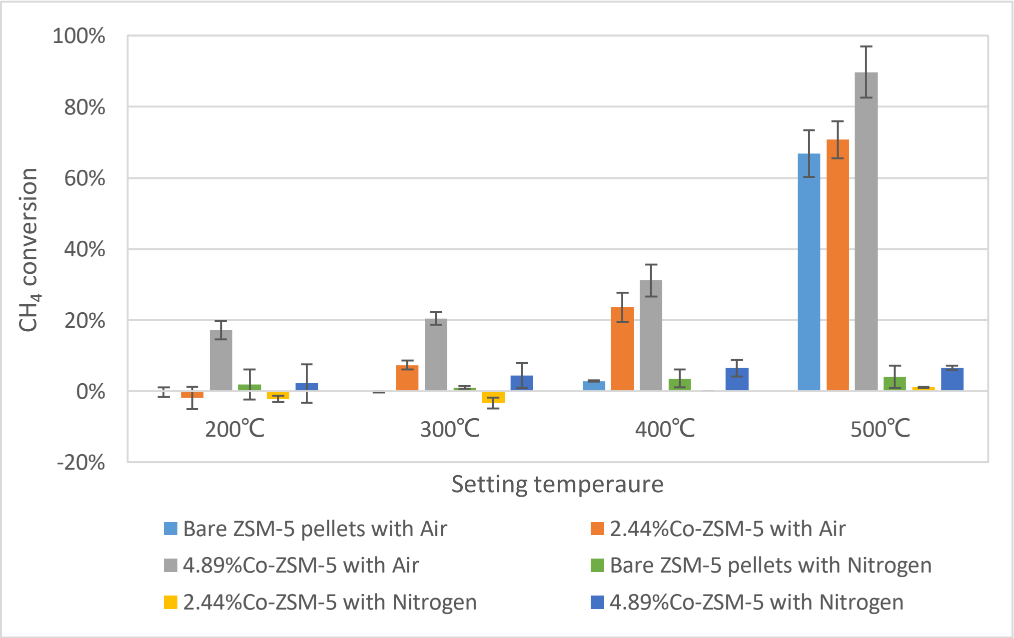

(b). CH_4 conversion

Figure 6.5: CH_4-SCR performance over 0.3g bare ZSM-5 and 2.44% & 4.89% Co-ZSM-5 (Si/Al=12.5) pellets under different feed gases and setting temperatures, feed gas conditions: [NOx]= 333ppm, [CH_4]= 0.67%, [O_2]= 6.98% (when air was applied in the tests), balance in N_2, 0.3 L/min.

6.3.3.1 Tests in the presence of air

Figures 6.5 (a) & (b) show the effect of the presence of excess oxygen on CH_4-SCR performance over bare and cobalt supporting ZSM-5 pellets (Si/Al=12.5) under different setting temperature conditions. As reaction 6.1 shown, oxygen works as the oxidizing agent and it is essential for CH_4-SCR theoretically. From Figures 6.5 (a) & (b), when comparing the NOx conversion rates in the presence of excess air, it can be found that bare ZSM-5 pellet had a neutral effect on CH_4-SCR though there was one exception of 24.90% NOx reduction happened at setting temperature of 500℃, which will be discussed later. On the other hand, cobalt supporting ZSM-5 pellets (Si/Al = 12.5) had a significantly positive impact on catalytic performance in terms of NOx and CH_4 reduction, especially at 400℃ setting temperature. Moreover, it seems that the catalytic performance was affected by Co loading of Co-ZSM-5 pellets. In this study, the performance of using 4.89% Co-ZSM-5 was better than that of using 2.44% Co-ZSM-5 over the entire temperature range. However, this found contradicted the conclusion of Bellmann et al. (2018). They proposed that the performance of 2.44% Co-ZSM-5 was better than 4.89% Co-ZSM-5 in terms of NO conversion and the catalyst with 2.5% to 3.0% Co loading had the optimum performance. One possible reason is that although the catalysts were made by the same synthesis method, setting conditions were largely different between two studies and they would have large impact on catalytic performance. The other possible reason is that the structure of Co/ZSM-5 in catalytic system is relatively complex when comparing with other metal iron supporting ZSM-5 catalysts (Kaucký et al., 2000). As a result, cobalt ions were relatively difficult to exchange into ZSM-5, resulting in lower Co loading of catalysts in actual applications as expected. Then, the variation of Co loading in catalysts may generate the different catalytic performance.

Regarding the NOx conversion over bare ZSM-5 pellets at 500℃ setting temperature, it can be explained by the reactions between NOx and CH_4 in the presence of air when feed gas was in high-temperature atmosphere as the phenomena of 'NOx drop' still happened in the test of empty reactor (without any pellet, see Figure A.11).

Until now, many researchers have focused on the performance of thermal interactions between NOx and hydrocarbons in fuel-lean conditions. It has been reported that adding small amounts of nitrogen oxides (NO or/and NO_2) such as presenting in the parts per million concentrations (ppm level) and even lower levels can enhance hydrocarbon oxidation to CO or/and CO_2 while at the same time hydrocarbon itself can also improve NOx conversion to N_2 or other intermediates (Bromly, 1991; Frassoldati, Faravelli and Ranzi, 2003). The challenging point is that the mechanism and efficiency are disparate when using NO or/and NO_2 and different types of hydrocarbon (Bendtsen, Glarborg and Dam-Johansen, 2000). Since there is air existing in this group of tests, NO and NO_2 can be easily interconverted. Specifically, some researchers have investigated the thermal NOx-CH_4 inter-reactions. For example, similar conditions to our study, Chan et al. (2011) tested the performance of 2.5% and 0.05% CH_4 in air atmosphere by introducing 0–100 ppm of NO or NO_2 within 550-750°C. The residence time was kept at approximately 0.35s. Small NOx conversion and significant CH_4 conversion were observed. They also concluded the mechanism of chain reactions among NOx, CH_4 and O_2 based on different testing temperatures. The equation list of important reactions can be found in Table A.2. In addition to that, based on their mechanism, reaction 6.4 rules at low testing temperature (600°C to 725°C) and reactions 6.5 and 6.6 dominate at high test temperature (over 725°C). Combined with all the reactions, it can be seen that HONO (nitrous acid gas) is one of the products of a key step in chain reactions, whether in the low or high-temperature range. That may result in the 'reduction' of NOx values when NOx-CH_4 chain reactions take place at a certain temperature.

$$\mathrm{CH_4 + NO_2 \rightarrow CH_3 + \ HONO} \qquad [6.4]$$

$$NO_2 + O \rightarrow NO + \ O_2 \qquad [6.5]$$

$$NO_2 + HO_2 \rightarrow HONO + \ O_2 \qquad [6.6]$$

Moreover, according to the conclusion of Chan et al. (2011), reaction temperature is another factor to determine the route of thermal NOx-CH_4 chain reactions mentioned above. In this study, the NOx variation over bare ZSM-5 pellets at 400°C setting temperature was pretty low (see Figure 6.5 a), which means the chain reaction did not happen practically in this temperature condition. Therefore, it can be concluded that the NOx conversion over Co supporting ZSM-5 at 400°C was contributed by CH_4-SCR (see reaction 6.1). However, it is more complicated in 500°C setting temperature condition. There was 24.90% NOx variation over bare ZSM-5 pellets, which represents that the thermal NOx-CH_4 chain reactions happened when taking the actual reaction temperature into account (See Table 6.1). On the other hand, the difference between values over bare ZSM-5 and Co-ZSM-5 shows that CH_4-SCR took place in that temperature condition as well. In that case, the NOx reduction caused by catalytic effect over 2.44% and 4.89% Co-ZSM-5 pellets at 500°C setting temperature was much lower than 400°C cases, only 5.98% and 22.2% respectively.

Figure 6.5 also illustrates that the pre-set furnace setting temperature is one of the factors to determine catalytic performance. The trend of NOx conversion rates (see Figure 6.5 a) displays a volcano-shape over the entire temperature range. The highest reduction took place at 400℃ setting temperature, 61.39% and 67.99% NOx conversion rates when using 2.44% and 4.89% Co-ZSM-5. However, with the setting temperature increasing to 500℃, the values of NOx reduction over both cobalt supporting ZSM-5 pellets had different degrees of declines. That proves there was an ideal (peak) reaction temperature for CH_4-SCR to achieve optimum NOx reduction performance, which was 400℃ setting temperature in this study. It is consistent with the conclusions of Li and Armor, (1993) and Wang, Chen and Sachtler, (2001). They proposed the optimum temperature for NOx reduction in CH_4-SCR system is at the range of 400-500℃ based on different operational settings such as gas hourly space velocity (GHSV) of feed gas.

Cobalt supporting ZSM-5 can not only be the promising catalyst for NOx abatement, but also be a suitable CH_4 oxidation catalyst, accelerating methane oxidation with O_2 to CO_2 and CO. For example, CH_4 conversion achieved 89.78% over 4.89% Co-ZSM-5 with the presence of O_2 and NOx at 500℃ setting temperature. When combining Figures 6.4 and 6.5 b, it can be seen that that CH_4 conversion rate can be divided into two parts. The thermal chain reactions between NOx and CH_4 contributed to the main part of CH_4 reduction when taking the conversion rate over bare ZSM-5 pellets under the same temperature condition into account. Then the performance of methane conversion was further improved by the catalytic effect of Co-ZSM-5 catalysts.

6.3.3.2 Tests in the absence of air

Firstly, it should be pointed out that CH_4 cracking did not take place in this case before discussing the reaction(s) between NOx and CH_4 in the absence of oxygen. It is acceptable that methane cracking occurs in the absence of air, but the reaction rate of non-catalytic methane cracking is pretty slow at temperature below 1000°C (Amin, Croiset and Epling, 2011). Although the reaction of methane cracking begins at 550°C, it only goes on a slow rate at 600–850°C and no more than 3.4% (Tsipouriari, Zhang and Verykios, 1998). Figure 6.5 (b) displays that CH_4 conversion was limited at any temperature (max 4.89% @ 400°C) when oxygen was unavailable in the feed gas. As a consequence, the effect of methane cracking is negligible in this study.

Compared with the obvious NOx reduction over Co supporting catalysts in the presence of oxygen, trend of NOx variation in the absence of oxygen (nitrogen condition) is less notable and different. As shown in Figure 6.5 (a), there was limited NOx reduction at 200°C or 300°C setting temperature. Then, NOx reduction began from 400°C setting temperature over both bare and Co supporting ZSM-5 pellets. Interestingly, NOx reduction among different pellet-use conditions was close at 400°C or 500°C setting temperature whether catalyst was used or not. For instance, the most considerable NOx variation among all nitrogen-environment tests happened at 500°C setting temperature, 17.17%, 14.87% and 11.31% NOx reduction when using 2.44% & 4.89% Co-ZSM-5 and bare ZSM-5 pellets. It can be attributed by the fact that NOx can be converted to N_2 with the help of CH_4 in the absence of oxygen as shown in reactions 6.7 and 6.8 (Desai et al., 2001; Takahashi et al., 2006):

$$CH_4 + 4NO \rightarrow 2N_2 + CO_2 + 2H_2O \qquad [6.7]$$

$$CH_4 + 2NO_2 \rightarrow N_2 + CO_2 + 2H_2O \qquad [6.8]$$

It can be seen that the reactions of NO- CH_4 and NO_2- CH_4 are slightly different though their final products are the same, N_2, CO_2 and water. Although it is known that NO can be easily converted into NO_2, it has to be in the atmosphere with oxygen. In this study, NO was used as the component of feed gas to represent NOx. Hence, the reaction underwent as described in reaction 6.7 when NO was under oxygen-free condition.

In the absence of oxygen, since there was no competitive reaction of CH_4 oxidation in the system, CH_4 can react with NOx under specific temperature without the help of catalyst. That explains why the NOx reduction values at 400°C or 500°C setting temperatures were close, whether Co-ZSM-5 catalyst was used or not. Moreover, when comparing the results of groups under oxygen-environment and nitrogen-environment, NOx- CH_4 reaction occurred above 400°C setting temperature in the absence of oxygen while that reaction took place over 300°C setting temperature in the presence of oxygen with the help of Co-ZSM-5 catalysts. Although there was some activity in terms of NOx reduction in the absence of oxygen, the performance could be remarkably promoted by adding excess oxygen to feed gas and using Co-ZSM-5 pellets as catalyst in the catalytic system.

6.3.4 Effect of Gas Hourly Space Velocity (GHSV) on CH_4-SCR over Co-ZSM-5

According to the literature, different NOx reduction efficiencies of CH_4-SCR were observed when using Co-ZSM-5 catalysts (Bellmann et al., 2018; Burch and Scire, 2010; Li, Battavio and Armor, 1993). It is found that apart from cobalt loading and reaction temperature, another factor that may affect NOx reduction performance is gas hourly space velocity (GHSV). The definition of GHSV is the ratio of feed gas flow rate, including inert and main components to the volume of bed which only refers to active phase, i.e. catalysts (Fogler, 2010). Hence, the effect of GHSV on CH_4-SCR coupling with Co-ZSM-5 catalyst was inspected in this section. Various computed GHSVs between 30000 h^{-1} and 90000 h^{-1} were obtained by changing the total reaction flow rates (0.3L/min, 0.6L/min and 0.9L/min) while the mass of Co-ZSM-5 catalyst was maintained at 0.3g ± 0.01g with 250-600 μm particle size (bulk density of zeolite = 0.5g/cm^3). Also, the main gas composition in feed gas mixture (NOx/ CH_4 / air) kept as the same as the last section to eliminate the effect of changing oxidizing and reducing environments. The setting details are shown in Table 6.2.

Table 6.2: Feed gas setting for the GHSV tests

GHSV	Total reaction flow rate (L/min)	Gas composition flow rate (NOx/ CH_4/ Air, L/min)
30000h^{-1}	0.3	0.1/0.1/0.1
60000h^{-1}	0.6	0.2/0.2/0.2
90000h^{-1}	0.9	0.3/0.3/0.3

Figures 6.6 and 6.7 compare the catalytic performance of 2.44% and 4.89% Co-ZSM-5 pellets in terms of NOx and CH_4 conversion rates under different GHSV conditions. From these figures, it is easily found that the adjustment of GHSV generated a big difference in the results of 300℃ and 400℃ setting temperature

conditions, but had limited influence on 500℃ conditions, especially for NOx reduction. For instance, NOx reduction dropped from over 60% to less than 40% when changing GHSV from 30000 h^{-1} to 60000 h^{-1} over both 2.44% and 4.89% Co-ZSM-5 pellets at 400℃ setting temperature while that difference over both catalysts was less than 5% at 500℃ setting temperature.

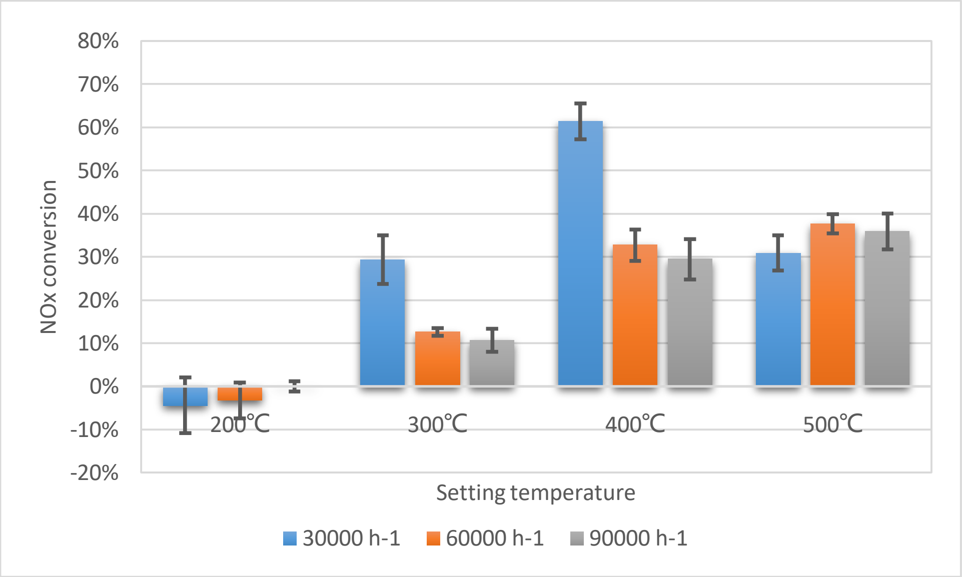

(a) NOx conversion

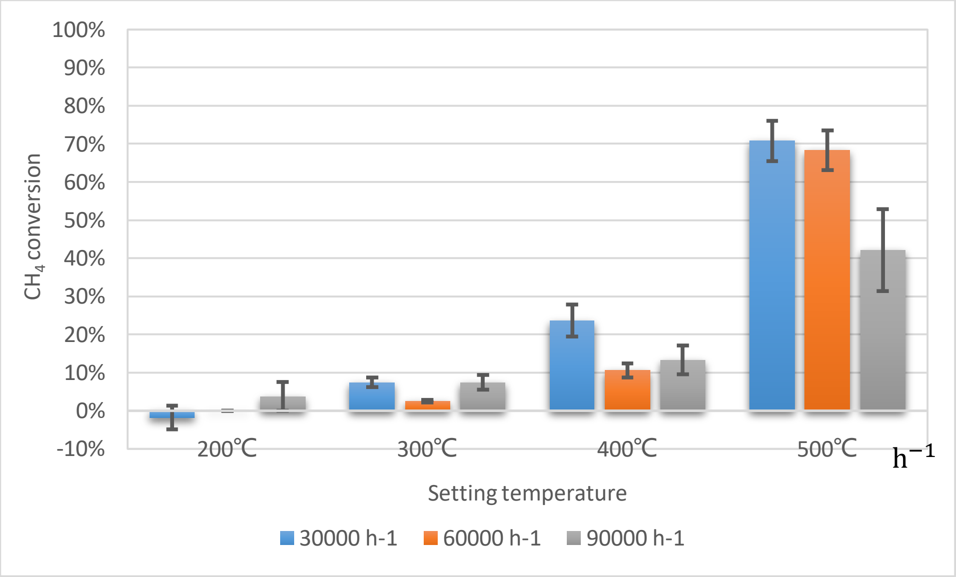

（b）CH_4 conversion

Figure 6.6: CH_4-SCR performance over 0.3g 2.44% Co-ZSM-5 (Si/Al=12.5) pellets under different GHSVs and setting temperatures, feed gas conditions: [NOx]= 333ppm, [CH_4]= 0.67%, [O_2]= 6.98%, balance in N_2

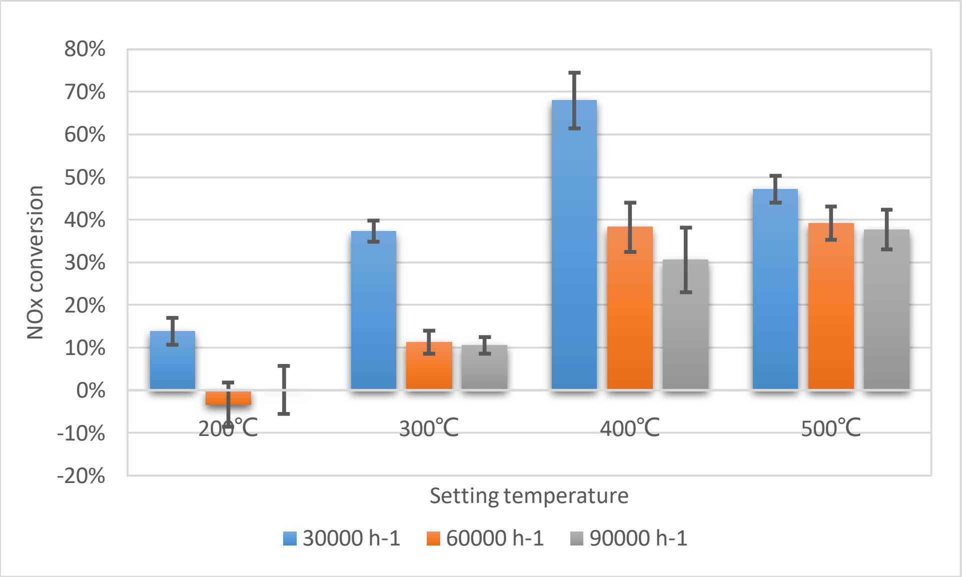

(a) NOx conversion

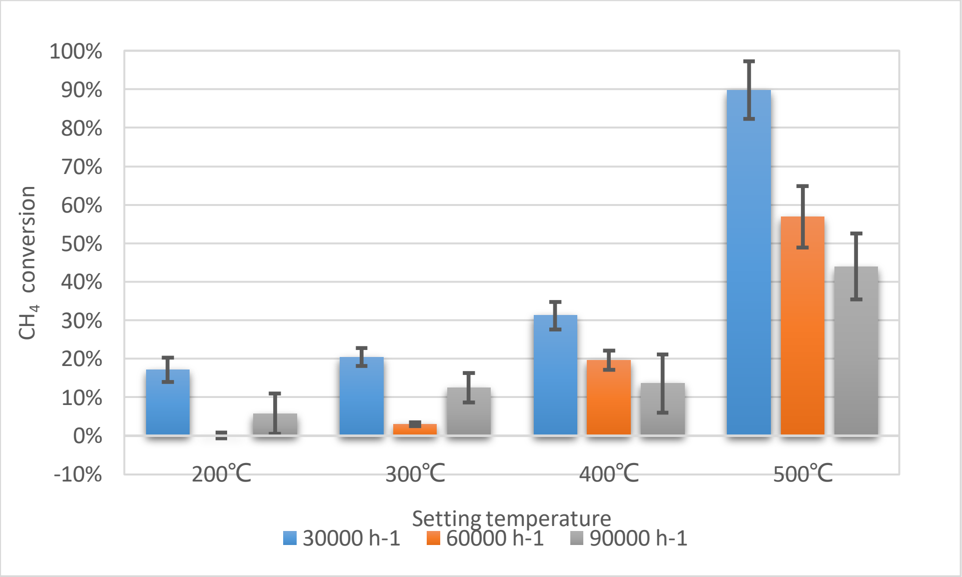

(b) CH_4 conversion

Figure 6.7: CH_4-SCR performance over 0.3g 4.89% Co-ZSM-5 (Si/Al=12.5) pellets under different GHSVs and setting temperatures, feed gas conditions: [NOx]= 333ppm, [CH_4]= 0.67%, [O_2]= 6.98%, balance in O_2

Concerning the phenomenon happened at low temperatures (300℃ and 400℃ cases), it can further confirm the variation of NOx was mainly caused by CH_4-SCR which affected by the change of GHSV. Higher GHSV (more specifically, larger flow rate in this case) led to less residence time and contact time between feed gas and catalysts. Therefore, the catalytic reaction of NOx- CH_4 was less inadequate compared with the reaction with smaller GHSV condition, then resulting in lower NOx reduction. However, as mentioned before, the reduction of NOx and CH_4 at 500℃ setting temperature was secondarily caused by the catalytic effect of CH_4-SCR, since it more depended on the reactions caused by temperature itself such as NOx- CH_4 chain reactions and direct CH_4 oxidation. In that case, the change of GHSV had an insignificant effect on values of NOx and CH_4 at 500℃ setting temperature though small temperature difference would be made when adjusting the reaction flow rates (see Table 6.1).

To sum up, although larger GHSV had minor impact on the reaction(s) mainly caused by high temperatures, it had an apparent negative effect on CH_4-SCR performance, especially for NOx reduction. Therefore, CH_4-SCR preferred small GHSV conditions and other potential methods which can improve mixing process between feed gas and catalysts need to be applied if large GHSV is unavoidable in practical applications.

6.3.5 Effect of Carbon Monoxide on CH_4-SCR over Co-ZSM-5

As mentioned in section 5.5, the presence of CO is inevitable when producing CH_4 in incomplete combustion. When CO meets sufficient oxygen, there are two possible routes for CO oxidation in the presence of NO. The first one is the direct oxidation of CO (see reaction 6.9) and the other one is indirect oxidation (reaction 6.11 followed by reaction 6.10). From these reactions, it can be seen that NO cannot be consumed in the presence of CO under non-catalytic atmosphere whether CO oxidation takes place via either direct or indirect route.

Direct oxidation of CO:

$$\mathrm{2CO + O_2 \rightarrow 2N_2 + CO_2} \qquad [6.9]$$

Indirect oxidation of CO:

$$\mathrm{2NO + O_2 \rightarrow 2NO_2} \qquad [6.10]$$

$$\mathrm{NO_2 + CO \rightarrow NO + CO_2} \qquad [6.11]$$

However, it has been reported that CO can work as a reductant, catalyzing NOx (NO and/or NO_2) to N_2 in the presence of N_2 under following reactions (reactions 6.12 to 6.15) over some specific catalysts (Mizuno, Tanaka and Misono, 1992).

For example, Gassan-Zade et al. (1979) studied the catalytic reaction between nitrogen dioxide (NO_2) and CO over NiO in the temperature range of 200°C-250°C.

The direct reaction between NO and CO to form $\mathrm{N_2}$:

$$\mathrm{2NO + 2CO \rightarrow N_2 + 2CO_2} \qquad [6.12]$$

The indirect reaction between NO and CO, generating $\mathrm{N_2O}$ first, then $\mathrm{N_2}$:

$$\mathrm{2NO + CO \rightarrow N_2O + CO_2} \qquad [6.13]$$

$$\mathrm{N_2O + CO \rightarrow N_2 + CO_2} \qquad [6.14]$$

Direct reaction between $\mathrm{NO_2}$ and CO to form $\mathrm{N_2}$:

$$\mathrm{2NO_2 + 4CO \rightarrow N_2 + 4CO_2} \qquad [6.15]$$

The reaction(s) between NOx and CO was investigated before adding CO to NOx-CH_4 (CH_4-SCR) system. To achieve it, again, 0.3g ± 0.01g pellet type Co-ZSM-5 catalysts with 250-600 μm particle size and 12.5 of Si/Al ratio were used in the fixed bed reactor. The tests of 0.1L/min 1500ppm CO and 0.1L/min 1000ppm NOx with either 0.1L/min air or 0.1L/min N_2 over empty reactor (no catalyst), bare ZSM-5 pellets and 2.44% & 4.89 Co-ZSM-5 pellets were carried out at the beginning of this stage (see Table 6.3). It should be mentioned that CO_2 was introduced together with CO from the same gas cylinder. Up to now, there is no evidence shows CO_2 is harmful to CH_4-SCR over ZSM-5 supporting catalysts though some information has been published regarding the disadvantage of CO_2 on metal oxide catalytic system. For instance, Xie, Rosynek and Lunsford, (1999) reported that CO_2 can partially poison SCR performance over Ba/MgO catalysts. In this stage, the variation of NOx was used to estimate the final performance of NOx-CO reaction(s). Also, the original concentration of CO was predicted by monitoring the value of CO_2 when testing in room-temperature condition because of the low concentration of CO in feed gas and relatively large measuring range of CO channel (0% to 5%) in the ABB gas analyzer.

Table 6.3: Feed gas setting for NOx-CO tests over different pellet-type catalysts

Condition	**Flow rate (L/min)**	**Composition concentration (balance in N_2)**			
		CO (ppm)	CO_2 (vol%)	NOx (ppm)	O_2 (vol%)
Test in air environment	0.1NOx/ 0.1CO/ 0.1Air	500	5.00	333	6.98
Test in Nitrogen environment	0.1NOx/ 0.1CO/ 0.1N_2				0.00

Figure 6.8 exhibits the NOx conversion rates of NOx-CO reaction(s) in the presence or absence of air over various types of pellets. It can be seen that NOx-CO reaction(s) took place in the presence of oxygen by observing the variation

of NOx values though oxygen itself was not involved in any mentioned reaction (reactions 6.12 to 6.15). Also, it looks like the reaction rate of NOx-CO mainly depended on reaction temperature. Specifically, among air-environmental tests, there was approximate 11% NOx conversion rate in all cases of 400℃ setting temperature and slightly less NOx reduction (7% approximately) at 500℃ setting temperature. On the contrary, the NOx conversion rate was relatively low (maximum 2.61% at 500℃ setting temperature) when there was no oxygen available in the feed gas. Moreover, Co supporting ZSM-5 catalysts did not affect the NOx-CO reaction(s).

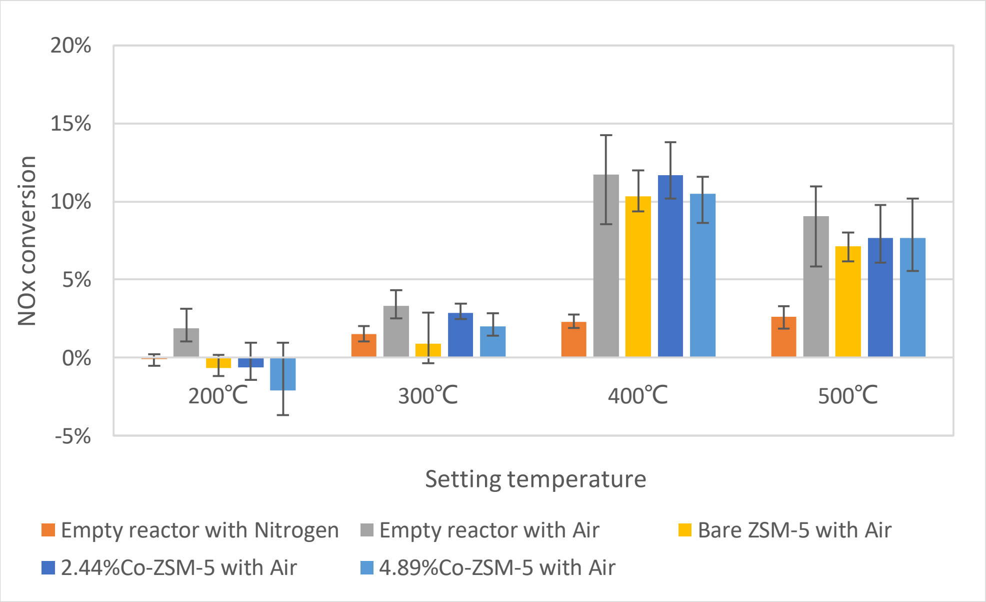

Figure 6.8: NOx conversion rates of NOx-CO reaction(s) over empty reactor, 0.3g bare ZSM-5 pellets and 2.44% & 4.89% Co-ZSM-5 (Si/Al=12.5) under different setting temperatures

After testing the NOx-CO reaction(s), CO was added into feed gas and its effect on the performance of CH_4-SCR was investigated. As the GHSP has shown its influence on CH_4-SCR performance, same flow setting condition (total testing flow rate maintained at 0.3 L/min) was used and 0.3g ± 0.01g Co supporting ZSM-5 catalysts were loaded into the same position of main reactor as before. In the feed gas, flow rates of 1000ppm NOx and air stayed at 0.1L/min, not only to make valid comparison with the results obtained in Figure 6.8, but also to eliminate the effect of amount of air (even it is stoichiometric excess in any tests) and NOx/CH_4 ratio on the performance of catalytic reaction(s). Also, since there is some activity of NOx-CO reactions at certain temperature, some conditions of different ratios of CH_4 /N_2 and CH_4 /CO were tested and more details of feed gas are shown in Table 6.4.

Table 6.4: Feed gas setting for NOx-CH_4-CO tests over 2.44% and 4.89% Co-ZSM-5 pellets

Condition	**Flow rate (L/min)**	**Composition concentration (balance in N_2)**				
		CH_4 (ppm)	CO (ppm)	CO_2 (vol%)	NOx (ppm)	O_2 (vol%)
100% CH_4	0.1CH_4	6667	0	0	333	6.98
50% CH_4/ 50% N_2	0.05 CH_4/ 0.05 N_2	3333	0	0		
50% CH_4/ 50% CO	0.05 CH_4/ 0.05 CO	3333	250	2.5		
25% CH_4/ 75% N_2	0.025 CH_4/ 0.075 N_2	1667	0	0		
25% CH_4/ 75% CO	0.025 CH_4/ 0.075 CO	1667	3.75	3.75		

As the results shown in Figures 6.5 and 6.8, reaction temperature is one of the critical factors to determine the performance of CH_4-SCR and NOx-CO reaction(s). Consequently, the effect of adding CO on CH_4-SCR performance was inspected at the temperature with optimum NOx reduction performance (furnace setting temperature of 400℃).

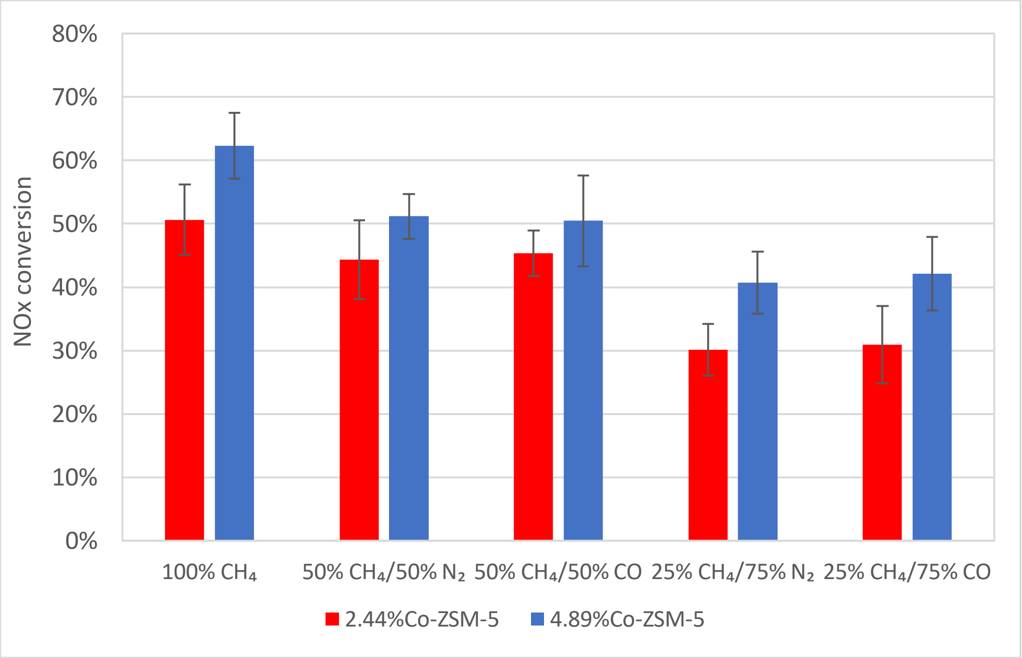

Figure 6.9: NOx conversion rates of CH_4-SCR over 0.3g 2.44% and 4.89% Co-ZSM-5 (Si/Al=12.5) pellets with different ratios of CH_4/ CO at setting temperature of 400℃

Figure 6.9 displays the performance of CH_4-SCR in terms of NOx conversion rates over 2.44% and 4.89% Co-ZSM-5 (Si/Al = 12.5) at 400℃ setting temperature when different ratios of CH_4/CO applied in the system. Firstly, it can be seen that the performance of 4.89% Co-ZSM-5 was better than 2.44%

one over the entire temperature range. The comparison of 100% CH_4 group between 2.44% and 4.89% Co-ZSM-5 has been discussed in section 6.3.3 and the same explanation can be used for other CH_4-N_2 groups (50% CH_4 /50%N_2 and 25% CH_4/75% N_2). It should be pointed out that the NOx conversion rates of both 2.44% and 4.89% Co-ZSM-5 in 100% CH_4 condition were not as high as the rates obtained in Figure 6.5. It can be partially explained by the activity loss of Co-ZSM-5 pellets after hundreds of hours of use. In that case, the durability and lifespan of Co-ZSM-5 pellets should be further investigated. Also, the conversion difference may relate to the change of pellet size or small temperature difference caused by V-DTF. Secondly, when comparing the NOx conversion rates of different ratio of CH_4/N_2 and 100%CH_4 with either 2.44% or 4.89% Co-ZSM-5 pellets, it can be seen that the amount of CH_4 affected NOx reduction performance of CH_4-SCR, even though CH_4 was stoichiometric excess in all conditions (see Table 6.4). The less CH_4 contained in feed gas led to a lower NOx conversion rate. Thirdly, the most critical one, the effect of adding CO on CH_4-SCR can be concluded when combining the groups contained CO and N_2 with either 2.44% or 4.89% Co-ZSM-5 pellets. A slightly higher NOx conversion can be observed when changing the composition from N_2 to CO in all comparative experiments. For instance, NOx reduction increased from 44.33% to 45.39% in the group of 50% CH_4/ 50% N_2 and 50% CH_4/ 50% CO with 2.44%

Co-ZSM-5 pellets. The small rise can be contributed by the reaction between NOx and CO since it has been proved to occur at setting temperature of 400℃ (see Figure 6.8). Unfortunately, the variation of CO cannot be detected effectively during the experiments due to the limitation of gas analyzers.

According to the discussion above, it can be concluded that the presence of CO did not inhibit the performance of CH_4-SCR though its positive effect on this catalytic system was also limited.

6.3.6 Effect of Si/Al Ratio of Co-ZSM-5 on CH_4-SCR

Si/Al ratio of metal exchanged ZSM-5 zeolites has found to play a crucial role in the nature of catalyst, which may further affect catalytic reactions. For example, in the study of Ferreira Madeira et al., (2012), they found Si/Al ratio of H-ZSM-5 influenced the catalytic performance in terms of transformation from ethanol (C_2H_6O) into hydrocarbons. Their result showed that the sample with Si/Al ratio of 60 had the optimum and stable performance since that ratio provided a great balance between active sites and the number of radicals.

In this section, an additional set of experiments was run to explore the influence of Si/Al ratio of Co-ZSM-5 on CH_4-SCR. New 2.44% and 4.89% Co-ZSM-5 pellets of the same particle size (250-600μm) with Si/Al ratio of 60 were prepared in laboratory using the same method as the ones with Si/Al ratio of 12.5. The feed gas was applied as the same condition presented in section 6.3.3.

Figure 6.10 (a) & (b) describe the comparison of CH_4-SCR performance over 2.44% and 4.89% Co-ZSM-5 pellets with different Si/Al ratios (12.5 and 60). It can be found that there was no catalytic activity observed in terms of NOx and CH_4 reduction at 300℃ and 400℃ setting temperatures when using Co-ZSM-5 pellets with Si/Al ratio of 60. Comparatively, at the same testing temperatures, the catalytic performance of Co-ZSM-5 pellets with Si/Al ratio of 12.5 was obvious, which has been illustrated in section 6.3.3. Moreover, although there was around 30% NOx and 65% CH_4 conversion at 500℃ setting temperature, it was contributed by the thermal inter-reactions between NOx and CH_4, not by catalytic effect.

Concerning the invalid use of catalysts with Si/Al ratio of 60, it may be explained that the catalytic performance of Co-ZSM-5 was affected by the number of active cobalt ions in catalysts. For the same amount and cobalt loading of catalyst, the catalyst having higher Si/Al ratio meant it had lower Al content in its framework while Al atoms were replaced by metal ions (cobalt in this case) during ion-exchanged synthesis process. Hence, compared with the catalysts with Si/Al ratio of 12.5, less cobalt ions 'entered' the Co-ZSM-5 pellets with Si/Al ratio of 60. Although silica-rich ZSM-5 pellets (high Si/Al ratio) may offer a relatively stable structure, it was not suitable for the catalytic use of Co-ZSM-5.

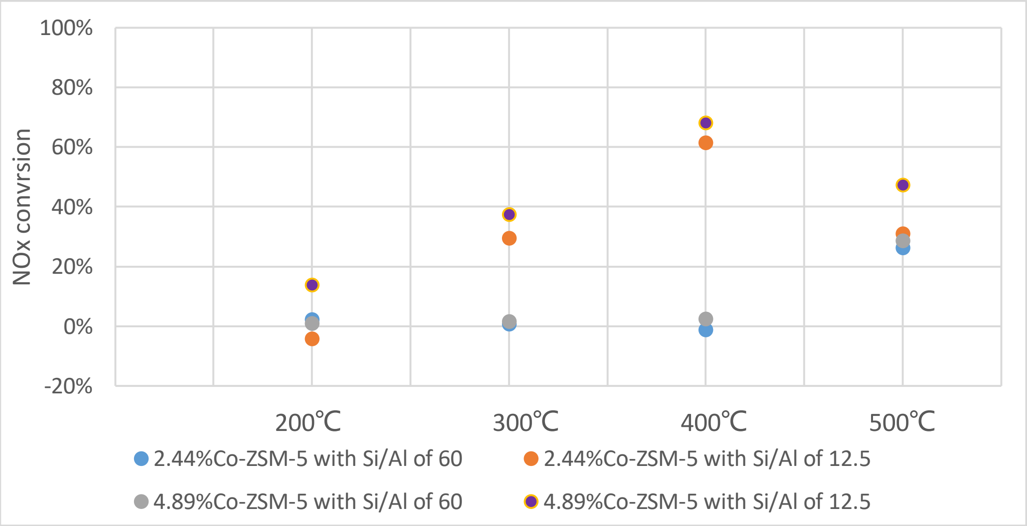

(a). NOx conversion

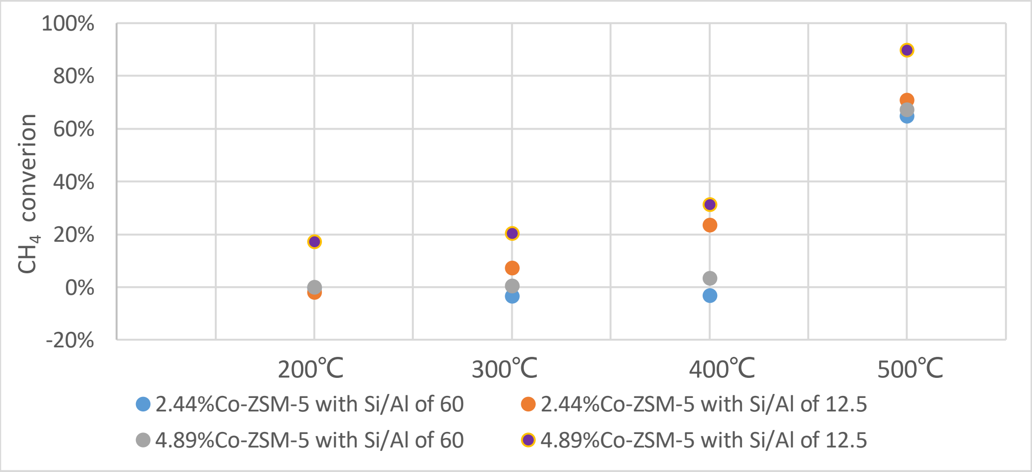

(b). CH_4 conversion

Figure 6.10: CH_4-SCR performance over 0.3g 2.44% and 4.89% Co-ZSM-5 pellets with different Si/Al ratios under various setting temperatures, feed gas conditions: [NOx]= 333ppm, [CH_4]= 0.67%, [O_2]= 6.98%, balance in N_2, 0.3 L/min.

6.4. Tests with Co-ZSM-5/SiC Foam(s)

After the tests of pellet-type Co-ZSM-5, further inspection of Co supporting catalysts was carried out by using Co-ZSM-5/SiC foam(s) with expected 4.89% Co loading which had greater practical significance. Its synthesis method has been presented in section 3.3.1.2. Same flow rate of feed gas and catalyst weight (expected 0.3g Co-ZSM-5 on three SiC foams in total) as pellet tests were applied in Co-ZSM-5/SiC foam tests to have a direct comparison. The measured reaction temperatures for foam tests are shown in Table 6.5.

Table 6.5: Reaction temperatures for the tests with foam-type catalysts

Setting temperature	**Reaction flow rate (0.3 L/min)**	
	Inlet temperature	**Outlet temperature**
Room temperature	18.2℃	18.1℃
200℃	292.0℃	272.5℃
300℃	409.6℃	404.2℃
400℃	503.1℃	518.3℃

Figure 6.11 compares the NOx conversion rates over Co-ZSM-5/SiC foams and bare SiC foams under different feed gas conditions. Different from the trend of NOx variation in tests of Co-ZSM-5 pellets, the highest NOx conversion rate happened at 200℃ (27.92%) when testing the feed gas contained NOx and CH_4

over Co-ZSM-5/SiC foams in the presence of air. With the increasing temperature, NOx conversion rate dropped rapidly until it disappeared at 400℃. Interestingly, the same trend even close rates can be found in the case of only NOx + air available in feed gas over Co-ZSM-5/SiC foams. However, that phenomenon was not observed in the case of bare SiC foams under the same condition. Hence, it can be concluded that the NOx conversion shown in Figure 6.11 was caused by physical and/ or chemical characteristics of Co-ZSM-5/SiC foams under air environment, not by catalytic reaction.

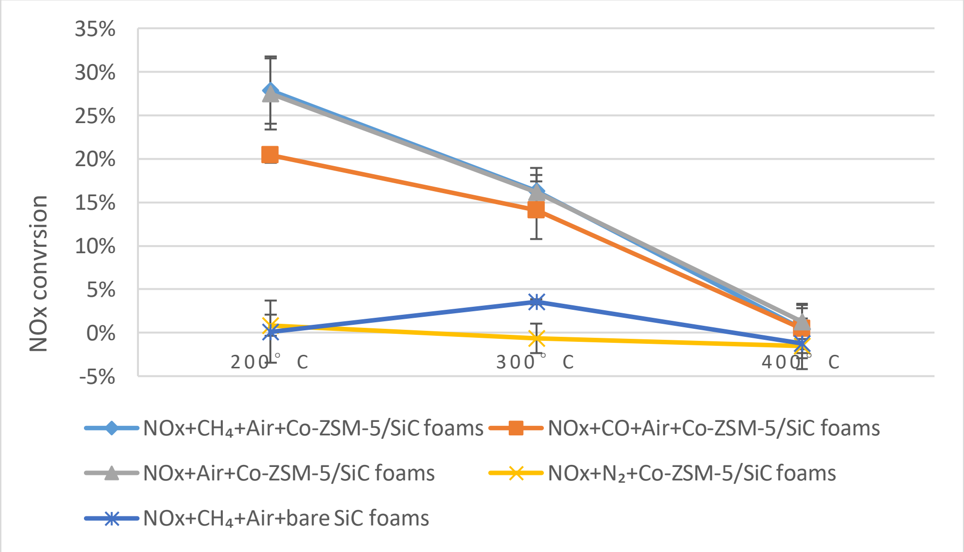

Figure 6.11: NOx variation rates of Co-ZSM-5/SiC foam tests

According to the findings from other research, the phenomenon can be explained by the existing form of Co cations. The trivalent Co (III) cations located in cavities of Co-ZSM-5 (inside ZSM-5 Channels) were active for the catalytic use of CH_4-SCR (Montanari et al., 2007). On the other hand, the isolated Co cations placed in Co-ZSM-5 can be acted as storage sites for NOx due to their chemisorption capacity. However, they cannot be treated as active sites and be active for CH_4-SCR (Chupin et al., 2006). In this study, the difference of existing forms of Co cations which affected NOx reduction performance may be caused by synthetic method. Although the synthetic methods of ion exchange were carried out in both Co-ZSM-5 and Co-ZSM-5/SiC foams, the growth process of ZSM-5 crystals on SiC foams may change the existing form of Co cations, which should be inspected in further research.

6.5. Tests with Fe-ZSM-5/SiC Foam(s)

Fe-ZSM-5, one of the most mature metal-exchanged zeolite catalysts, has been well studied so far. It has shown its remarkable activity and stability to reduce NOx in NH_3-SCR with a wide working temperature range (Krishna and Makkee, 2006; Ma and Grünert, 1999). Also, Fe-ZSM-5 has a considerable impact on SCR performance with higher hydrocarbons such as propene (C_3H_6), benzene (C_6H_6), n-decane (n-$C_{10}H_{22}$), (Guzmán-Vargas et al., 2005; Pérez-Ramírez et al., 2000; Wichtelová, Sobalík and Dědeček, 2003).

However, comparing with Co/ZSM-5, it is found that Fe/ZSM-5 is not working with methane (CH_4) in the DeNOx system. In the report of Chen, Voskoboinikov and Sachtler (1998), there was a noticeable NOx decrease in the system when using Fe/ZSM-5 with propene (C_3H_6), propane (C_3H_8) or isobutene (C_4H_8) as reductants. In contrast, CH_4 was inactive within all the measured temperature range (200℃ - 500℃). Similarly, Wang, Chen and Sachtler, (2001) investigated CH_4 and isobutane (i-C_4H_{10}) over Fe/ZSM-5 and Co/ZSM-5 catalysts in dry feed conditions. The results displayed that the Co/ZSM-5 catalyst showed remarkable activity for CH_4-SCR, achieving near 35% NOx reduction. However, Fe/ZSM-5 was unable to catalyze NOx reduction with CH_4.

On the other hand, iron and iron oxides have been proposed as possible catalysts to reduce NOx and CO simultaneously. Specifically, NO could be reduced by metallic iron to form N_2 while Fe could be oxidized to $\mathrm{Fe_xO_y}$ in the same reaction (see reaction 6.16).

$$\mathrm{NO + Fe \rightarrow Fe_xO_y + N_2} \qquad [6.16]$$

Concurrently, CO could be consumed by $\mathrm{Fe_xO_y}$ to generate $\mathrm{CO_2}$ and metallic iron could be regenerated (see reaction 6.17).

$$\mathrm{CO + Fe_xO_y \rightarrow Fe + CO_2} \qquad [6.17]$$

When combining both reactions (reactions 6.16 and 6.17), the net reaction is following.

$$\mathrm{CO} + \mathrm{NO} \rightarrow \mathrm{CO_2} + {}^{1}\!/_{2}\,\mathrm{N_2} \qquad [6.18]$$

It should be pointed out that the form of iron product (Fe_xO_y) has not been fully understood until now. The type could be iron (II) oxide (FeO), iron (III) oxide (Fe_2O_3), iron (II, III) oxide (Fe_3O_4) or other mixtures based on different conditions. For example, Hayhurst and Lawrence (1997) proposed that iron oxide included most of FeO and a small amount of Fe_2O_3. Su et al. (2014) suggested that the type of iron oxide was more dependent on working temperature. Fe_3O_4 was the primary iron oxide at lower temperature (around 550°C) while Fe_2O_3 dominated the iron oxide at a higher temperature (about 1100°C).

From reactions 6.16 to 6.18, it is interesting to find that the reactions of NO-Fe_xO_y and Fe_xO_y-CO could happen at the same time if both NO and CO are available in the feed gas. Fe, the potential catalyst, can exist in any chemical form in catalytic NO-CO reactions theoretically. Fennell and Hayhurst (2002) proposed that it was possible to use particles of pure metallic iron, any type of iron oxide and even industrial waste products. According to the experiments conducted by University of Manchester, Fe (III) (Fe_2O_3) dominated the Fe-ZSM-5/SiC foam (the catalyst used in this section) though there was a small amount of metal Fe containing in the framework of zeolite when they applied X-ray photoelectron spectroscopy on Fe-ZSM-5/SiC foams. In this section, the use of Fe ions (III) coupling with ZSM-5 and SiC foams was explored by testing CH_4-SCR and catalytic NO-CO reactions.

6.5.1 CH_4-SCR over Fe-ZSM-5/SiC Foams

The activity of CH_4-SCR (NOx-CH_4 reaction with O_2) over Fe-ZSM-5/SiC foams was tested in this section. Similar setting conditions of feed gas as previous CH_4-SCR tests were used in order to make a comparable performance. In this series of experiments, the feed gas contained 0.1L/min NOx (1000ppm, balance in N_2), 0.1L/min CH_4 (2%, balance in N_2) and either 0.1L/min air or nitrogen and the details are following (see Table 6.6).

Table 6.6: Feed gas setting for NOx-CH_4 tests over Fe-ZSM-5/SiC foams

Condition	**Flow rate (L/min)**	**Composition concentration (balance in N_2)**		
		NOx (ppm)	CH_4 (vol%)	O_2 (vol%)
Test in air environment	0.1NOx/ 0.1CH_4/ 0.1Air	333	0.67	6.98
Test in Nitrogen environment	0.1NOx/ 0.1CH_4/ 0.1N_2			0.00

Figure 6.12 shows the NOx variation of NOx-CH_4 reaction over bare SiC and Fe-ZSM-5/SiC foams in air or nitrogen environment at different setting temperatures. In the presence of O_2, the use of bare SiC foams had a neutral effect on NOx-CH_4 reaction though there was NOx reduction (25.73%) happened at 500℃ setting temperature, which was caused by thermal inter-reaction of NOx-CH_4 and has been discussed in section 6.3.3.1. More importantly, Fe-ZSM-5/SiC foam was inactive in the CH_4-SCR system (NOx-CH_4 reaction in the presence of oxygen), which was consistent with the conclusion of Chen, Voskoboinikov and Sachtler (1998), Chen, Voskoboinikov and Sachtler (1999) and Chen and Sachtler (2001). There were negative NOx conversion rates from 200℃ to 500℃ setting temperatures (around 43ppm NOx at room temperature and over 55ppm NOx at higher temperatures). It might be contributed by the adsorption capacity of NO on Fe-ZSM-5 at low temperatures (Mihaylov et al., 2009). Then the desorption process happened with the increasing operating temperatures to 'achieve' negative NOx conversion. That also explains why the negative NO conversion was getting lower from 200℃ (-22.57%) to 300℃ (-39.41%) and keeping relatively constant at 400℃ setting temperature (-38.22%). In the end, the value increased to -30.41% at 500℃ setting temperature as the thermal reaction occurred between NO and CH_4 in the presence of oxygen. On the other hand, comparing with the results over bare SiC foams, Fe-ZSM-5/SiC foams significantly enhanced the activity of NOx- CH_4 reaction in terms of NOx conversion (92.62% @500℃) when there was no O_2 available in the feed gas.

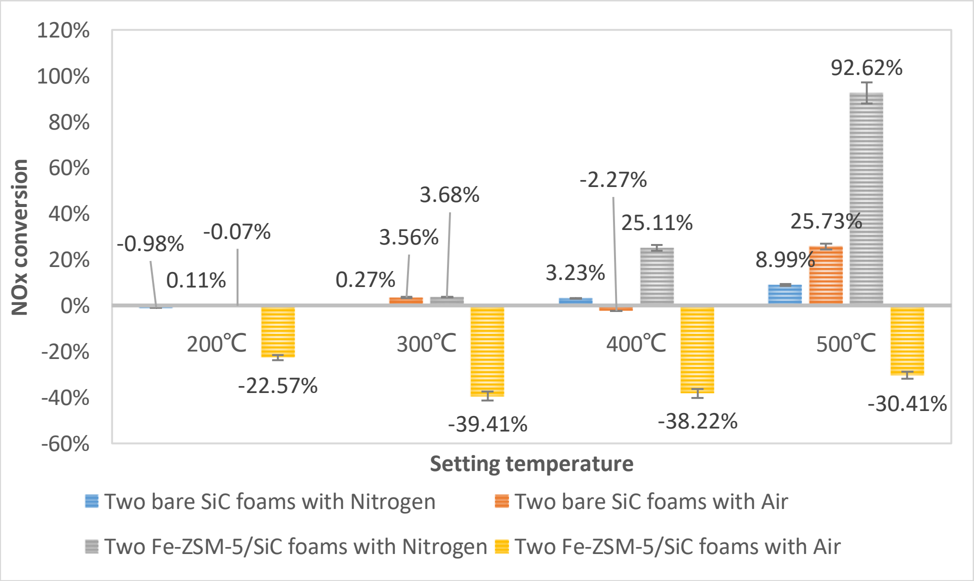

Figure 6.12: NOx variation rates of NOx-CH_4 reaction(s) over Fe-ZSM-5/SiC foams with various feed gases and setting temperatures

6.5.2 Catalytic NOx-CO Reactions over Fe-ZSM-5/SiC Foams

In the group of NOx-CO tests over Fe-ZSM-5/SiC foams, the use of catalyst and analytical methods were kept as last section. The only difference was to use CO to replace CH_4 in the feed gas and the setting details are presented in Table 6.7.

Table 6.7: Feed gas setting for NOx-CO tests over Fe-ZSM-5/SiC foams

Condition	**Flow rate (L/min)**	**Composition concentration (balance in N_2)**			
		NOx (ppm)	CO (ppm)	CO_2 (vol%)	O_2 (vol%)
Test in air environment	0.1NOx/ 0.1CO/ 0.1Air	333	500	5.00	6.98
Test in nitrogen environment	0.1NOx/ 0.1CO/ $0.1N_2$				0.00

Figure 6.13 shows the NOx conversion rates of NOx-CO reactions over Fe-ZSM-5/SiC foams in air or nitrogen environment with different reaction temperatures. In the presence of oxygen, NOx variation was caused by the adsorption capacity of CO on Fe-ZSM-5 at low temperatures and inter-reaction between CO and NO at high temperatures. Differently, in the absence of oxygen, an apparent NOx reduction can be observed in the NOx-CO reactions with the help of Fe-ZSM-5/SiC foams. Unfortunately, the variation of CO cannot be detected effectively in both air and nitrogen environment due to its low concentration for the measuring channel of gas analyzers. However, the rough trend of CO can be found when using large gas flow rates (see Figure A.12). From Figure A.12, it can be seen that there was no obvious NOx and CO variation when using bare SiC foam(s), but both of NOx and CO values had clear downward trends over Fe-ZSM-5/SiC foam(s) in the absence of oxygen.

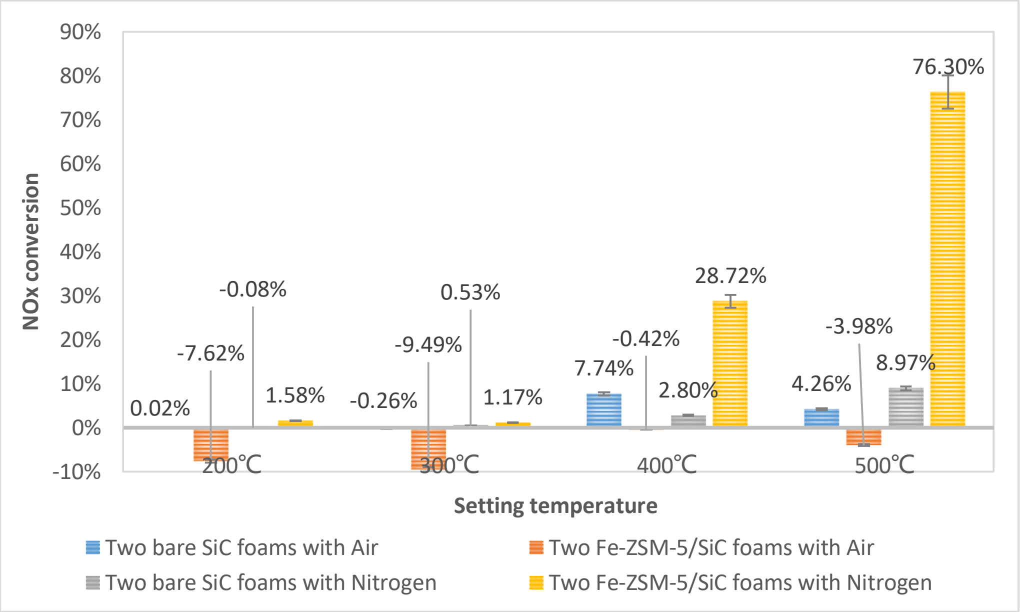

Figure 6.13: NOx conversion rates of NOx-CO reactions over Fe-ZSM-5/SiC foams with different feed gas components and setting temperatures

Also, Figure A.15 shows the trends of NOx, CO and CO_2 values in catalytic NOx-CO reaction(s) over Fe-ZSM-5/SiC foam(s) when feed gas had a various ratio of air/ N_2 (large flow rate setting). From Figure A.15 (b), a slight descending trend of CO value can be found when feed gas was in oxygen-free environment. However, when there was oxygen in feed gas, CO values had faster downward trends. The rapid decline can be explained by the CO oxidation with oxygen and its oxidation rate was much quicker than the reaction rate of catalytic NOx-CO reactions.

Furthermore, Figure A.14 displays that O_2 had a huge negative effect on NOx reduction by NOx-CO catalytic reaction(s). Even 0.36% O_2 (0.1 air/ 2.9 N_2) in feed gas could cause insignificant NOx reduction in the test. Based on the experimental results, CO preferred to have oxidation with O_2, not NOx-CO reactions even with the help of catalyst. A similar result can be found in the paper of Su, Zhao and Deng (2015). As conclusion, the catalytic reactions between NOx and CO can be only efficient in the absence of oxygen (fuel-rich condition). The efficiency of NOx reduction would be largely affected by the presence of oxygen (fuel-lean condition).

6.5.3 Effect of Number of Fe-ZSM-5/SiC foams on Catalytic NOx-CO Reactions

This section tested the effect of the number of Fe-ZSM-5/SiC foams on catalytic NOx-CO reactions. The tests were carried out in nitrogen environment (preferred catalytic condition), and other detail of the flow setting was the same as Table 6.7 described. The tests with one Fe-ZSM-5/SiC foam was added to compare with the results with two Fe-ZSM-5/SiC foams which obtained in last section.

Figure 6.14 illustrates the NOx variation of catalytic NOx-CO reactions over one or two Fe-ZSM-5/SiC foams with various setting temperatures. As expected, the performance of two Fe-ZSM-5/SiC foams was better than the case using one foam, especially at 400°C and 500°C setting temperatures. Although there was small temperature difference created by different amount of Fe-ZSM-5/SiC foams, the difference of NOx conversion rates between one and two-foam tests was mainly contributed by the longer residence time between feed gas and catalyst and the amount of catalysts (III Fe ions).

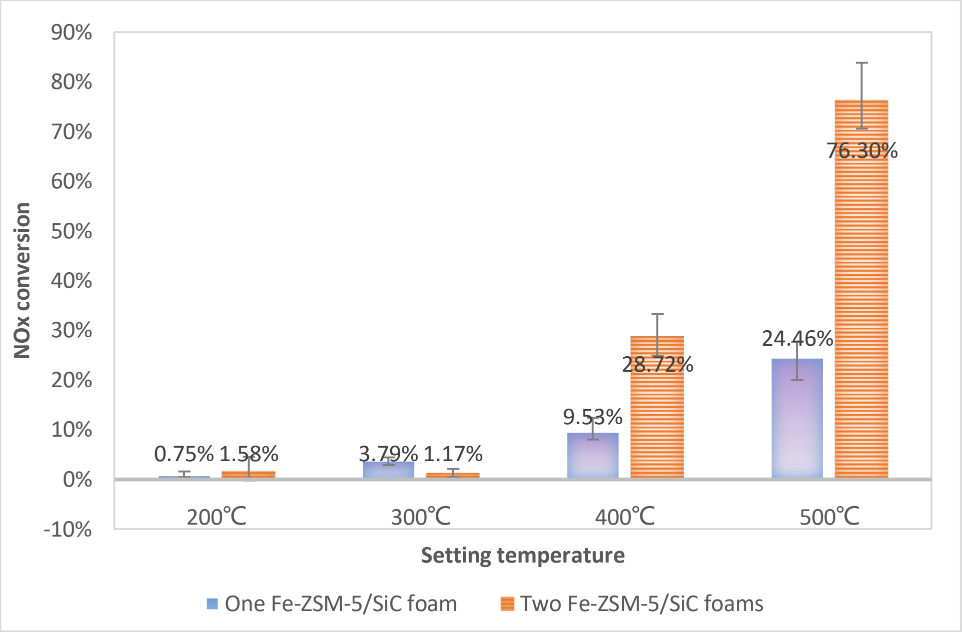

Figure 6.14: NOx conversion rates of NOx-CO reaction over a different number of Fe-ZSM-5/SiC foams with various setting temperatures, feed gas conditions: [NOx] = 333ppm, [CO] = 500ppm, [CO_2] = 5.00%, balance in N_2, 0.3 L/min.

6.6 Summary

The performance of CH_4-SCR over Cobalt (Co) supporting catalysts (ZSM-5 pellets and ZSM-5/SiC foams) in terms of NOx reduction has been investigated in a lab-scale fixed bed reactor by applying a simulated flue gas. The activity of catalytic NOx-CO reactions over iron (Fe) supporting ZSM-5/SiC foams was also explored in this chapter. The following conclusions can be drawn:

- Co-ZSM-5 catalyst was active for CH_4-SCR in the presence of oxygen. It not only reduced NOx emissions but also further promoted CH_4 oxidation in the catalytic system. However, Co-ZSM-5 was not working in oxygen-free atmosphere although there was thermal reaction happened between NOx and CH_4 under high temperature conditions.
- The NOx reduction efficiency of CH_4-SCR over Co-ZSM-5 was affected by many factors including Co loading, reaction temperature, Gas Hourly Space Velocity (GHSV) and Si/Al ratio. The highest NOx reduction (over 60%) was observed when using 4.89% Co-ZSM-5 with Si/Al ratio of 12.5 at 400℃ furnace setting temperature (GHSV=30000h^{-1}).
- Carbon monoxide (CO) as a product of incomplete combustion could react with NOx at high temperatures, whether Co-ZSM-5 was used or not. Also, CO had a near neutral effect on CH_4-SCR as it had a negligible effect on further NOx reduction.
- Fe-ZSM-5/SiC foam was inactive in CH_4-SCR system over the entire tested temperature range. However, it could effectively enhance the catalytic NOx-CO reaction in the absence of oxygen under high

temperature conditions and the catalytic performance was severely inhibited by the presence of oxygen.

CHAPTER 7. CONCLUSIONS AND FUTURE WORK

7.1 Conclusions

The overarching aims of this research were to investigate the combustion behaviours of biomass fuels and explore the catalytic methods to control harmful emissions (NOx, CO and CH_4) for potential applications in domestic biomass boilers. The specific conclusions from this work are summarized as follows:

（1） The combustion behaviours of biomass fuels were investigated by burning individual pellet samples (wood, straw, miscanthus, peanut shell and torrefied wood) in a visual drop tube furnace (V-DTF) under both air and oxy-fuel combustion atmospheres. Based on the measured temperature distributions of individual pellet tests, four combustion phases, namely pre-heating, volatile combustion, volatile/ char overlap combustion and char combustion were identified. Higher combustion temperature led to a shorter total burnout time of pellet which was mainly contributed to the more rapid char combustion. Increasing the fraction of oxygen (21% to 30%) in oxy-fuel atmospheres could significantly accelerate the pellet combustion in oxy-fuel combustion atmospheres while the total burnout time of conventional air (21% O_2-79% N_2) combustion was between those of 21% O_2-79% CO_2 and 25% O_2-75% CO_2 atmospheres. Also, the total burning time of most pellet fuels except torrefied wood in air was shorter than that in 21% O_2-79% CO_2 atmosphere. In the case of torrefied wood combustion, the more active C-CO_2 gasification during the char combustion led to shorter char combustion time hence shorter total combustion in 21% O_2-79% CO_2. With the help of high-speed camera, the volatile flame brightness was found to increase with O_2 fraction in oxy-fuel combustions while the brightness of volatile flame in air was close to the one in 30% O_2-70% CO_2 atmosphere.

（2） The small-scale (50kW) Ashwell biomass boiler was found to have good performance in terms of NOx emissions under all air setting conditions. Continuously fluctuating CH_4 and CO were detected in the combustion chamber during combustion process due to insufficient mixing and limited combustion chamber space. Furthermore, both CH_4 and CO concentrations followed the same variation trends. Compared with normal air setting, the reduction of primary air generated more CH_4 and CO while the reduction of secondary air had a minor effect on additional CH_4 and CO emissions. On the other hand, either primary or secondary air reduction had a limited impact on NOx emission as its value was largely dependent on the nitrogen content of fuel type (wood) in this small-scale biomass boiler.

（3） The CH_4-SCR and catalytic NOx-CO reactions were tested in a lab-scale fixed bed reactor. For CH_4-SCR, Co-ZSM-5 was active to reduce NOx in the syngas of NOx + CH_4 + air which was used to simulate the flue gas of typical domestic biomass heating boilers. The optimum NOx conversion rate could be over 60% when using 2.89% or 4.89% Co-ZSM-5 (Si/Al ratio of 12.5) at the furnace setting temperature of 400℃. The catalytic performance in terms of NOx conversion disappeared in the oxygen-free atmosphere due to the lack of oxygen though there was still thermal NOx-CH_4 reactions happened at high temperatures. Co-ZSM-5/SiC foam showed its adsorption capacity to NOx, but failed to show its catalytic capacity. This was primarily caused by the difference of existing forms of cobalt cations in different Co-supporting catalysts. For catalytic NOx-CO system, Fe-ZSM-5/SiC foam could promote NOx-CO reaction in the absence of O_2 at high temperatures, but the catalytic performance was severely inhibited by the presence of oxygen. Meanwhile, Fe-ZSM-5/SiC foam was inactive in CH_4-SCR system.

7.2 Future Work

This research was mainly focused on the study of biomass combustion and potential catalytic method(s) to control NOx, CO and CH_4 (representing hydrocarbon) emissions for domestic biomass boilers. However, due to the limitations of experiment apparatus and time, there are some fields of research that can be improved further. The following points can be considered for future work based on this research:

- The research shown in Chapter 4 mainly focused on the combustion stage of biomass fuels. It is known that the ignition stage (especially ignition delay) is also significant for biomass combustion under both air and oxy-fuel atmospheres. Since the ignition delay normally takes place in a short time, it requires more accurate time measurement. Because of the limitation in this research, although the start time of visible flame emerging on video can be accurately determined, the exact time when pellet sample inserted into V-DTF cannot be discerned. Thus, it is recommended to investigate the effect of oxy-fuel atmospheres on ignition delay of biomass combustion by improving the experimental method.

- Following the first point, spectral intensities of free radicals such as Na and K can also be monitored and quantified to compare the combustion behaviours of different biomass fuels (especially non-woody types) by choosing suitable filters with the help of high-speed camera.
- In this work, due to the structure of heat exchanger, only part of temperature distribution of tubes was measured in the Ashwell biomass boiler. Then, the experimental results showed uneven combustion in the chamber. For further exploration, software such as Computational Fluid Dynamics (CFD) can be used to predict the temperature distribution over the entire heat exchanger. The measured temperature can be used to verify or calibrate the simulated results.
- Co-ZSM-5 has proven its activity in CH_4-SCR using a lab-scale fixed bed reactor. As the experimental results shown in Chapter 6, the catalytic performance showed a certain decline after several hundred hours of testing. Thus, the lifespan and stability of Co-ZSM-5 need to be investigated in future. Moreover, its application with suitable support in actual domestic boilers needs further investigation.

REFERENCES

AIR POLLUTION IN THE UK 2016. (2017). 1st ed.

AMIN, A.M., CROISET, E. AND EPLING, W. (2011). Review of methane catalytic cracking for hydrogen production. International Journal of Hydrogen Energy, 36(4), pp.2904-2935.

AMORIM, E., CARVALHO, J., SOARES NETO, T., ANSELMO, E., SAITO, V., DIAS, F. AND SANTOS, J. (2013). Influence of specimen size, tray inclination and air flow rate on the emission of gases from biomass combustion. Atmospheric Environment, 74, pp.52-59.

ATTYA, A.M. AND WHITELAW, J.H. (1981). Velocity, temperature and species concentrations in unconfined kerosene spray flames. Am. Soc. Mech. Eng.,(Pap.);(United States), 81.

AYLOR, A.W., LOBREE, L.J., REIMER, J.A. AND BELL, A.T. (1996). An infrared study of NO reduction by CH_4 over Co-ZSM-5. In Studies in Surface Science and Catalysis (Vol. 101, pp. 661-670). Elsevier.

BAE, S., ROH, S. AND KIM, S. (2006). NO removal by reducing agents and additives in the selective non-catalytic reduction (SNCR) process. Chemosphere, 65(1), pp.170-175.

BACH, C. AND EGGENSCHWILER, P.D. (2011). Ceramic foam catalyst substrates for diesel oxidation catalysts: Pollutant conversion and operational issues (No. 2011-24-0179). SAE Technical Paper.

BÄFVER, L., BOMAN, C. AND RÖNNBÄCK, M. (2011). Reduction of particle emissions by using additives. In Central European Biomass Conference, Graz, Austria, Jan (pp. 26-29).

BALAT, H. AND KIRTAY, E. (2010). Hydrogen from biomass – Present scenario and future prospects. International Journal of Hydrogen Energy, 35(14), pp.7416-7426.

BAUKAL, C., 2005. Everything you need to know about NOx. Metal finishing, 103(11), pp.18-24.

BELLMANN, A., ATIA, H., BENTRUP, U. AND BRÜCKNER, A. (2018). Mechanism of the selective reduction of NO x by methane over Co-ZSM-5. Applied Catalysis B: Environmental, 230, pp.184-193.

BENDTSEN, A.B., GLARBORG, P. AND DAM-JOHANSEN, K.I.M. (2000). Low temperature oxidation of methane: the influence of nitrogen oxides. Combustion science and technology, 151(1), pp.31-71.

BENSAID, S., DEORSOLA, F., FINO, D. AND RUSSO, N. (2012). After-treatment of household wood-fired stove emissions: From catalyst formulation to full-scale system. Catalysis Today, 197(1), pp.76-89.

BEZNIS, N., VAN LAAK, A., WECKHUYSEN, B. AND BITTER, J. (2011). Oxidation of methane to methanol and formaldehyde over Co–ZSM-5 molecular sieves: Tuning the reactivity and selectivity by alkaline and acid treatments of the zeolite ZSM-5 agglomerates. Microporous and Mesoporous Materials, 138(1-3), pp.176-183.

BEZNIS, N., WECKHUYSEN, B. AND BITTER, J. (2009). Partial oxidation of methane over Co-ZSM-5: Tuning the oxygenate selectivity by altering the preparation route. Catalysis Letters, 136(1-2), pp.52-56.

BIANCHI, E., HEIDIG, T., VISCONTI, C., GROPPI, G., FREUND, H. AND TRONCONI, E. (2012). An appraisal of the heat transfer properties of metallic open-cell foams for strongly exo-/endo-thermic catalytic processes in tubular reactors. Chemical Engineering Journal, 198-199, pp.512-528.

BROHEZ, S., DELVOSALLE, C. AND MARLAIR, G. (2004). A two-thermocouples probe for radiation corrections of measured temperatures in compartment fires. Fire Safety Journal, 39(5), pp.399-411.

BROMLY, J.H., 1991. The formation of nitrogen oxides in gas combustion (Doctoral dissertation, Murdoch University).

BRUNNER, THOMAS, INGWALDOBERNBERGER, AND ROBERT SCHARLER. "Primary measures for low-emission residential wood combustion–comparison of old with optimised modern systems." Proceedings of the 17th European Biomass Conference & Exhibition. 2009.

BUCHMAYR, M., GRUBER, J., HARGASSNER, M. AND HOCHENAUER, C. (2015). Experimental investigation of the primary combustion zone during staged combustion of wood-chips in a commercial small-scale boiler. Biomass and Bioenergy, 81, pp.356-363.

BUHRE, B., ELLIOTT, L., SHENG, C., GUPTA, R. AND WALL, T. (2005). Oxy-fuel combustion technology for coal-fired power generation. Progress in Energy and Combustion Science, 31(4), pp.283-307.

BURCH, R. AND SCIRE, S. (2010). ChemInform Abstract: Selective Catalytic Reduction of Nitric Oxide with Ethane and Methane on Some Metal Exchanged ZSM-5 Zeolites. ChemInform, 25(37), p.no-no.

CALVO, A.I., TARELHO, L.A.C., DUARTE, M., EVTYUGINA, M. AND ALVES, C.A. (2011). May. Operating conditions of a Portuguese wood stove. In Proceedings of the 4th International Congress of Energy and Environment Engineering and Management (CIIEM), Merida, Spain.

CAMPA, M., DE ROSSI, S., FERRARIS, G. AND INDOVINA, V. (1996). Catalytic activity of Co-ZSM-5 for the abatement of NOx with methane in the presence of oxygen. Applied Catalysis B: Environmental, 8(3), pp.315-331.

ČAPEK, L., DĚDEČEK, J., WICHTERLOVÁ, B., CIDER, L., JOBSON, E. AND TOKAROVÁ, V. (2005). Cu-ZSM-5 zeolite highly active in reduction of NO with decane.Applied Catalysis B: Environmental, 60(3-4), pp.147-153.

CAPOSCIUTTI, G. AND ANTONELLI, M. (2018). Experimental investigation on air displacement and air excess effect on CO, CO_2 and NO emissions of a small size fixed bed biomass boiler. Renewable Energy, 116, pp.795-804.

CARNO, J. (1996). Catalytic abatement of emissions from small-scale combustion of wood: A comparison of the catalytic effect in model and real flue gases. Fuel, 75(8), pp.959-965.

CARROLL, J., FINNAN, J., BIEDERMANN, F., BRUNNER, T. AND OBERNBERGER, I. (2015). Air staging to reduce emissions from energy crop combustion in small scale applications.Fuel, 155, pp.37-43.

CARVALHO, L., WOPIENKA, E., POINTNER, C., LUNDGREN, J., VERMA, V., HASLINGER, W. AND SCHMIDL, C. (2013). Performance of a pellet boiler fired with agricultural fuels. Applied Energy, 104, pp.286-296.

CERRI, I. (2000). Methane combustion over low-emission catalytic foam burners. Catalysis Today, 60(1-2), pp.21-32.

CHAN, Y., BARNES, F., BROMLY, J., KONNOV, A. AND ZHANG, D. (2011). The differentiated effect of NO and NO_2 in promoting methane oxidation. Proceedings of the Combustion Institute, 33(1), pp.441-447.

CHEN, H., VOSKOBOINIKOV, T. AND SACHTLER, W. (1998). Reduction of NOx over Fe/ZSM-5 Catalysts: Adsorption complexes and their reactivity toward hydrocarbons. Journal of Catalysis, 180(2), pp.171-183.

CHEN, H., VOSKOBOINIKOV, T. AND SACHTLER, W. (1999). Reduction of NOx over Fe/ZSM-5 catalysts: mechanistic causes of activity differences between alkanes. Catalysis Today, 54(4), pp.483-494.

CHEN, Q., ZHANG, X., ZHOU, J., SHARIFI, V. AND SWITHENBANK, J. (2015). Effects of flue gas recirculation on emissions from a small scale wood chip fired boiler. Energy Procedia, 66, pp.65-68.

CHENG, X. AND BI, X. (2014). A review of recent advances in selective catalytic NOx reduction reactor technologies. Particuology, 16, pp.1-18.

CHUPIN, C., VANVEEN, A., KONDURU, M., DESPRES, J. AND MIRODATOS, C. (2006). Identity and location of active species for NO reduction by CH_4 over Co-ZSM-5. Journal of Catalysis, 241(1), pp.103-114.

DAMOE, A., WU, H., FRANDSEN, F., GLARBORG, P. AND SANDER, B. (2014). Impact of Coal Fly ash addition on combustion aerosols (PM 2.5) from full-scale suspension-firing of pulverized wood. Energy & Fuels, 28(5), pp.3217-3223.

DEENG, K., MOHAMED, A. AND BHATIA, S. (2004). Process optimization studies of structured Cu–ZSM-5 zeolite catalyst for the removal of NO using design of experiments (DOE). Chemical Engineering Journal, 103(1-3), pp.147-157.

DESAI, A.J., LOMBARDO, E.A., KOVALCHUK, V.I. AND D'ITRI, J.L. (2001). Interaction of CH_4 with NO and NO_2 over Pt-ZSM-5 in the absence of O_2. Catalysis letters, 72(1-2), pp.65-70.

DE LUCAS, A., VALVERDE, J., DORADO, F., ROMERO, A. AND ASENCIO, I. (2005). Influence of the ion exchanged metal (Cu, Co, Ni and Mn) on the selective catalytic reduction of NOx over mordenite and ZSM-5. Journal of Molecular Catalysis A: Chemical, 225(1), pp.47-58.

DIAS, J., COSTA, M. AND AZEVEDO, J. (2004). Test of a small domestic boiler using different pellets. Biomass and Bioenergy, 27(6), pp.531-539.

DIETRICH, B. (2012). Pressure drop correlation for ceramic and metal sponges.Chemical Engineering Science, 74, pp.192-199.

DIMOPOULOS EGGENSCHWILER, P., TSINOGLOU, D., SEYFERT, J., BACH, C., VOGT, U. AND GORBAR, M. (2009). Ceramic foam substrates for automotive catalyst applications: fluid mechanic analysis. Experiments in Fluids, 47(2), pp.209-222.

DOGGALI, P., KUSABA, H., EINAGA, H., BENSAID, S., RAYALU, S., TERAOKA, Y. AND LABHSETWAR, N. (2011). Low-cost catalysts for the control of indoor CO and PM emissions from solid fuel combustion. Journal of Hazardous Materials, 186(1), pp.796-804.

DUAN, F., ZHANG, J., CHYANG, C., WANG, Y. AND TSO, J. (2014). Combustion of crushed and pelletized peanut shells in a pilot-scale fluidized-bed combustor with flue gas recirculation.Fuel Processing Technology, 128, pp.28-35.

EDDINGS, E., MCAVOY, D. AND COATES, R. (2017). Co-firing of pulverized coal with pinion pine/juniper wood in raw, torrefied and pyrolyzed forms. Fuel Processing Technology, 161, pp.273-282.

ERÄNEN, K., LINDFORS, L., KLINGSTEDT, F. AND MURZIN, D. (2003). Continuous reduction of NO with octane over a silver/alumina catalyst in oxygen-rich exhaust gases: combined heterogeneous and surface-mediated homogeneous reactions. Journal of Catalysis, 219(1), pp.25-40.

ERKFELDT, S., PALMQVIST, A. AND PETERSSON, M. (2011). Influence of the reducing agent for lean NOx reduction over Cu-ZSM-5. Applied Catalysis B: Environmental, 102(3-4), pp.547-554.

FAN, W., ZHU, T., SUN, Y. AND LV, D. (2014). Effects of gas compositions on NOx reduction by selective non-catalytic reduction with ammonia in a simulated cement precalciner atmosphere. Chemosphere, 113, pp.182-187.

FENNELL, P. AND HAYHURST, A. (2002). The kinetics of the reduction of NO to N_2 by reaction with particles of Fe. Proceedings of the Combustion Institute, 29(2), pp.2179-2185.

FERNANDES, A., ALVES, C., GONÇALVES, C., TARELHO, L., PIO, C., SCHIMDL, C. AND BAUER, H. (2011). Emission factors from residential combustion appliances burning Portuguese biomass fuels. Journal of Environmental Monitoring, 13(11), p.3196.

FERREIRA MADEIRA, F., BEN TAYEB, K., PINARD, L., VEZIN, H., MAURY, S. AND CADRAN, N. (2012). Ethanol transformation into hydrocarbons on ZSM-5 zeolites: Influence of Si/Al ratio on catalytic performances and deactivation rate. Study of the radical species role. Applied Catalysis A: General, 443-444, pp.171-180.

FINO, D., RUSSO, N., SARACCO, G. AND SPECCHIA, V. (2005). Multifunctional Filter for treatment of the flue gases from municipal waste incinerators. Industrial & Engineering Chemistry Research, 44(25), pp.9542-9548.

FOGLER, H.S., 2010. Essentials of chemical reaction engineering: Essenti Chemica Reactio Engi. Pearson Education.

FORESTRY.GOV.UK. (2016). What is biomass (Forest Research). [online] Available at: http://www.forestry.gov.uk/fr/beeh-9uhlqv [Accessed 15 Nov. 2016].

FOURNEL, S., MARCOS, B., GODBOUT, S. AND HEITZ, M. (2015). Predicting gaseous emissions from small-scale combustion of agricultural biomass fuels. Bioresource Technology, 179, pp.165-172.

FOURNEL, S., PALACIOS, J., MORISSETTE, R., VILLENEUVE, J., GODBOUT, S., HEITZ, M. AND SAVOIE, P. (2015). Particulate concentrations during on-farm combustion of energy crops of different shapes and harvest seasons. Atmospheric Environment, 104, pp.50-58.

FOURNEL, S., PALACIOS, J.H., MORISSETTE, R., VILLENEUVE, J., GODBOUT, S., HEITZ, M. AND SAVOIE, P. (2015). Influence of biomass properties on technical and environmental performance of a multi-fuel boiler during on-farm combustion of energy crops. Applied Energy, 141, pp.247-259.

FRASSOLDATI, A., FARAVELLI, T. AND RANZI, E. (2003). Kinetic modeling of the interactions between NO and hydrocarbons at high temperature. Combustion and Flame, 135(1-2), pp.97-112.

FRIEDL, A., PADOUVAS, E., ROTTER, H. AND VARMUZA, K. (2005). Prediction of heating values of biomass fuel from elemental composition. Analytica Chimica Acta, 544(1-2), pp.191-198.

FU, M., LI, C., LU, P., QU, L., ZHANG, M., ZHOU, Y., YU, M. AND FANG, Y. (2014). A review on selective catalytic reduction of NOx by supported catalysts at 100–300 ℃—catalysts, mechanism, kinetics. Catal.Sci. Technol, (4), pp.14-25.

GAO, X., YU, Q. AND CHEN, L., (2003). Selective catalytic reduction of NO with methane. Journal of Natural Gas Chemistry, 12(4), pp.264-270.

GARRIGÓS-PASTOR, G., PARRES-ESCLAPEZ, S., BUENO-LÓPEZ, A., ILLÁN-GÓMEZ, M. AND SALINAS-MARTÍNEZ DE LECEA, C. (2009). Power-bench demonstration of the Pt-catalysed C_3H_6-SCR of NOx in a diesel exhaust. Applied Catalysis A: General, 354(1-2), pp.63-71.

GASSAN-ZADE, G.Z., MUKHERJEE, T.K. AND ALKHAZOV, T.G. (1979). Effect of oxygen on the catalytic reduction of nitric oxides by carbon monoxide over NiO. Reaction Kinetics and Catalysis Letters, 12(4), pp.525-529.

GAWADE, P., C. ALEXANDEER, A., SILVER, R. AND OZKAN, U. (2012). Effect of engine exhaust parameters on the hydrothermal stability of Hydrocarbon-Selective Catalytic Reduction (SCR) catalysts for lean-burn systems. Energy Fuels, 26(12), pp.7084–7091.

GOV.UK. (2016). Welcome to GOV.UK. [online] Available at: https://www.gov.uk/ [Accessed 15 Nov. 2016].

GUZMÁN-VARGAS, A., DELAHAY, G., COQ, B., LIMA, E., BOSCH, P. AND JUMAS, J. (2005). Influence of the preparation method on the properties of Fe-ZSM-5 for the selective catalytic reduction of NO by n-decane. Catalysis Today, 107-108, pp.94-99.

HAMELINCK, C., FAAIJ, A., UIL, H. AND BOERRIGTER, H. (2004). Energy, 29 (2004), pp.1743-1771.

HAYHURST, A. AND LAWRENCE, A. (1997). The reduction of the nitrogen oxides NO and N_2O to molecular nitrogen in the presence of iron, its oxides, and carbon monoxide in a hot fluidized bed. Combustion and Flame, 110(3), pp.351-365.

HECK, R. (1999). Catalytic abatement of nitrogen oxides–stationary applications. Catalysis Today, 53(4), pp.519-523.

HECK, R., GULATI, S. AND FARRAUTO, R. (2001). The application of monoliths for gas phase catalytic reactions. Chemical Engineering Journal, 82(1-3), pp.149-156.

HEINRICH, F., SCHMIDT, C., LÖFFLER, E., MENZEL, M. AND GRÜNERT, W. (2002). Fe–ZSM-5 catalysts for the selective reduction of NO by isobutane—The problem of the active sites. Journal of Catalysis, 212(2), pp.157-172.

HEUER, S., SENNECA, O., WÜTSCHER, A., DÜDDER, H., SCHIEMANN, M., MUHLER, M. AND SCHERER, V. (2016). Effects of oxy-fuel conditions on the products of pyrolysis in a drop tube reactor. Fuel Processing Technology, 150, pp.41-49.

HEITOR, M. AND MOREIRA, A. (1993). Thermocouples and sample probes for combustion studies. Progress in Energy and Combustion Science, 19(3), pp.259-278.

HIGMAN, C. AND BURGT, M. (2003). Gasification. Boston: Elsevier/ Gulf Professional Pub

HINDASAGERI, V., VEDULA, R. AND PRABHU, S. (2013). Thermocouple error correction for measuring the flame temperature with determination of emissivity and heat transfer coefficient. Review of Scientific Instruments, 84(2), p.024902.

HODŽIĆ, N., KAZAGIĆ, A. AND SMAJEVIĆ, I. (2016). Influence of multiple air staging and reburning on NOx emissions during co-firing of low rank brown coal with woody biomass and natural gas. Applied Energy, 168, pp.38-47.

HORNE, P. AND WILLIAMS, P. (1996). Influence of temperature on the products from the flash pyrolysis of biomass. Fuel, 75(9), pp.1051-1059.

HOSSAIN, M., LU, G., SUN, D. AND YAN, Y. (2013). Three-dimensional reconstruction of flame temperature and emissivity distribution using optical tomographic and two-colour pyrometric techniques. Measurement Science and Technology, 24(7), p.074010.

HOUSHFAR, E., KHALIL, R., LØVÅS, T. AND SKREIBERG, Ø. (2012). Enhanced NOx reduction by combined staged air and flue gas recirculation in biomass grate combustion. Energy& Fuels, 26(5), pp.3003-3011.

HOUSHFAR, E., SKREIBERG, Ø.,LØVÅS, T., TODOROVIĆ, D. AND SØRUM, L. (2011). Effect of excess air ratio and temperature on NOx emission from grate combustion of biomass in the staged air combustion scenario. Energy& Fuels, 25(10), pp.4643-4654.

HUMS, E. (1998). Is advanced SCR technology at a standstill? A provocation for the academic community and catalyst manufacturers. Catalysis Today, 42(1-2), pp.25-35.

HUSTAD, J., SKREIBERG, Ø. AND SØNJU, O. (1995). Biomass combustion research and utilisation in IEA countries. Biomass and Bioenergy, 9(1-5), pp.235-255.

INAYAT, A., FREUND, H., SCHWAB, A., ZEISER, T. AND SCHWIEGER, W. (2011). Predicting the specific surface area and pressure drop of reticulated ceramic foams used as catalyst support. Advanced Engineering Materials, 13(11), pp.990-995.

INAYAT, A., KLUMPP, M., LÄMMERMANN, M., FREUND, H. AND SCHWIEGER, W. (2016). Development of a new pressure drop correlation for open-cell foams based completely on theoretical grounds: Taking into account strut shape and geometric tortuosity. Chemical Engineering Journal, 287, pp.704-719.

INCERA GARRIDO, G., PATCAS, F., LANG, S. AND KRAUSHAAR-CZARNETZKI, B. (2008). Mass transfer and pressure drop in ceramic foams: A description for different pore sizes and porosities. Chemical Engineering Science, 63(21), pp.5202-5217.

IVANOVA, S., LOUIS, B., MADANI, B., TESSONNIER, J., LEDOUX, M. AND PHAM-HUU, C. (2007). ZSM-5 coatings on β-SiC monoliths: possible new structured catalyst for the methanol-to-olefins process. The Journal of Physical Chemistry C, 111(11), pp.4368-4374.

IWAMOTO, M., YAHIRO, H., KUTSUNO, T., BUNYU, S. and KAGAWA, S. (1989). ChemInform abstract: Enhancement of catalytic activity of copper ion-exchanged Y type zeolites for the decomposition of nitrogen monoxide. ChemInform, 20(22).

IWAMOTO, M., YAHIRO, H., MIZUNO, N., ZHANG, W.X., MINE, Y., FURUKAWA, H. AND KAGAWA, S., (1992). Removal of nitrogen monoxide through a novel catalytic process. 2. Infrared study on surface reaction of nitrogen monoxide adsorbed on copper ion-exchanged ZSM-5 zeolites. The Journal of Physical Chemistry, 96(23), pp.9360-9366.

JIAO, Y., JIANG, C., YANG, Z. AND ZHANG, J. (2012). Controllable synthesis of ZSM-5 coatings on SiC foam support for MTP application. Microporous and Mesoporous Materials, 162, pp.152-158.

JOHANSSON, L., LECKNER, B., GUSTAVSSON, L., COOPER, D., TULLIN, C. AND POTTER, A. (2004). Emission characteristics of modern and old-type residential boilers fired with wood logs and wood pellets. Atmospheric Environment, 38(25), pp.4183-4195.

KAUCKÝ, D., VONDROVÁ, A., DĚDEČEK, J. AND WICHTERLOVÁ, B. (2000). Activity of Co Ion Sites in ZSM-5, Ferrierite, and Mordenite in selective catalytic reduction of NO with methane. Journal of Catalysis, 194(2), pp.318-329.

KHODAEI, H., GUZZOMI, F., YEOH, G., REGUEIRO, A. AND PATIÑO, D. (2016). An experimental study into the effect of air staging distribution and position on emissions in a laboratory scale biomass combustor. Energy.

KIM, M. AND NAM, I. (2001). Water tolerance of DeNOx SCR catalysts using hydrocarbons: Findings, improvements and challenges. Korean Journal of Chemical Engineering, 18(5), pp.725-740.

KIM, S. AND LEE, C. (2014). A review on manufacturing and application of open-cell metal foam.Procedia Materials Science, 4, pp.305-309.

KLUSKA, J., TURZYŃSKI, T. AND KARDAŚ, D. (2018). Experimental tests of co-combustion of pelletized leather tannery wastes and hardwood pellets. Waste Management, 79, pp.22-29.

KOEBEL, M., ELSENER, M. AND KLEEMANN, M. (2000). Urea-SCR: a promising technique to reduce NOx emissions from automotive diesel engines. Catalysis Today, 59, pp.335-345.Heck, R. (1999). Today, (53), pp.519-523.

KONG, D., ECKHOFF, R. AND ALFERT, F. (1995). Auto-ignition of CH_4/air, C_3H_8/air, CH_4/C_3H_8/air and CH_4/CO_2/air using a 11 ignition bomb. Journal of Hazardous Materials, 40(1), pp.69-84.

KRISHNA, K. AND MAKKEE, M. (2006). Preparation of Fe-ZSM-5 with enhanced activity and stability for SCR of NOx. Catalysis Today, 114(1), pp.23-30.

KUBACKA, A., JANAS, J., WŁOCH, E. AND SULIKOWSKI, B. (2005). Selective catalytic reduction of nitric oxide over zeolite catalysts in the presence of hydrocarbons and the excess of oxygen. Catalysis Today, 101(2), pp.139-145.

KUMAR, P. AND TOPIN, F. (2014). Investigation of fluid flow properties in open cell foams: Darcy and weak inertia regimes. Chemical Engineering Science, 116, pp.793-805.

KUO,K.K. Principles and combustion. 2nd edition.JohnWiley&Sons, Inc. 2005

KYMÄLÄINEN, M., HAVIMO, M. AND LOUHELAINEN, J. (2014). Sorption properties of torrefied wood and charcoal. Wood Material Science & Engineering, 9(3), pp.170-178.

LACROIX, M., NGUYEN, P., SCHWEICH, D., PHAM HUU, C., SAVIN-PONCET, S. AND EDOUARD, D. (2007). Pressure drop measurements and modeling on SiC foams. Chemical Engineering Science, 62(12), pp.3259-3267.

LAST, J., SUN, W. AND WITSCHI, H. (1994). Ozone, NO, and NO_2: oxidant air pollutants and more. Environmental Health Perspectives, 102 (suppl 10), pp.179-184.

LEMAIRE, R. AND MENANTEAU, S. (2017). Assessment of radiation correction methods for bare bead thermocouples in a combustion environment. International Journal of Thermal Sciences, 122, pp.186-200.

LI, Y. AND ARMOR, J. (1993). Selective catalytic reduction of NOx with methane over metal exchange zeolites. Applied Catalysis B: Environmental, 2(2-3), pp.239-256.

LI, Y. AND ARMOR, J. (1994). Selective Reduction of NO by methane on Co-Ferrierites. Journal of Catalysis, 150(2), pp.376-387.

LI, Y., BATTAVIO, P. AND ARMOR, J. (1993). Effect of water vapor on the selective reduction of NO by methane over Cobalt-exchanged ZSM-5. Journal of Catalysis, 142(2), pp.561-571.

LI, Y., LIN, Y., ZHAO, J., LIU, B., WANG, T., WANG, P. AND MAO, H. (2019). Control of NOx emissions by air staging in small- and medium-scale biomass pellet boilers. Environmental Science and Pollution Research, 26(10), pp.9717-9729.

LI, Z., WU, J. AND WU, L. (2017). Effect of Zr, Ca and Mn as promoters on the Co/SiC catalysts for the Fischer–Tropsch synthesis. Reaction Kinetics, Mechanisms and Catalysis, 122(2), pp.887-900.

LIN, C., WANG, J. and LUNSFORD, J. (1988). ChemInform Abstract: oxidative dimerization of methane over sodium-promoted calcium oxide. ChemInform, 19(38).

LIU, H., CHANEY, J., LI, J. AND SUN, C. (2013). Control of NOx emissions of a domestic/small-scale biomass pellet boiler by air staging. Fuel, 103, pp.792-798.

LIU, H., ZAILANI, R. AND GIBBS, B. (2005). Comparisons of pulverized coal combustion in air and in mixtures of O/CO. Fuel, 84(7-8), pp.833-840.

LÓNYI, F., SOLT, H., PÁSZTI, Z. AND VALYON, J. (2014). Mechanism of NO-SCR by methane over Co,H-ZSM-5 and Co,H-mordenite catalysts. Applied Catalysis B: Environmental, 150-151, pp.218-229.

LU, M., LI, M., SHAN, Y., SESHAN, K. AND LEFFERTS, L. (2008). Reduction of NO_2 in flue gas by CO and Propylene over CuO-CeO_2/SiO_2 in the presence of O_2. Chinese Journal of Chemistry, 26(6), pp.1035-1040.

LUO, J., OH, H., HENRY, C. AND EPLING, W. (2012). Effect of C_3H_6 on selective catalytic reduction of NOx by NH_3 over a Cu/zeolite catalyst: A mechanistic study. Applied Catalysis B: Environmental, 123-124, pp.296-305.

MA, A. AND GRÜNERT, W. (1999). Selective catalytic reduction of NO by ammonia over Fe-ZSM-5 catalysts. Chemical Communications, (1), pp.71-72.

MACHIDA, M. AND WATANABE, T. (2004). Effect of Na-addition on catalytic activity of Pt-ZSM-5 for low-temperature NO–H_2–O_2 reactions. Applied Catalysis B: Environmental, 52(4), pp.281-286.

MAHJOOB, S. AND VAFAI, K. (2008). A synthesis of fluid and thermal transport models for metal foam heat exchangers. International Journal of Heat and Mass Transfer, 51(15-16), pp.3701-3711.

MATTHES, M. AND HARTMANN, I. (2017). Improvement of efficiency and emissions from wood log stoves by retrofit solutions. Chemical Engineering & Technology, 40(2), pp.340-350.

MEUNIER, F., ZUZANIUK, V., BREEN, J., OLSSON, M. AND ROSS, J. (2000). Mechanistic differences in the selective reduction of NO by propene over cobalt- and silver-promoted alumina catalysts: kinetic and in situ DRIFTS study. Catalysis Today, 59(3-4), pp.287-304.

MIHAYLOV, M., IVANOVA, E., DRENCHEV, N. AND HADJIIVANOV, K. (2009). Coordination Chemistry of Fe2+ Ions in Fe,H-ZSM-5 Zeolite as Revealed by the IR Spectra of Adsorbed CO and NO. The Journal of Physical Chemistry C, 114(2), pp.1004-1014.

MISHRA, R. AND MOHANTY, K. (2018). Pyrolysis kinetics and thermal behavior of waste sawdust biomass using thermogravimetric analysis. Bioresource Technology, 251, pp.63-74.

MIZUNO, N., TANAKA, M. AND MISONO, M. (1992). Reaction between carbon monoxide and nitrogen monoxide over perovskite-type mixed oxides. Journal of the Chemical Society, Faraday Transactions, 88(1), p.91.

MONGKOLSIRI, N., PRASERTHDAM, P., SILVESTON, P. AND HUDGINS, R. (2000). Transient study of the effect of residual cations in Cu/ZSM-5 for SCR of NO by hydrocarbon. Chemical Engineering Science, 55(12), pp.2249-2256.

MONTANARI, T., MARIE, O., DATURI, M. AND BUSCA, G. (2007). Searching for the active sites of Co-H-MFI catalyst for the selective catalytic reduction of NO by methane: A FT-IR in situ and operando study. Applied Catalysis B: Environmental, 71(3-4), pp.216-222.

MRAD, R., AISSAT, A., COUSIN, R., COURCOT, D. AND SIFFERT, S. (2015). Catalysts for NOx selective catalytic reduction by hydrocarbons (HC-SCR). Applied Catalysis A: General, 504, pp.542-548.

NASIR UDDIN, M., DAUD, W. AND ABBAS, H. (2013). Potential hydrogen and non-condensable gases production from biomass pyrolysis: Insights into the process variables. Renewable and Sustainable Energy Reviews, 27, pp.204-224.

NATI, C., SPINELLI, R. AND FABBRI, P. (2010). Wood chips size distribution in relation to blade wear and screen use. Biomass and Bioenergy, 34(5), pp.583-587.

N.D. MULTI-COMPONENT GAS ANALYZER VA-3000 SERIES. [ebook] JAPAN: HORIBA. Available at: <https://www.horiba.com/fileadmin/uploads/Process-Environmental/Documents/HRE2854C-VA_VS_Series.pdf> [Accessed 15 February 2020].

MUNIR, S., NIMMO, W. AND GIBBS, B. (2011). The effect of air staged, co-combustion of pulverised coal and biomass blends on NOx emissions and combustion efficiency. Fuel, 90(1), pp.126-135.

NUSSBAUMER, T. (2003). Combustion and co-combustion of biomass: fundamentals, technologies, and primary measures for emission reduction . Energy & Fuels, 17(6), pp.1510-1521.

OLSSON, J.G., U. JAGLIG, AND J.B. PETTERSSON. Energy Fuels 11 (1997): 779-784. Print.

OU, X., PILITSIS, F., XU, N., TAYLOR, S., WARREN, J., GARFORTH, A., ZHANG, J., HARDACRE, C., JIAO, Y. AND FAN, X. (2018). On developing ferrisilicate catalysts supported on silicon carbide (SiC) foam catalysts for continuous catalytic wet peroxide oxidation (CWPO) reactions. Catalysis Today.

PATCAS, F., GARRIDO, G. AND KRAUSHAAR-CZARNETZKI, B. (2007). CO oxidation over structured carriers: A comparison of ceramic foams, honeycombs and beads. Chemical Engineering Science, 62(15), pp.3984-3990.

PÉREZ-RAMÍREZ, J., GARCÍA-CORTÉS, J., KAPTEIJN, F., ILLÁN-GÓMEZ, M., RIBERA, A., SALINAS-MARTÍNEZ DE LECEA, C. AND MOULIJN, J. (2000). Dual-bed catalytic system for NOx–N_2O removal: a practical application for lean-burn deNOx HC-SCR. Applied Catalysis B: Environmental, 25(2-3), pp.191-203.

PIETERSE, J., BRINK, R., BOONEVELD, S. AND DE BRUIJIN, F. (2003).Appl. Catal., B 46, pp.239-250.

PITTS, W.M., BRAUN, E., PEACOCK, R.D., MITLER, H.E., JOHNSSON, E.L., RENEKE, P.A. AND BLEVINS, L.G., (1998). Temperature uncertainties for bare-bead and aspirated thermocouple measurements in fire environments (NISTIR 6242) (No. NIST Interagency/Internal Report (NISTIR)-6242).

QIU, G. (2013). Testing of flue gas emissions of a biomass pellet boiler and abatement of particle emissions.Renewable Energy, 50, pp.94-102.

RABAÇAL, M., FERNANDES, U. AND COSTA, M. (2013). Combustion and emission characteristics of a domestic boiler fired with pellets of pine, industrial wood wastes and peach stones. Renewable Energy, 51, pp.220-226.

RACKLEY, S. (2017). Carbon capture and storage. 2nd ed. Joy Hayton, p.P23.

RATHNAM, R., ELLIOTT, L., WALL, T., LIU, Y. AND MOGHTADERI, B. (2009). Differences in reactivity of pulverised coal in air (O_2/N_2) and oxy-fuel (O_2/CO_2) conditions. Fuel Processing Technology, 90(6), pp.797-802.

REICHERT, G., SCHMIDL, C., HASLINGER, W., STRESSLER, H., STURMLECHNER, R., SCHWABL, M., WÖHLER, M. AND HOCHENAUER, C. (2018). Impact of oxidizing honeycomb catalysts integrated in firewood stoves on emissions under real-life operating conditions. Fuel Processing Technology, 177, pp.109-118.

RIAZA, J., AJMI, M., GIBBINS, J. AND CHALMERS, H. (2017). Ignition and combustion of single particles of coal and biomass under O_2/CO_2 atmospheres. Energy Procedia, 114, pp.6067-6073.

RIAZA, J., GIBBINS, J. AND CHALMERS, H. (2017). Ignition and combustion of single particles of coal and biomass. Fuel, 202, pp.650-655.

RIAZA, J., KHATAMI, R., LEVENDIS, Y., ÁLVAREZ, L., GIL, M., PEVIDA, C., RUBIERA, F. AND PIS, J. (2014). Combustion of single biomass particles in air and in oxy-fuel conditions. Biomass and Bioenergy, 64, pp.162-174.

ROBINSON, C. AND SMITH, D. (1984). The auto-ignition temperature of methane. Journal of Hazardous Materials, 8(3), pp.199-203.

ROY, S., HEGDE, M. AND MADRAS, G. (2009). Catalysis for NOx abatement. Applied Energy, 86(11), pp.2283-2297.

SABER, M., HUU, T., PHAM-HUU, C. AND EDOUARD, D. (2012). Residence time distribution, axial liquid dispersion and dynamic–static liquid mass transfer in trickle flow reactor containing β-SiC open-cell foams.Chemical Engineering Journal, 185-186, pp.294-299.

SARROZA, A., BENNET, T., EASTWICK, C. AND LIU, H. (2017). Characterising pulverised fuel ignition in a visual drop tube furnace by use of a high-speed imaging technique. Fuel Processing Technology, 157, pp.1-11.

SAWATMONGKHON, B. (2011). Modelling of catalytic after treatment of NOx emissions using hydrocarbon as a reducant. Ph.D. University of Birmingham.

SCHURICHT, F. AND RESCHETILOWSKI, W. (2012).Simultaneous selective catalytic reduction (SCR) of NOx and N_2O over Ag/ZSM-5 – Catalytic studies and mechanistic implications. Microporous and Mesoporous Materials, 164, pp.135-144.

SCHWIEGER, W., RAUSCHER, M., MÖNNIG, R., SCHEFFLER, F. AND FREUDE, D., (2000). Supported Crystallization of MFI-and FER-type Molecular Sieves on Porous Glasses. In Studies in Surface Science and Catalysis (Vol. 129, pp. 121-130). Elsevier.

SEO, C., CHOI, B., KIM, H., LEE, C. AND LEE, C. (2012). Effect of ZrO_2 addition on de-NOx performance of Cu-ZSM-5 for SCR catalyst. Chemical Engineering Journal, 191, pp.331-340.

SHAN, F., LIN, Q., ZHOU, K., WU, Y., FU, W., ZHANG, P., SONG, L., SHAO, C. AND YI, B. (2017). An experimental study of ignition and combustion of single biomass pellets in air and oxy-fuel. Fuel, 188, pp.277-284.

SHELEF, M., MONTREUIL, C. AND JEN, H. (1994). NO_2 formation over Cu-ZSM-5 and the selective catalytic reduction of NO. Catalysis Letters, 26(3-4), pp.277-284.

SINGH, D., CROISET, E., DOUGLAS, P. AND DOUGLAS, M. (2003). Techno-economic study of CO_2 capture from an existing coal-fired power plant: MEA scrubbing vs. O_2/CO_2 recycle combustion. Energy Conversion and Management, 44(19), pp.3073-3091.

SINGH, R. AND SHUKLA, A. (2014). A review on methods of flue gas cleaning from combustion of biomass. Renewable and Sustainable Energy Reviews, 29, pp.854-864.

SKIBINSKI, J., CWIEKA, K., KOWALKOWSKI, T., WYSOCKI, B., WEJRZANOWSKI, T. AND KURZYDLOWSKI, K. (2015). The influence of pore size variation on the pressure drop in open-cell foams. Materials& Design, 87, pp.650-655.

SMEETS, P., MENG, Q., CORTHALS, S., LEEMAN, H. AND SCHOONHEYDT, R. (2008). Co–ZSM-5 catalysts in the decomposition of N_2O and the SCR of NO with CH_4: Influence of preparation method and cobalt loading. Applied Catalysis B: Environmental, 84(3-4), pp.505-513.

SOARES NETO, T., CARVALHO, J., VERAS, C., ALVARADO, E., GIELOW, R., LINCOLN, E., CHRISTIAN, T., YOKELSON, R. AND SANTOS, J. (2009). Biomass consumption and CO_2, CO and main hydrocarbon gas emissions in an Amazonian forest clearing fire. Atmospheric Environment, 43(2), pp.438-446.

SOMMERSACHER, P., BRUNNER, T., OBERNBERGER, I., KIENZL, N. AND KANZIAN, W. (2013). Application of novel and advanced fuel characterization tools for the combustion related characterization of different wood/ kaolin and straw/kaolin mixtures. Energy & Fuels, 27(9), pp.5192-5206.

SONG, X., J. H. JOHNSON, AND J. D. NABER. (2014). A review of the literature of selective catalytic reduction catalysts integrated into diesel particulate filters. International Journal of Engine Research 16.6: 738-749. Web.

STAKHEEV, A., LEE, C., PARK, S. AND CHONG, P. (1996). Appl. Catal., B9, pp.65-86.

STÅHL, M., GRANSTRÖM, K., BERGHEL, J. AND RENSTRÖM, R. (2004). Industrial processes for biomass drying and their effects on the quality properties of wood pellets. Biomass and Bioenergy, 27(6), pp.621-628.

STAROKON, E.V., VEDYAGIN, A.A., PIRUTKO, L.V. AND MISHAKOV, I.V., 2015. Oxidation of CO and hydrocarbons with molecular oxygen over Fe–ZSM-5 zeolite. Journal of Porous Materials, 22(2), pp.521-527.

STEWART, R. (2012). Conversion of biomass boiler emission concentration data for comparison with Renewable Heat Incentive emission criteria.

STREGE, J., ZYGARLICKE, C., FOLKEDAHL, B. and MCCOLLOR, D. (2006). Bench-scale study of interactions between flue gas and cofired ash in an SCR. Fuel, 85(17-18), pp.2439-2444.

SU, Y.X., REN, L.M. AND DENG, W.Y., 2014. Effect of CO/CH_4 on redox of iron during NO reduction by XRD/SEM. In Applied Mechanics and Materials (Vol. 448, pp. 559-563). Trans Tech Publications.

SU, Y., ZHAO, B. AND DENG, W., 2015. NO reduction by methane over iron oxides: Characteristics and mechanisms. Fuel, 160, pp.80-86.

SULLIVAN, J. AND CUNNINGHAM, J. (1998). Selective catalytic reduction of NO with C_2H_4 over Cu/ZSM-5: Influences of oxygen partial pressure and incorporated rhodia. Applied Catalysis B: Environmental, 15(3-4), pp.275-289.

SUN, T., FOKEMA, M. AND YING, J. (1997). Mechanistic study of NO reduction with methane over Co2+ modified ZSM-5 catalysts. Catalysis Today, 33(1-3), pp.251-261.

TAKAHASHI, M., NAKATANI, T., IWAMOTO, S., WATANABE, T. AND INOUE, M., (2007). Performance of solvothermally prepared Ga_2O_3-Al_2O_3 catalysts for SC. R of NO with methane. Applied Catalysis B: Environmental, 70(1-4), pp.73-79

TANKSALE, A., BELTRAMINI, J. AND LU, G. (2010). A review of catalytic hydrogen production processes from biomass. Renewable and Sustainable Energy Reviews, 14(1), pp.166-182.

TAYYEBJAVED, M., IRFAN, N. AND GIBBS, B. (2007). Control of combustion-generated nitrogen oxides by selective non-catalytic reduction. Journal of Environmental Management, 83(3), pp.251-289.

TISSARI, J., SIPPULA, O., KOUKI, J., VUORIO, K. AND JOKINIEMI, J. (2008). Fine particle and gas emissions from the combustion of agricultural fuels fired in a 20 kW Burner. Energy & Fuels, 22(3), pp.2033-2042.

TRUONG-PHUOC, L., TRUONG-HUU, T., NGUYEN-DINH, L., BAAZIZ, W., ROMERO, T., EDOUARD, D., BEGIN, D., JANOWSKA, I. AND PHAM-HUU, C. (2014). Silicon carbide foam decorated with carbon nanofibers as catalytic stirrer in liquid-phase hydrogenation reactions. Applied Catalysis A: General, 469, pp.81-88.

TSIPOURIARI, V.A., ZHANG, Z. AND VERYKIOS, X.E., 1998. Catalytic partial oxidation of methane to synthesis gas over Ni-based catalysts: I. Catalyst performance characteristics. Journal of Catalysis, 179(1), pp.283-291.

UDDIN, M., KOMATSU, T. AND YASHIMA, T. (1993). Catalytic activity of framework iron in MFI-type ferrisilicate for the oxidation of carbon monoxide. Microporous Materials, 1(3), pp.201-205.

VANSETTEN, B., SPITTERS, C., BREMMER, J., MULDERS, A., MAKKEE, M. AND MOULIJN, J. (2003). Stability of catalytic foam diesel-soot filters based on CsO, MoO, and CsSO molten-salt catalysts. Applied Catalysis B: Environmental, 42(4), pp.337-347.

VASSILEV, S., BAXTER, D., ANDERSEN, L. AND VASSILEVA, C.(2010). An overview of the chemical composition of biomass. Fuel, 89(5), pp.913-933.

VERMA, V., BRAM, S., GAUTHIER, G. AND DE RUYCK, J. (2011). Performance of a domestic pellet boiler as a function of operational loads: Part-2. Biomass and Bioenergy, 35(1), pp.272-279.

VICENTE, E., DUARTE, M., CALVO, A., NUNES, T., TARELHO, L. AND ALVES, C. (2015). Emission of carbon monoxide, total hydrocarbons and particulate matter during wood combustion in a stove operating under distinct conditions. Fuel Processing Technology, 131, pp.182-192.

WANG, X., CHEN, H. AND SACHTLER, W. (2001). Mechanism of the Selective Reduction of NOx over Co/MFI: Comparison with Fe/MFI. Journal of Catalysis, 197(2), pp.281-291.

WANG, X., CHEN, H. AND SACHTLER, W. (2001). Selective reduction of NOx with hydrocarbons over Co/MFI prepared by sublimation of $CoBr_2$ and other methods. Applied Catalysis B: Environmental, 29(1), pp.47-60.

WENNERSTEN, R., SUN, Q. AND LI, H. (2015). The future potential for carbon capture and storage in climate change mitigation – an overview from perspectives of technology, economy and risk. Journal of Cleaner Production, 103, pp.724-736.

WERTHER, J., SAENGER, M., HARTGE, E., OGADA, T. AND SIAGI, Z. (2000). Combustion of agricultural residues. Progress in Energy and Combustion Science, 26(1), pp.1-27.

WICHTELOVÁ, B., SOBALÍK, Z. AND DĚDEČEK, J. (2003). Redox catalysis over metallo-zeolites. Applied Catalysis B: Environmental, 41(1-2), pp.97-114.

WILLIAMS, A., JONES, J., MA, L. AND POURKASHANIAN, M. (2012). Pollutants from the combustion of solid biomass fuels. Progress in Energy and Combustion Science, 38(2), pp.113-137.

WÖGERBAUER, C., MACIEJEWSKI, M., BAIKER, A. AND GÖBEL, U., 2001. Ir/H-ZSM-5 catalysts in the selective reduction of NOx with hydrocarbons. Topics in Catalysis, 16(1-4), pp.181-186.

WÖHLER, M., JAEGER, D., PELZ, S. AND THORWARTH, H. (2017). Potential of integrated emissions reduction systems in a firewood stove under real life operation conditions. Energy & Fuels, 31(7), pp.7562-7571.

WONG, T.W. ED., 2009. Handbook of zeolites: Structure, properties and applications. Nova Science Pub Incorporated.

WOODLETS. (2019). What does ENPlus A1 mean?. [online] Available at: https://www.woodlets.co.uk/faqs/enplus-a1-mean/ [Accessed 12 Apr. 2019].

WORLD HEALTH ORGANIZATION. Air quality guidelines: global update 2005: particulate matter, ozone, nitrogen dioxide, and sulfur dioxide. World Health Organization, 2006. Air quality guidelines: global update 2005: particulate matter, ozone, nitrogen dioxide, and sulfur dioxide. World Health Organization, 2006.

XIE, S., ROSYNEK, M. AND LUNSFORD, J. (1999). Catalytic reactions of NO over 0–7 mol% Ba/MgO Catalysts. Journal of Catalysis, 188(1), pp.32-39.

XU, J., QIN, Y., WANG, H., GUO, F. AND XIE, J., 2020. Recent advances in copper-based zeolite catalysts with low-temperature activity for the selective catalytic reduction of NOx with hydrocarbons. New Journal of Chemistry, 44(3), pp.817-831.

YANG, S., WANG, X., CHU, W., SONG, Z. AND ZHAO, S. (2011). An investigation of the surface intermediates of H_2-SCR of NOx over Pt/H-FER. Applied Catalysis B: Environmental, 107(3-4), pp.380-385.

YU, Q., RICHTER, M., LI, L., KONG, F., WU, G. AND GUAN, N. (2010). The promotional effect of Cr on catalytic activity of Pt/ZSM-35 for H_2-SCR in excess oxygen. Catalysis Communications, 11(11), pp.955-959.

YU, YUNBO, H. HONG, AND J. CHIN. Catalysis Science &Techonology 24 (2003): 385-390. Print.

ZENG, T., WELLER, N., POLLEX, A. AND LENZ, V. (2016). Blended biomass pellets as fuel for small scale combustion appliances: Influence on gaseous and total particulate matter emissions and applicability of fuel indices. Fuel, 184, pp.689-700.

ZHANG, X., WALTERS, A. AND VANNICE, M. (1994). Catalytic reduction of NO by CH_4 over Li-Promoted MgO. Journal of Catalysis, 146(2), pp.568-578.

ZHAO, X., ZHANG, X., XU, Y., LIU, Y., WANG, X. AND YU, Q. (2015). The effect of H_2O on the H_2-SCR of NOx over Pt/HZSM-5. Journal of Molecular Catalysis A: Chemical, 400, pp.147-153.

APPENDIX

Table A. 1: Properties of tested pellet samples (pre-set V-DTF temperature of 800°C)

Pre-set Furnace Temperature : 800C							
Combustion environment		Fuel					Duration
Ratio (% age)	Flow rate (L/min)	Category	Code	Weight (g)	Length (mm)	Diameter (mm)	Time
Air	10	Wood	W1	0.8190	26.85	6.20	04:55
			W2	0.7756	24.72	6.13	04:40
			W3	0.9585	29.44	6.11	05:05
		Straw	S1	1.0667	27.41	6.67	04:50
			S2	0.8417	24.39	6.37	04:40
			S3	0.9556	24.21	6.66	04:48
		Miscanthus	M1	0.6583	21.37	6.14	03:57
			M2	0.6594	20.77	6.49	03:46
			M3	0.7610	24.22	6.18	03:39
		Peanut	P1	1.5419	26.88	8.50	07:53
			P2	11,428	21.60	8.23	06:54
			P3	1.3451	23.65	8.20	08:21
		Torrefied wood	T1	0.8716	26.05	6.13	05:44
			T2	0.7588	23.44	6.11	05:23
			T3	0.8701	26.40	6.10	05:37
21% O2/ 79% CO2	2.1/7.9	Wood	W19	0.868	27.98	6.01	04:41
			W20	0.7599	25.42	6.02	04:35
			W21	0.8729	27.35	6.07	04:57
		Straw	S18	0.9055	21.47	6.61	04:43
			S19	0.9663	28.55	6.29	03:54
			S22	0.7076	23.31	6.40	04:31
			S23	0.9770	24.42	6.76	05:49
		Miscanthus	M20	0.8322	25.92	6.29	04:49
			M21	0.7437	23.03	6.54	05:38
			M22	0.7707	23.44	6.29	05:08
		Peanut	P21	1.4508	24.60	8.60	08:46
			P22	1.2798	22.12	8.33	07:41
			P23	1.433	26.65	8.41	09:43
		Torrefied wood	T21	0.6971	22.13	6.19	06:20
			T22	0.6295	19.17	6.14	05:41
			T23	0.5512	17.86	6.10	04:45
			T24	0.5555	17.18	6.07	04:47
25% O2/ 75% CO2	2.5/7.5	Wood	W22	0.8316	26.97	6.03	03:44
			W23	0.7089	24.24	6.02	03:28
			W24	0.8117	25.65	6.15	03:49
		Straw	S25	0.9576	23.90	6.66	04:17
			S26	0.9327	26.04	6.30	04:01
			S27	0.7913	25.61	6.42	03:28
		Miscanthus	M23	0.6504	19.87	6.33	03:19
			M24	0.7270	23.00	6.12	03:34
			M25	0.6652	20.48	6.31	03:31
		Peanut	P24	1.3411	23.70	8.62	06:46
			P25	1.2885	22.48	8.39	06:34
			P26	1.5391	27.03	8.69	07:04
		Torrefied wood	T25	0.6057	20.66	6.15	03:39
			T27	0.5970	18.91	6.11	03:56
			T28	0.6264	19.56	6.17	03:51
30% O2/ 70% CO2	3.0/ 7.0	Wood	W25	0.9427	29.42	6.00	03:23
			W26	0.9078	28.27	6.10	03:12
			W27	0.6357	21.45	6.02	02:55
		Straw	S29	0.6730	21.85	6.37	03:16
			S30	0.7311	21.58	6.37	02:58
			S31	0.8599	25.88	6.14	03:27
		Miscanthus	M26	0.7013	24.02	8.18	02:53
			M27	0.6033	20.33	6.08	02:48
			M28	0.6057	19.74	6.09	02:48
		Peanut	P27	1.2216	23.36	8.14	05:26
			P28	1.2577	23.21	8.22	04:52
			P29	1.2412	21.60	8.57	05:22
		Torrefied wood	T30	0.5925	19.87	6.12	03:12
			T31	0.6092	19.79	6.14	03:05
			T32	0.5486	18.13	6.07	02:58

Table A. 2: Properties of tested pellet samples (pre-set V-DTF temperature of 800°C)

Pre-set Furnace Temperature : 900C							
Combustion environment		Fuel					Duratation
Ratio (% agerage)	Flow rate (L/min)	Category	Code	Weight (g)	Length (mm)	Diameter (mm)	Time
Air	10	Wood	W4	0.7992	26.77	6.02	03:56
			W5	0.7052	25.95	5.98	03:40
			W6	0.7512	24.49	6.05	03:29
		Straw	S4	0.9199	22.35	6.57	04:12
			S5	0.7138	23.51	6.12	03:22
			S7	0.8333	26.36	6.19	03:54
		Miscanthus	M4	0.6891	22.76	6.18	03:27
			M5	0.798	24.63	6.12	03:42
			M6	0.6943	25.88	6.31	03:25
		Peanut	P4	1.277	23.58	8.62	06:26
			P5	1.3844	22.6	8.98	06:52
			P6	1.2845	24.2	8.1	06:49
		Torrefied wood	T4	0.8369	25.33	6.19	05:12
			T5	0.7715	23.17	6.12	04:43
			T6	0.8529	25.81	6.19	05:31
21% O2/ 79% CO2	2.1/7.9	Wood	W7	0.8166	26.57	6.08	03:29
			W8	0.8014	25.67	6.07	03:25
			W9	0.834	25.76	6.1	03:39
		Straw	S8	1.095	27.05	6.36	04:28
			S9	0.9111	26.94	6.17	03:44
			S10	0.8242	25.89	6.24	03:38
		Miscanthus	M7	0.7014	21.88	6.45	03:24
			M8	0.7754	23.91	6.32	03:35
			M9	0.8425	24.92	6.15	03:48
		Peanut	P7	1.4192	26.35	8.03	05:55
			P9	1.4885	27.2	8.04	06:40
			P10	1.1364	20.59	8.4	05:58
		Torrefied wood	T7	0.6541	20.52	6.15	04:03
			T8	0.782	24.36	6.12	04:01
			T9	0.6597	21.17	6.03	03:45
25% O2/ 75% CO2	2.5/7.5	Wood	W11	0.8068	26.23	6.16	02:57
			W12	0.7223	24.13	6.07	02:56
			W13	0.853	29.18	6.18	02:56
		Straw	S11	0.8717	25.67	6.42	03:45
			S13	0.9009	24.55	6.49	03:36
			S14	0.8692	25.75	6.22	03:05
		Miscanthus	M10	0.6742	20.79	6.09	02:57
			M11	0.7546	23.81	6.28	02:57
			M13	0.8251	23.86	6.42	03:09
		Peanut	P11	1.5518	27.6	8.48	05:33
			P13	1.2838	21.95	8.74	05:18
			P14	1.2814	24.26	8.29	05:23
			P15	1.0905	22.58	8.06	04:46
		Torrefied wood	T13	0.6782	21.6	6.14	03:09
			T14	0.6578	20.38	6.18	03:11
			T15	0.6653	20.45	6.18	03:18
30% O2/ 70% CO2	3.0/ 7.0	Wood	W16	0.8198	27.86	6.13	02:22
			W17	0.9487	29.43	6.12	02:34
			W18	0.9352	29.05	6.1	02:28
		Straw	S15	0.82	23.84	6.16	02:42
			S16	0.867	26.6	6.26	02:33
			S17	0.8034	25.7	6.21	01:38
		Miscanthus	M14	0.7288	22.6	6.41	02:27
			M16	0.6352	21.77	6.25	01:25
			M17	0.5735	18.96	6.52	02:04
			M19	0.6558	21.31	6.13	02:30
		Peanut	P16	1.2647	22.81	8.56	04:14
			P19	1.3311	24.35	8.47	04:17
			P20	1.2111	21.38	8.6	04:10
		Torrefied wood	T17	0.6076	19.5	6.24	02:34
			T18	0.6667	20.25	6.13	02:35
			T19	0.6232	19.37	6.08	02:30
			T20	0.6237	18.95	6.11	02:44

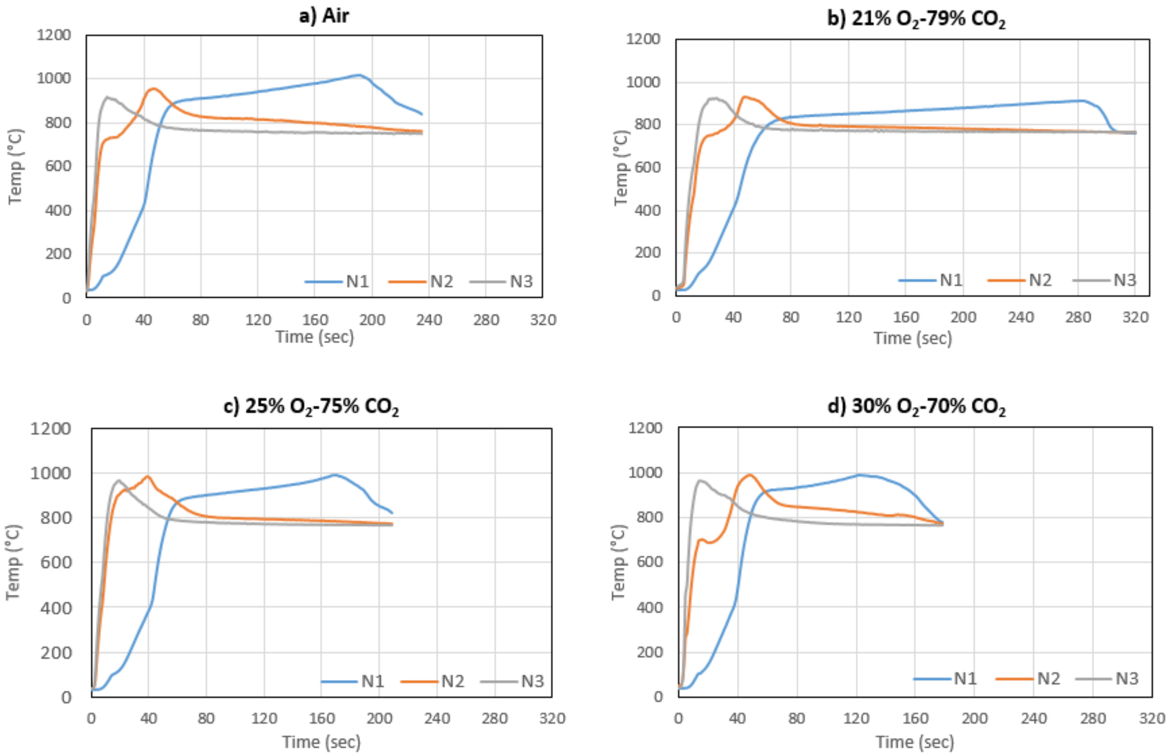

Figure A. 1: Temperature distributions of miscanthus pellet combustion test with the furnace set temperature of 800°C: a) air; b) 21%O_2-79%CO_2; c) 25%$O_2$75% CO_2; d) 30%O_2-70%CO_2

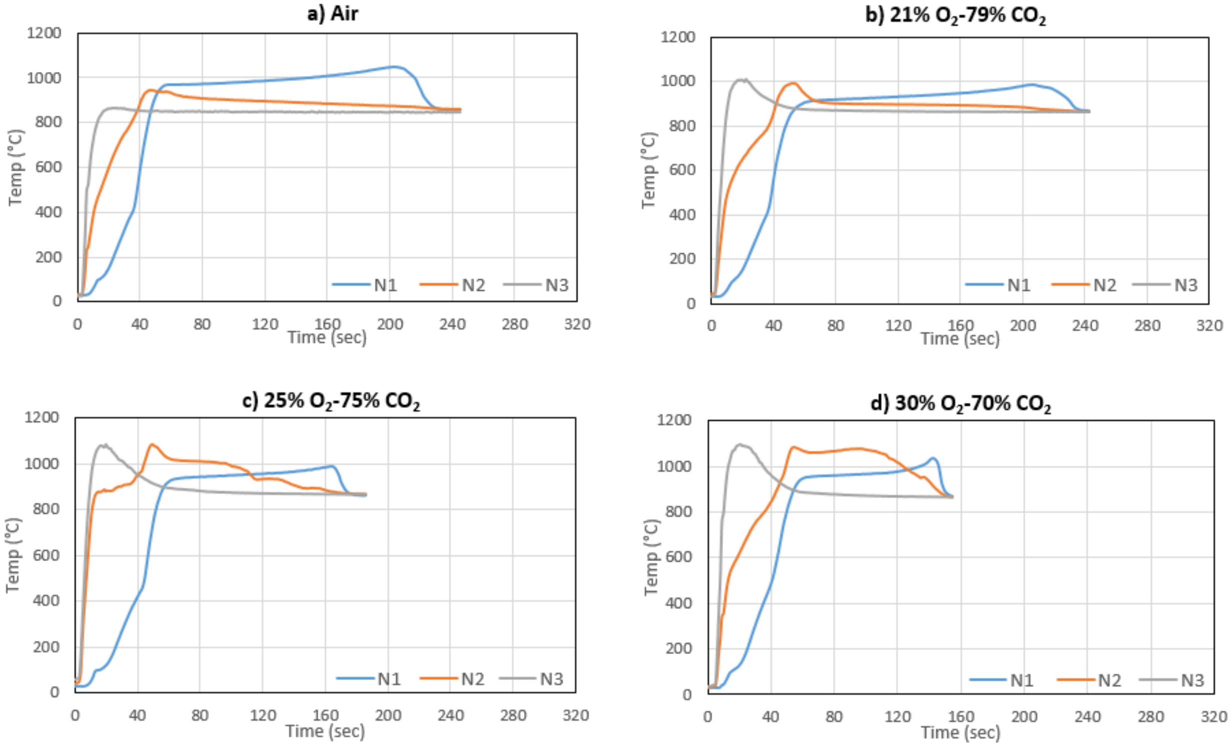

Figure A. 2: Temperature distributions of miscanthus pellet combustion test with the furnace set temperature of 900°C: a) air; b) 21%O_2-79%CO_2; c) 25%$O_2$75% CO_2; d) 30%O_2-70%CO_2

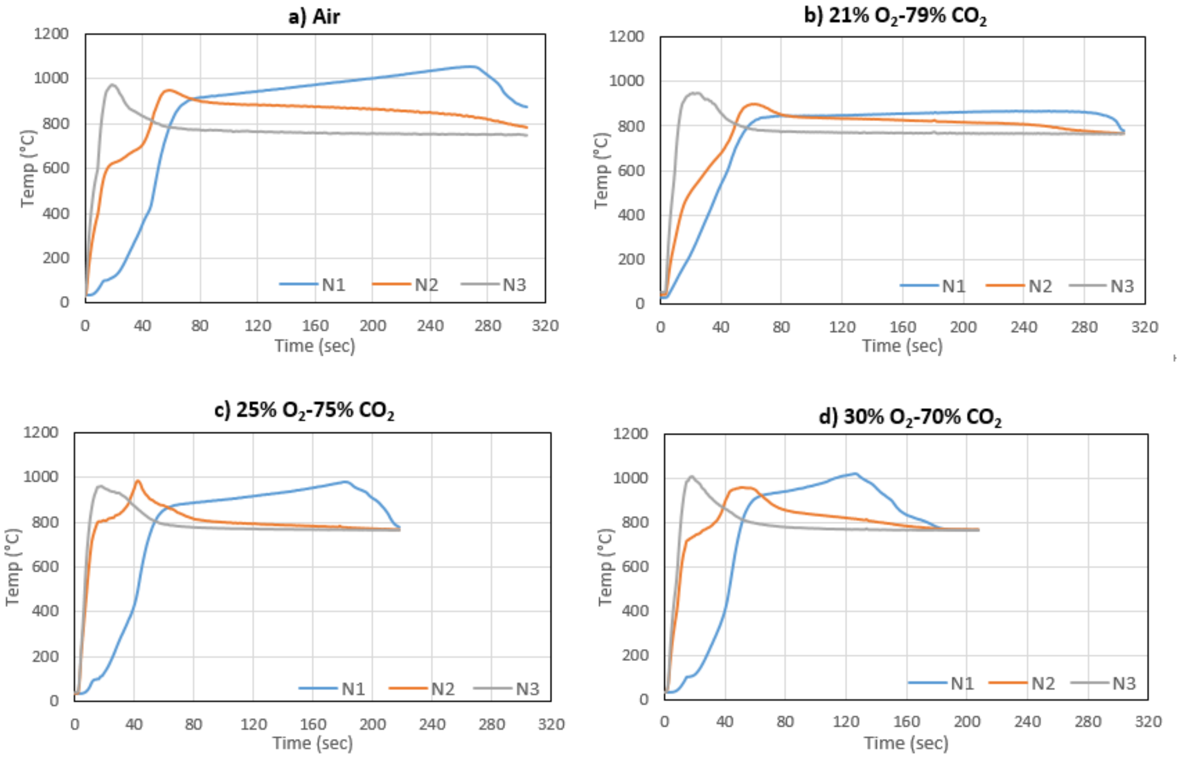

Figure A. 3: Temperature distributions of straw pellet combustion test with the furnace set temperature of 800°C: a) air; b) 21%O_2-79%CO_2; c) 25%$O_2$75% CO_2; d) 30%O_2-70%CO_2

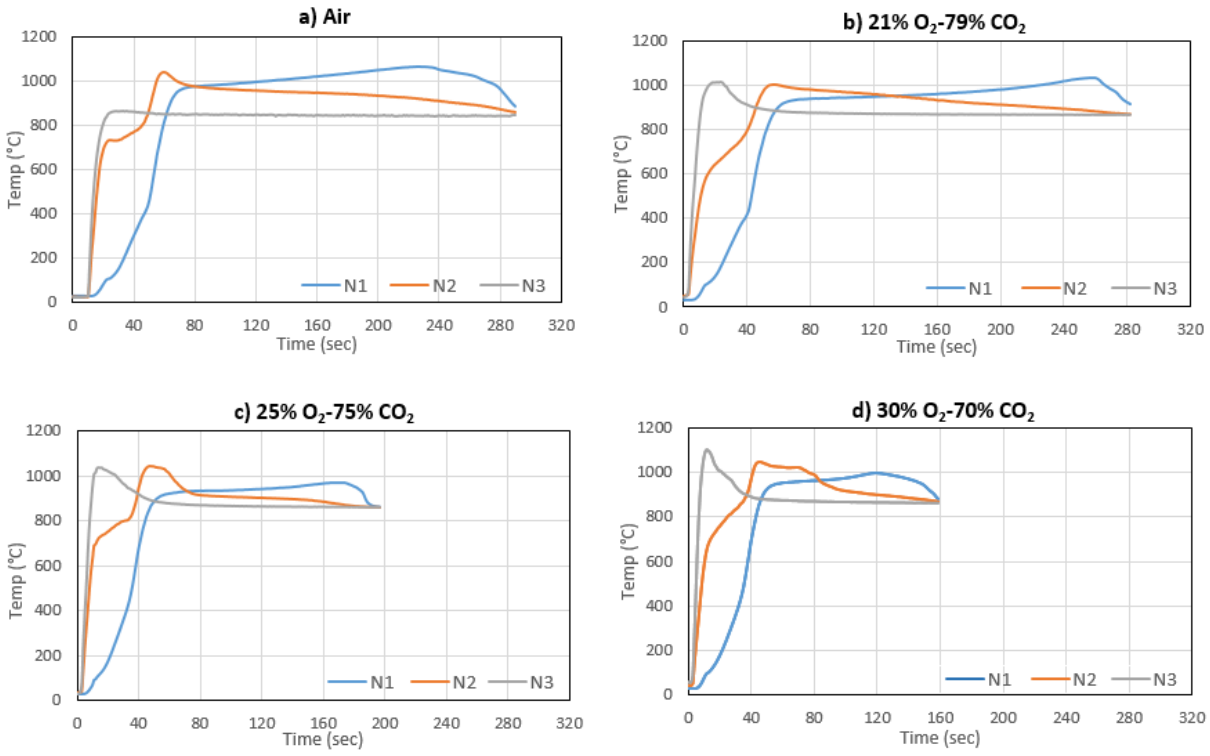

Figure A. 4: Temperature distributions of straw pellet combustion test with the furnace set temperature of 900°C: a) air; b) 21%O_2-79%CO_2; c) 25%$O_2$75% CO_2; d) 30%O_2-70%CO_2

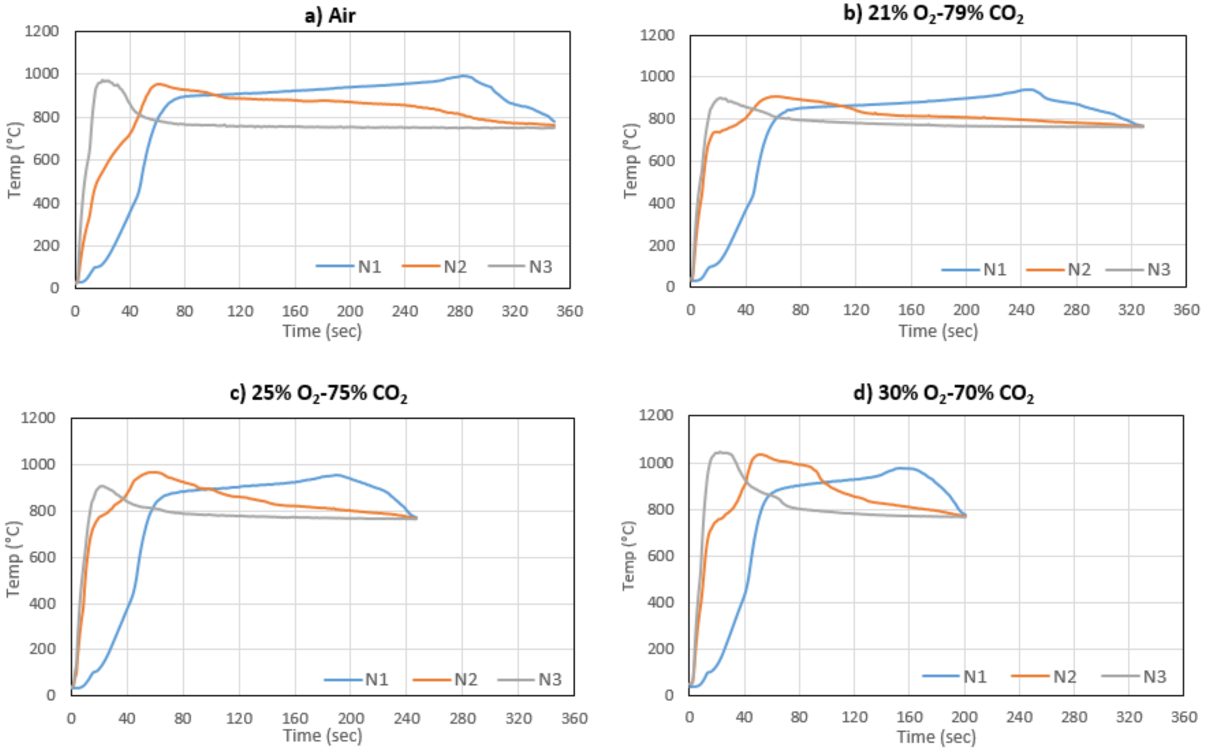

Figure A. 5: Temperature distributions of torrefied wood pellet combustion test with the furnace set temperature of 800°C: a) air; b) 21%O_2-79%CO_2; c) 25%$O_2$75% CO_2; d) 30%O_2-70%CO_2

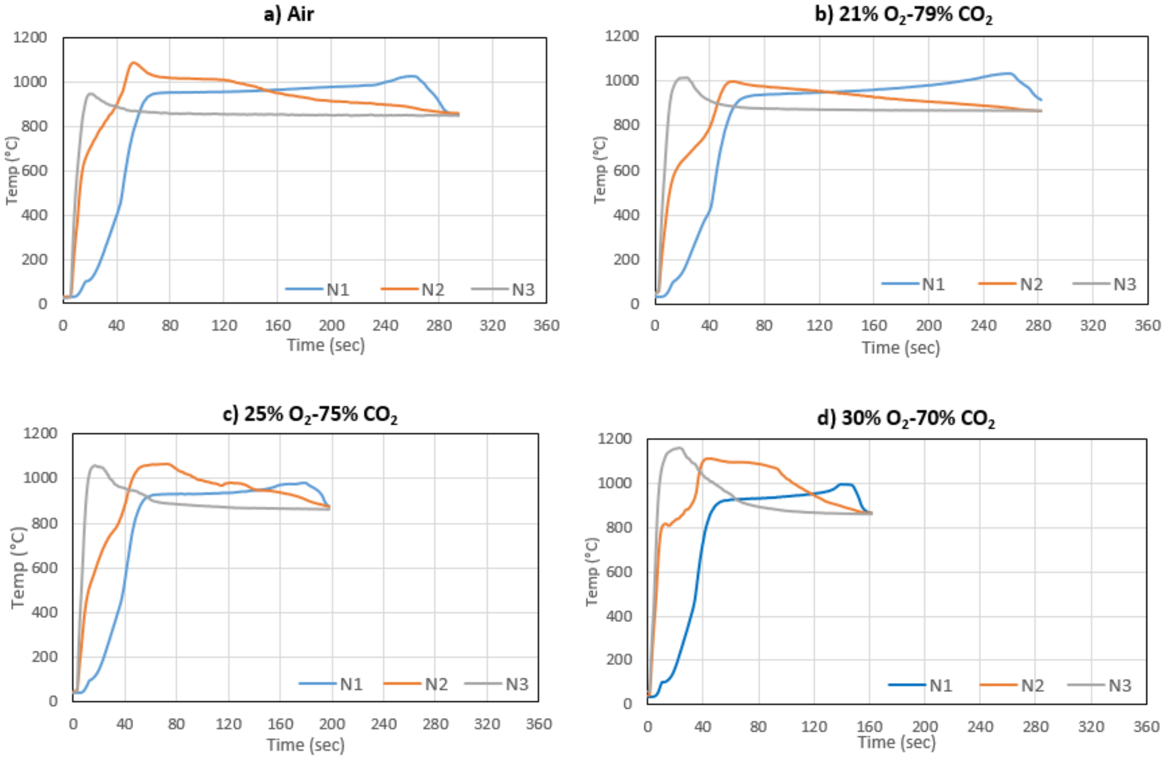

Figure A. 6: Temperature distributions of torrefied wood pellet combustion test with the furnace set temperature of 900°C: a) air; b) 21%O_2-79%CO_2; c) 25%$O_2$75% CO_2; d) 30%O_2-70%CO_2

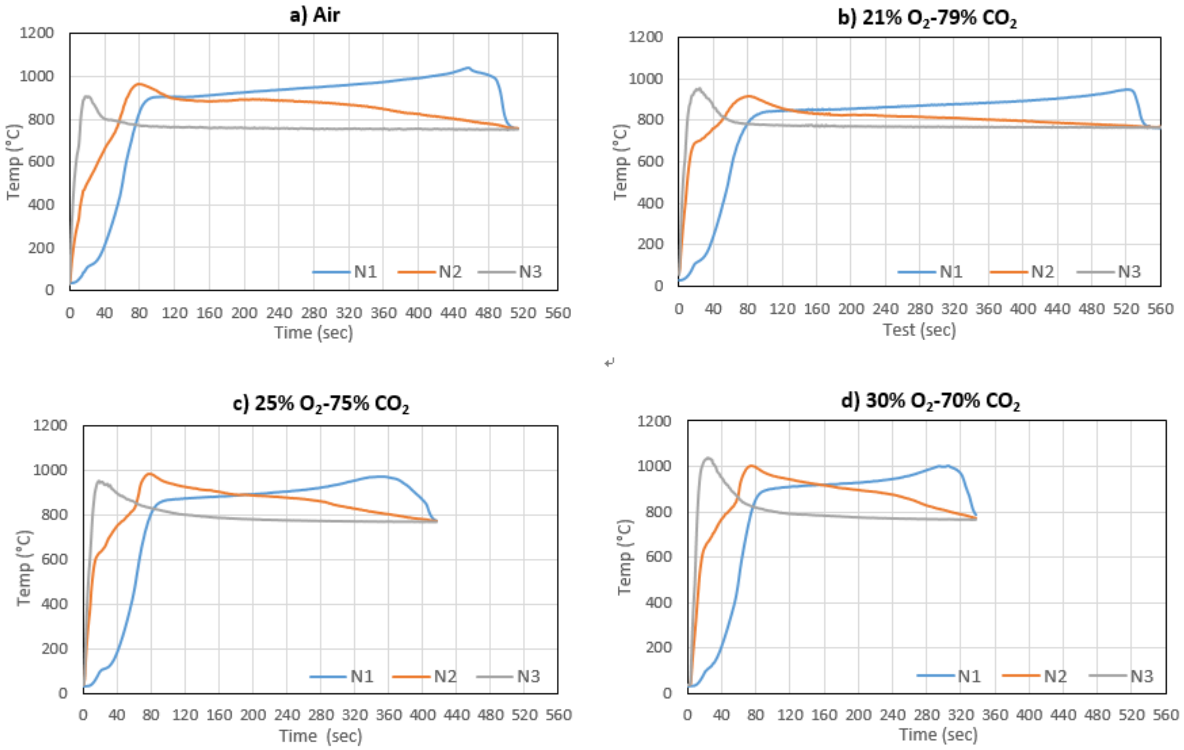

Figure A. 7: Temperature distributions of peanut pellet combustion test with the furnace set temperature of 800°C: a) air; b) $21\%O_2$-$79\%CO_2$; c) $25\%O_2 75\%$ CO_2; d) $30\%O_2$-$70\%CO_2$

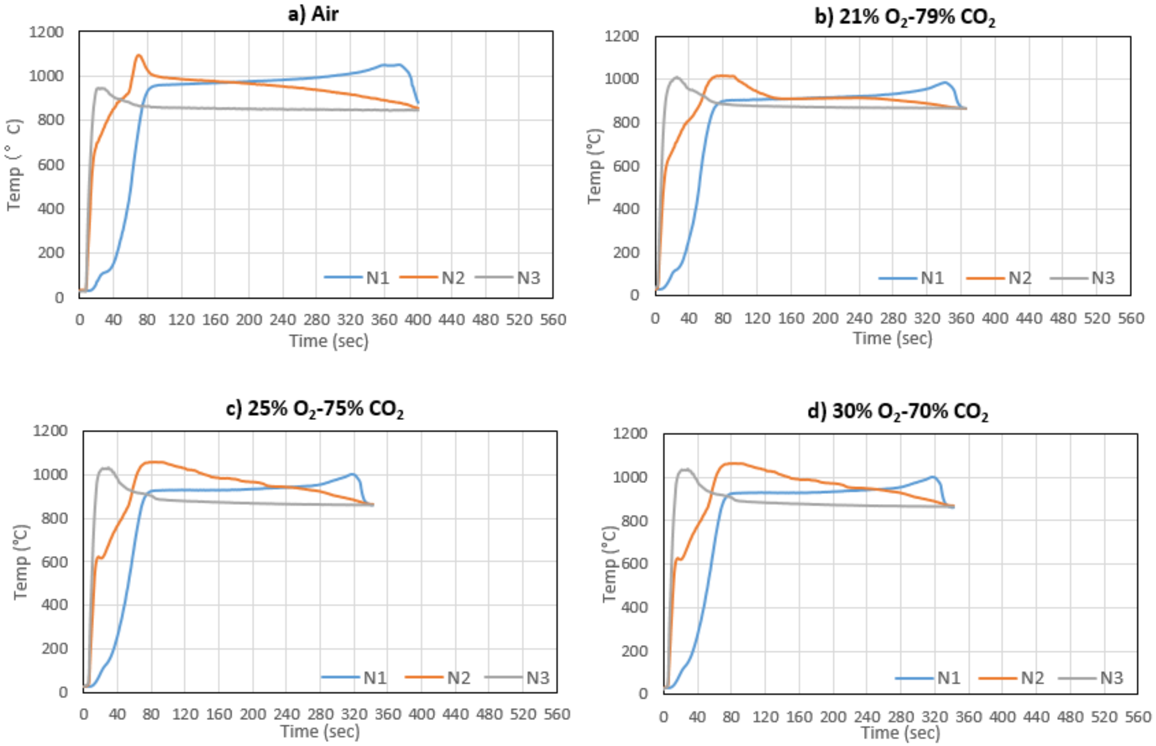

Figure A. 8: Temperature distributions of peanut pellet combustion test with the furnace set temperature of 900°C: a) air; b) 21%O_2-79%CO_2; c) 25%$O_2$75% CO_2; d) 30%O_2-70%CO_2

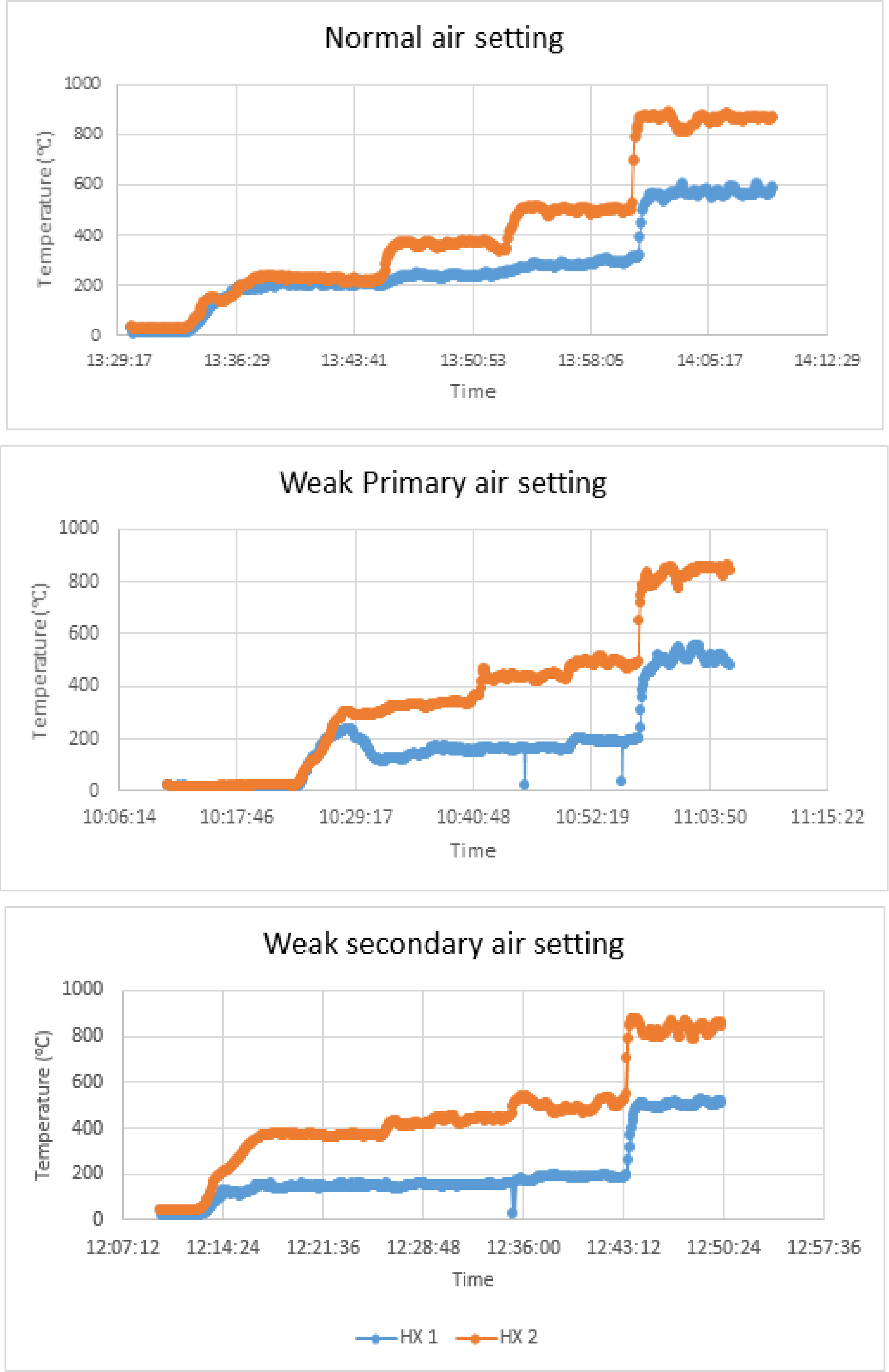

Figure A. 9: Temperature variation of four tubes from 300mm height to heat exchanger inlet (HX 1 and HX 2)

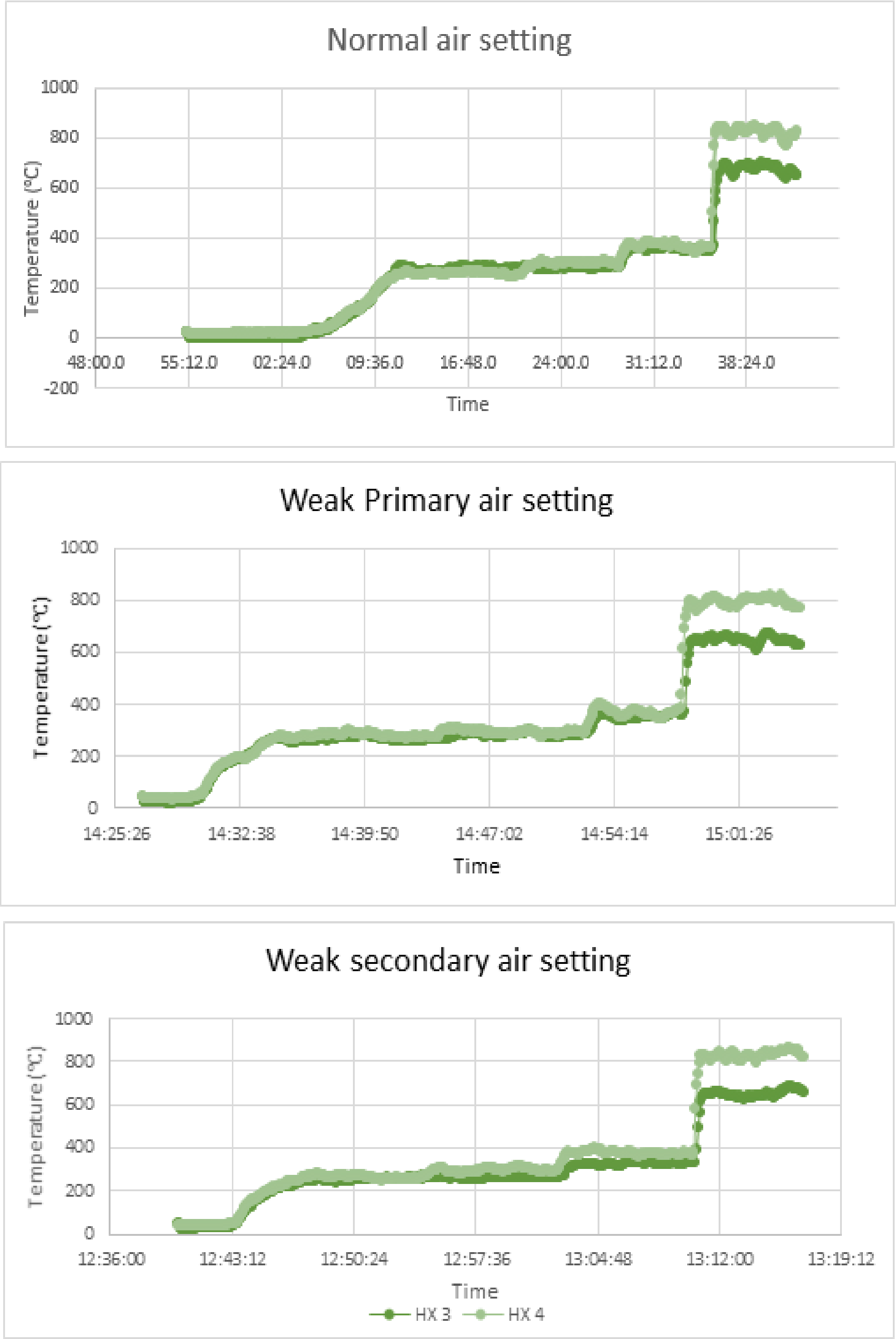

Figure A. 10: Temperature variation of four tubes from 300mm height to heat exchanger inlet (HX 3 and HX 4)

Table A. 3: Reaction gas variation of catalytic methane oxidation over 2.44% Co-ZSM-5 (Si/Al=12.5) under different setting temperatures

	CO (vol %)	CO_2 (vol %)	O_2 (vol %)	CH_4 (vol %)
Room Temperature	-0.0012	0.038	15.59	0.112
200℃	-0.0021	0.038	18.59	0.110
300℃	-0.0030	0.039	18.60	0.109
400℃	-0.0016	0.039	18.61	0.106
500℃	0.0042	0.042	18.57	0.0843

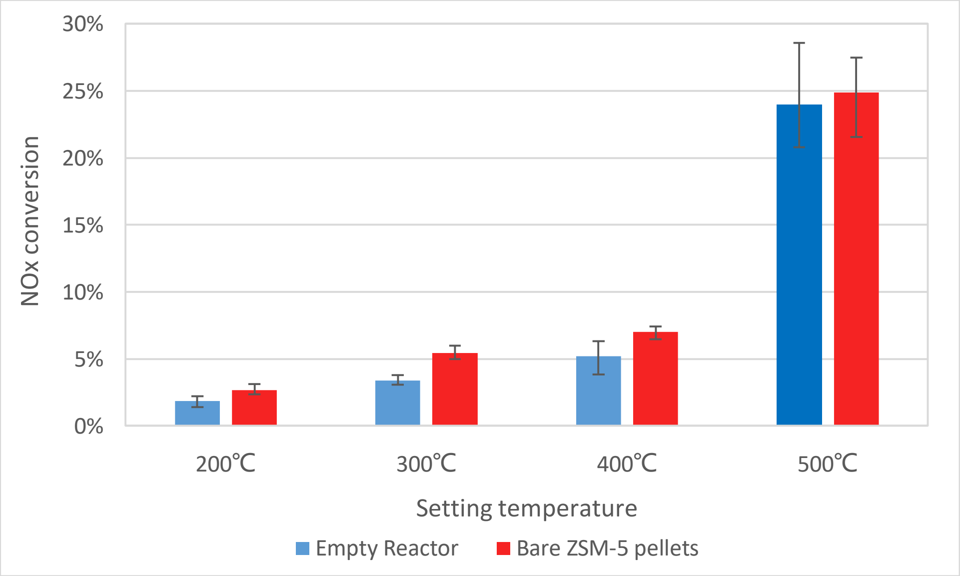

Figure A. 11: Comparison of NOx conversion on CH_4-SCR over empty reactor and bare ZSM-5 pellets in the presence of oxygen, feed gas conditions: [NOx]= 333ppm, $[CH_4]$= 0.67%, $[O_2]$= 6.98%, balance in N_2, 0.3 L/min.

Table A. 4: Main reactions of methane oxidation in the presence of air and low-level NOx (Chan et al., 2011)

$$\mathrm{H} + \mathrm{O_2} \rightarrow \mathrm{OH} + \mathrm{O} \tag{1}$$

$$\mathrm{H} + \mathrm{O_2} + \mathrm{M} \rightarrow \mathrm{HO_2} + \mathrm{M} \tag{2}$$

$$\mathrm{CH_2O} + \mathrm{OH} \rightarrow \mathrm{HCO} + \mathrm{H_2O} \tag{3}$$

$$\mathrm{CH_4} + \mathrm{OH} \rightarrow \mathrm{CH_3} + \mathrm{H_2O} \tag{4}$$

$$\mathrm{CH_4} + \mathrm{O} \rightarrow \mathrm{CH_3} + \mathrm{OH} \tag{5}$$

$$\mathrm{CH_3} + \mathrm{O_2} \rightarrow \mathrm{CH_2O} + \mathrm{OH} \tag{6}$$

$$\mathrm{CH_3} + \mathrm{O_2} \rightarrow \mathrm{CH_2O} + \mathrm{O} \tag{7}$$

$$\mathrm{CH_3} + \mathrm{CH_3}(+\mathrm{M}) \rightarrow \mathrm{C_2H_6}\ (+\mathrm{M}) \tag{8}$$

$$\mathrm{NO} + \mathrm{HO_2} \rightarrow \mathrm{NO_2} + \mathrm{OH} \tag{9}$$

$$\mathrm{NO_2} + \mathrm{O} \rightarrow \mathrm{NO} + \mathrm{NO_2} \tag{10}$$

$$\mathrm{NO_2} + \mathrm{HO_2} \rightarrow \mathrm{HONO} + \mathrm{O_2} \tag{11}$$

$$\mathrm{CH_3} + \mathrm{NO_2} \rightarrow \mathrm{CH_3O} + \mathrm{NO} \tag{12}$$

$$\mathrm{CH_3O_2} + \mathrm{NO} \rightarrow \mathrm{CH_3O} + \mathrm{NO_2} \tag{13}$$

$$\mathrm{CH_3} + \mathrm{HONO} \rightarrow \mathrm{CH_4} + \mathrm{NO_2} \tag{14}$$

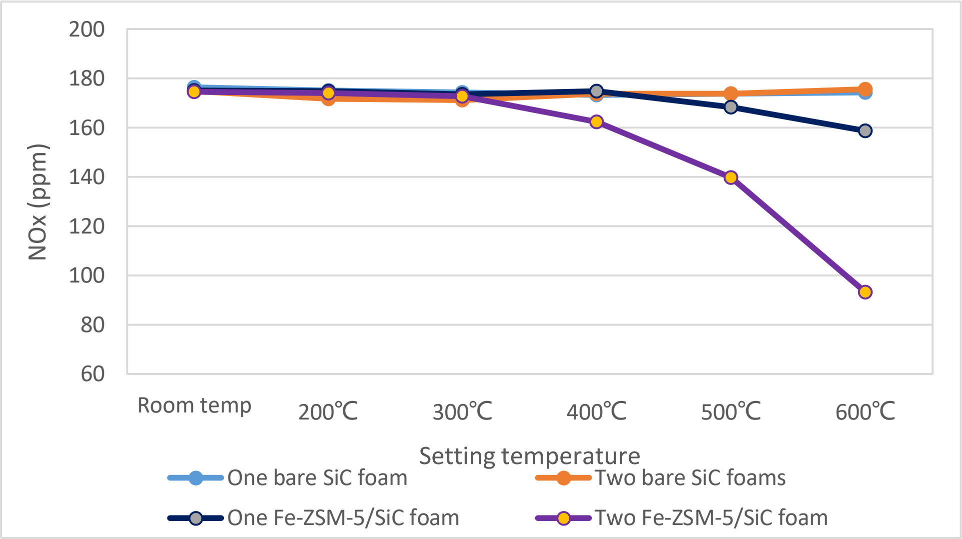

(a). Variation of NOx

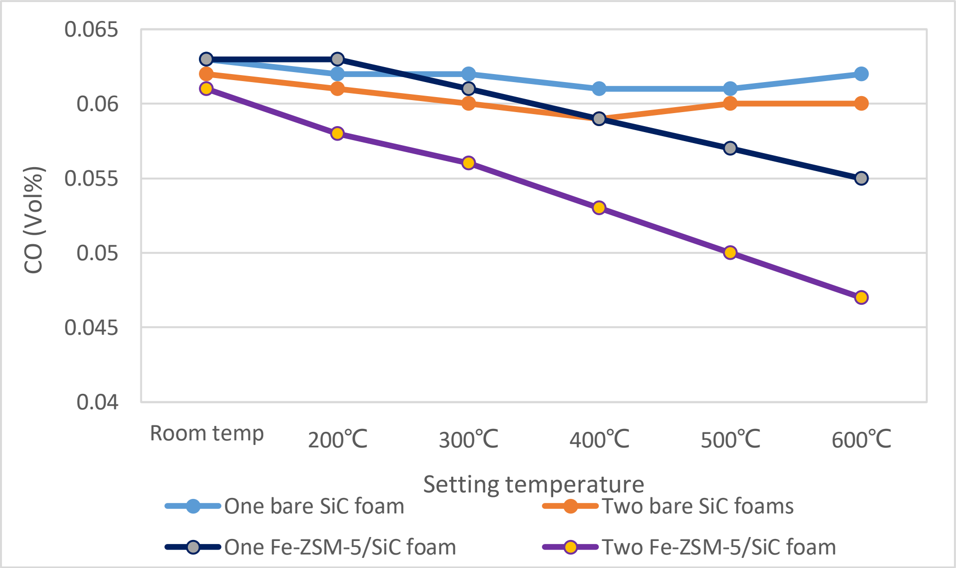

(b). Variation of CO

Figure A.12: Trends of NOx and CO in catalytic NOx-CO reaction(s) over Fe-ZSM-5/SiC foam(s) in the absence of oxygen under large flow rate setting, feed gas conditions: [NOx]= 167ppm, [CO]= 250ppm, $[CO_2]$= 2.5%, balance in N_2, 6 L/min.

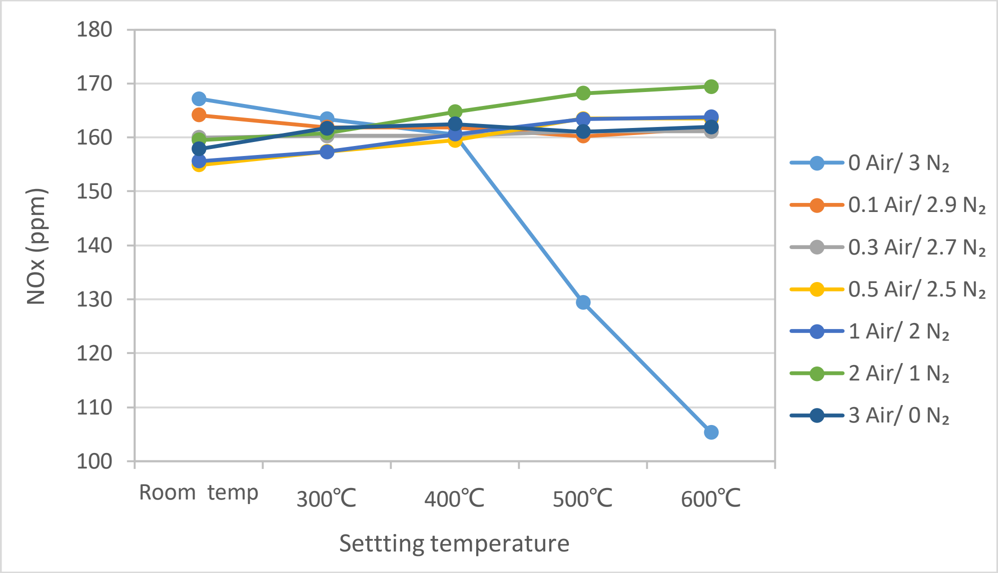

(a). Variation of NOx

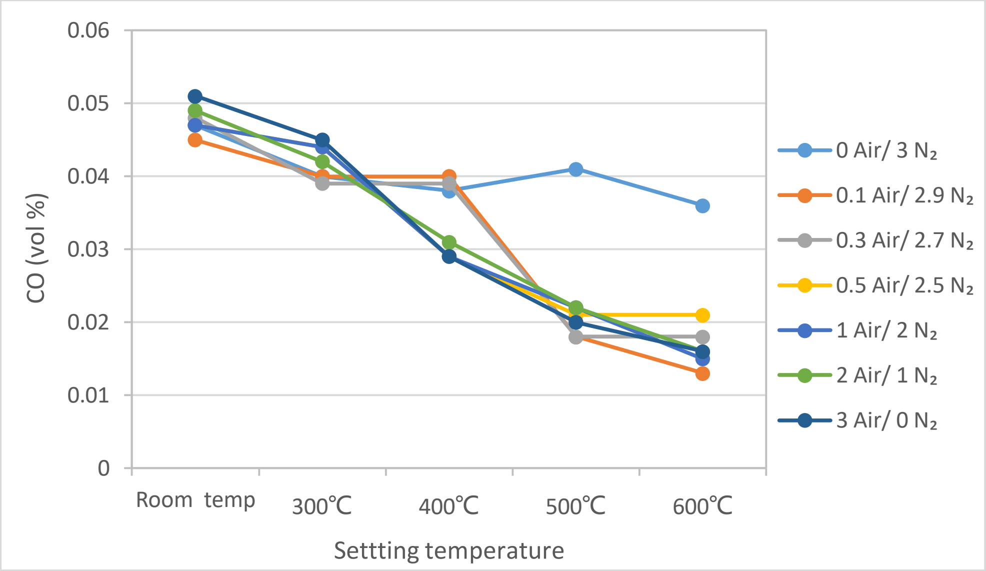

(b). Variation of CO

Figure A.13: Trends of NOx and CO in catalytic NOx-CO reaction(s) over Fe-ZSM-5/SiC foam(s) under various ratio of air/ N_2 (large flow rate setting), feed gas conditions: [NOx]= 167ppm, [CO]= 250ppm, [CO_2]= 2.5% and different ratios of air/ N_2 (L/min), 6 L/min.